APPLICATIONS AND EXTENSIONS OF THE THEORY OF ATOMS IN MOLECULES

By

MARSHALL TODD CARROLL, B.Sc.

A Thesis

Submitted to the School of Graduate Studies

in Partial Fulfilment of the Requirements

for the Degree

Doctor of Philosophy

McMaster University

APPLICATIONS AND EXTENSIONS OF THEORY OF ATOMS IN MOLECULES

DOCTOR OF PHILOSOPHY (1989) McMASTER UNIVERSITY

(Chemistry) Hamilton, Ontario

TITLE: Applications and Extensions of the Theory of Atoms in Molecules

AUTHOR: Marshall Todd Carroll, B.Sc. (University of Winnipeg)

SUPERVISOR: Dr. R. F. W. Bader

NUMBER OF PAGES: xix, 456

ABSTRACT

This thesis applies and extends the theory of atoms in molecules. The charge distributions of diatomic molecules, hydrocarbons, hydrogen-bonded complexes and complexes containing NN bonds are examined.

The theory of atoms in molecules provides a quantum mechanical definition of an atom in a molecule and its properties. The topology of the charge distribution is the observational basis for the elements of molecular structure, structural change and stability.

The theory is reviewed in Chapter 1. Studies of hydrocarbons and diatomic molecules are made and the new concept of atomic volume is introduced. Electronegativity schemes are explored and extended.

The nature of the hydrogen bond is discussed in Chapter 2. The charge redistribution which allows for mutual penetration of the van der Waals envelopes of the base atom and the H-bonded H atom is investigated.

Chapter 3 shows how the Laplacian of the charge density can be used to predict structures and geometries of hydrogen-bonded complexes. Reactivities of activated double bonds to nucleophilic attack are predicted by $\nabla^2\rho$.

Chapter 4 surveys a set of complexes containing NN bonds and proposes a bond order and bond energy scheme for these bonds.

Chapter 5 uses density functional theory to construct correlation energy functionals. The correlation energies of atoms in

molecules can then be studied and total energies of molecules calculated.

ACKNOWLEDGEMENTS

I wish to thank all the members of the Theoretical Chemistry Laboratory for their assistance, cooperation and friendship during my stay at McMaster. In chronological order they are Tom Slee, Clem Lau, Preston MacDougall, Jane Bailey, Jeurgen Gauss, Annie Larouche, Cheng Chang, Jim Cheeseman, Carlo Gatti, Weiliang Cao, Kathy Gough, Keith Laidig and Danny Legare. I wish to give special thanks to my supervisor, Richard Bader, for teaching me Science.

This thesis is dedicated to Sharon.

TABLE OF CONTENTS

TABLE OF CONTENTS (con'd)

TABLE OF CONTENTS (con'd)

LIST OF FIGURES

LIST OF FIGURES (con'd)

LIST OF FIGURES (con'd)

LIST OF FIGURES (con'd)

LIST OF TABLES

LIST OF TABLES (con'd)

LIST OF TABLES (con'd)

LIST OF TABLES (con'd)

LIST OF TABLES (con'd)

LIST OF TABLES (con'd)

INTRODUCTION

Science is observation, identification, classification, explanation and prediction. The first observation of the theory of atoms in molecules was that if the charge density in a region of real three-dimensional space was similar in form between different systems, then so was its kinetic energy density. This observation led to the proposition of zero flux surfaces and to the identification of these (mononuclear) regions as atoms. Second- and third-row diatomic molecules were then considered and the interatomic surfaces were classified on the basis of their shape and the number of valence electrons (vacancies) on the electron donor (acceptor). Atomic interactions were classified as shared ($\nabla^2\rho(r_c) < 0$) or closed-shell ($\nabla^2\rho(r_c) > 0$). Hydrogen-bonded complexes (Chapters 2 and 3) are examples of closed-shell interactions while molecules containing nitrogen nitrogen bonds (Chapter 4) are examples of shared interactions.

An explanation of hydrogen bonding is given by the theory of atoms in molecules. The charge distributions of the approaching atoms that will form the H-bond polarize in such a way as to facilitate mutual penetration of their van der Waals envelopes. As the degree of penetration increases, so does the strength of the hydrogen-bond. The theory also explains the geometry of OCO-HF (Chapter 3), the similarities between isoelectronic NN and CC complexes (Chapter 4), and the trends in correlation energies of the hydrides for example

(Chapter 5).

The theory predicts the electron population of an atom in a diatomic molecule (Chapter 1), the structures and geometries of H-bonded complexes (Chapter 3), the greater toxicity of the acrylates as compared to the methacrylates (Chapter 3) and the bond orders and bond energies of complexes containing NN bonds (Chapter 4).

The goal of this work is to apply and extend the theory of atoms in molecules to various chemical systems within the framework of the scientific method.

CHAPTER 1

THE THEORY OF ATOMS IN MOLECULES AND ITS APPLICATION TO MOLECULAR CHARGE DISTRIBUTIONS

This chapter introduces the concepts used in the theory of atoms in molecules (Bader 1985, Bader and Nguyen-Dang 1981, Bader et al 1981). Discussions of the topological properties of the electronic charge distribution and the Laplacian of the electronic charge distribution and the atomic properties of atoms in molecules are emphasized as these ideas are central to the original work presented in this and the following chapters.

Section 1.1 details the construction of the charge distribution. Sections 1.2 and 1.3 describe the topological features of the molecular charge distribution, ρ, and the Laplacian of the charge distribution, $\nabla^2\rho$, respectively. Section 1.4 shows how these features can be used to characterize atomic interactions. Section 1.5 outlines the quantum mechanical derivation of the theory of atoms in molecules and delineates the atomic properties of interest in this work. It also demonstrates the transferability of these properties in a series of hydrocarbons. Section 1.6 illustrates the concepts of the theory through a study of second-row diatomic molecules and second- and third-row hydrides. Non-relativistic stationary state quantum mechanics using the Schrödinger representation (or picture) and the coordinate representation is used throughout the thesis. Atomic units ($\hbar = e = m_e = 1$) are used in the equations and results throughout this

work unless otherwise noted.

1.1 CONSTRUCTION OF THE CHARGE DISTRIBUTION

An isolated molecular system composed of N nuclei, denoted α, β, ..., and n electrons, denoted i, j, ..., is described by its Hamiltonian operator, $\hat{H}$, and a wavefunction Ψ satisfying the stationary state Schrödinger equation

$$\hat{H}\Psi_1 = E_1\Psi_1 \qquad [1.1.1]$$

(Schrödinger 1926; For introductory accounts of quantum mechanics see Levine 1983 or Hehre et al 1986, for example). In this time-independent equation, E_1 is a real constant (an eigenvalue), $1 = 0,1,\ldots$ and $\hat{H}$ is given by

$$\hat{H} = \Sigma_\alpha \frac{-1}{2M_\alpha}\nabla^2_\alpha + \frac{-1}{2}\Sigma_i\nabla^2_i + \Sigma_{\alpha<\beta}\frac{Z_\alpha Z_\beta}{R_{\alpha\beta}} - \Sigma_{\alpha,i}\frac{Z_\alpha}{r_{i\alpha}} + \Sigma_{i<j}\frac{1}{r_{ij}} \qquad [1.1.2]$$

The mass and charge of nucleus α are denoted M_α and Z_α respectively. The Laplacian operator with respect to the coordinates of the indicated particle (nucleus or electron) is denoted ∇^2_α or ∇^2_i respectively. The expression for the Laplacian operator is

$$\nabla^2 = \partial^2/\partial x^2 + \partial^2/\partial y^2 + \partial^2/\partial z^2 \qquad [1.1.3]$$

The symbols $R_{\alpha\beta}$, $r_{i\alpha}$ and r_{ij} denote the distances between the respective particles.

Adopting the Born-Oppenheimer approximation (1927), where the nuclear and electronic motions are decoupled and noting that in all applications of the theory in this thesis molecular systems are

considered in their ground states (therefore the 1 subscript can be dropped) allows the state function to be written as

$$\Psi(X,x) = \theta(X)\psi(x;X) \qquad [1.1.4]$$

Here X denotes the collection of the nuclear coordinates, x denotes the collection of electronic space and spin coordinates, $\theta(X)$ is the nuclear state function and $\psi(x;X)$ is the properly antisymmetrized electronic state function which must satisfy the electronic Schrodinger equation

$$\hat{H}_{el}\psi(x;X) = E(X)\psi(x;X) \qquad [1.1.5]$$

The electronic Hamiltonian is given by

$$\hat{H}_{el} = \frac{-1}{2}\Sigma_i\nabla^2_i - \Sigma_{\alpha,i}\frac{Z_\alpha}{r_{i\alpha}} + \Sigma_{i<j}\frac{1}{r_{ij}} \qquad [1.1.6]$$

$\hat{H}_{el}$ depends on X only through the term

$$\hat{V}_{en} = -\Sigma_{\alpha,i}\frac{Z_\alpha}{r_{i\alpha}} \qquad [1.1.7]$$

and this term is responsible for the parametric dependence of the solutions to equation [1.1.5] on X. For notational convenience, hereafter this dependence will be implicitly assumed. The Roothaan-Hartree-Fock Self Consistent Field procedure (1951), as implemented in the GAUSSIAN series of programs (Frisch et al 1988) for example, is used to find solutions to [1.1.5].

The charge distribution for a system containing N electrons is defined by

$$\rho(r) = n\Sigma_{spins}\int\{\prod_{j\neq 1}dr_j\}\psi^*(x)\psi(x) \qquad [1.1.8]$$

where ψ is a solution to equation [1.1.5], x is the collection of electronic space and spin coordinates and r is the space coordinates of

one electron. In an abbreviated fashion, equation [1.1.8] may be written as

$$\rho(r) = n\int d\tau' \Psi^*(x)\Psi(x) \qquad [1.1.8]$$

where τ' denotes the Cartesian coordinates of all the electrons but one and the spin coordinates of all the electrons.

The electronic charge distribution $\rho(r)$ (also known as the electron distribution, charge distribution, electron density or charge density) is an observable scalar field defined in real three dimensional space. It determines the distribution of any one of the electrons as determined by an average over the motions of the remaining electrons. The electron density can be determined both experimentally from x-ray crystallography (Stewart 1979, Lau et al 1986) and theoretically. In this work theoretical charge densities obtained from single determinant state functions are analyzed. Since the Roothaan-Hartree Fock SCF procedure is used, $\rho(r)$ can be expressed as

$$\rho(r) = \Sigma_i \lambda_i \phi_i(x)\phi_i(x) \qquad [1.1.10]$$

where λ_i is the electron occupation number of the i^{th} real Hartree-Fock spin orbital $\phi_i(x)$. The series of computer programs collectively known as PROAIM operates on $\rho(r)$ generated from equation [1.1.10] (Biegler-König et al 1982).

1.2 TOPOLOGY OF MOLECULAR ELECTRONIC CHARGE DISTRIBUTIONS

Having defined the charge density of interest for this work, $\rho(\mathbf{r})$, it is essential to describe the topological features of this distribution. Figure 1.2.1 displays contour plots of the charge density of formaldehyde in the molecular plane, a plane perpendicular to this containing C and O, and a plane perpendicular to the CO bond axis containing the CO bond critical point. The contour lines connect points of equal charge density. Figure 1.2.2 displays the corresponding relief plots. The figures show that maxima in ρ occur only at the position of the nuclei and that saddle points in ρ are found between C and O and C and H. To concisely and quantitatively summarize these observations, a critical point analysis is performed (Table 1.2.1).

A critical point of $\rho(\mathbf{r})$ is a point where the associated gradient vector $\nabla\rho(\mathbf{r})$ vanishes. A critical point is classified according to its rank and signature, written as (rank, signature). The rank of a critical point at $\mathbf{r}_c$ equals the number of nonzero eigenvalues (principal curvatures) of the Hessian matrix A where

$$A_{ij} = (\partial^2\rho/(\partial r_i \partial r_j))_{\mathbf{r}=\mathbf{r}_c} \qquad [1.2.1]$$

is a real symmetric matrix which can be diagonalized. Associated with the principal curvatures are the corresponding principal axes (the eigenvectors λ_1, λ_2 and λ_3). The signature is the sum of the signs of the eigenvalues.

In the charge distributions studied in the present work, only critical points of rank 3 are found. They are of four types: (3,-3), (3,-1), (3,+1) or (3,+3). Nuclear positions behave topologically as (3,-3) critical points (local maxima) in ρ (Bader and Nguyen-Dang 1981).

The two negative eigenvectors (λ_1 and λ_2) associated with the negative eigenvalues of a (3,-1) critical point define a surface in which the critical point is a local maximum. The eigenvector (λ_3) associated with the positive eigenvalue defines a unique axis along which ρ increases for motion away from the critical point most rapidly, the value of $\rho(r_c)$ being the local minimum along this axis. The saddle-like nature of this critical point is displayed in Figure 1.2.1 (a) and (b) where the critical point on the carbon oxygen internuclear axis is viewed in a plane defined by the eigenvectors associated with λ_3 and either one of λ_1 or λ_2. Figure 1.2.1 (c) illustrates that in the plane defined by the eigenvectors associated with the negative eigenvalues a (3,-1) critical point is a local maximum. The molecular structure hypothesis (vide infra) states that two atoms are bonded if a (3,-1) critical point exists between them. Thus, C and O are bonded as are C and H and the (3,-1) critical point is termed a bond critical point.

The values of $\rho(r_c)$ are given in Table 1.2.1. There is a total of three bond critical points in formaldehyde. The value of the charge density evaluated at any of these bond critical points is a positive value which gives a measure of the degree of accumulation of electronic charge between the given nuclei. It is a general observation that

increasing strength through a similar series of bonds is reflected in a corresponding increase in the amount of charge density at the bond critical point. The values of ρ_b have been used to define a bond order relationship for CC, CO, CN and OO bonds (Bader et al 1983, Kraka 1984) and NN bonds in the present work (Chapter 4).

In a bond with cylindrical symmetry such as CO or HF (Figure 1.2.3) the two negative curvatures of ρ at the bond critical point (λ_1 and λ_2) are of equal magnitude. However, if electronic charge is preferentially accumulated in a given plane along the bond path (as it is for a bond with π-character, the CO bond in H_2CO for example) then the rate of falloff in ρ from its maximum value $\rho(r_a)$ in the interatomic surface is less along the axis lying in this plane than along the one perpendicular to it, and the magnitude of the corresponding curvature of ρ is smaller. If λ_2 is taken to be the value of the smallest curvature, then the ellipticity of the bond

$$\epsilon = (\lambda_1/\lambda_2 - 1) \qquad [1.2.2]$$

provides a measure of the extent to which charge is preferentially accumulated in a given plane. The axis of the softer curvature (λ_2), the major axis, determines the relative orientation of this plane within a molecule. The CO bond in H_2CO has a substantial ellipticity with ϵ = 0.058 reflecting the π-character of the bond (Table 1.2.1). The concepts of σ and π-electron populations and atomic quadrupole moments (given in Section 1.5) also describe quantitatively preferential accumulation of charge in a given plane.

A (3,+1) critical point is called a ring critical point because it only exists in ring structures such as cyclopropane. The

eigenvectors associated with the two positive eigenvalues generate an infinite set of gradient paths which originate at the critical point and which define the ring surface. The remaining eigenvector generates a pair of gradient paths which terminate at the critical point and define a unique axis perpendicular to the ring surface at the critical point. The value of ρ at a ring critical point is necessarily smaller than the value of ρ evaluated at the surrounding bond critical points (Table 1.2.1).

A (3,+3) critical point, a local minimum in $\rho(\mathbf{r})$, is called a cage critical point because it exists only in molecules possessing cage structures such as tetrahedral N_4 (Table 1.2.1). The eigenvectors associated with it generate an infinity of gradient paths which originate at the critical point. Cage and ring critical points are found only in a few of the charge distributions analyzed in this work.

To gain more understanding of critical points and their properties, and to define the elements of molecular structure, it is instructive to examine the gradient vector field of the charge density (Figure 1.2.4). Each orthogonal trajectory or gradient path of ρ is a line of steepest ascent through the scalar field $\rho(\mathbf{r})$. The gradient path is the integral curve of the differential equation

$$d\mathbf{r}(s)/ds = \nabla\rho(\mathbf{r}(s)) \qquad [1.2.3]$$

for some initial value $\mathbf{r}(0) = \mathbf{r}_o$. Thus the points $\mathbf{r}(s)$ of the gradient path through $\mathbf{r}_o$ are given by

$$\mathbf{r}(s) = \mathbf{r}_o + \int_o^s \nabla\rho(\mathbf{r}(t))dt \qquad [1.2.4]$$

Each and every such path starts and finishes at a critical point or at infinity. The starting point is called the α-limit set

$$\alpha(r_0) = \lim_{s \to -\infty} r(s) \qquad [1.2.5]$$

and the terminus is the ω-limit set

$$\omega(r_0) = \lim_{s \to +\infty} r(s) \qquad [1.2.6]$$

The α-limit set is termed the repellor and the ω-limit set is termed the attractor of the path (Bader et al 1981).

A (3,-3) critical point is the ω-limit set of all paths starting from and contained in some neighbourhood of the critical point. It is an attractor of $\nabla\rho$. Thus, nuclei act as the attractors of the gradient vector field of $\rho(r)$. The largest neighbourhood containing trajectories such that any trajectory originating in it terminates at a nucleus is called a basin. An atom, free or bound, is defined topologically as the union of an attractor and its associated basin.

Alternatively, the atom can be defined in terms of its boundary. The basin of a single nucleus in an isolated atom spans the entire three dimensional space R^3. For an atom in a molecule the atomic basin is a subset of R^3. This atom is separated from neighbouring atoms by interatomic surfaces. The existence of an interatomic surface S_{AB} implies the presence of a (3,-1) critical point. The surface S_{AB} consists of all gradient paths which terminate at the (3,-1) critical point. It is generated by the two eigenvectors associated with λ_1 and λ_2. The atomic surface S_A of an atom A is defined as the boundary of the basin. In general this boundary is the union of a number of interatomic surfaces, separating two neighbouring basins, and some portions which may be infinitely distant from the attractor. The interatomic surfaces and the surfaces found at infinity

are the only surfaces S of R^3 which satisfy the equation

$$\nabla\rho(\mathbf{r})\cdot\mathbf{n}(\mathbf{r}) = 0 \quad \text{for every } \mathbf{r}\in S \qquad [1.2.7]$$

where n is the unit vector outward normal to the surface at r. A surface satisfying the zero flux condition (equation [1.2.7]) is called a zero flux surface. An atom, isolated or bound, is a region of real space containing a single nucleus and bounded by a zero flux surface. The zero flux surfaces displayed in Figure 1.2.4 represent the intersection of the atomic surfaces with the given plane.

Also shown in Figure 1.2.4 is a pair of gradient paths in a given plane which originates at a (3,-1) critical point and terminates at neighbouring nuclei. These gradient paths are generated by λ_3 and they define a line through the charge distribution along which $\rho(\mathbf{r})$ is a maximum with respect to any lateral displacement. This line is termed an atomic interaction line. For a molecular system at an equilibrium geometry this line can be further classified as a bond path. Since only equilibrium geometries are examined in this work, exclusive use of the term bond path will be made. Two atoms are bonded to each other if a bond path connects the two atoms. Since a bond exists between two atoms if and only if a bond path, and hence a (3,-1) critical point, exist between them, a (3,-1) critical point is called a bond critical point and its coordinates are denoted $\mathbf{r}_b$.

The length of the bond path R_b between atoms A and B is always $\geq$ the corresponding straight-line geometrical internuclear separation R_e (Table 1.2.1). The difference is greatest for electron-rich and electron-deficient molecules which possess curved bonds. The bond path angle α_b, the limiting value of the angle subtended at a nucleus by two

bond paths, when compared to the corresponding geometrical angle α_o (bond angle), is important in quantifying the idea of bond strain (Wiberg et al 1987a). In general, $\Delta\alpha = \alpha_b - \alpha_o$ gives a measure of the degree of relaxation of the charge density away from the geometrical constraints imposed by the nuclear framework. In Chapter 4, a study of NN complexes, large values of $\Delta\alpha$ are observed and these concepts are discussed in more detail.

The network of bond paths linking pairs of nuclei is called the molecular graph of the system (Figure 1.2.5). A molecular graph summarizes which atoms are bonded to one another, i.e. the molecular structure. In many instances the molecular graph is in agreement with chemical expectations. It is important to note that only one bond path links two bonded atoms. The C and O nuclei in H_2CO are linked by one bond path; "double bonds" do not appear in ρ as two lines linking C and O; only a single path is observed.

The concept of molecular structure is different from that of molecular geometry. A molecular structure is a representation of which atoms are bonded to one another in a molecule. It is a generic property. A molecular geometry gives the internuclear distances and angles in the molecule. Geometry is a non-generic property since any infinitesimal change in a set of nuclear coordinates results in a different geometry. The molecular geometry may be varied without changing the molecular structure but the converse is not true. All molecular geometries having the same molecular structure belong to the same structure region. The mechanisms of structural change, as described using catastrophe theory, have been reviewed by Bader et al

(1981).

The final columns in Table 1.2.1 list the atomic bonded and nonbonded radii values. The distances of the carbon and oxygen nuclei to their common bond critical point in H_2CO are called the bonded radii r_C and r_O. The bonded radii values are useful when studying a homologous series of molecules and the shift in bond critical point toward an atom may be related to the electronegativity of that atom (Section 1.6).

A nonbonded radius r_A^o is the distance of a nucleus from a chosen contour of the nonbonded charge density. The outer charge density contour, of value 0.001 au, is used in the determination of nonbonded radii as this yields molecular sizes and atomic diameters in good agreement with gas phase van der Waals radii (Bader and Preston 1970). A large value for r_A^o implies a large diffuse region of nonbonded charge distribution. In Figure 1.2.3, this is seen to be most evident in the carbon of CO. In general, atomic first moments (Section 1.5) also increase with increasing nonbonded radius. Nonbonded and bonded radii values are needed to quantify the concept of mutual penetration of two isolated reactants to form a complex. Mutual penetration is described in the hydrogen bond work (Chapter 2).

The notion of defining the shape of the molecule has been extensively studied (Bader et al 1987a). In the theory of atoms in molecules, molecular shape does not mean the arrangement of nuclei in three dimensional space. Nor is the shape given by the intersection of spherical van der Waals surfaces. Rather the shape is given by the 0.001 au charge density envelope (Figure 1.2.6). The volume enclosed

by the envelope is termed the molecular volume v_M. Each atom in a molecule has an atomic volume $v(\Omega)$ and $\Sigma_\Omega v(\Omega) = v_M$ (Section 1.5).

The topology of a molecular charge distribution yields a unified theory of molecular structure, one that defines atoms, bonds, structure and the mechanisms of structural change. However, the topology of ρ does not give any evidence of a shell structure in an atom or of maxima in ρ corresponding to bonded or nonbonded pairs of electrons as is anticipated on the basis of the Lewis model or the model of localized electron pairs - models important in the understanding of chemical reactivity and molecular geometry. These models are recovered in the properties and topology of the Laplacian of ρ.

Figure 1.2.1

Contour plots of the electron density in three planes of the formaldehyde molecule H_2CO. (a) The plane containing the nuclei. Nuclear positions are denoted by + signs. (b) The plane perpendicular to the above and containing the carbon-oxygen internuclear axis. (c) The plane perpendicular to the carbon-oxygen internuclear axis at its bond critical point. The outermost contour of ρ has a value of 0.001 au and the contours then increase in steps of 2×10^{n}, 4×10^{n}, and 8×10^{n} with n beginning at -3 and increasing in steps of unity. This set of contour values is used throughout the thesis unless otherwise noted. In (a) and (b) zero-flux surfaces and bond critical points (black dots) are included. The charge densities have been generated from statefunctions calculated using the RHF/6-311++G**//6-31G** scheme.

a

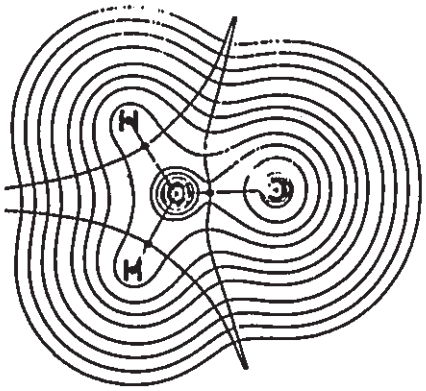

b

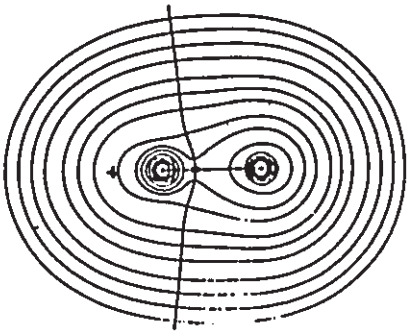

c

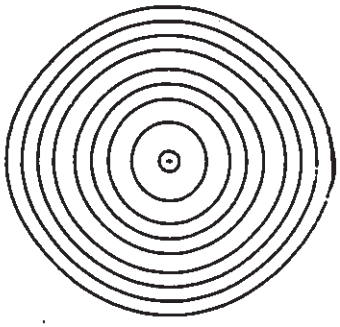

Figure 1.2.2

Relief plots in the three planes of the formaldehyde molecule H_2CO considered in Figure 1.2.1.

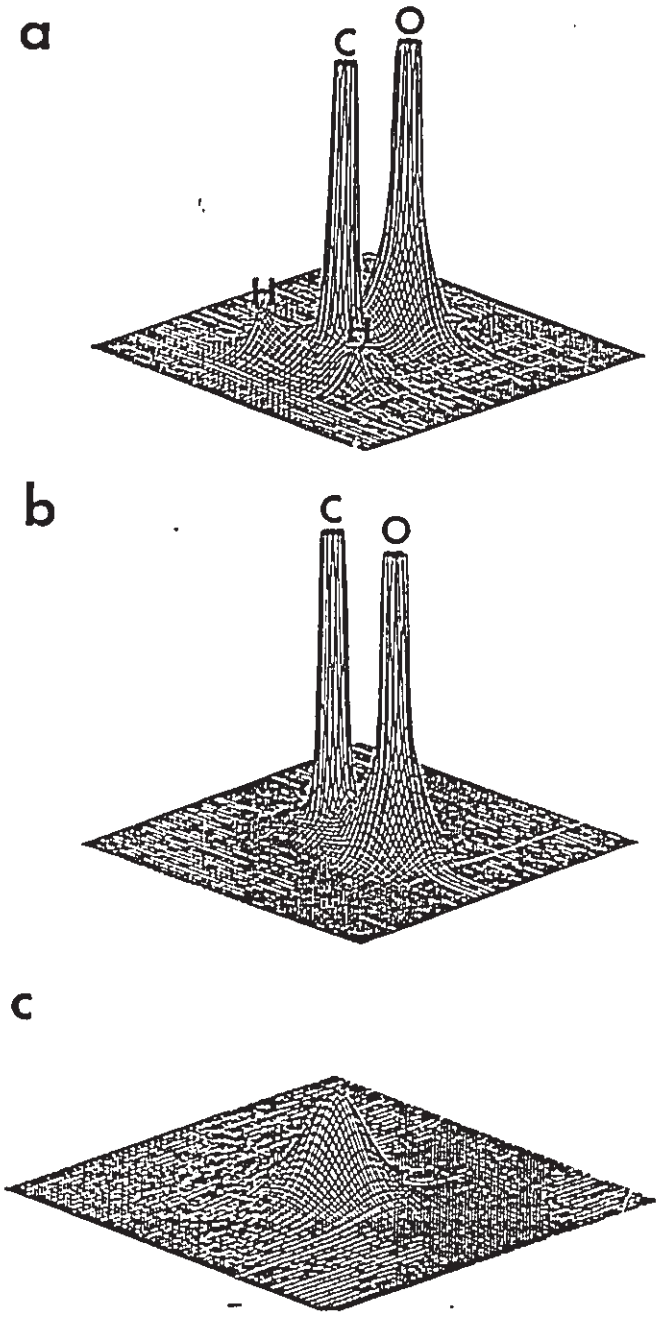
a
C
O
H
H
b
C
O
c

Figure 1.2.3

Contour maps of the charge distributions of hydrogen fluoride and carbon monoxide are presented. Included are zero flux surfaces and bond critical points (black dots).

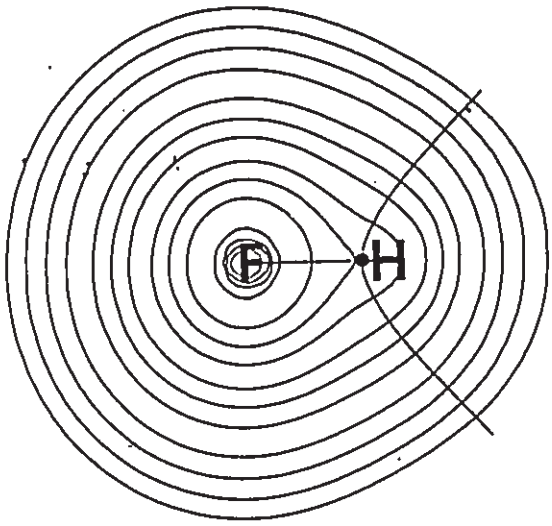
F
H

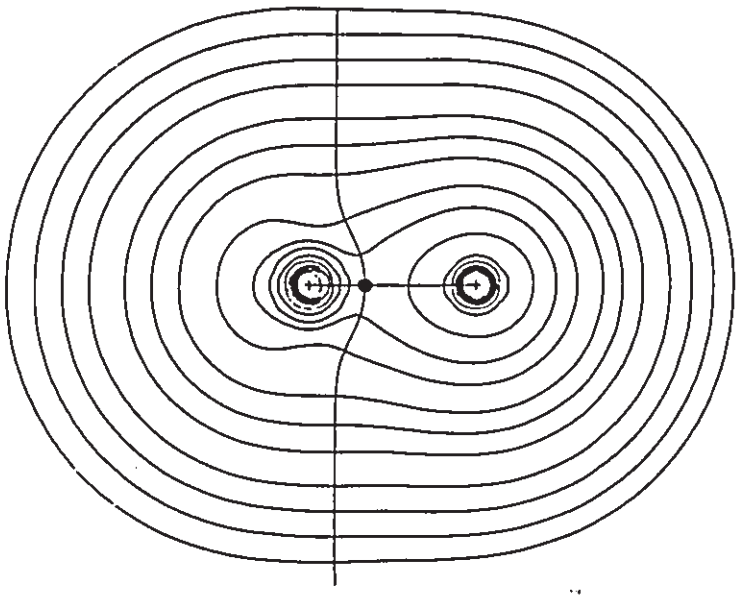

Figure 1.2.4

(a) A map of the gradient vector field of the charge density for the plane containing the nuclei of the formaldehyde molecule superimposed on the charge density contours of formaldehyde. Included are zero flux surfaces (bold lines), bond paths and bond critical points (black dots). Each line represents a trajectory of $\nabla\rho$.

(b) A map of the gradient vector field of the charge density for the plane containing the nuclei of the trans-N_2H_2 molecule. Included are zero flux surfaces, bond paths and bond critical points (black dots). Each line represents a trajectory of $\nabla\rho$.

a

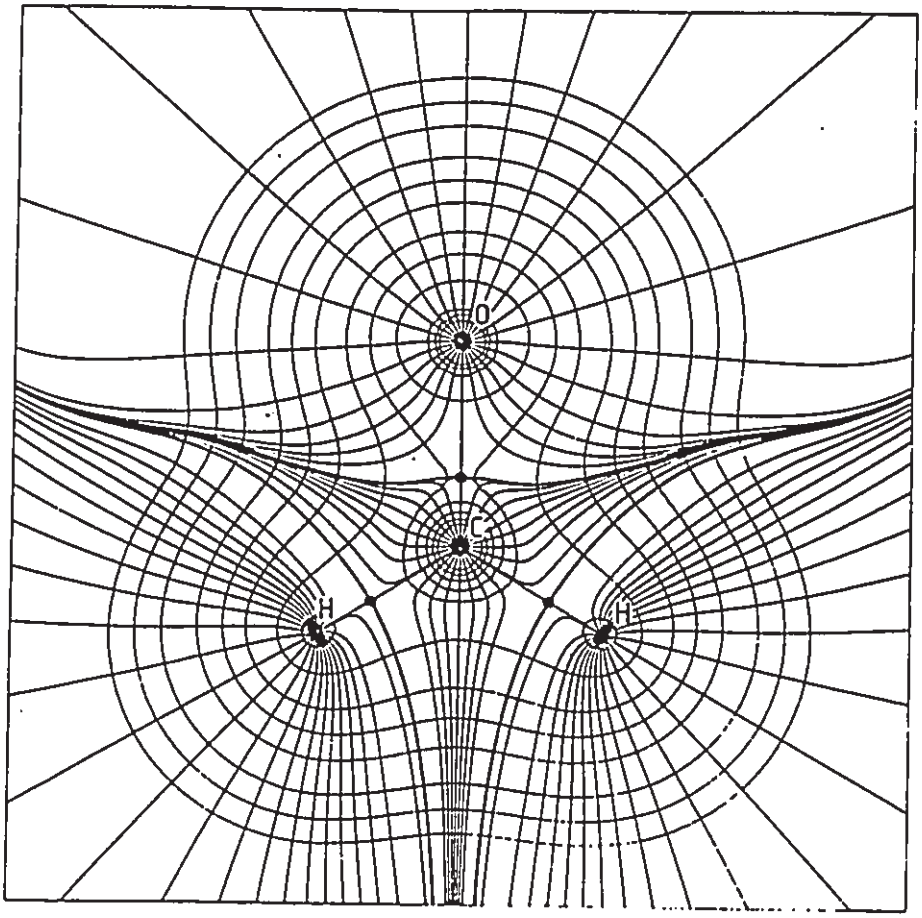

b

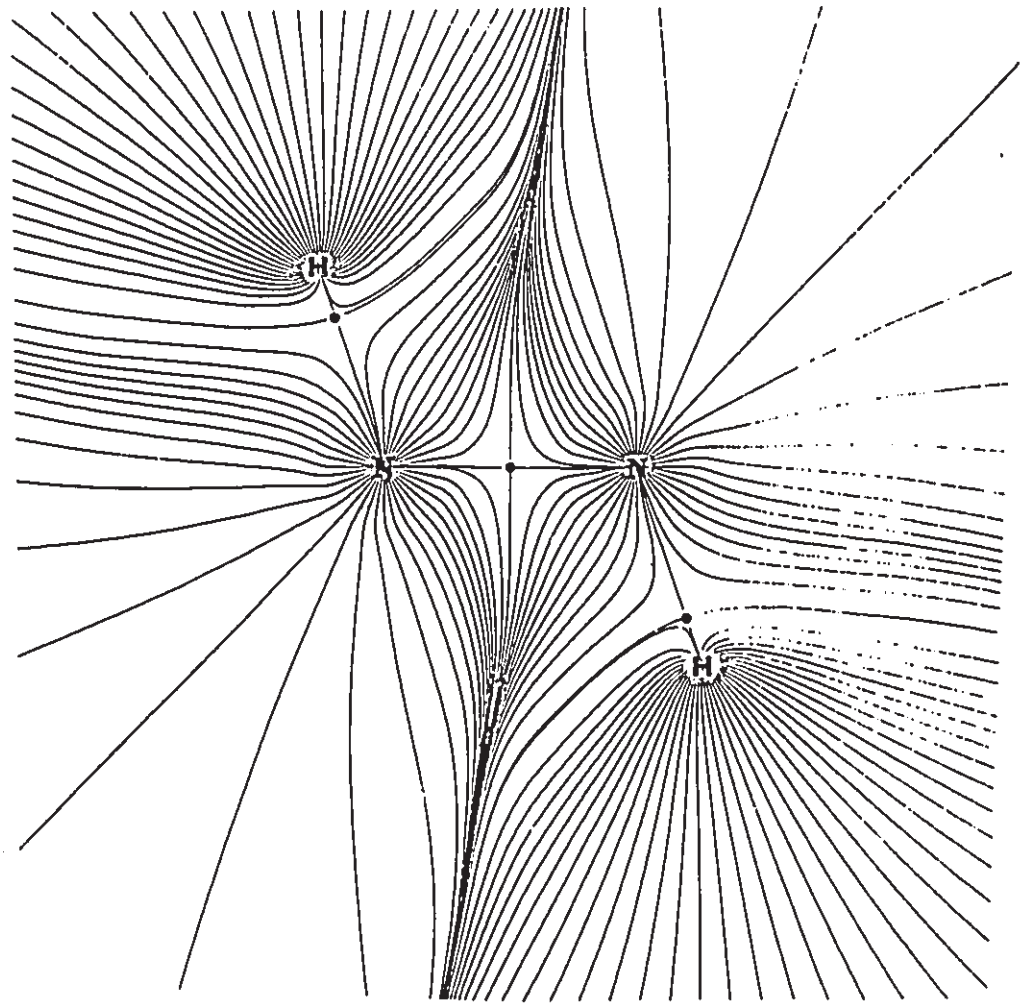

Figure 1.2.5

Molecular graphs of H_2CO and other second- and third-row molecules of interest in this thesis are presented. Black dots denote bond critical points. Values of $q(\Omega)$, the net charge of atom Ω, and directions of the atomic first moment $\mu(\Omega)$ (shown as arrows drawn to scale) are given.

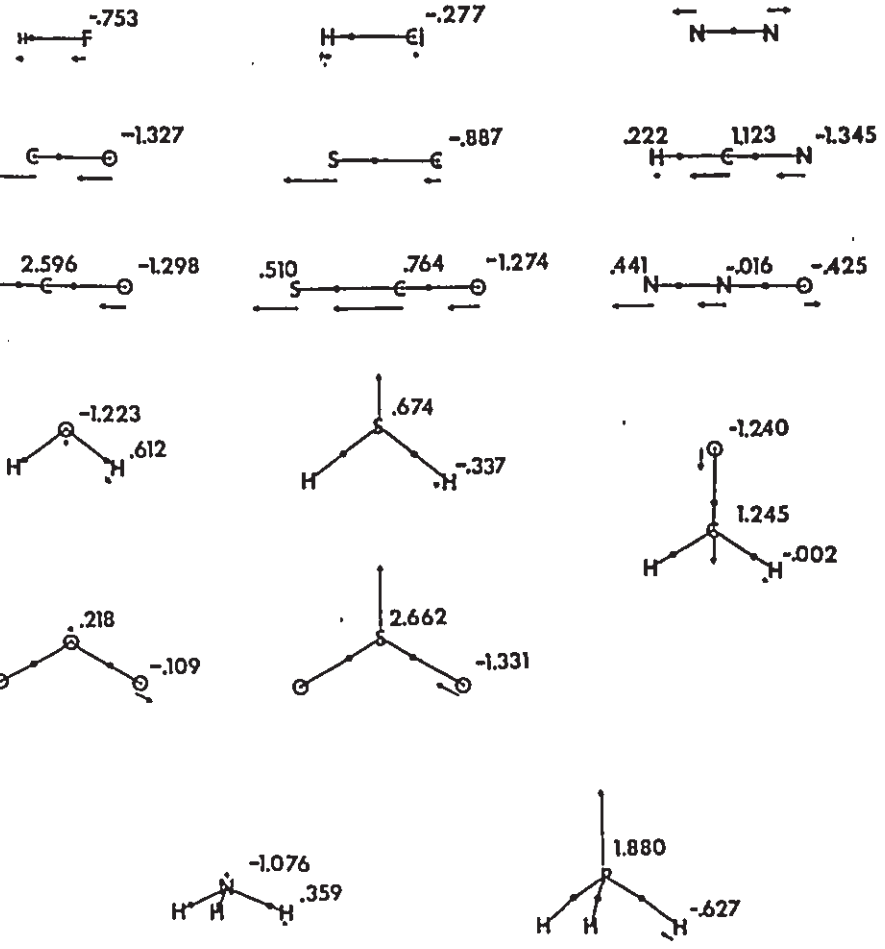
-.753
H F
-.277
H Cl
N N
-1.327
C O
-.887
S C
.222 1.123 -1.345
H C N
2.596 -1.298
C O
.510 .764 -1.274
S C O
.441 -.016 -.425
N N O
-1.223
H H .612
.674
H H -.337
-1.240
1.245
H H -.002
.218
-.109
2.662
-1.331
-1.076
H H H .359
1.880
H H H -.627

Figure 1.2.6

The 0.001 au charge density envelopes, i.e. the molecular shapes, of some hydrocarbon molecules are presented: a) CH_4 b) C_2H_6 c) C_3H_8 d) C_4H_{10} e) C_5H_{12} f) C_6H_{14} g) iso-C_4H_{10} h) neo-C_5H_{12} i) C_3H_6 j) C_4H_8 k) C_6H_{12} l) bicyclo[1.1.0]butane m) [1.1.1]propellane. The intersection of the zero flux interatomic surfaces with these envelopes are readily drawn in by eye to yield the methyl and methylene groups. The formaldehyde molecule (labelled n) is included at the bottom of the figure.

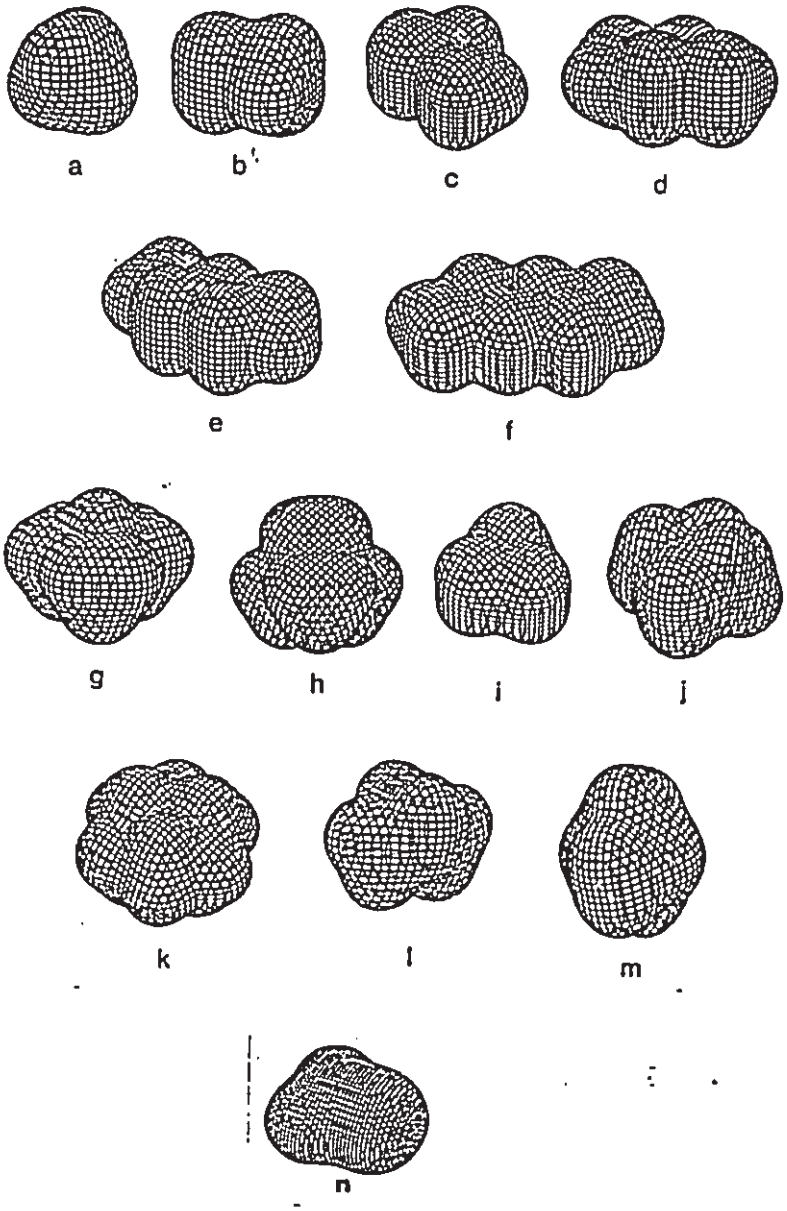
a
b
c
d
e
f
g
h
i
j
k
l
m
n

Table 1.2.1. Critical Point Properties for H_2CO, CO, HF, C_3H_8 and N_4.[a]

System	Bond AB	R_a	R_b	$\rho(r_c)$	λ_1	λ_2	λ_3	$\nabla^2\rho(r_c)$	ϵ
H_2CO	CO	2.2382	2.2382	0.4308	-1.2499	-1.1815	2.8808	0.4593	0.0580
	CH	2.0661	2.0662	0.2925	-0.7881	-0.7813	0.4592	-1.1103	0.0087
CO	CO	2.1047	2.1047	0.5069	-1.8323	-1.8323	4.6441	0.8796	0.0000
HF	FH	1.7018	1.7018	0.3923	-2.8052	-2.8052	2.2409	-3.3695	0.0000
C_3H_8	CC	2.8289	2.8449	0.2478	-0.4807	-0.3172	0.2575	-0.5404	0.5154
	CH	2.0334	2.0336	0.2894	-0.7501	-0.7267	0.4193	-1.0575	0.0322
	ring			0.2049	-0.3821	0.2326	0.2326	0.0831	
N_4	NN	2.6360	2.6632	0.3385	-0.6641	-0.6374	0.7690	-0.5324	0.0419
	ring			0.2609	-0.3621	0.5171	0.5171	0.6721	
	cage			0.2398	0.3493	0.3493	0.3493	1.0478	

System	Bond AB	r_A	r_B	r_A^o	r_B^o
H_2CO	CO	0.7427	1.4955		3.42
	CH	1.3257	0.7405		2.60
CO	CO	0.7081	1.3966	3.78	3.28
HF	FH	1.4441	0.2576	3.18	2.04
C_3H_8	CC	1.4182	1.4182		
	CH	1.2786	0.7548		2.56
	ring				
N_4	NN	1.3220	1.3220	3.50	3.50
	ring				
	cage				

[a] All values are in au. The charge densities are calculated using the RHF/6-311++G**//6-31G** scheme.

1.3. TOPOLOGY OF THE LAPLACIAN OF THE ELECTRON CHARGE DENSITY

The Laplacian of ρ is defined by the equation

$$\nabla^2\rho(\mathbf{r}) = \partial^2\rho/\partial x^2 + \partial^2\rho/\partial y^2 + \partial^2\rho/\partial z^2 \qquad [1.3.1]$$

It is the sum of the three principal curvatures of the Hessian of ρ. It determines where electronic charge is locally concentrated and depleted (Bader 1989, Bader et al 1988, Bader and MacDougall 1985, Bader and Essén 1984, Bader et al 1984). From the definition of a second derivative one finds that $\rho(\mathbf{r})$ is greater than the average of its values over an infinitesimal sphere centered on $\mathbf{r}$ when $\nabla^2\rho(\mathbf{r}) < 0$ and less than this average when $\nabla^2\rho(\mathbf{r}) > 0$. Thus a local maximum (minimum) in $-\nabla^2\rho$ signifies a local concentration (depletion) of electronic charge. The Laplacian of ρ, a scalar field, occurs throughout the theory of atoms in molecules multiplied by $-\hbar^2/4m$, that is, as an energy density (Bader and Nguyen-Dang 1981).

In general the maxima in $-\nabla^2\rho$ duplicate in number and in kind the nonbonded electron pairs of the Lewis model (1916) and the VSEPR model of geometry (Gillespie 1972). However, the Laplacian is a property of the total system and not a model. Its values provide a quantitative measure of the local charge concentrations as well as fixing their number and positions. The extrema in $\nabla^2\rho$ are found by locating their critical points, points where $\nabla(\nabla^2\rho) = 0$. A maximum in the $-\nabla^2\rho$ field, a (3,-3) critical point, denotes the presence of a region of local charge concentration. A minimum in the $-\nabla^2\rho$ field, a (3,+3) critical point, denotes the presence of a region of local charge

depletion.

The Laplacian recovers the shell model of electronic structure in an atom by displaying a corresponding number of alternating shells of charge concentration and charge depletion beginning with a region of charge concentration at the nucleus. Within the outer or valence shell of charge concentration (VSCC), an isolated atom exhibits a uniform sphere over which the valence electronic charge is maximally concentrated. The curvature of $-\nabla^2\rho$ normal to the surface of this sphere, the radial curvature, is negative. The two remaining curvatures, those tangential to the surface, are equal to zero. Upon chemical combination this surface will, in general, persist (the derivative of $-\nabla^2\rho$ normal to the surface is still zero and the corresponding curvature is negative), but the surface is no longer one of uniform concentration as the tangential curvatures assume either positive or negative values. This distortion causes the formation of regions of local charge concentration and charge depletion.

Figure 1.3.1 serves as an example of the above features of $\nabla^2\rho$. Contour plots of $\nabla^2\rho$ for formaldehyde in the molecular plane and a perpendicular plane along the CO axis are displayed along with corresponding relief plots. In the molecular plane there are two equivalent oxygen nonbonded maxima which are large in magnitude and serve as sites of electrophilic attack (by H in HF for example). In the perpendicular plane there are regions of charge depletion which are large in magnitude in the carbon valence shell and serve as sites of nucleophilic attack (by OH^- for example).

In addition to nonbonded maxima in the VSCC of O in H_2CO, there

also exist bonded maxima between C and O and C and H (Figure 1.3.1). Bonded maxima, in general, are smaller in magnitude and more tightly bound since they are shared between two nuclei. In H_2CO, for example, the nonbonded O maxima have a value of 7.10 au while the bonded maxima adjacent to O and C respectively in the C-O bond have values of only 3.12 and 1.57 au (ρ is calculated using the RHF/6-31G**//6-31G** scheme in this section).

The maximum in the VSCC of an atom increase in magnitude and decrease in distance from the nucleus on traversing a row of the periodic table from left to right. The average distances for C, N, O, and F are 0.50, 0.42, 0.36 and 0.30Å and 0.76 0.68, 0.62Å respectively for P, S, and Cl (Carroll et al 1988).

The alignment of a maximum in $-\nabla^2\rho$ with a region of charge depletion may be discussed using the local virial theorem which shows that it corresponds to the combination of a region of excess potential energy with a region of excess kinetic energy (Bader and MacDougall 1985, Bader and Essén 1984). The local virial theorem is given (in au) by

$$(1/4)\nabla^2\rho(\mathbf{r}) = V(\mathbf{r}) + 2G(\mathbf{r}) \qquad [1.3.2]$$

where $V(\mathbf{r})$ is the potential energy density and $G(\mathbf{r})$ is the kinetic energy density. Since the integral of the Laplacian vanishes over an atom Ω as well as over the the total system (Section 1.5), one obtains the virial theorem

$$V(\Omega) + 2T(\Omega) = 0 \qquad [1.3.3]$$

upon integration over the basin of an atom or over the total system. Since $V(\mathbf{r}) < 0$ and $G(\mathbf{r}) > 0$ for all $\mathbf{r}$, equation [1.3.2] states that the

lowering of the potential energy dominates the total energy in regions where electronic charge density is concentrated, where $\nabla^2\rho < 0$, and the kinetic energy is dominant in regions where electronic charge density is depleted, where $\nabla^2\rho > 0$. The reaction of an acid with a base or an electrophile with a nucleophile is therefore the reaction of a region of excess kinetic energy with one of excess potential energy to yield a system where the virial theorem is again satisfied.

The reactive surface of a molecule is defined as the $\nabla^2\rho = 0.0$ au envelope. Inside (outside) this envelope, charge is concentrated (depleted). These surfaces are displayed for isolated KrF^+ and HCN in Figure 1.3.2. The VSCC envelope for Kr is but a belt of charge concentration. This arrangement exposes the Kr core (the inner spherical shell of charge concentration) to the approaching nitrogen.

Figure 1.3.1

Left hand side: Contour plots of $\nabla^2\rho$ for the molecular plane of formaldehyde (top) and a plane perpendicular to this and along the C-O axis. The dashed (solid) lines denote regions of charge concentration (depletion). The Laplacian is also negative within the region bounded by the innermost solid contour enclosing each C and O nucleus. The top diagram shows the positions of the three bonded charge concentrations in the VSCC of carbon and the single bonded and two nonbonded concentrations in the valence shell of oxygen. The zero flux surfaces and bond critical points (black dots) are also shown. The bottom diagram shows the two critical points (indicated by solid triangles) which determine the sites of nucleophilic attack at carbon. Starting at a zero contour, contour values change in steps of $\pm 2\times10^{n}$, $\pm 4\times10^{n}$ and $\pm 8\times10^{n}$ with n beginning at -3 and increasing in steps of unity.

Right hand side: Corresponding relief plots of $\nabla^2\rho$.

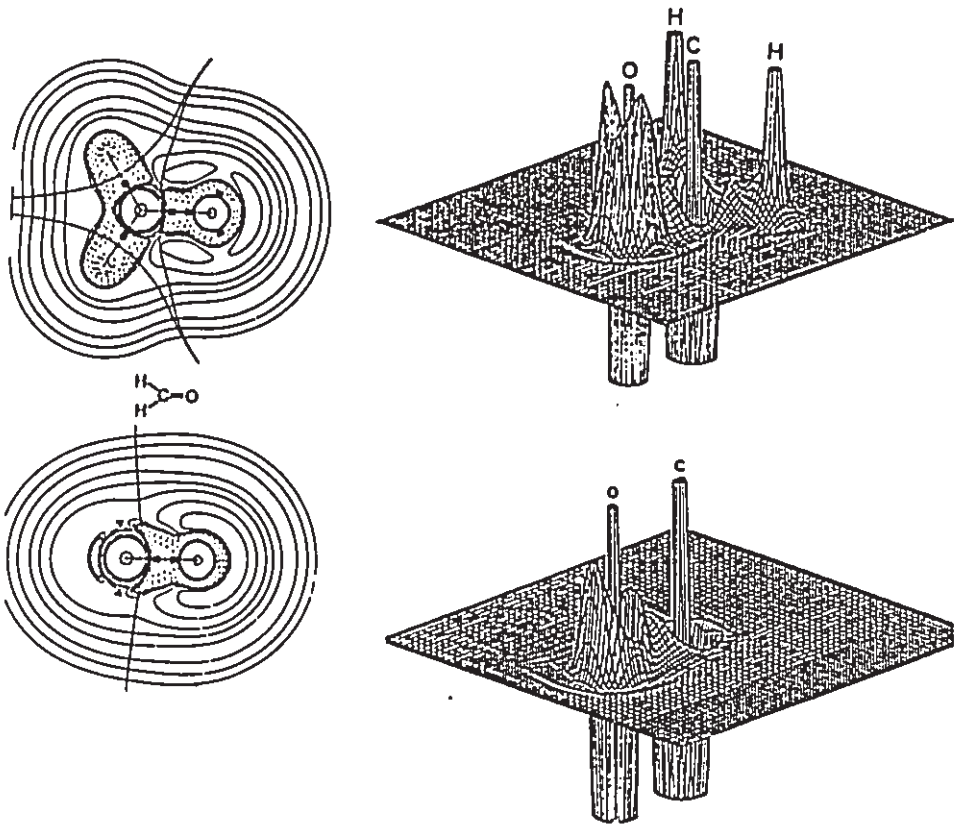
H
C
O
H
O
C

Figure 1.3.2

Reactive surfaces (i.e. zero envelopes of the Laplacian distributions ($\nabla^2\rho = 0$ for all points on the surface)) for isolated KrF^+ and HCN shown aligned for adduct formation and shown to the same scale. The internuclear separation between Kr and N is 5 A (MacDougall et al 1989).

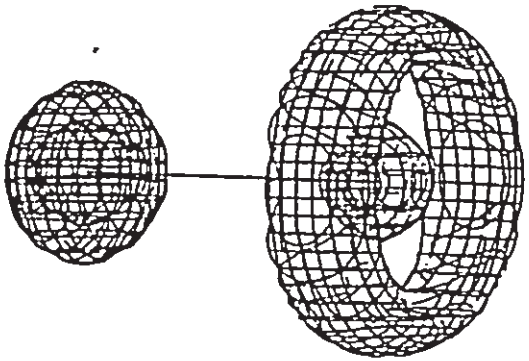
F
Kr

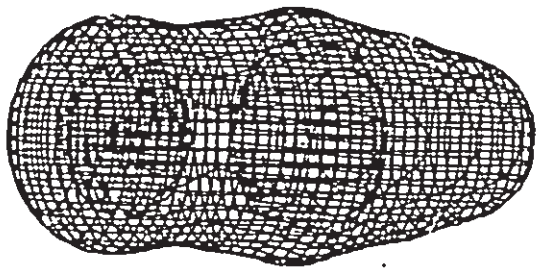
N
C
H

1.4. CHARACTERIZATION OF ATOMIC INTERACTIONS

An understanding of the topology of both the ρ and $\nabla^2\rho$ fields is necessary in the characterization of atomic interactions. The interaction of two atoms leads to the formation of a critical point in ρ. The charge density is a maximum in an interatomic surface at the critical point, and charge is locally concentrated there since the two curvatures of ρ (λ_1 and λ_2) perpendicular to the bond path are negative. The charge density is a local minimum at the critical point along the bond path since the third curvature (λ_3) is positive and charge is locally depleted at r_c with respect to neighbouring points along the bond path. Thus the formation of an interatomic surface and a chemical bond is the result of a competition between the perpendicular contractions of ρ, which lead to a concentration or compression of charge between the nuclei towards and along the bond path, and the parallel expansion of ρ which leads to the separate concentration of charge in the basins of the neighbouring atoms. The sign of $\nabla^2\rho$ at r_c determines which of the two competing effects is dominant. It also determines, through the local expression for the virial theorem, the regions where the potential energy makes its dominant contributions to the lowering of the energy.

When $\nabla^2\rho(r_c) < 0$ the perpendicular contractions in ρ dominate the interaction and the result is a sharing of electronic charge between the nuclei as is typical of covalent or polar covalent bonds (Figure 1.4.1: H_2, B_2, N_2, O_2 and NO). Such behavior is also, for

example, found for the polar F-H, N-H and O-H bonds. Since charge is concentrated between the nuclei along the bond path in these cases, the values of ρ and $|-\nabla^2\rho|$ at a bond critical point are relatively large: $\rho(r_c) = 0.352$ au, $\nabla^2\rho(r_c) = -1.758$ au for N-H in H_3N, $\rho(r_c) = 0.387$ au, $\nabla^2\rho(r_c) = -2.865$ au for O-H in H_2O and $\rho(r_c) = 0.392$ au, $\nabla^2\rho(r_c) = -3.370$ au for F-H in FH (values are from ρ calculated using RHF/6-311++G**//6-31G**; Carroll and Bader 1988). As a consequence of the local form of the virial theorem, equation [1.3.2], the atoms in these molecules are bound because of the lowering of the potential energy associated with the charge concentrated between the nuclei.

When $\nabla^2\rho(r_c) > 0$ the contraction of each atomic density towards its nucleus dominates the interaction, resulting in a depletion of charge at r_c and in the interatomic surface. These interactions are called closed-shell because they represent interactions between closed-shell atoms as found in noble gas repulsive states, ionic bonds and hydrogen bonds. The values of the charge density at a critical point arising from a closed-shell interaction are, in general, at least an order of magnitude smaller than those found in shared interactions. These values are indicative of a relative depletion of charge in the interatomic surface - a consequence of the requirements of the Pauli exclusion principle. In a closed-shell interaction there is little shared concentration of charge. Instead, the charge concentrations and the corresponding regions of excess potential energy are separately localized in the basins of the neighbouring atoms. Since these charge concentrations can be polarized into the nonbonded or bonded regions of the basins of the individual atoms, closed-shell

interactions can give rise to unbound or bound states respectively (Figure 1.4.1: unbound: He_2, Ar_2; bound: KF, LiCl and NaCl).

The Laplacian map for Ar_2 shows that more electronic charge is concentrated on the nonbonded than on the bonded side of each argon atom. Charge is depleted from the internuclear region to a greater extent than it is from the nonbonded region of each nucleus. Thus the net forces on the nuclei are repulsive in agreement with the unbound nature of Ar_2.

A subset of closed-shell interactions which are bound are ionic interactions. For an ionic diatomic molecule to achieve electrostatic equilibrium the charge distributions of both the anion and cation must be polarized in a direction counter to the direction of electron transfer. The cationic nucleus is attracted by the net negative field of the anion and the charge distribution of the cation must polarize away from the anion to balance this attractive force. The anionic nucleus is repelled by the net positive field of the cation and the charge distribution of the anion must polarize towards the cation to balance this repulsive force. These features are displayed in the Laplacian distribution of KF, LiCl and NaCl (Figure 1.4.1).

Figure 1.4.1

a) Contour maps of $\nabla^2\rho$ for molecules with shared and closed-shell interactions.

b) Relief maps of $\nabla^2\rho$ for N_2 and Ar_2.

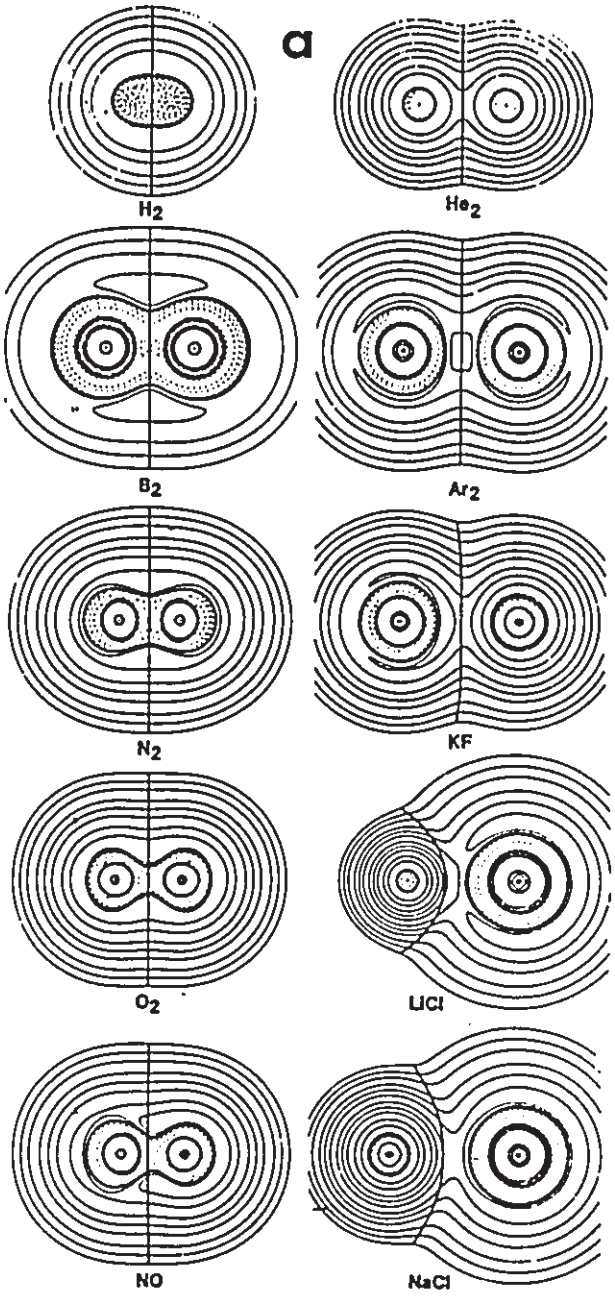
a
H_2
He_2
B_2
Ar_2
N_2
KF
O_2
LiCl
NO
NaCl

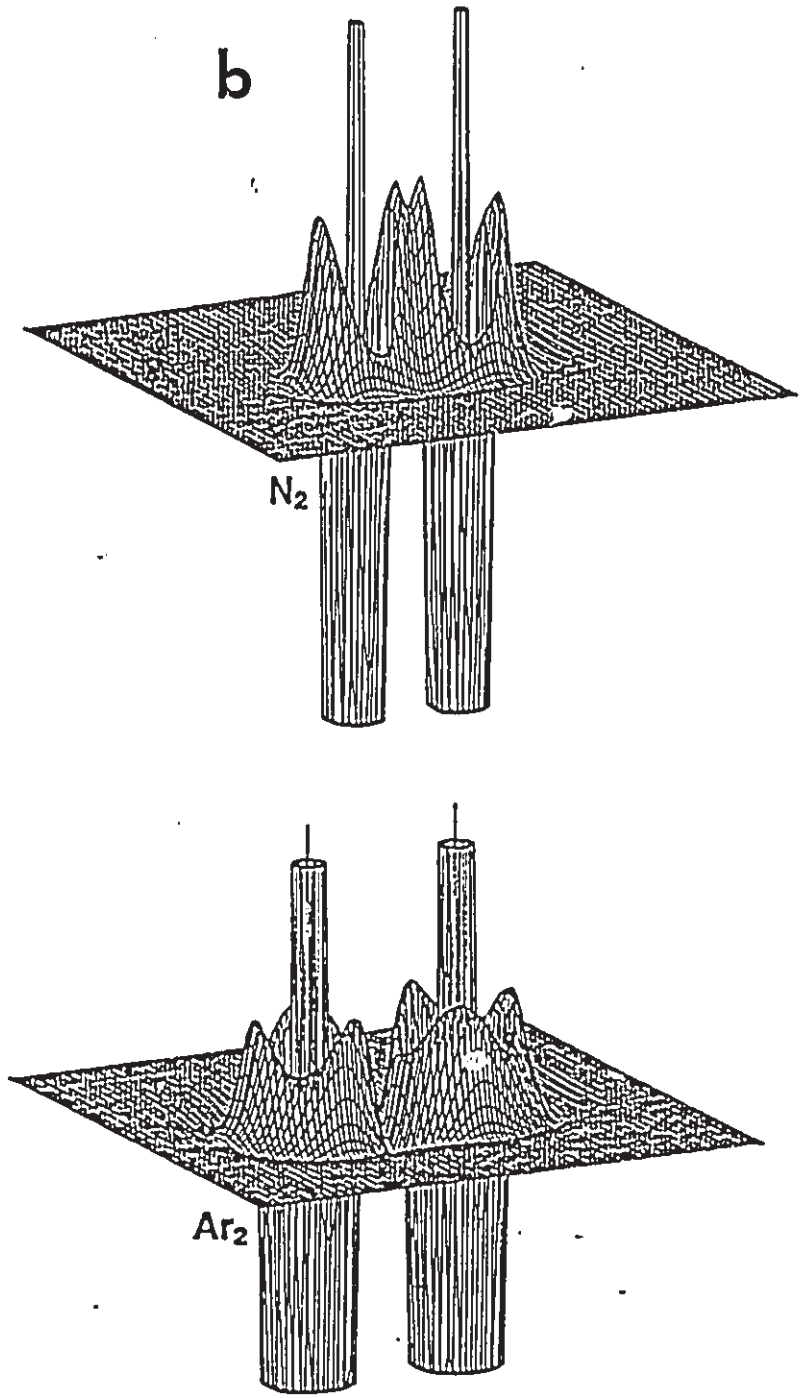
b
N_2
Ar_2

1.5 THE QUANTUM MECHANICS OF ATOMS IN MOLECULES

The quantum mechanical basis for the definition of an atom in a molecule and its properties has been developed by Bader and co-workers (Bader 1988, Bader 1985, Bader and Nguyen-Dang 1981). Though we are concerned with the stationary state only, it is important to note that the theory of atoms in molecules is completely general and holds for the time-dependent case also (Bader and Nguyen-Dang 1981).

The theory of atoms in molecules extends quantum mechanics to subdomains. This theory is based upon a generalization of quantum mechanics to a subsystem of a total system, a generalization that is possible only if the subsystem is bounded by a surface through which the flux in the gradient vector field of the charge density is zero,

$$\nabla\rho(\mathbf{r})\cdot\mathbf{n}(\mathbf{r}) = 0 \quad \text{for all points on the surface.} \qquad [1.5.1]$$

The operational statement of this theory for a subsystem Ω is the variational statement of the Heisenberg equation of motion for the observable G. For a stationary state the corresponding statement is a variational expression for the hypervirial theorem

$$\delta E[G\phi,\Omega] = -(\epsilon/2)\{(i/\hbar)\langle\phi[H,G]\phi\rangle_\Omega + \text{complex conjugate}\}/\langle\phi,\phi\rangle_\Omega \qquad [1.5.2]$$

The quantity $\delta E[G\phi,\Omega]$ is the subsystem projection of the variation in the total energy of the system as caused by the action of the generator of an infinitesimal (ϵ) change, $-(i\epsilon/\hbar)G$, on the state function ϕ. In general, because of the topology of molecular charge distributions, the zero flux boundary condition leads to a disjoint partitioning of the

space of a molecule into a set of subsystems each of which contains a single nucleus - a partitioning into atoms. The average value of every observable, together with its Heisenberg equation of motion is defined for every atom Ω in a molecule and the average value of a property M for the total system is given by the sum of the atomic averages M(Ω),

$$\langle M \rangle = \Sigma_\Omega M(\Omega) \qquad [1.5.3]$$

The atomic statement of the hypervirial theorem as given in equation [1.5.2] yields a variational derivation of all the theorems derived from the Heisenberg equation of motion, including the virial and Ehrenfest theorems. The atomic virial theorem is obtained by setting the operator $\hat{G}$ equal to $\hat{\mathbf{r}}\cdot\hat{\mathbf{p}}$ and is of a form identical to that for a total system, namely

$$2T(\Omega) = - V(\Omega) \qquad [1.5.4]$$

This theorem defines the kinetic energy T(Ω) and potential energy V(Ω) of the electrons in Ω. Both of these quantities are determined by the quantum mechanical stress tensor which is a functional of the one-electron density matrix and both are therefore, expressible as corresponding densities which can be integrated over the basin of an atom. The total energy of atom Ω, which also obeys the requirements of the virial theorem, is

$$E(\Omega) = T(\Omega) + V(\Omega) = - T(\Omega) = (1/2)V(\Omega) \qquad [1.5.5]$$

Atomic Properties

An atomic property is determined by integrating the corresponding property density over the basin of an atom Ω. For example, the average electron population of an atom, N(Ω), is found by

integrating the electron density over the basin of an atom:

$$N(\Omega) = \int_\Omega dr\rho(r) \qquad [1.5.6]$$

The net charge $q(\Omega)$ is given by

$$q(\Omega) = Z_\Omega - N(\Omega) \qquad [1.5.7]$$

where Z_Ω is the nuclear charge. Values of $N(\Omega)$ and $q(\Omega)$ for H_2CO are given in Table 1.5.1. The quantity $|\Sigma N(\Omega) - N(\text{molecule})|$ gives a measure of the numerical integration error and is zero, to three decimal places, for H_2CO. In all calculations done in this work, this value never exceeds 0.001 electrons.

Where orbitals of pure σ and pure π symmetry can be distinguished, the quantities $N_\sigma(\Omega)$ and $N_\pi(\Omega)$ can be determined:

$$N_\sigma(\Omega) = \int_\Omega dr\rho_\sigma(r)$$

$$N_\pi(\Omega) = \int_\Omega dr\rho_\pi(r) \qquad [1.5.8]$$

Intraatomic polarizations of electron density from σ density to π density are reflected in these results (Chapter 2).

The quantities $N_\alpha(\Omega)$ and $N_\beta(\Omega)$ are important in the description of electron correlation and density functional theory (Chapter 5). The population of electrons with spin α in atom Ω is given by

$$N_\alpha(\Omega) = \int_\Omega dr\rho_\alpha(r) \qquad [1.5.8]$$

where $\rho_\alpha(r)$ is the α-spin (or spin-up) electron density. For a closed-shell system $\rho_\alpha(r) = \rho_\beta(r)$ and, hence $N_\alpha(\Omega) = N_\beta(\Omega)$.

There have been other attempts to determine the electron population of an atom in a molecule. The population analysis scheme, based on basis set partitioning, developed by Mulliken (1955) is still the most popular method. It is interesting that in 1971 Mulliken said that owing to the inconsistent and unsatisfactory results of this

admittedly arbitrary scheme, it would be desirable to compute atomic charges directly from the molecular electronic charge distribution. This would be accomplished by integrating ρ over regions associated with the individual atoms (Politzer and Mulliken 1971). At about the same time Bader and co-workers were just beginning their work on the zero flux surface (Bader and Beddall 1972). Why the theory of atoms in molecules was not embraced by the chemical community at that time is puzzling but even more puzzling is that almost twenty years after Mulliken's denunciation of his population method, chemists are continuing to use it.

The first moment (or atomic dipole) of atom Ω, denoted $\mu(\Omega)$, is the atomic average of the electronic position vector $r_\Omega = r - X_\Omega$ where X_Ω is the position vector of the nucleus of atom Ω measured from an origin. Thus,

$$\mu(\Omega) = -\int_\Omega r_\Omega \rho(r)dr \qquad [1.5.10]$$

The cartesian components of $\mu(\Omega)$ are calculated as follows:

$$\mu_x(\Omega) = -\int_\Omega x_\Omega \rho(r)dr$$

$$\mu_y(\Omega) = -\int_\Omega y_\Omega \rho(r)dr$$

$$\mu_z(\Omega) = -\int_\Omega z_\Omega \rho(r)dr \qquad [1.5.11]$$

The atomic first moment measures the distortion of the charge density of Ω from sphericity. It quantitatively describes to what extent the charge density is polarized in a given direction.

The dipole moment of a neutral molecule, μ, may be expressed as a sum over the net charge $q(\Omega)$ and first moment $\mu(\Omega)$ of every atom in the molecule as

$$\mu = \Sigma_\Omega[q(\Omega)X_\Omega + \mu(\Omega)] \qquad [1.5.12]$$

where X_Ω is the position vector of the nucleus of atom Ω measured from some arbitrary origin. While the individual atomic contributions $q(\Omega)X_\Omega$ depend upon the choice of origin, their sum does not, and thus each molecular dipole moment is uniquely determined by a charge transfer contribution arising from the net charge on the atoms

$$\mu_c = \Sigma_\Omega q(\Omega)X_\Omega \qquad [1.5.13]$$

and a first moment contribution arising from the polarization of the atomic charge densities

$$\mu_a = \Sigma_\Omega \mu(\Omega) \qquad [1.5.14]$$

Hydrocarbon and diatomic molecular dipole moments will be discussed in the following sections.

The components of the traceless symmetric quadrupole moment tenscr Q for atom Ω are given as follows:

$$Q_{xx}(\Omega) = - \int_\Omega (3x^2 - r_\Omega^2)\rho(r)dr$$

$$Q_{xy}(\Omega) = - \int_\Omega (3xy)\rho(r)dr$$

$$Q_{xz}(\Omega) = - \int_\Omega (3xz)\rho(r)dr$$

$$Q_{yy}(\Omega) = - \int_\Omega (3y^2 - r_\Omega^2)\rho(r)dr$$

$$Q_{yz}(\Omega) = - \int_\Omega (3yz)\rho(r)dr$$

$$Q_{zz}(\Omega) = - \int_\Omega (3z^2 - r_\Omega^2)\rho(r)dr \qquad [1.5.15]$$

Q can always be diagonalized, and so, we examine $Q_{xx}(\Omega)$, $Q_{yy}(\Omega)$ and $Q_{zz}(\Omega)$. These components reflect the preferential accumulation of charge in a given plane. For a spherical distribution, $Q_{xx}(\Omega) = Q_{yy}(\Omega) = Q_{zz}(\Omega) = 0$. Each of these diagonal elements has the form of a d_z^2 orbital. If the sphere is flattened at its poles to yield an oblate spheroid, then (with the polar axis along z) $Q_{zz}(\Omega) > 0$ and $Q_{xx}(\Omega) = Q_{yy}(\Omega) = -(1/2)Q_{zz}(\Omega)$. If $Q_{zz}(\Omega) > 0$ for a linear molecule, electron

density is removed from the internuclear axis and concentrated in a torus like distribution about that axis. The quadrupole moment is the density complement of an orbital π population. The changes in quadrupole moments upon hydrogen bond formation are described in Chapter 2.

To discuss the local single-particle kinetic energy densities, it is first necessary to describe the first-order density matrix $\Gamma^{(1)}(r',r)$. This matrix can be written in the form

$$\Gamma^{(1)}(r',r) = n\int\Psi^*(r_1',r_2',r_3',\ldots,r_n')\Psi(r_1,r_2,r_3,\ldots,r_n)dr_2\ldots dr_n. \qquad [1.5.16]$$

The diagonal elements yield the charge density:

$$\Gamma^{(1)}(r',r)_{r'=r} = \rho(r) \qquad [1.5.17]$$

$K(r)$, termed the "Schrodinger kinetic energy density" is given by

$$K(r) = (-1/4)\{(\nabla^2 + \nabla'^2)\Gamma^{(1)}(r,r')\}_{r=r'} \qquad [1.5.18]$$

and $G(r)$, termed the "gradient kinetic energy density" is given by

$$G(r) = (1/2)\{\nabla\cdot\nabla'\Gamma^{(1)}(r,r')\}_{r=r'} \qquad [1.5.19]$$

The difference between these two values is the Lagrangian density $L(r)$:

$$L(r) = K(r) - G(r) = (-1/4)\nabla^2\rho(r) \qquad [1.5.20]$$

As a consequence of the zero flux condition of the atomic surface, when the above equation is integrated over an atom in a molecule, $L(r)$ vanishes,

$$\int_\Omega dr\nabla^2\rho(r) = \oint dS_\Omega(r)\nabla\rho(r)\cdot n(r) = 0 \qquad [1.5.21]$$

and $K(\Omega) = G(\Omega)$. Thus, the average kinetic energy of an atom is uniquely defined:

$$T(\Omega) = K(\Omega) = \int_\Omega drK(r) = G(\Omega) = \int_\Omega drG(r) \qquad [1.5.22]$$

For single-determinantal statefunctions, G(Ω) and K(Ω) may be written as sums over functions of orbitals, that is,

$$G(\Omega) = (1/2)\int_\Omega(\Sigma_i\lambda_i\nabla\phi_i\cdot\nabla\phi_i)dr \text{ and} \qquad [1.5.23]$$

$$K(\Omega) = (-1/2)\int_\Omega(\Sigma_i\lambda_i\phi_i\nabla^2\phi_i)dr \qquad [1.5.24]$$

and this is the manner in which PROAIM calculates these values. Theoretically, they should be equal but since numerical approximation methods are used in PROAIM, they differ slightly and L(Ω), though small, is not equal to zero. The L(Ω) value has been used as a criterion by which the quality of the integration over the given atom is based. If $L(\Omega) < 1\times10^{-4}$, a "good" integration is observed. Otherwise, the atom must be reintegrated using a larger number of points for the gaussian quadrature.

The total energy of an atom in a molecule, the atomic energy E(Ω) is obtained using the virial relationship, that is

$$E(\Omega) = -T(\Omega) = (1/2)V(\Omega) \qquad [1.5.25]$$

Practically speaking, this equation is not exactly satisfied for a finite basis set calculation (6-31G** for example). The ratio -V/T differs slightly from the correct value of two for an equilibrium geometry. To correct for the error in the virial, each atomic kinetic energy must be multiplied by the factor (V/T + 1) to obtain a set of atomic energies that correctly sum to the total energy of the molecule. In formaldehyde, we see that the quantity $|\Sigma E(\Omega) - E_{SCF}|$ is 0.01 kcal mol^{-1}. For the molecules studied in this thesis, this error will rarely be larger than 1 kcal mol^{-1}.

In Chapter 2, V(Ω) is broken down as follows:

$$V(\Omega) = V_A(\Omega) + V_R(\Omega) \qquad [1.5.26]$$

where the quantity, $V_A(\Omega)$, the total attractive potential energy, is the interaction of all the nuclei in the system with the charge density of Ω and $V_R(\Omega)$ is the total repulsive potential energy. Explicitly,

$$V_A(\Omega) = - \int_\Omega (\Sigma_\alpha (Z_\alpha / r_\alpha)) \rho(r) dr. \qquad [1.5.27]$$

Further,

$$V_R(\Omega) = V_{ee}(\Omega) + V_{NN}(\Omega) \qquad [1.5.28]$$

where $V_{ee}(\Omega)$ is the repulsive electron-electron contribution to the potential energy and $V_{NN}(\Omega)$ is the repulsive nuclear-nuclear contribution to the potential energy. Also of interest is $V_\Omega(\Omega)$ which is the potential energy of interaction of the charge density within the basin of Ω with its own nucleus, that is,

$$V_\Omega(\Omega) = - \int_\Omega (Z_\Omega / r_\Omega). \qquad [1.5.29]$$

Since the virial theorem is not exactly satisfied, the potential energies must be corrected. This is accomplished by multiplying the above potential energy values by the term $2(1+V/T)/(V/T)$.

Discussion of the atomic properties associated with atomic localization are deferred to Chapter 5 in which the relationships between density functional theory and the theory of atoms in molecules are examined.

An atomic surface is the union of a number of interatomic surfaces, one such surface for each bonded neighbour, and if the atom is not an interior atom, some portions which may be infinitely distant from the nucleus. The latter open portions of the atomic surface are replaced by a particular density envelope in the calculation of an atomic volume. An atomic volume is defined to be a measure of the region of real space enclosed by the intersection of the atomic surface

of zero flux and a particular envelope of the charge density:

$$v(\Omega) = \int_{\Omega} dr \qquad [1.5.30]$$

The 0.001 au charge density envelope is chosen because it has previously been shown that the 0.001 au charge density contour for methane and the inert gases gives good agreement with the equilibrium diameters of these molecules as determined by second virial coefficient or viscosity data fitted with a Lennard-Jones 6-12 potential (Bader and Preston 1970). Further, the 0.001 au density envelope contains at least 96% of the electronic charge (Bader et al 1987a).

The shapes of some hydrocarbon molecules, the 0.001 au charge density envelopes, are displayed in Figure 1.2.6 and contour maps are displayed in Figure 1.5.1. The lengths, widths and atomic volumes have been calculated (Bader et al 1987a). What is to be stressed here is that the volumes of methyl and methylene groups in normal hydrocarbons are transferable, as are their charge distributions, populations, dipoles and energies (Bader et al 1987a,b) (Table 1.5.2).

Additivity and Transferability of Functional Group Properties

All of the average properties of an atom, isolated or in a molecule, are defined by quantum mechanics. The average value of an observable M for the total system is given by the sum of the corresponding atomic averages M(Ω)

$$\langle M \rangle = \Sigma_{\Omega} M(\Omega) \qquad [1.5.31]$$

For example, the molecular volume v_M is obtained by summing the volumes of the constituent atoms v(Ω). Similarly, the volume of a methyl group is obtained by summing the volumes of the one carbon and three

hydrogens comprising this group. Such a group is bounded by a surface of zero flux in the gradient vector of the charge density and is a quantum subsytem with well defined properties.

The theory of atoms in molecules determines to what extent atomic properties are transferable between molecules. Atoms are the most transferable pieces of a system defined in R^3 and therefore they maximize the transfer of information between systems. The constancy in the average values of an atom's observables is found to be directly determined by the constancy in its distribution of charge as found in different systems. When the distribution of charge over an atom or some functional group of atoms is the same in the real space of two different systems, then it makes the same contribution to the value of the total property in both systems. If the form of an atom changes slightly or greatly, its energy and other properties change by corresponding amounts. Examples of near perfect transferability of atoms and functional groups of atoms have been given (Bader et al 1987a,b, Bader 1986, Wiberg et al 1987a, Bader and Nguyen-Dang 1981). Functional group properties of the methyl and methylene groups of some normal alkanes, $CH_3(CH_2)_mCH_3$, starting with m = 0, are given in Table 1.5.2.

The experimentally determined heats of formation of these molecules obey a group additivity scheme (Domalski and Hearing 1988, Benson 1968, Allen 1959, Franklin 1949, Prosen et al 1946). Fixed values are assigned to the methyl and methylene groups and the experimental value is fitted to the expression 2A + mB where A and B are the methyl and methylene contributions respectively. The change in

H_T on going from 298 to zero Kelvin, the zero point energies and the correlation energy corrections are well represented by group equivalents (Schulman and Disch 1985, Wiberg 1984). What is exciting from the theoretical point of view, is that energies calculated for the vibrationless molecules at zero Kelvin may also be fitted to the expression E = 2A + mB with errors less than experimental. Here, A = -39.61912 au which is half the energy of ethane (RHF/6-31G**//6-31G* results: Table 1.5.2) and B = -39.03779 ± 0.00014 au which is the energy increment per methylene group.

Hydrogen is slightly more electronegative than carbon in saturated hydrocarbons. This is also the case in the diatomic molecule CH (Section 1.6). The order of the group electron withdrawing ability in hydrocarbon molecules without geometric strain is H > CH_3 > CH_2 > CH > C. The population and energy of the methyl group are constant when it is bonded to a methylene group (within the accuracy of the numerical integrations). Thus, the methyl group is the same in all of the members past ethane. This transferable methyl group is more stable relative to methyl in ethane by an amount ΔE = -10.5 ± 0.5 kcal mol^{-1} and its electron population is greater by an amount ΔN = 0.018 ± 0.001 electrons. The electrons and stability gained by the methyl group are taken from the methylene group. The energy gained by methyl is equal to the energy lost by methylene and this accounts for the additivity observed in this series. Table 1.5.2 lists the energies of the methylene groups relative to the energy increment B above. In propane, where methylene is bonded to two methyls, the energy of the methylene group is B - $2\Delta E$ and its charge is $+2\Delta N$ where the values of ΔE and ΔN

have been given above in this paragraph. In butane, each methylene is bonded to a single methyl and their energies are given by B - ΔE and their charges by +ΔN. The corresponding methylene groups in pentane and hexane, those bonded to a single methyl, have the same properties as the methylene group in butane. This implies that the central methylenes in these molecules, those bonded only to other methylenes, shoud have an energy equal to B and a zero net charge and this is the case (Table 1.5.2). In other words, the charge transfer to methyl is damped by a single methylene. The major reason that additivity is observed in these molecules is that the change in energy for a change in population $\Delta E/\Delta N$ is the same for both the methyl and methylene groups. The small amount of charge shifted from methylene to methyl makes the same contribution to the total energy (Bader et al 1987 a,b).

We have alluded to the correlation energies of these hydrocarbons and how their group contributions are additive. Indeed, correlation energies exhibit constant values for the transferable methyl group and the two kinds of transferable methylene groups. In Chapter 5, a correlation energy functional developed by Langreth and Mehl (1983), denoted ϵ, is shown to give the best overall results when compared to experiment for atoms and molecules. This expression is a complicated functional of the charge density involving gradient corrections. The important point is that this functional depends on the charge density, and so, if the forms of a methyl or methylene group, for example, remain unchanged in two different molecules, then so do their correlation energies (Table 1.5.2). Unfortunately, ϵ is still not of chemical accuracy but once an accurate functional is

found, the theory of atoms in molecules will allow the determination of the total energies of the groups responsible for the additivity schemes and total energies of large molecules will be predicted using groups and properties defined by the theory (see Chapter 5).

The study of the molar volumes of these molecules provided the earliest example of the additivity of group properties (Kopp 1855). This scheme works only if the molar volumes of the functional groups are nearly transferable within the homologous series. As Table 1.5.2 shows, indeed this is the case. The molar volume of the methyl group in ethane is slightly larger than that of the methyl groups in the remaining members whose volumes vary by only ±0.02 au from their average value. The volume of the methylene group bonded to two methyls in propane is slightly greater than the volumes of the methylene bonded to one methyl in butane, pentane and hexane, their volumes varying by ±0.02 au from their average value. The methylene groups bonded only to other methylenes, as found in pentane and hexane, have similar values for their volumes. The small differences between the latter two kinds of methylene groups are displayed in Figure 1.5.1. The charge density of the methylene bonded to one methyl is less compressed than the charge density of the methylene bonded only to other methylenes and this is expressed in the larger volume of the former.

Experimentally, the CH_2 group makes an additive contribution of 22.0 cm^3 to the molar volume of a hydrocarbon at its boiling point (Glasstone 1946). The calculated molar volume of the transferable methylene group, corrected to take into account the free volume between

molecules (Marcus 1977), is 21.9 cm^3, in good agreement with experiment.

The behavior of the group dipoles parallels that of the energy and the electron population. The magnitude of the methyl group moment is unique for ethane but nearly constant for the remaining members of the series. The methylene groups give two transferable values, one for methylene attached to a single methyl and the other for a methylene attached only to other methylenes. This latter value is smaller because the charge density of this kind of methylene is more compressed than that of the former.

In all methyl and methylene groups, the hydrogens form the negative end of the group dipole. As was the case with the magnitudes, the directions of these moments are also transferable. The moment of the methyl group is parallel to the bond path linking the neighbouring carbon nucleus to within 0.5° through the series. The direction of the methylene moment, in those cases where it is not dictated by symmetry, lies 0.05° off the axis bisecting the HCH angle in pentane and 1.1° and 1.2° off this axis in butane and hexane respectively. These group moments, along with the group charges, may be used in equation [1.5.12] to calculate the total dipole moment of a hydrocarbon molecule. For propane and pentane, these magnitudes are 0.0237 (0.0236) and 0.0230 (0.0230) au respectively where the SCF moments are enclosed in parantheses. The moments are directed along the twofold symmetry axis bisecting the central HCH angle with the positive end in the direction of the methylene hydrogens in propane and the reverse in pentane. Thus, the total moments are dominated by the moments and charges of the

methyl groups. The SCF moments are 0.0236 and 0.0230 au. The magnitude of the experimental moment for propane is 0.0327 au (Lide 1960). Charge densities calculated using multi-determinantal state functions are needed to improve our agreement with experiment.

For various series of molecules, it has been shown that the electron populations, energies, dipole moments, volumes and correlation energies of functional groups are transferable. What is currently of interest in this laboratory is the possibility of constructing the charge distributions and predicting the properties of large biological molecules, or their relevant portions, from the distributions of the groups that serve as the building blocks for these large systems. Studies on the DNA base pairs, amino acids, high energy phosphates and other biological molecules are in progress.

Figure 1.5.1

Contour maps of the charge density in pentane and hexane including the bond paths and interatomic surfaces. The maps make clear that the union of the interatomic surfaces and the outer density envelope bound an atomic region. The two middle maps are displays of the central methylene group in pentane (lhs) and of one of the two such groups in hexane (rhs) in a plane perpendicular to the plane containing the chain of carbon nuclei as displayed in the upper and lower maps. These two methylene groups possess identical properties and they are interchangeable between the two molecules, as are the methyl groups.

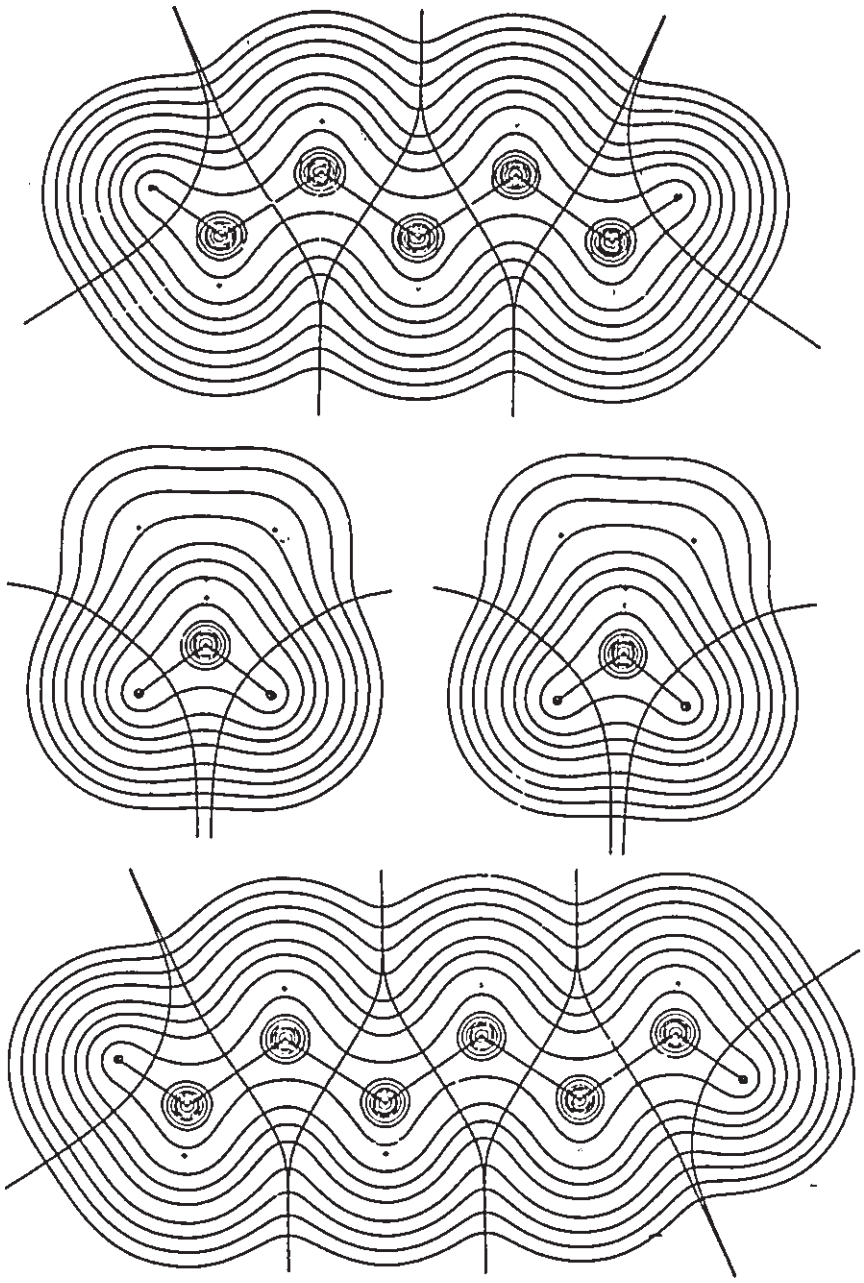

Table 1.5.1. Atomic Properties for H_2CO, CO and HF (RHF/6-311++G**//6-31G**).[a]

System	Ω	N(Ω)	q(Ω)	E(Ω)	v(Ω)	μ(Ω)[b]
H_2CO	O	9.2403	-1.2403	-75.61290	137.74	0.597
	C	4.7547	1.2453	-37.03508	58.71	0.912
	H	1.0025	-0.0025	-0.62749	49.85	0.122
	H	1.0025	-0.0025	-0.62749	49.85	0.122
total		16.0000	0.0000	-113.90296	296.15	
SCF				-113.90298		
CO	O	9.3269	-1.3269	-75.89051	139.47	0.984
	C	4.6731	1.3269	-36.88065	112.74	1.718
total		14.0000	0.0000	-112.77116	252.21	
SCF				-112.77113		
HF	F	9.7527	-0.7527	-99.78607	128.26	0.373
	H	0.2474	0.7526	-0.26725	13.02	0.109
total		10.0001	-0.0001	-100.05332	141.28	
SCF				-100.05336		

[a] All values are in au.
[b] See Figure 1.2.5 for directions of moments.

Table 1.5.2 Group Properties in Hydrocarbons (RHF/6-31G**//6-31G*).

	Methyl Group Properties[a]					Methylene Group Properties[b]									
Molecule	$\Delta N(CH_3)$ (au)	$\Delta E(CH_3)$ (kcal mol^{-1})	$\mu(CH_3)^c$ (au)	ε^d (au)	Molar Volume (cm^3)	$\Delta N(CH_2)$ (au)		$\Delta E(CH_2)$ (kcal mol^{-1})		$\mu(CH_2)^c$ (au)		ε^d (au)		Molar Volume (cm^3)	
Ethane	0.000	0.0	0.253	-0.3456	19.77										
Propane	0.017	-10.9	0.244	-0.3484	19.73	0.037		+21.7		0.307		-0.3180		14.18	
Butane	0.018	-10.8	0.243	-0.3486	19.70	-0.019		+10.8		0.305		-0.3208		14.12	
Pentane	0.017	-9.9	0.249	-0.3486	19.71	-0.019	-0.001	+10.9	0.0	0.310	0.304	-0.3210	-0.3238	14.08	13.98
Hexane	0.018	-9.9	0.245	-0.3485	19.74	-0.020	0.000	+10.6	-1.1	0.306	0.300	-0.3208	-0.3237	14.09	14.03

[a] Differences are relative to methyl group in ethane.

[b] Differences are relative to standard methylene group. The entries beginning with propane are for CH_2 groups bonded to one methyl group. The set beginning with pentane is for CH_2 groups bonded only to other CH_2 groups.

[c] Calculated with carbon nucleus as origin.

[d] Correlation Energy calculated using Langreth and Mehl (1983) density functional.

1.6 THE THEORY OF ATOMS IN MOLECULES APPLIED TO DIATOMIC MOLECULES

In this section, the ground state charge distributions of the second- and third-row hydrides and the second-row homo- and heteronuclear neutral diatomic molecules at their experimental internuclear separations are analyzed using the theory of atoms in molecules. The charge distributions are cylindrically averaged and are constructed from near-Hartree-Fock quality state functions (Cade and Huo 1973, 1974, 1975) using Slater-type functions for the basis set.

The motivation for this study is three-fold: Firstly, the diatomic molecules provide a chemically interesting set for which to explore the topology of ρ and the atomic properties both qualitatively and quantitatively. Secondly, although all the second- and third-row hydrides and second-row homonuclear diatomics have been previously studied, values of their atomic volumes, quadropole moments and correlation energies are presented for the first time in this thesis. Thirdly, results calculated using the theory of atoms in molecules of only about fifty percent of the second-row heteronuclear diatomic molecules have been previously published while in the present work all are considered.

Topology of the Charge Density and Atomic Properties

Figures 1.6.1 - 1.6.5 display contour maps of the charge distributions and Laplacian distributions of the diatomic molecules. There are only two (3,-3) critical points, one for each nucleus in each

diatomic molecule except for C_2 and Li_2 where a non-nuclear maximum is found at the geometric midpoint. Non-nuclear maxima have been found in Li and Na clusters and their properties have been shown to be related to the metallic character of these clusters (Gatti et al 1987, Cao et al 1987). The charge density evaluated at the (3,-3) critical point associated with the nucleus of larger Z is greater in value than the charge density evaluated at the other nucleus for the heteronuclear AB systems. This is apparent in the figures (CF for example in Figure 1.6.5 where the inner contours around F are more contracted than those around C).

There exists only one bond critical point in each of the diatomic charge distributions (with the exception of Li_2 and C_2). Only for the homonuclear diatomic molecules is it located at the geometric midpoint. For the heteronuclear diatomics, it is located nearer to the nuclei of smaller Z and in each hydride series, the bond critical point shifts towards the proton on traversing each period from left to right (Table 1.6.1). Bond paths and zero flux surfaces (which contain the bond critical point) are included in the figures. Molecular systems have been classified in terms of the shape of the zero flux surface (Bader and Beddall 1973) and this scheme is reviewed in conjunction with a necessary discussion of the atomic properties and topological features of the diatomic molecules examined.

Table 1.6.1 lists the experimental bond lengths, the bonded and nonbonded radii, the maximum perpendicular nonbonded radii r_p, the values of ρ and $\nabla^2\rho$ at the bond critical points (denoted, for brevity as ρ_b and $\nabla^2\rho_b$) and the principal curvatures of the Hessian of ρ. The

bonded and nonbonded radii are measured along the axis coincident with the bond path. The nonbonded radii together with r_p give an indication of the size of the molecule. Since the densities are cylindrically averaged, $\lambda_1 = \lambda_2$ and the ellipticity values are zero. It should be noted that the charge distributions for LiBe and BC are calculated using the HF/6-311G*//6-311G* scheme as the Cade and Huo wavefunctions are not available for these molecules and the BC charge distribution is not cylindrically averaged.

Table 1.6.2 lists the net charges, atomic dipoles, atomic quadropoles and atomic volumes. In all cases, the A nucleus is at the origin and the B nucleus is in the positive z direction. A positive value of $\mu(A)$ means that the centroid of negative charge in this atom is directed along the negative z direction. Since ρ is cylindrically averaged, $Q_{xx}(A) = Q_{yy}(A)$ and therefore $Q_{zz}(A) = -2Q_{xx}(A)$.

Table 1.6.3 lists the atomic energies. The difference between E_{SCF} and E(AB) gives a measure of the numerical integration errors encountered in PROAIM. The largest errors occur for the third-row hydrides. The relative energies $E_{rel}(A)$ and $E_{rel}(B)$ are relative to the separated atoms in their ground states (Clementi and Roetti 1974).

Figures 1.6.6 - 1.6.8 summarize the net charges, atomic volumes and relative energies of the atoms in the diatomic molecules in bar graph form. Tables 1.6.1 - 1.6.3 and Figures 1.6.1 - 1.6.8 now are used to discuss each series.

Second- and Third-Row Hydrides

Bader and Beddall (1973) and Bader and Messer (1974) were the

first to examine second- and third-row diatomic hydrides, respectively, using the theory of atoms in molecules. It is appropriate in the present work to outline only the most important features through a summary of the results as the details were thoroughly discussed by these authors. Figures 1.6.1 and 1.6.2 display the contour maps of ρ and $\nabla^2\rho$ for the second- and third-row diatomic hydrides respectively. There are three types of charge distributions which the diatomic hydrides may possess as characterized by the shape of the zero flux surface (denoted S(x)): Class I, Class II and Class III (Table 1.6.4).

A Class I system displays the following features: There is a large extent of electron transfer from one atom to the other and the number of valence electrons of the donor atom is equal to or less than the number of vacancies in the acceptor atom. The donor atom (denoted D) approaches the limiting tight core distribution of the D^+ or D^{2+} cation and S(x) is paraboloid in shape with arms in general curving back to encompass the electropositive atom.

A Class II system is obtained when the number of valence electrons of the donor is greater than the number of vacancies of the acceptor in systems containing no more than ten valence electrons. In such cases, the remaining valence charge density of the donor is strongly polarized into its nonbonded region in the form of a relatively diffuse distribution. Indeed, the nonbonded radii of these atoms are the largest of those in any class. Electron transfer in these systems is reflected in the initial paraboloid nature of S(x) about the bond critical point. However, the diffuse valence density remaining on D extends into the outer reaches of the internuclear

region, causing a reversal in the curvature of the outer arms of S(x).

Class III systems differ from Class II systems only in that the diffuse nonbonded valence density in the donor is present as an equatorial rather than as an axial distribution. MgH($A^2\pi$) obtained from MgH($X^2\Sigma^+$) by a σ to π transition is an example as is BeH($A^2\pi$) (Figure 1.6.9). None of the ground-state hydrides are of Class III.

There are no examples of Class IV systems in the diatomic hydrides. Rather, Class IV systems are found in heteronuclear diatomic molecules with eleven or more valence electrons. The zero flux surface is paraboloid with a very small curvature sloping towards the more electronegative atom.

The zero flux surfaces for the second-row hydrides plotted with respect to a fixed position for the proton are given in Figure 1.6.10. Along with the tables and other figures, this figure concisely shows that electrons are transferred from A to H in LiH, BeH and BH and increasingly from H to A in NH, OH and FH. In CH the transfer of charge is near zero. The sharp transition from Class I to Class II occurs at corresponding members of the second- and third-row hydrides: BeH and MgH. The general characteristics of a Class II system persist until the direction of electron transfer is reversed to H to A. This occurs at NH in the second-row and ClH in the third-row. In both periods, the molecule immediately preceding this change is transitional in its behavior. Thus the number of electrons transferred in CH and SH is very small but still in the direction A to H. However, S(x) for these two molecules are typical of Class I and similar to the following members in each series with electron transfer H to A.

The transition from electron donor to electron acceptor relative to hydrogen occurs two elements to the right in the third-row as compared to the second-row. This is most easily seen in Figure 1.6.6. In the second-row series, q(A) > 0.75 for LiH to BH and then drops sharply at CH. In the third-row, q(A) > 0.78 for NaH to SiH and then drops gradually through PH to a near zero value at SH. In general, the decrease in electronegativity associated with the increased core size in the third-row A atoms is reflected in the q(A) results. Shortly, we will examine electronegativity schemes in more detail.

Figure 1.6.10 shows that the bond critical point progressively shifts towards the proton on going from LiH to FH. While r_H, r^o_H, N(H), and v(H) monotonically decrease, ρ_b increases. Similar conclusions are drawn upon examination of the third-row hydrides and the fourth-row hydrides (Boyd and Edgecombe 1987). The small, tight, hard, positively charged hydrogen in FH will serve as the acidic hydrogen in the BASE-HF studies in the following chapter.

In LiH, more than nine-tenths of an electron are transferred from Li to H. Essentially, lithium approaches a spherical Li^+ cation, and consequently, its nonbonded radius is relatively small compared to the other r^o_A values and its atomic first moment is absolutely small. The other r^o_A values decrease from BeH to FH. The maximum distance out from the A nucleus perpendicular to the AH bond axis is greater than the corresponding distance from the proton with the exception of LiH (Figure 1.6.1). Similar conclusions are drawn for the third-row hydrides except that μ(Na) is larger in magnitude than μ(Li). Not as

many electrons are transferred from Na to H in NaH compared to Li to H in LiH. In NaH, the Na nucleus experiences a net attractive force from the hydrogen and to balance this the remaining charge density in Na is polarized away from the hydrogen. This is quantified by the atomic first moment of NaH (0.018 au; Table 1.6.2). The positive sign means that the centroid of negative charge is positioned in the negative z direction. The proton is repelled by the net positive field of Na and consequently the hydrogen charge density is polarized towards Na (μ(H) = 0.135 au). Of course, H is polarized towards Li in LiH but Li is not polarized significantly owing to the extreme tightness of its charge distribution.

LiH and NaH are examples of closed-shell interactions because ρ_b is relatively small and $\nabla^2\rho_b$ is positive. The systems CH - FH and SH - ClH are examples of shared interactions: ρ_b is relatively large and $\nabla^2\rho_b$ is negative and large in magnitude. The atomic interactions in the molecules BeH - BH and MgH - PH have properties which bridge those of the ionic systems at the closed-shell limit and those of the covalent and polar covalent systems of the shared interactions. In these intermediate systems, the valence charge density remaining on A is strongly polarized into the nonbonded region of the A atom, because of the net negative field exerted on it by the negatively charged hydrogen atom, where it forms a separate region of charge increase (Figures 1.6.1 and 1.6.2). This strong polarization away from the internuclear region is quantified by the largest magnitudes for μ(A) and r_A^o of all the hydrides examined. Another characteristic of these intermediate systems is that the nodal surface in $\nabla^2\rho$ is nearly

coincident with the interatomic surface. These atomic interactions correspond to a relatively hard core of density on A with the remaining valence density of A strongly polarized into its nonbonded region interacting with a softer more polarizable region of charge concentration on the bonded side of the proton dominated by contractions of ρ towards the bond path (Bader and Essén 1984).

In general, for the diatomic hydrides and the AB systems studied in this work, the atom gaining electrons is stabilized and the atom losing electrons is destabilized relative to the separated reactants (Table 1.6.3). We graphically summarize the results (Figure 1.6.8). An extensive treatment of the energy changes accompanying hydride formation has been given by Bader and Beddall (1973) and Bader and Messer (1974).

Like the hydrocarbons in the previous section, the hydrides may be used to illustrate transferability. Figure 1.6.11 displays the charge distributions of BeH and BeH_2. The distributions of charge in H in the two systems is very similar. The degree of constancy in N(H) and E(H) between these systems (Table 1.6.5) is found in spite of the very large differences in the individual forces acting on H in the two molecules. For example, from BeH to BeH_2, the electron nuclear attractive energy of H changes by -228 kcal mol^{-1}. However, the sum of the changes in the electron electron and nuclear nuclear repulsive contributions is of almost equal magnitude and opposite in sign and hence the change in the total virial of H is small (3 kcal mol^{-1}). Thus when the total virial field acting on an atom changes by a small amount, the changes in the atom are correspondingly small. Table 1.6.5

gives a complete list of the changes in populations and energies on going from a diatomic hydride AH to a binary hydride AH_n. Both second- and third-row hydrides are listed. The changes are small in all cases.

While H bonded to a given A has a characteristic set of properties which vary between relatively narrow limits (Table 1.6.5), it is also evident from this table that the properties of H are quite different when bonded with different A. When bonded to Li, Be, B or C, H gains electrons and is more stable than an isolated H atom; when bonded to N, O or F, H loses electrons and is less stable. An examination of the population and energy changes of H in combination with various A provides a quantitative probe of the relative bonding properties of A. In fact, the populations of A in combination with H may be used to predict the populations of A and A′ in combination with each other (Bader and Beddall 1973 and electronegativity subsection below).

The Lithium Series

Since we have already discussed LiH and Li_2, the members of the lithium series now examined are LiBe, LiB, LiC, LiN, LiO and LiF. The following monotonic trends are observed on going from LiBe to LiF: q(Li), ρ_b, $\nabla^2\rho_b$ and $E_{rel}(Li)$ increase; r_{Li}, r_B, r_B^o, r_p, $\mu(B)$, v(A) and v(B) decrease. Of all the diatomic molecules studied in this work, it is in LiF where the greatest percentage of valence electrons are transferred (93.8% from Li to F) and where the smallest atomic volume is observed ($v(Li)_{LiF}$ = 25.4 au).

The large nonbonded radius of Li in LiBe (and consequently, r_p, μ(Li) and V(Li)) arises from the small degree of electron transfer from Li to Be and the subsequent polarization of the remaining Li valence density into lithium's nonbonded region. The large nonbonded radii of Be, B and C in the respective diatomic lithium complexes correlate with the large magnitude of their $Q_{zz}(\Omega)$ values. Upon complex formation, the nonbonded charge density of these atoms is stretched out along the z-axis resulting in a prolate spheroid.

All the members of this series are examples of closed-shell interactions as ρ_b is small and $\nabla^2\rho_b$ is positive. In fact in all polyatomic molecules containing Li-E bonds (where E is any other atom) so far studied using the theory of atoms in molecules, this is the case.

The molecules LiF, LiO and LiH were among the first to be studied in the context of transferability of atoms bounded by zero flux surfaces (Bader and Beddall 1972). In these systems, the distribution of charge in Li is remarkably similar in spite of the very different natures of the atoms to which it is bonded, and thus the values of q(Li) are very similar. The kinetic energy distributions in Li (and hence E(Li)) exhibit a corresponding degree of constancy as that of the Li charge distribution. This is because the Li atom changes in response to the virial of the net force exerted on it and not to changes in the individual contributions (Bader and Nguyen-Dang 1981).

The Remaining Series

The molecules BeB, BeC, BeN, BeO and BeF are considered. The

following trends are observed: q(Be) increases till it reaches a maximum in BeO. In BeF, it is smaller because F has only one vacancy. ρ_b, $\nabla^2\rho_b$, μ(B) and E_{Fel}(Be) also peak at BeO. r_{Be}, r_B, $\overset{o}{r}_{Be}$, v(Be) decrease to BeO and then increase while $\overset{o}{r}_B$, r_p and v(B) monotonically decrease. The value of v(Be) (and $\overset{o}{r}_{Be}$) in BeO is very small owing to the pinch effect common for Class I systems for which Z_B exceeds Z_A by at least three units (Bader et al 1971).

BeB is an example of an interaction intermediate between the shared and closed-shell limits while the heavier members are examples of closed-shell interactions.

From B_2 to BF the values of the nonbonded radius of the atom bonded to boron and r_p monotonically decrease, ρ_b and $\nabla^2\rho_b$ peak at BO, and r_A reaches a minimum at BO. B_2 exhibits the poperties of a shared interaction but the others are closed-shell.

From CN to CF $\nabla^2\rho_b$ and v(C) monotonically increase while $\overset{o}{r}_B$, r_p and v(B) decrease. There has been much controversy over the sign of the CO dipole moment. The experimental dipole moment is O^+C^- but the magnitude is very small. We can account for this small magnitude as follows: There is a charge transfer of 1.3e from C to O. The remaining valence charge density on C is strongly polarized into its nonbonded region (Figure 1.6.5). There are large atomic first moments in both C and O with directions counter to the direction of charge transfer. These moments nullify the charge transfer moment and the resultant dipole moment has a magnitude of 0.108 au (equation 1.5.12). Although $\nabla^2\rho_b$ is positive in CO, the interaction is intermediate between that of shared and closed-shell because the nodal surface in

$\nabla^2\rho$ is nearly coincident with the interatomic surface. CF is the first example of a Class IV system.

From N_2 to NF r_B and $\nabla^2\rho_b$ increase while r_N, r^o_B, r_p, ρ_b and v(B) decrease. These systems are examples of shared interactions and NO and NF are Class IV systems. The partitioning surfaces for all the AB molecules (where A or B = N) plotted with respect to a fixed position for N is given in Figure 1.6.10).

From O_2 to OF, r_O, r_B, $\nabla^2\rho_b$, q(O) and v(O) increase while r^o_O, r^o_B, r_p, ρ_b and v(B) decrease. The partitioning surfaces relative to a fixed position for O are given in Figure 1.6.10.

In F_2, the contraction of ρ towards each nucleus dominates the (closed-shell) interaction. The strong attractive potential field exerted on the valence electrons in F provide the major source of binding in fluorides through an electron transfer to F but also cause the weak binding found in F_2. (Bader and Essen 1984). There is a very pronounced intraatomic correlation in F which limits the interatom exchange and the pairing of electrons between atoms and this is why F_2 is only weakly bound (Carroll et al 1987; Chapter 5).

Electronegativity Schemes

Figure 1.6.6 displays the net charges in the AH and AB systems. Consider a diagonal line sloping downward from left to right from Li_2 to F_2. All the atoms above and to the right of this diagonal will gain electrons from their partner while those below and to the left will lose electrons. Chemists have long been interested in determining the electron withdrawing abilities of the elements. Electronegativity has

been defined as the power of an atom in a molecule to attract electrons to itself (Pauling 1960). Empirical scales based upon thermochemical data of average electronegativities have been developed (Pauling 1960, Allred 1961). These scales show that electronegativity increases from left to right in a given row of the periodic table and decreases from top to bottom in a given group.

The properties of the diatomic hydrides, as found using the theory of atoms in molecules, have been used to create an electronegativity scale in the following manner (Boyd and Edgecombe 1988): The electronegativity factor F_A associated with atom A in the diatomic hydride AH is given by

$$F_A = r_H/(r_{\alpha}^{b}Val_A) \qquad [1.6.1]$$

where Val_A is the number of valence electrons in A and the other quantities have been previously defined. The F_A values are converted into values comparable to those of Pauling's using the expression

$$x_A = a[F_A^{b}] \qquad [1.6.2]$$

where a and b are two parameters chosen to give electronegativities of one and four for Li and F respectively. The observed trends in electron withdrawing abilities are predicted by this scale and the mean deviation from the empirical results (Allred 1961) is only 0.08. Large Gaussian basis sets were used in the construction of the diatomic hydride statefunctions. In the present work we use Slater functions, and following the same procedure as Boyd and Edgecombe (1988) we get a mean deviation of only 0.05 for the set of second- and third-row hydrides compared to 0.06 for the Gaussian basis set (Table 1.6.6).

Following the procedure described above, group

electronegativities relative to H have been determined (Boyd and Edgecombe 1988). In general the N(H) values calculated using the theory of atoms in molecules decrease as the electronegativity of the A group increases (Table 1.6.7).

While these electronegativity scales are useful, in general, to predict the relative electron withdrawing abilities of atoms or groups of atoms relative to H, what would also be valuable is a way in which to predict the actual electron population of an atom in a molecule. To this end, Bader and Beddall (1973) have developed the following method: Consider the second-row hydrides AH. The electron population of A in AH is used to define an electronegativity which in turn is used to predict electron populations in other systems. The electronegativity of A relative to H is

$$x_A = 1 - N(H)_{AH} \qquad [1.6.3]$$

where $N(H)_{AH}$ is the electron population of H in AH. A value of x_A greater than (less than) zero means an electron withdrawing ability for A greater (or smaller) than that of H (column 6 of Table 1.6.6). The population of A in AB is

$$N(A)_{AB} = N(A)_A - v[x_B - x_A] \qquad [1.6.4]$$

where $N(A)_A$ is the electron population in the isolated A atom (i.e. the atomic number of A) and v equals the number of valence electrons in A or vacancies in B, whichever is smaller. Further, if $|x_B - x_A| > v$, then the second term on the right-hand side of equation [1.6.4] is set equal to v. This condition is imposed to prevent an atom from losing more than its full complement of valence electrons. In the present work we extend this scheme to third-row atoms, and thereby examine a

larger set of systems. The results (Table 1.6.8) predicted from this procedure are in good agreement with the actual electron populations with the exceptions of the oxides, nitrides and carbides of beryllium and boron. It is noteworthy that in general these exceptions have large values for both r_A^o and r_B^o, and so, the model falters for these systems with large regions of nonbonded charge distribution.

Figure 1.6.1

(a) Contour maps of the charge density for hydrogen and the neutral ground-state second-row hydrides. Nuclear positions are denoted by + signs. Bond paths and interatomic surfaces are included and bond critical points are denoted by black dots. Left hand side from top: H_2, LiH, BeH, BH; Right hand side from top: CH, NH, OH and FH.

(b) Corresponding plots for the Laplacian of the charge density.

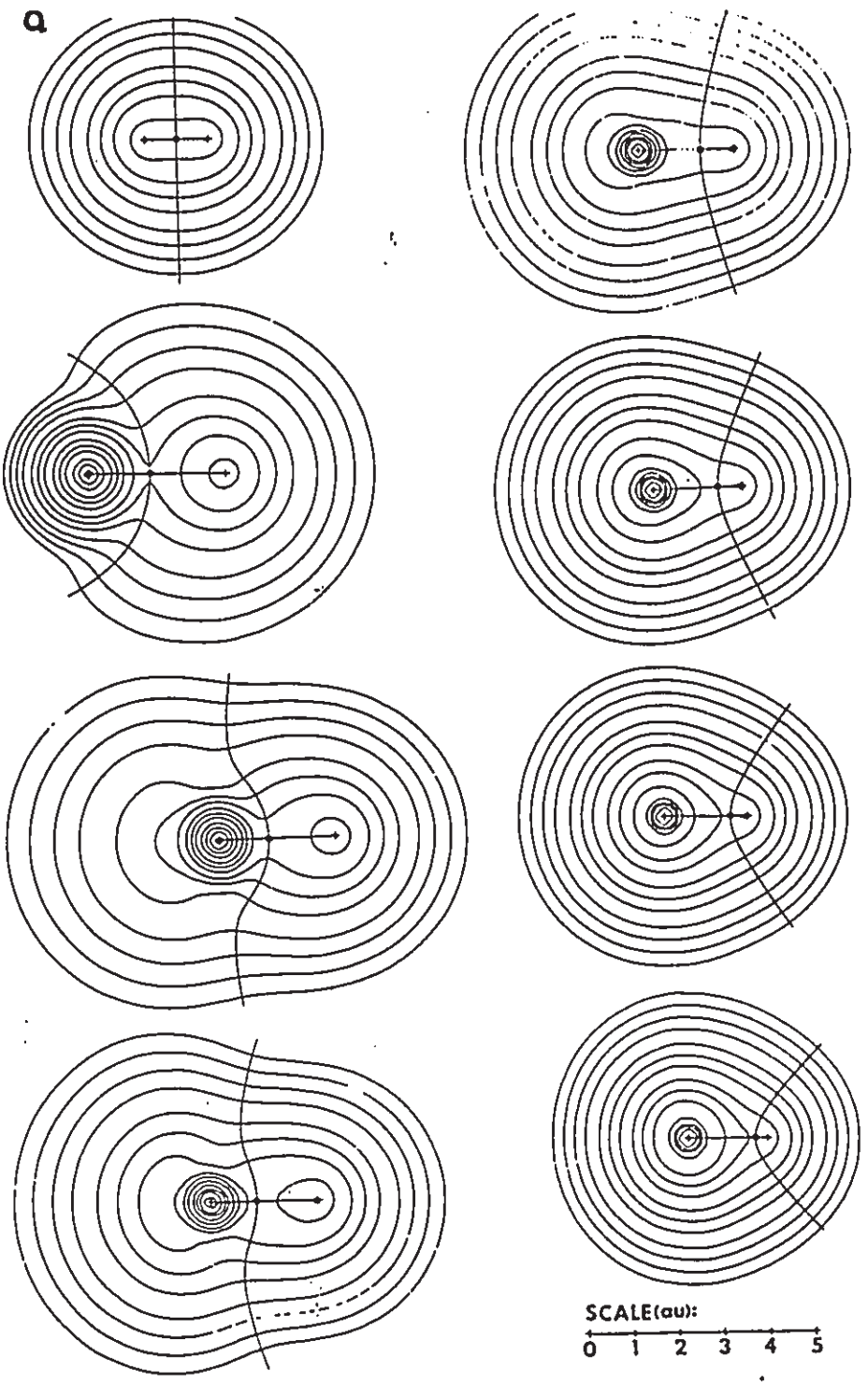
a
SCALE(au):
0 1 2 3 4 5

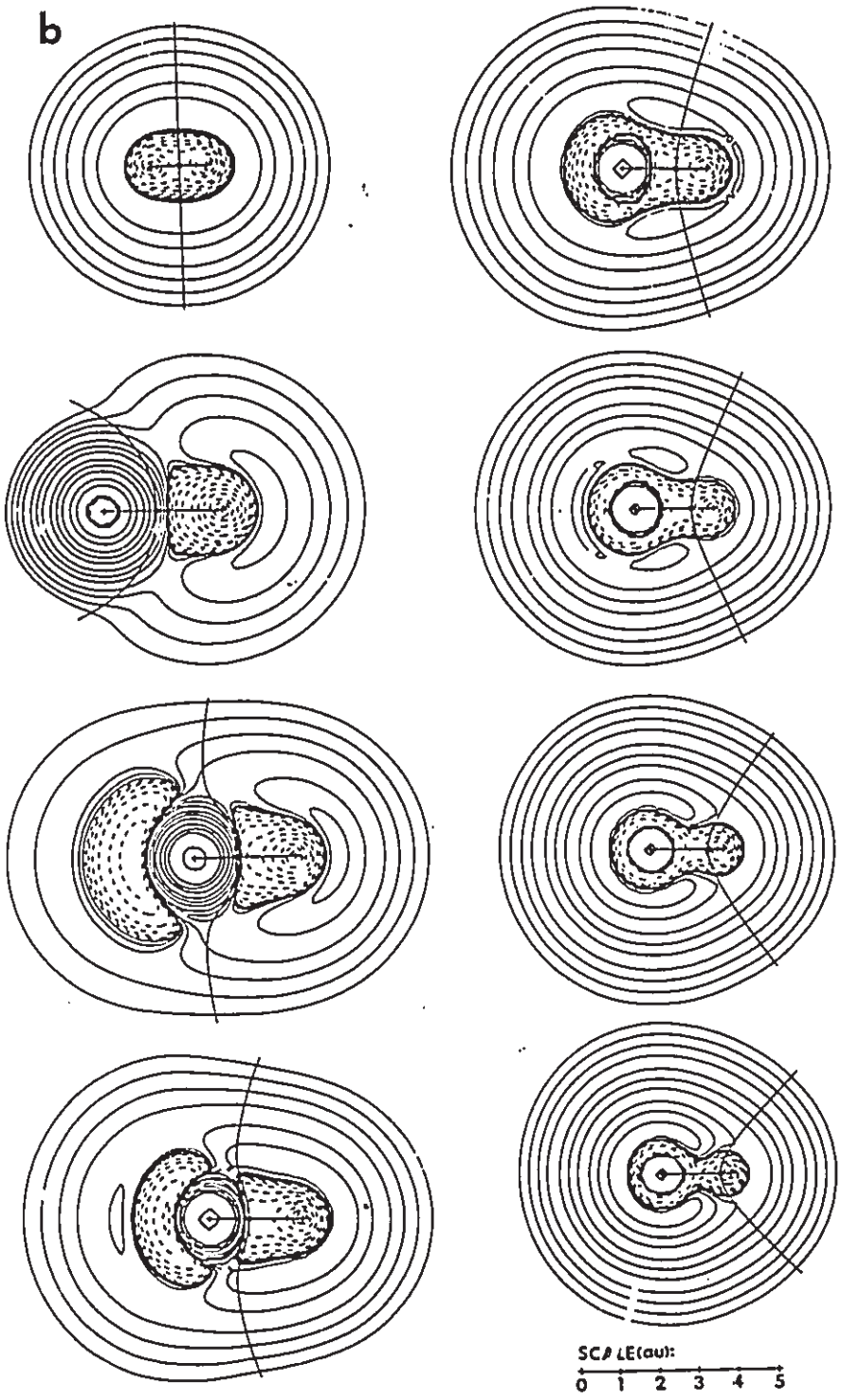
b
SCALE(au):
0 1 2 3 4 5

Figure 1.6.2

(a) Contour maps of the charge density for neutral ground-state third-row hydrides. Nuclear positions are denoted by + signs. Bond paths and interatomic surfaces are included and bond critical points are denoted by black dots. Left hand side from top: NaH, MgH, AlH, SiH; Right hand side from top: PH, SH, ClH.

(b) Corresponding plots for the Laplacian of the charge density.

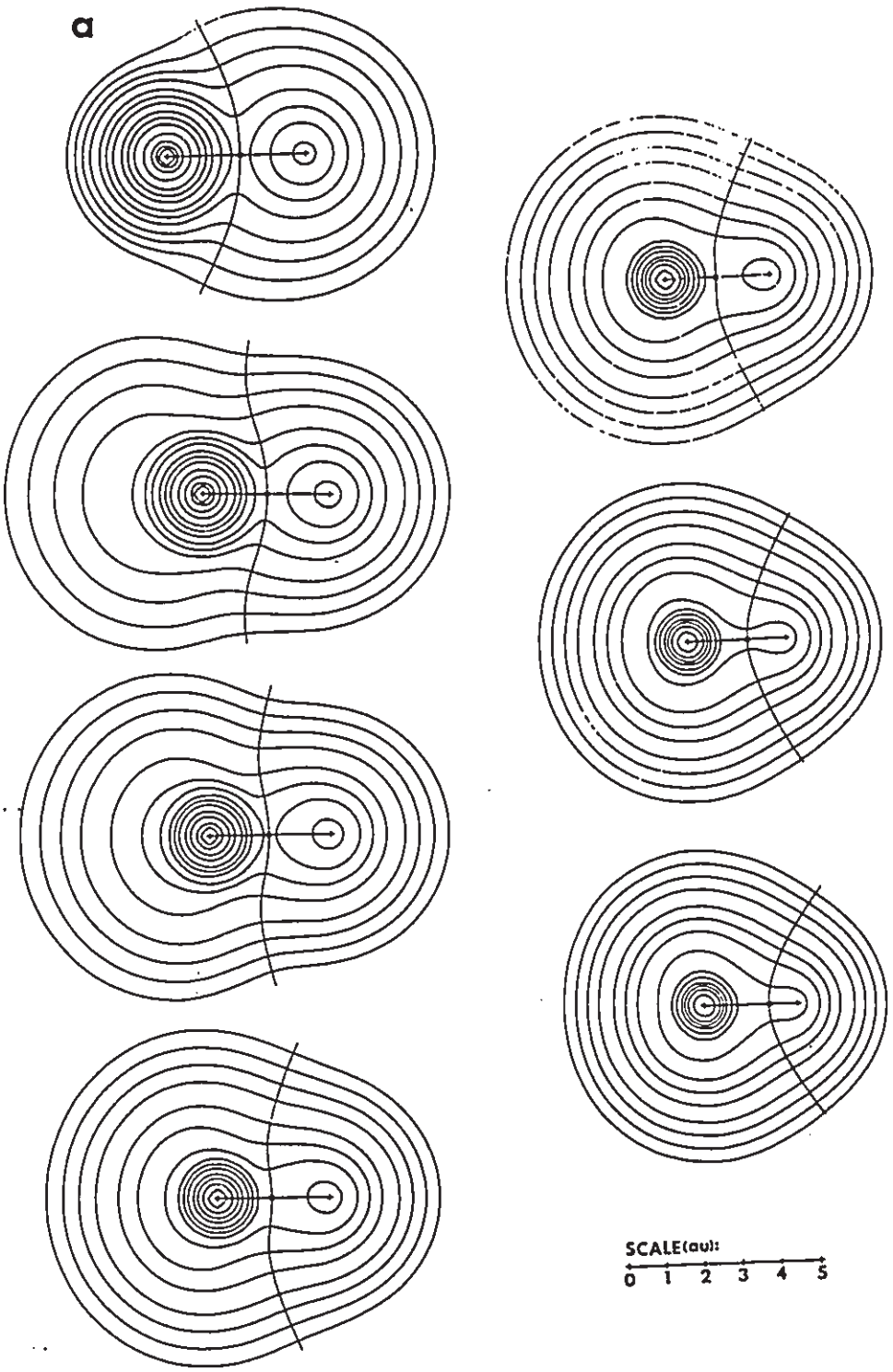
a
SCALE(au):
0 1 2 3 4 5

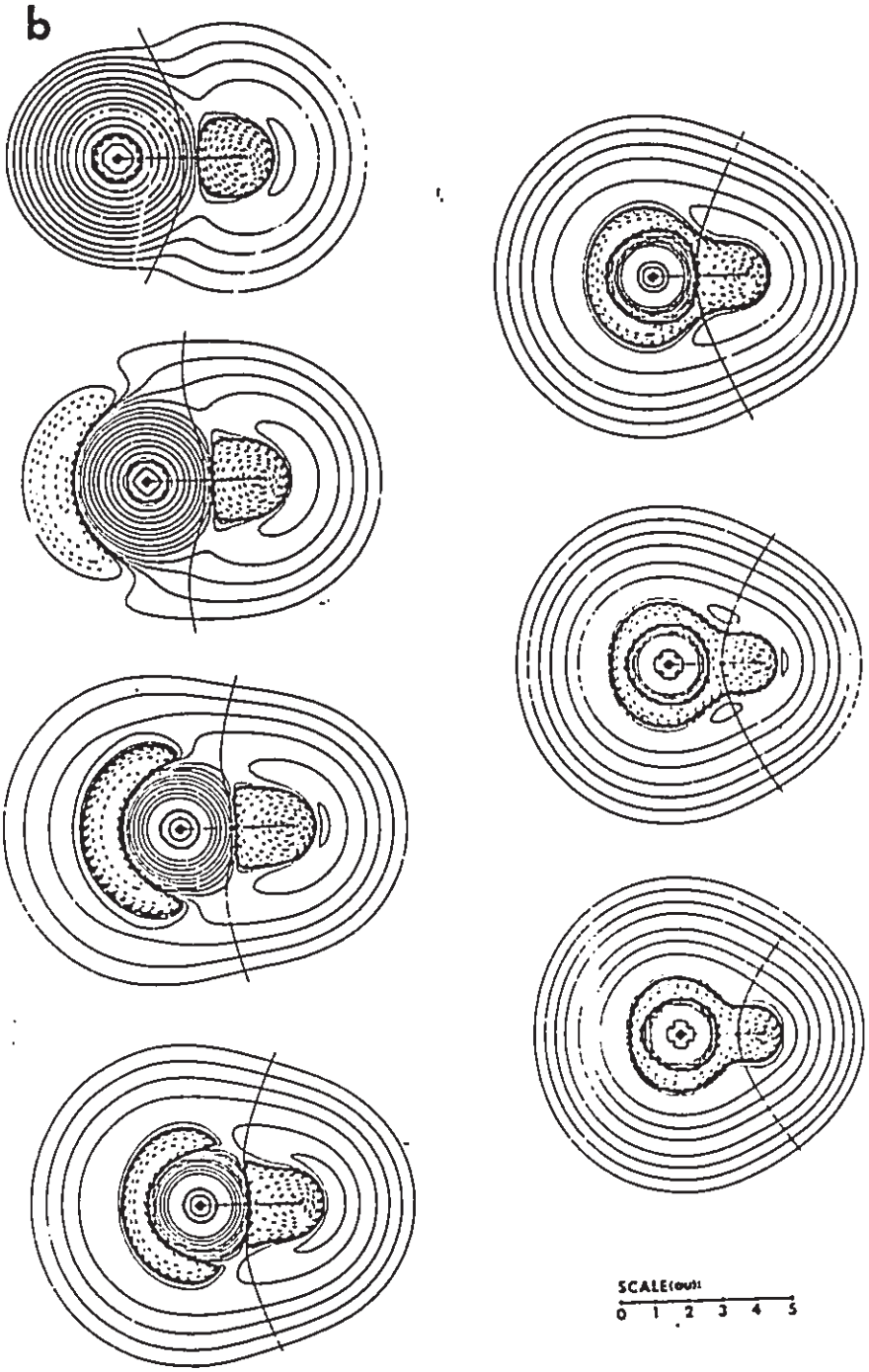
b
SCALE(cm)
0 1 2 3 4 5

Figure 1.6.3

(a) Contour maps of the charge density for lithium-containing diatomics. Nuclear positions are denoted by + signs. Bond paths and interatomic surfaces are included and bond critical points are denoted by black dots. Left hand side from top: Li_2, LiBe, LiB, LiC; Right hand side from top: LiN, LiO, LiF.

(b) Corresponding plots for the Laplacian of the charge density.

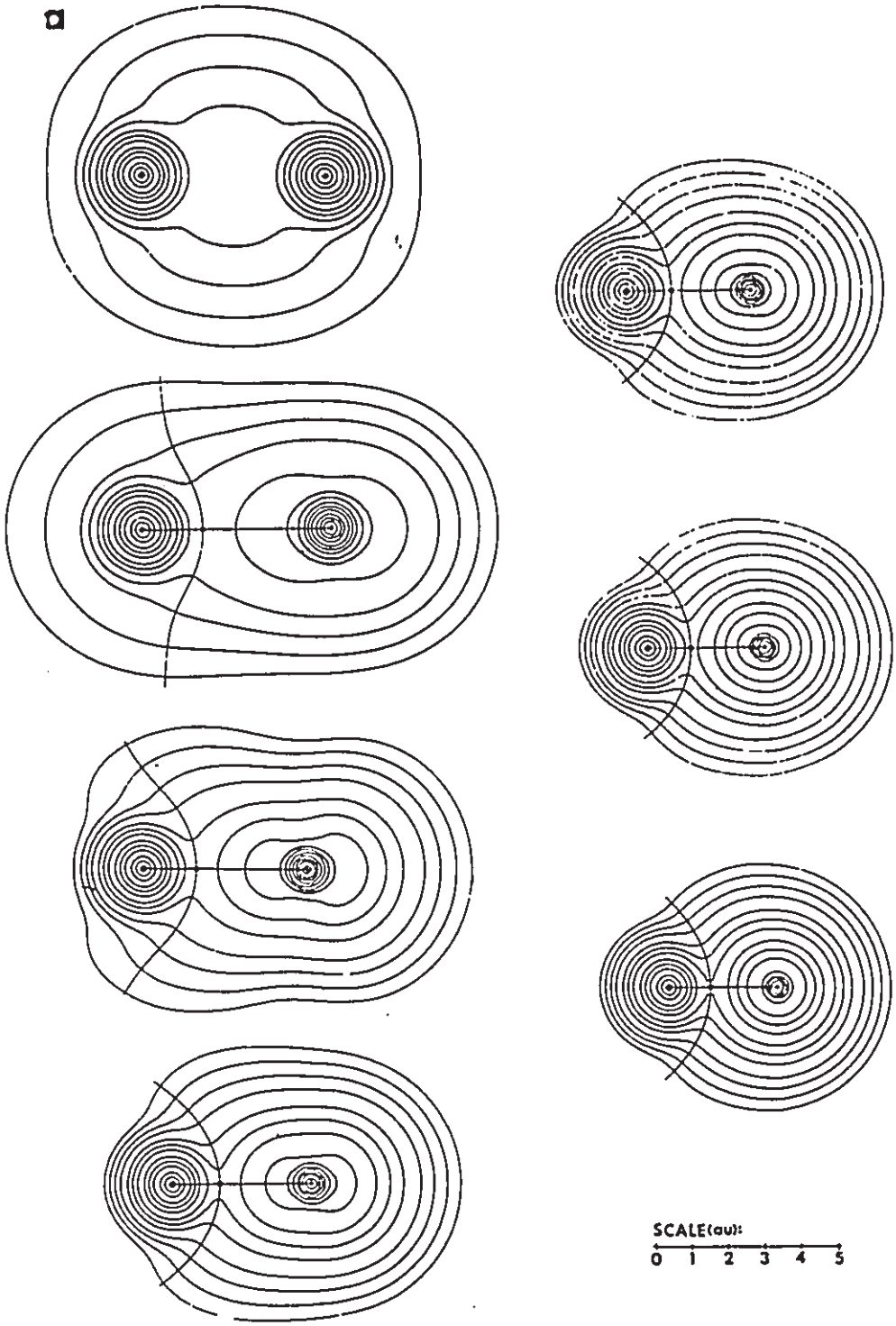
SCALE(au):
0 1 2 3 4 5

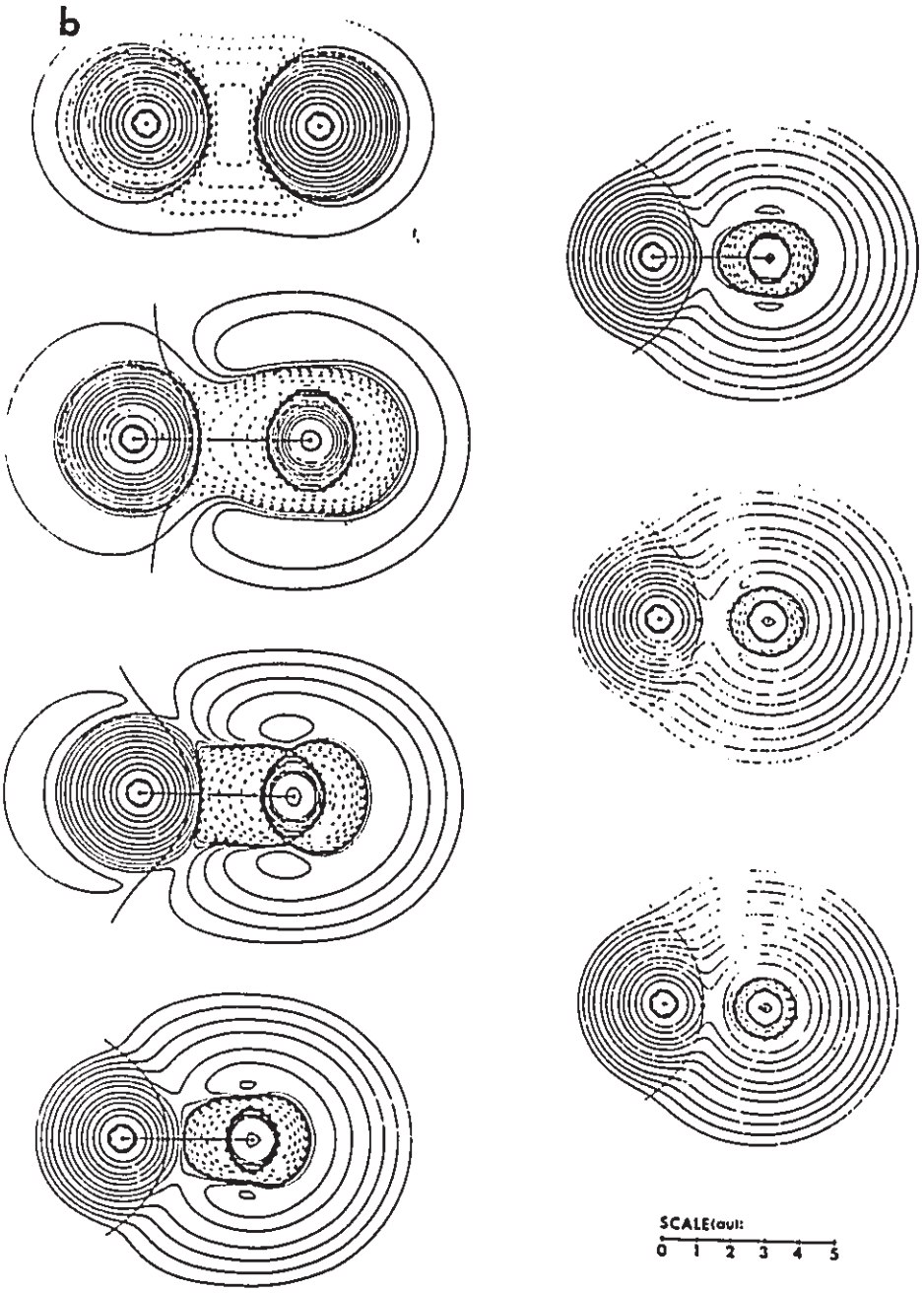
b
SCALE(au):
0 1 2 3 4 5

Figure 1.6.4

(a) Contour maps of the charge density for beryllium-containing diatomics (left hand side) and boron-containing diatomics (right hand side). Nuclear positions are denoted by + signs. Bond paths and interatomic surfaces are included and bond critical points are denoted by black dots. Left hand side from top: BeB, BeC, BeN, BeO, BeF; Right hand side from top: B_2, BC, BN, BO, BF.

(b) Corresponding plots for the Laplacian of the charge density.

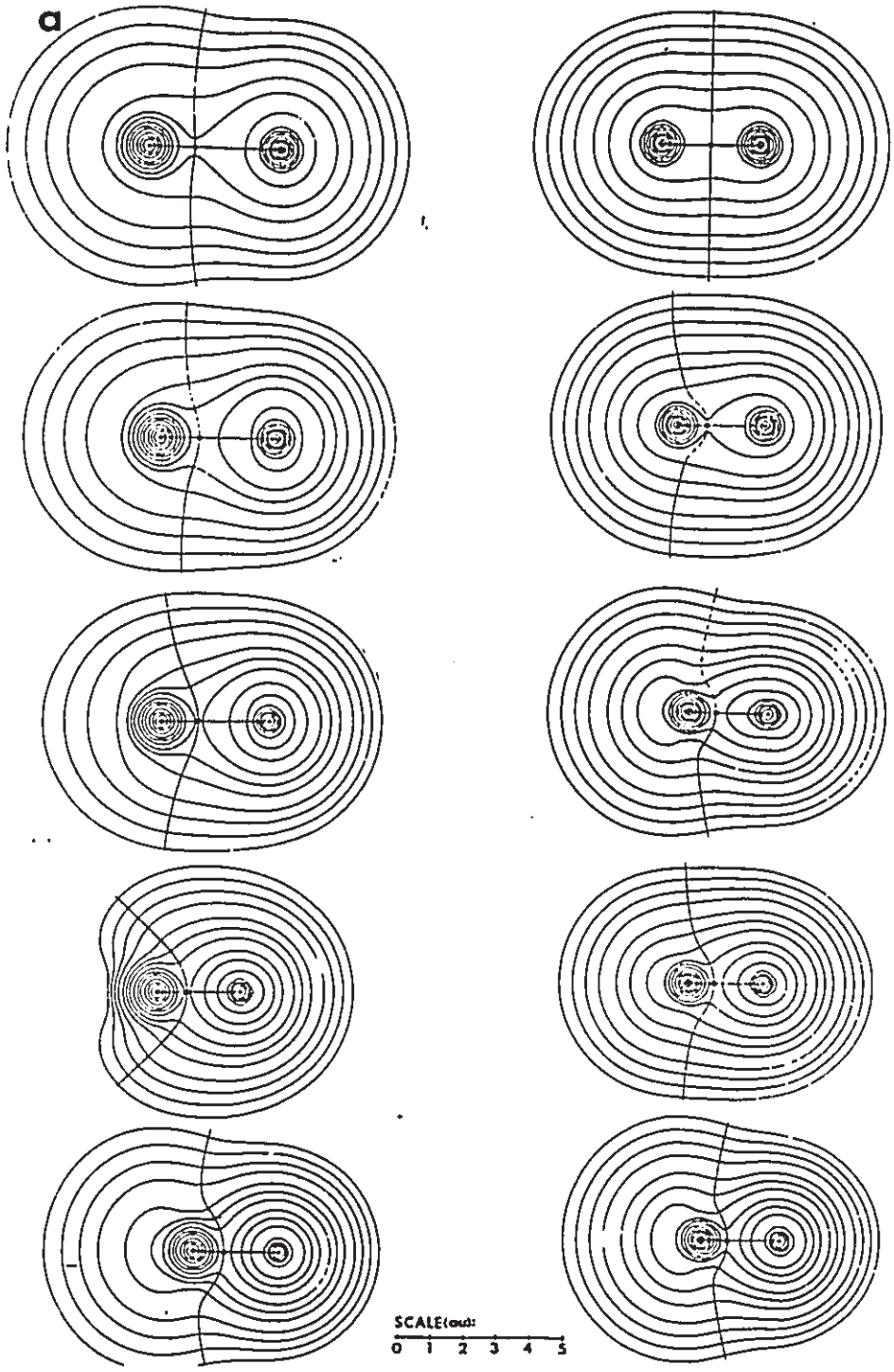
a
SCALE(au):
0 1 2 3 4 5

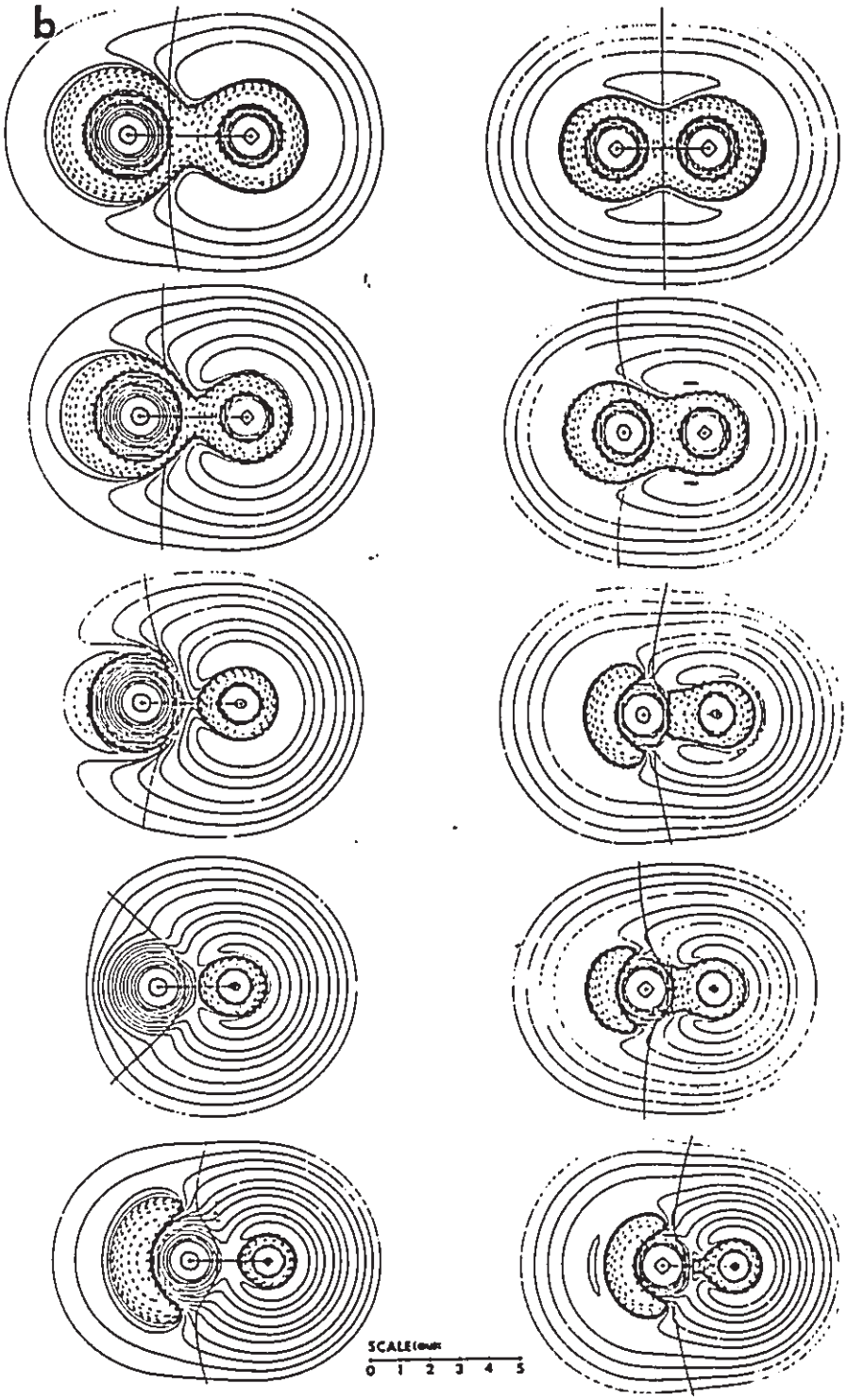
b
SCALE(au)
0 1 2 3 4 5

Figure 1.6.5

(a) Contour maps of the charge density for remaining carbon, nitrogen, oxygen and fluorine-containing diatomics. Nuclear positions are denoted by + signs. Bond paths and interatomic surfaces are included and bond critical points are denoted by black dots.

(b) Corresponding plots for the Laplacian of the charge density.

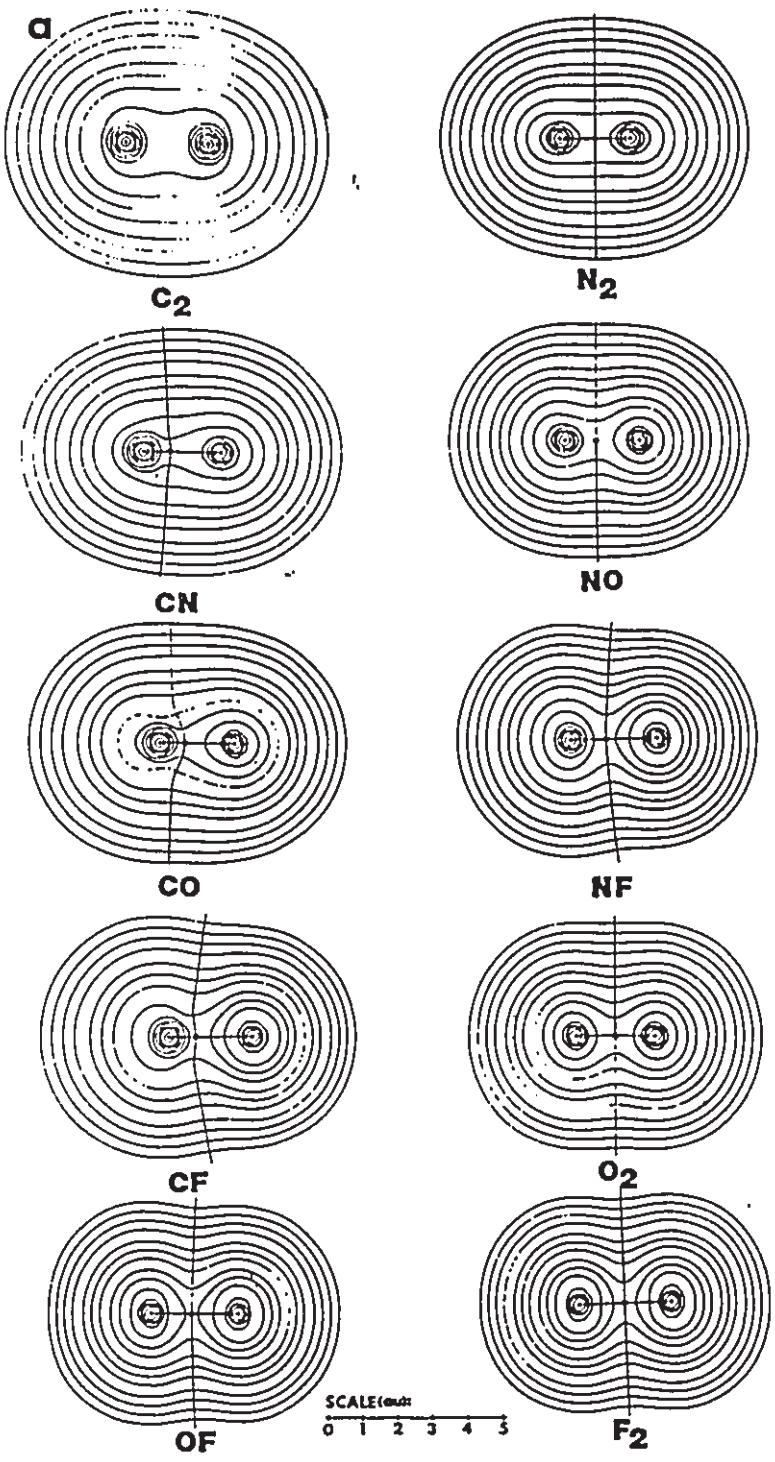
a
C_2
N_2
CN
NO
CO
NF
CF
O_2
OF
F_2
SCALE(au):
0 1 2 3 4 5

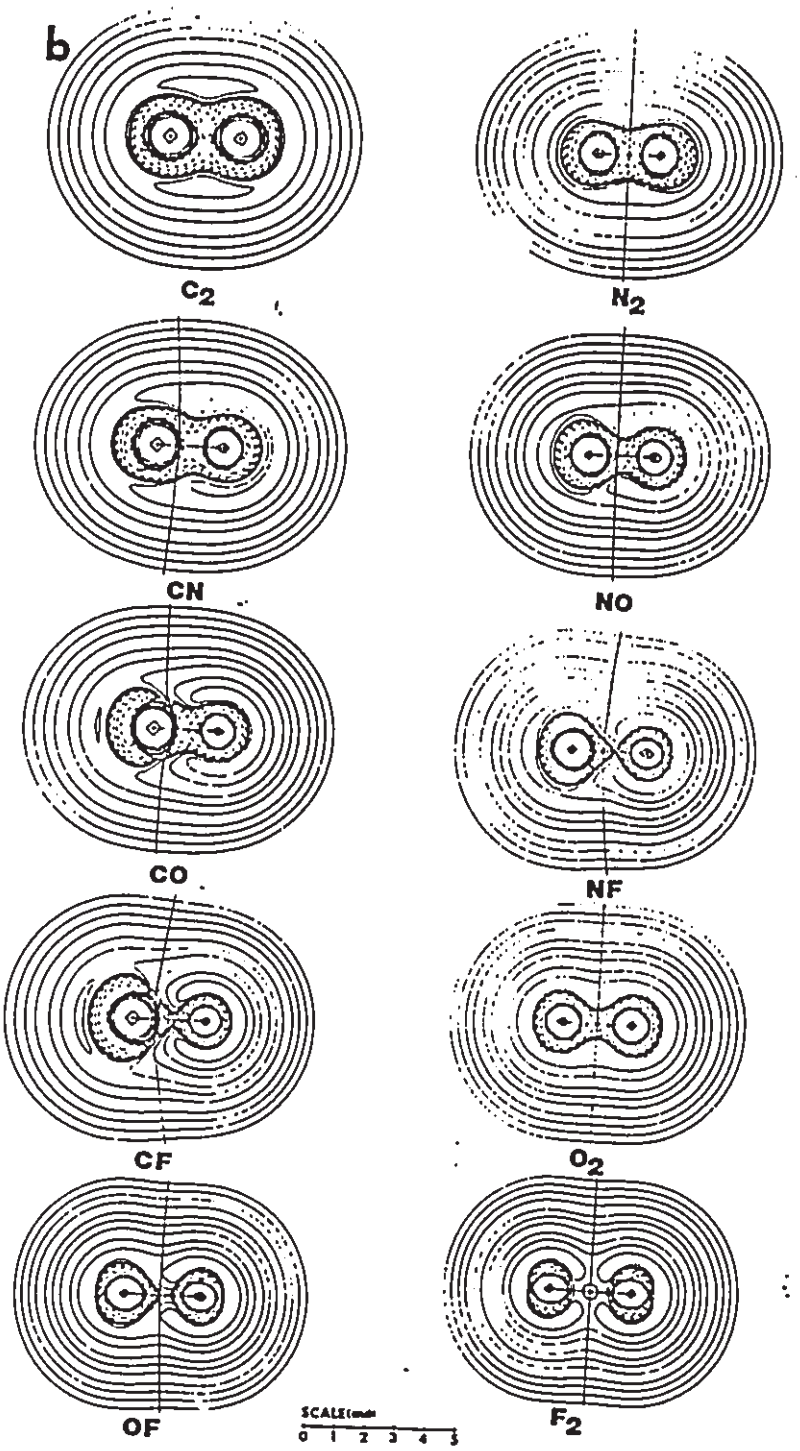
b
C2
N2
CN
NO
CO
NF
CF
O2
OF
F2
SCALE(mdu)
0 1 2 3 4 5

Figure 1.6.6

(a) Net charges of atoms in second-row diatomic molecules.

(b) Comparison of q(H) between second- and third-row hydrides.

a

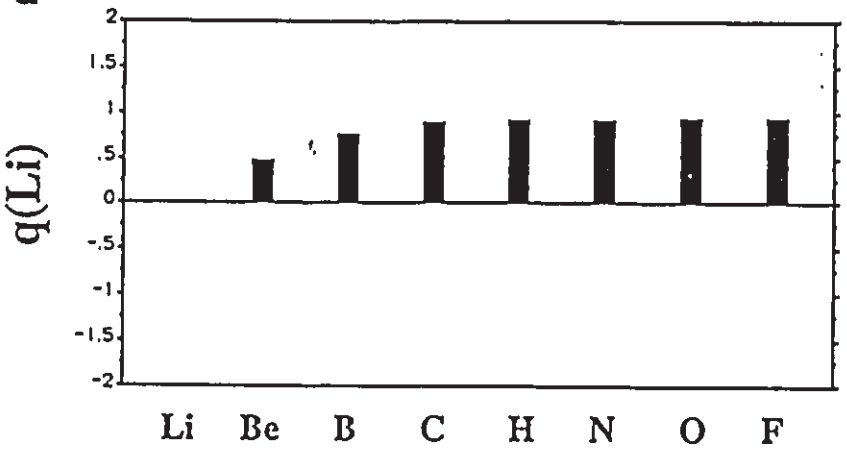
q(Li)
2
1.5
1
.5
0
-.5
-1
-1.5
-2
Li Be B C H N O F

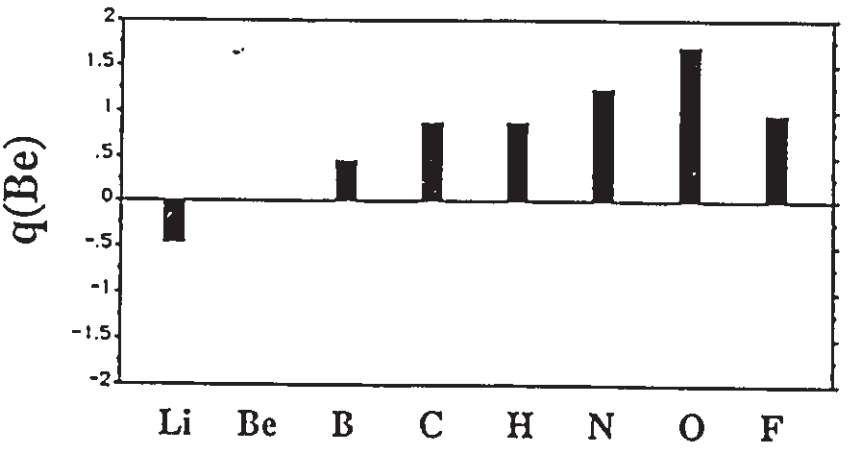
q(Be)
2
1.5
1
.5
0
-.5
-1
-1.5
-2
Li Be B C H N O F

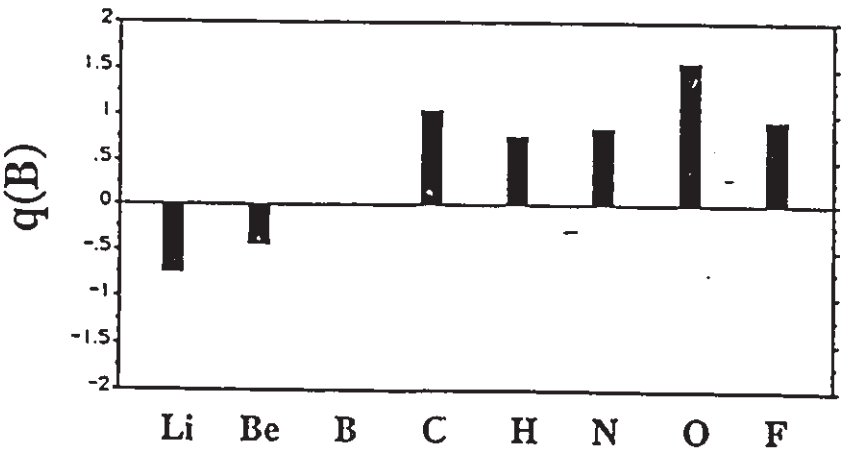
q(B)
2
1.5
1
.5
0
-.5
-1
-1.5
-2
Li Be B C H N O F

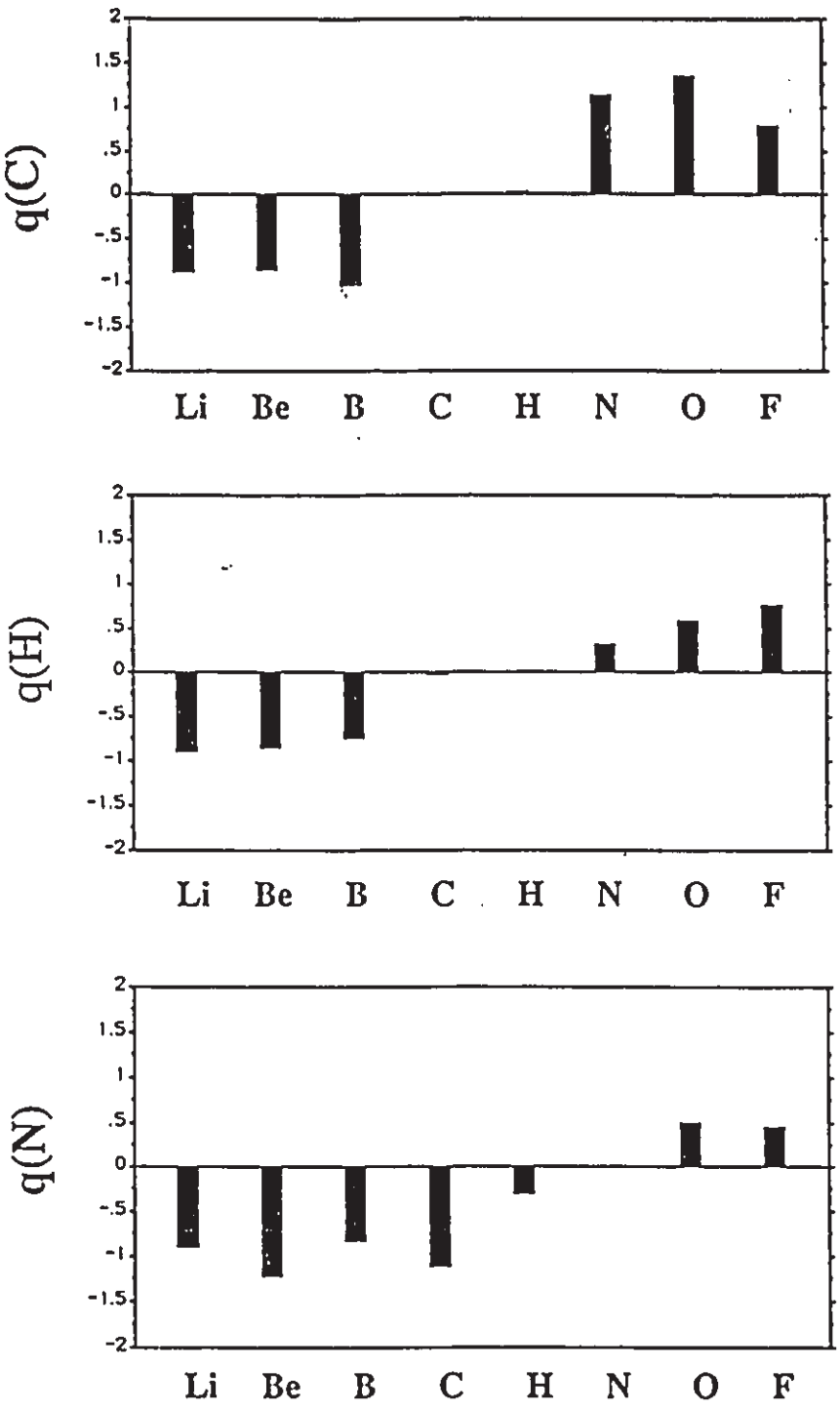
q(C)
q(H)
q(N)
2
1.5
1
.5
0
-.5
-1
-1.5
-2
Li
Be
B
C
H
N
O
F

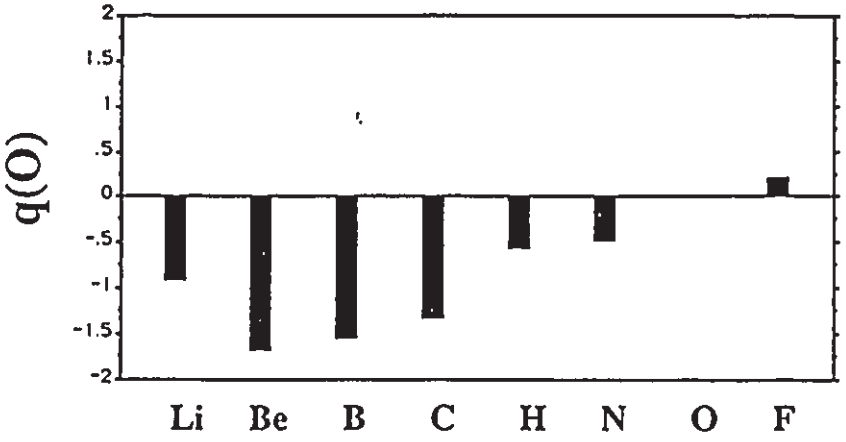
q(O)
2
1.5
1
.5
0
-.5
-1
-1.5
-2
Li
Be
B
C
H
N
O
F

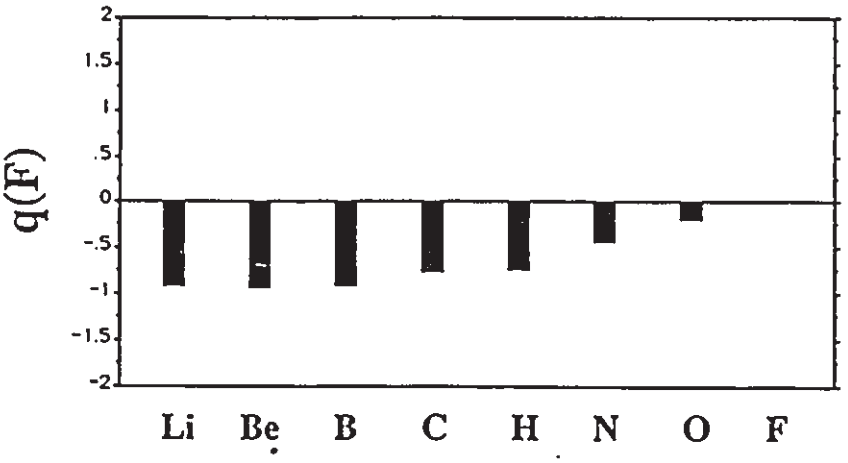
q(F)
2
1.5
1
.5
0
-.5
-1
-1.5
-2
Li
Be
B
C
H
N
O
F

b

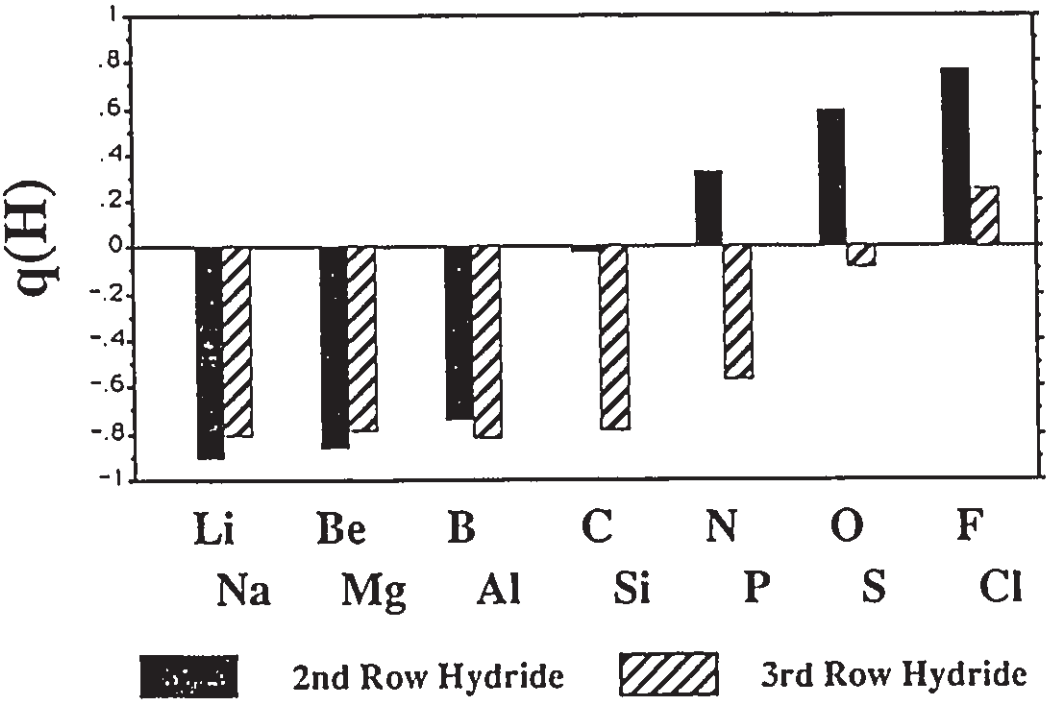
q(H)
1
.8
.6
.4
.2
0
-.2
-.4
-.6
-.8
-1
Li Be B C N O F
Na Mg Al Si P S Cl
2nd Row Hydride
3rd Row Hydride

Figure 1.6.7

(a) Volumes of atoms in second-row diatomic molecules.

(b) Comparison of $v(\Omega)$ within and between second- and third-row hydrides.

a

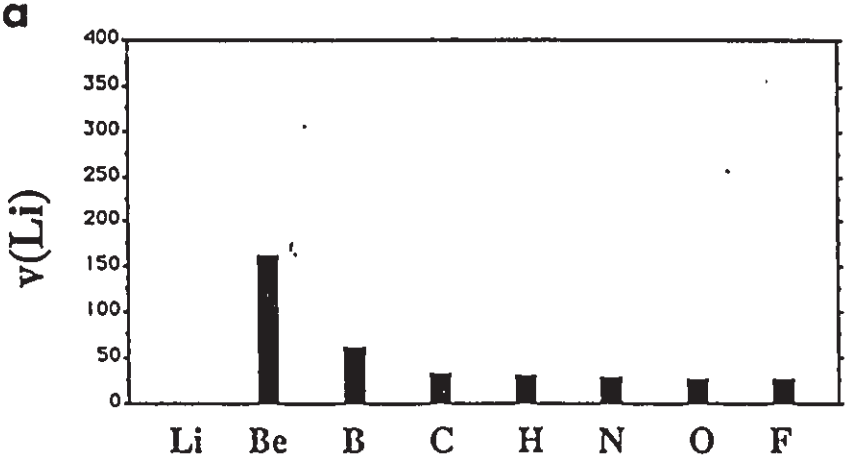
v(Li)
400
350
300
250
200
150
100
50
0
Li Be B C H N O F

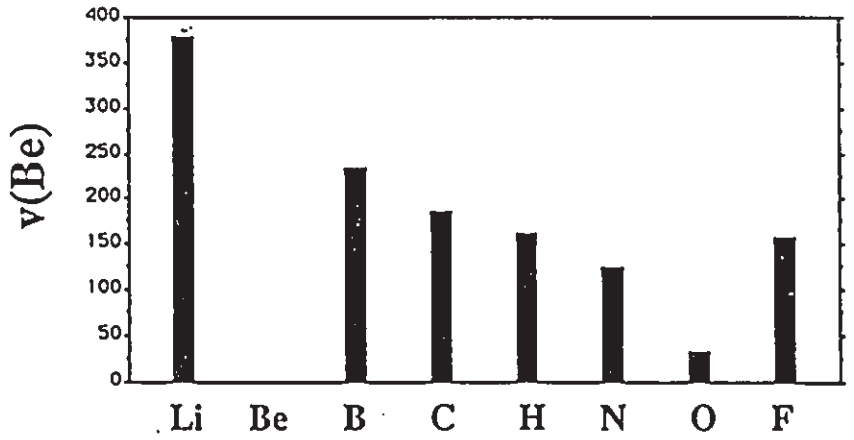
v(Be)
400
350
300
250
200
150
100
50
0
Li Be B C H N O F

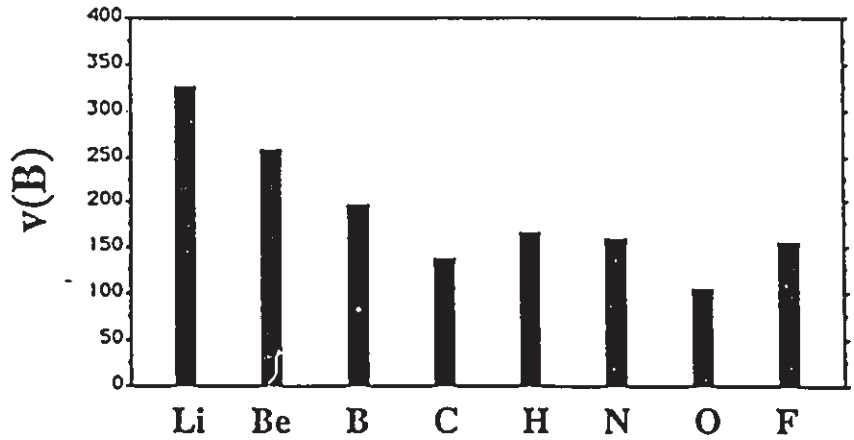
v(B)
400
350
300
250
200
150
100
50
0
Li Be B C H N O F

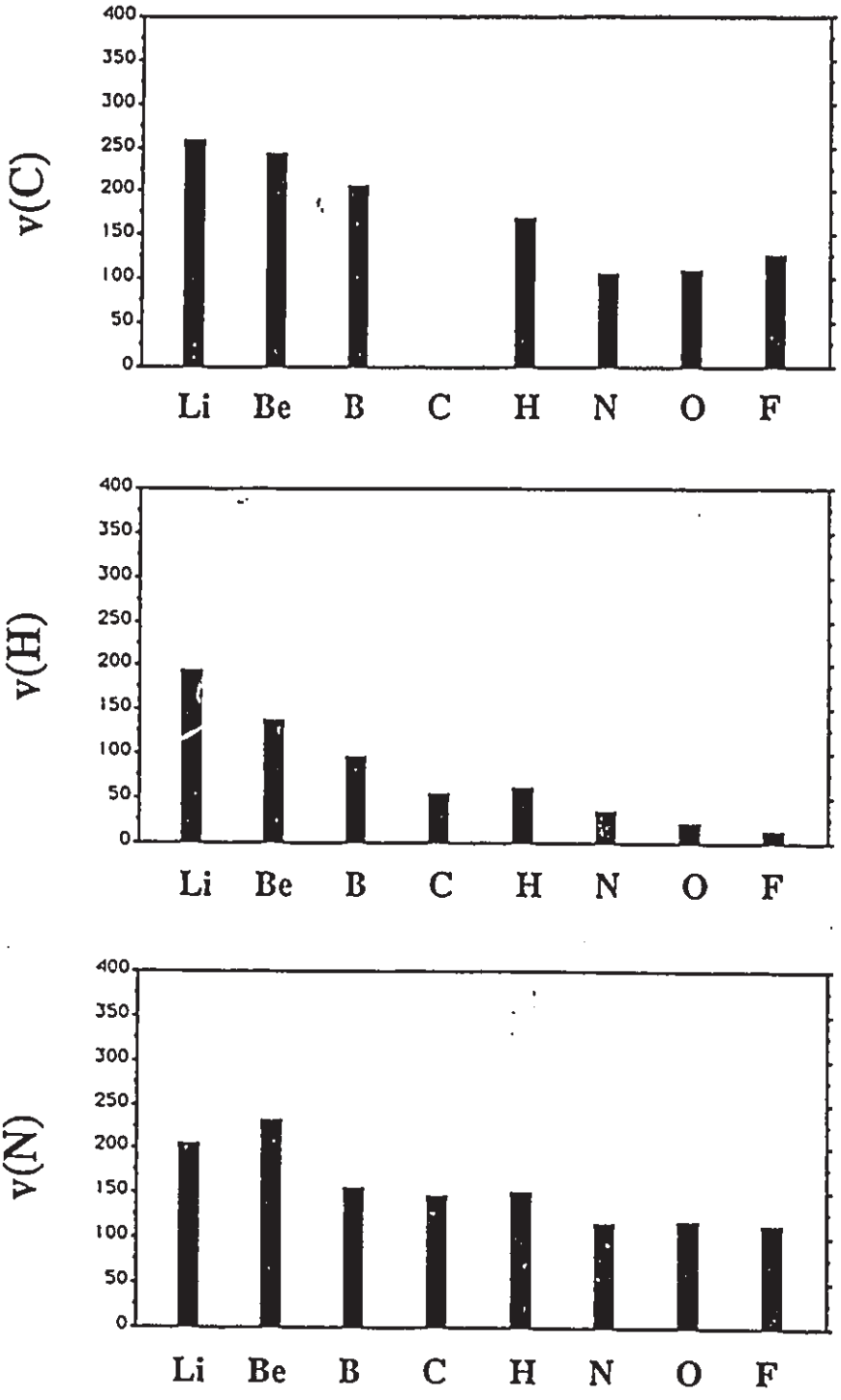
ν(C)
400
350
300
250
200
150
100
50
0
Li Be B C H N O F
ν(H)
400
350
300
250
200
150
100
50
0
Li Be B C H N O F
ν(N)
400
350
300
250
200
150
100
50
0
Li Be B C H N O F

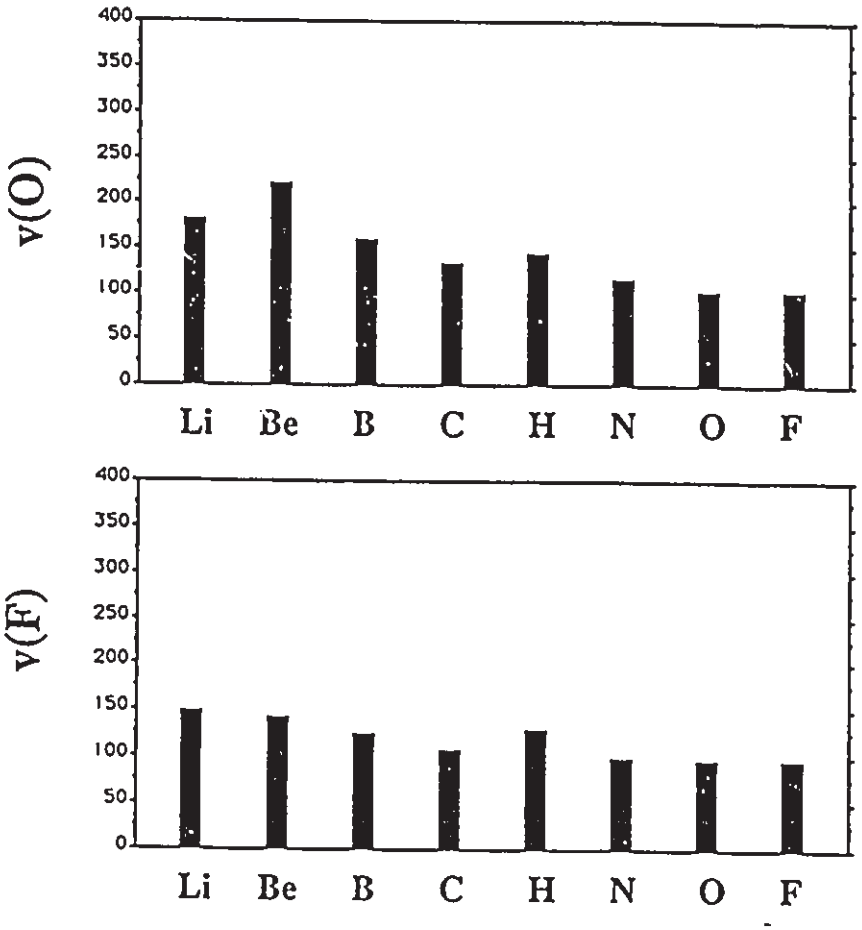
ν(O)
400
350
300
250
200
150
100
50
0
Li Be B C H N O F
ν(F)
400
350
300
250
200
150
100
50
0
Li Be B C H N O F

b

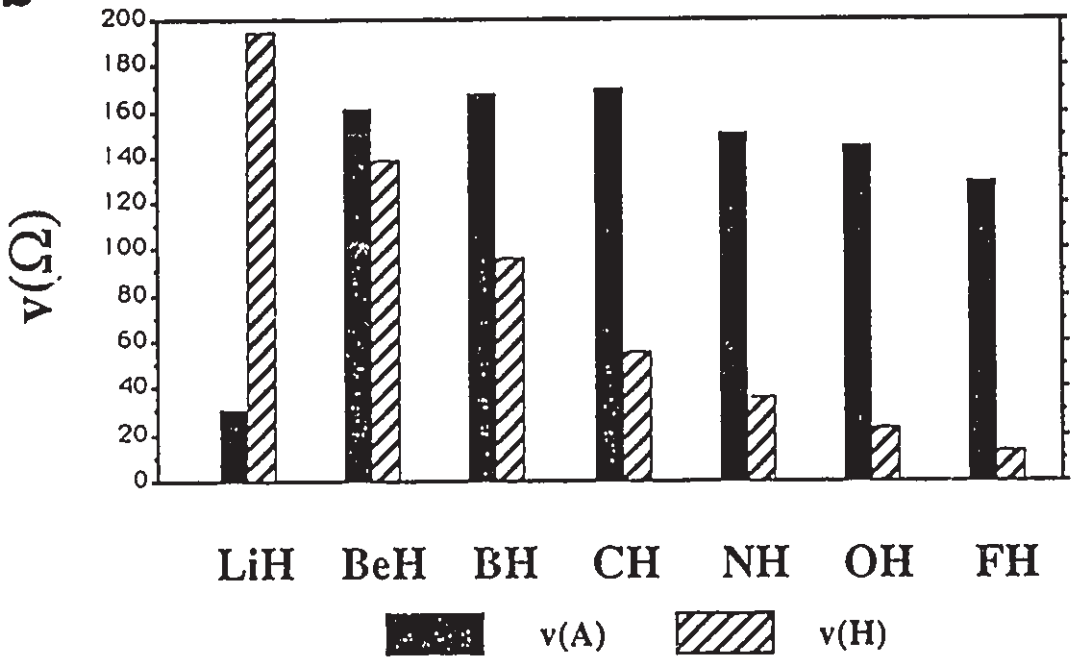
200
180
160
140
120
100
80
60
40
20
0
ν(Ω)
LiH
BeH
BH
CH
NH
OH
FH
ν(A)
ν(H)

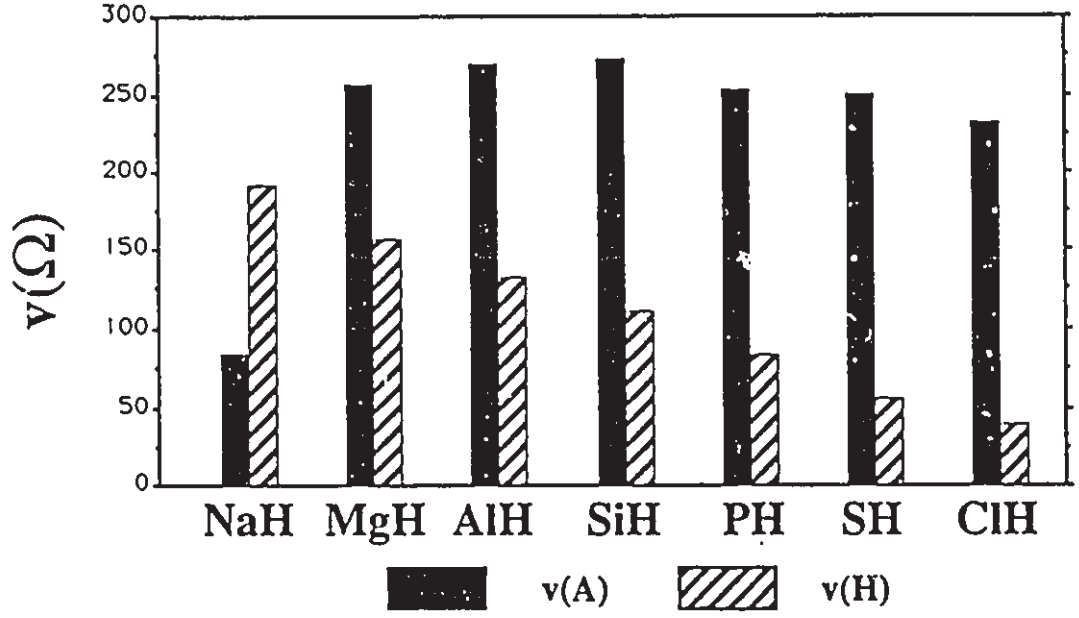
300
250
200
150
100
50
0
ν(Ω)
NaH
MgH
AlH
SiH
PH
SH
ClH
ν(A)
ν(H)

Figure 1.6.8

Relative energies of atoms in second-row diatomic molecules.

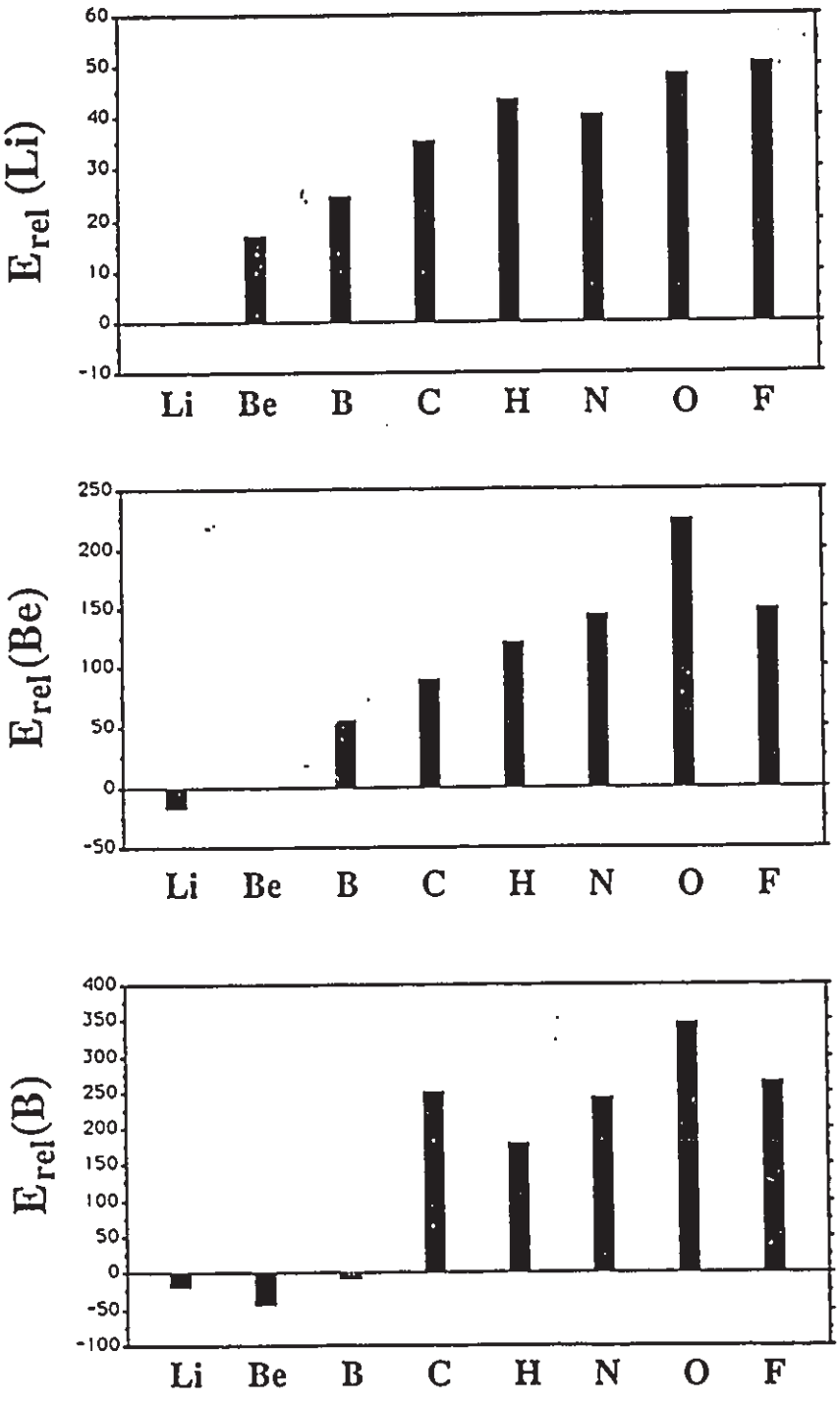
E_{rel} (Li)
60
50
40
30
20
10
0
-10
Li Be B C H N O F
E_{rel}(Be)
250
200
150
100
50
0
-50
Li Be B C H N O F
E_{rel}(B)
400
350
300
250
200
150
100
50
0
-50
-100
Li Be B C H N O F

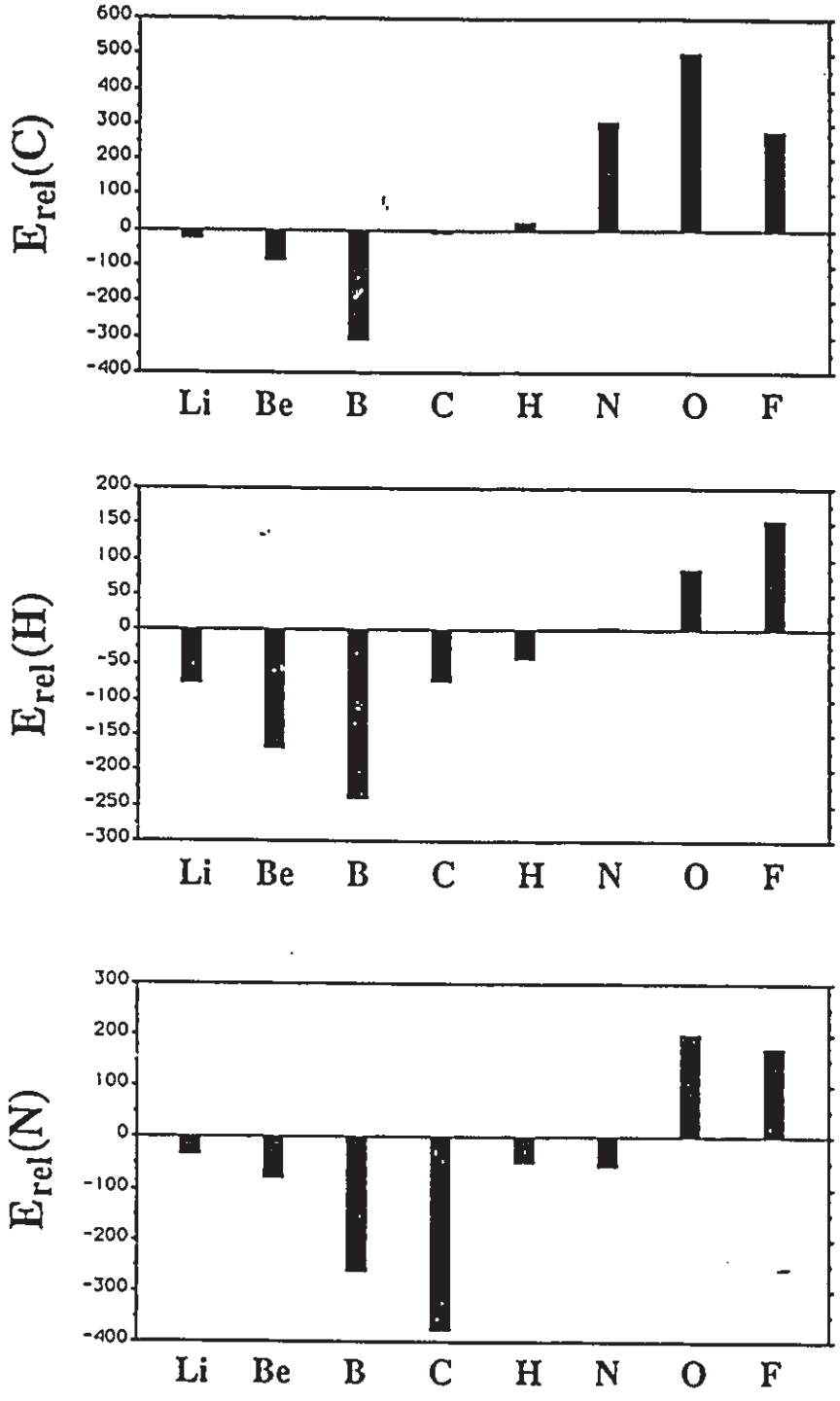
$E_{rel}(C)$
600
500
400
300
200
100
0
-100
-200
-300
-400
Li Be B C H N O F
$E_{rel}(H)$
200
150
100
50
0
-50
-100
-150
-200
-250
-300
Li Be B C H N O F
$E_{rel}(N)$
300
200
100
0
-100
-200
-300
-400
Li Be B C H N O F

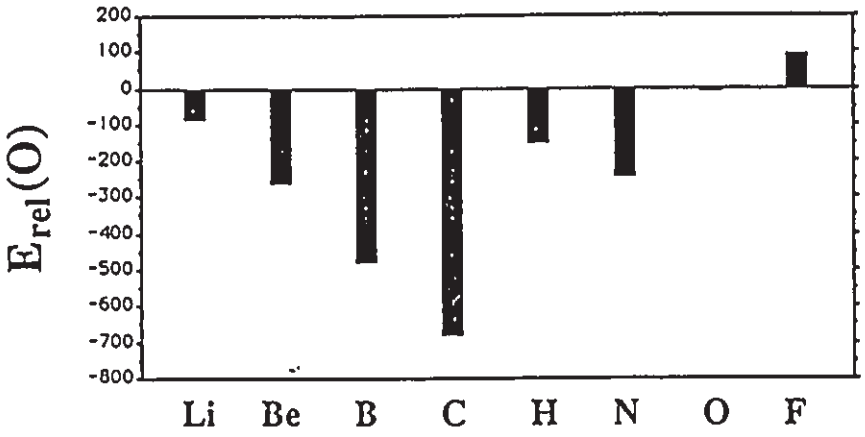
$E_{rel}(O)$
200
100
0
-100
-200
-300
-400
-500
-600
-700
-800
Li
Be
B
C
H
N
O
F

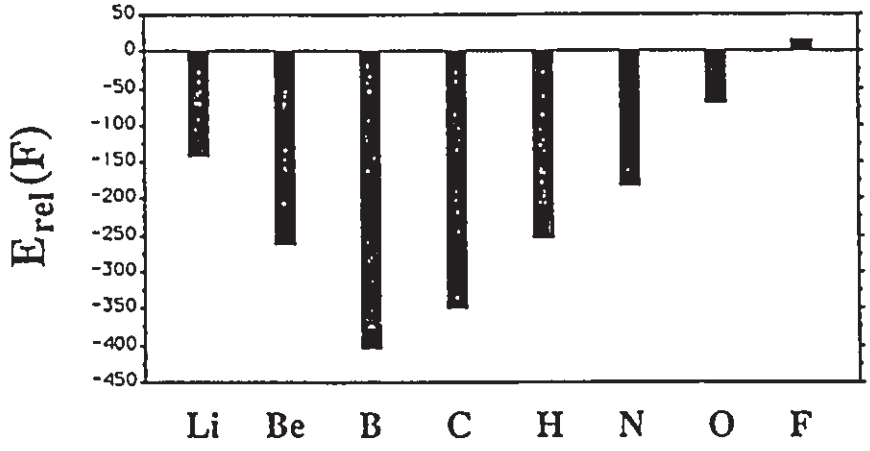
$E_{rel}(F)$
50
0
-50
-100
-150
-200
-250
-300
-350
-400
-450
Li
Be
B
C
H
N
O
F

Figure 1.6.9

Left hand side: Contour maps of the charge density for states of the BeH system illustrating the three classes of hydride molecules, BeH^+ ($X^1\Sigma^+$) (class I); BeH ($X^2\Sigma^+$) (class II); BeH ($A^2\pi_r$) (class III). The smallest contour value is 0.002 au. Right hand side: Corresponding comparison for the MgH system.

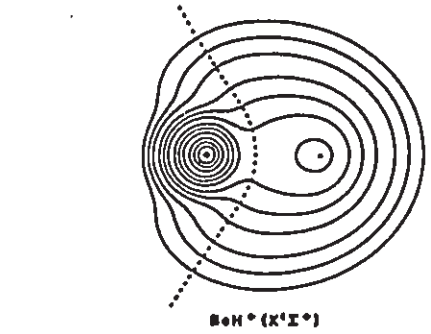

BeH$^+$ ($X^1\Sigma^+$)

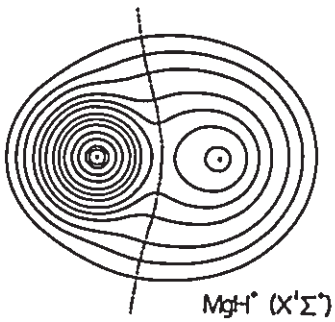

MgH$^+$ ($X^1\Sigma^+$)

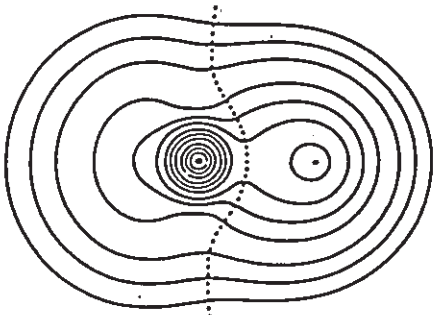

BeH ($X^2\Sigma^+$)

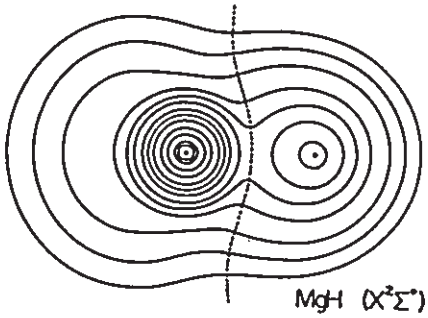

MgH ($X^2\Sigma^+$)

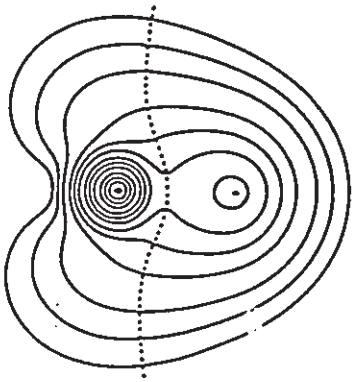

BeH ($A^2\Pi_r$)

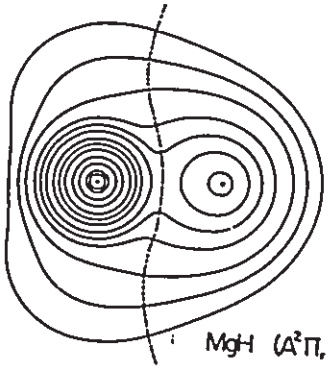

MgH ($A^2\Pi_r$)

Figure 1.6.10

The partitioning surfaces for families of neutral, ground state, diatomic molecules. The surfaces are plotted with respect to a fixed position of the reference nucleus in each family. Because of axial symmetry only the upper half of each surface is shown.

upper left: surfaces for diatomic fluorides

upper right: surfaces for diatomic oxides

lower left: surfaces for diatomic hydrides

lower right: surfaces for diatomic nitrides

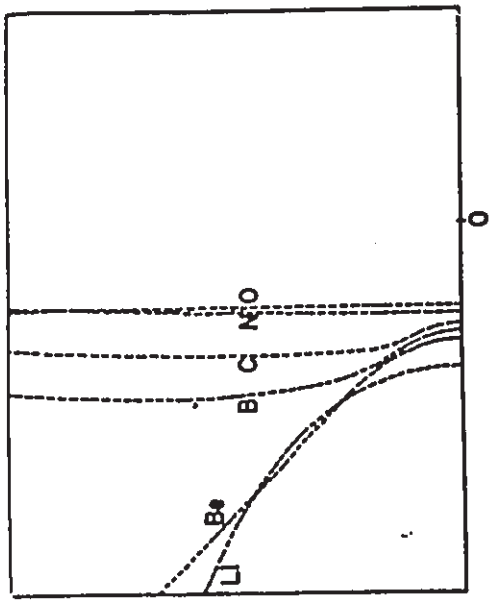
O
N
C
B
Be
Li

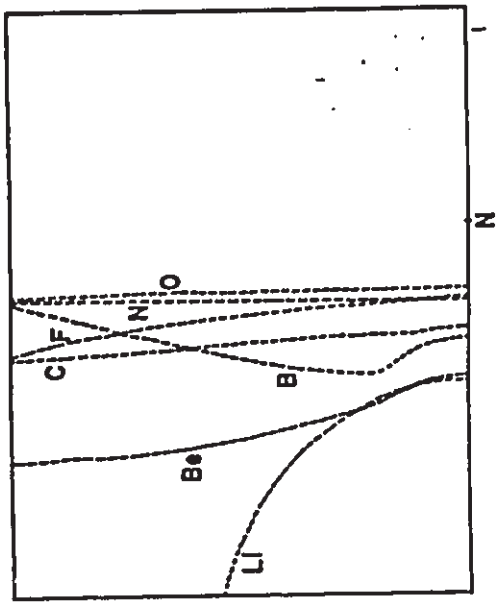
N
O
F
C
B
Be
Li

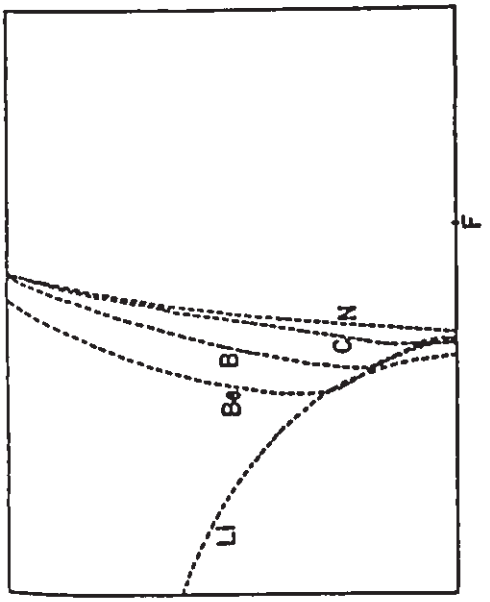
F
N
C
B
Be
Li

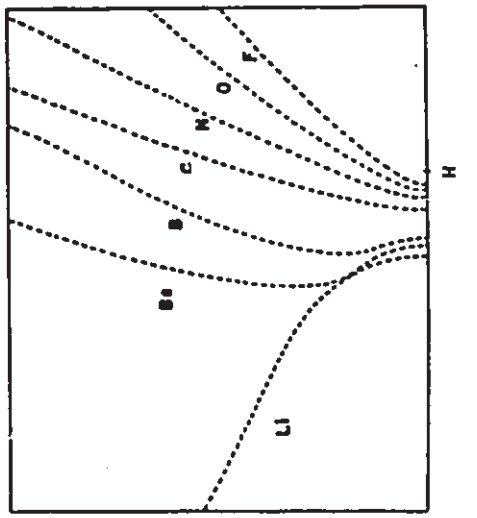
F
O
N
C
B
Be
Li

Figure 1.6.11

Contour maps of the charge density for BeH_2 and BeH. Zero flux surfaces (dashed lines) are included. Note the great similarity in the charge distribution for the hydrogen atom in the two systems.

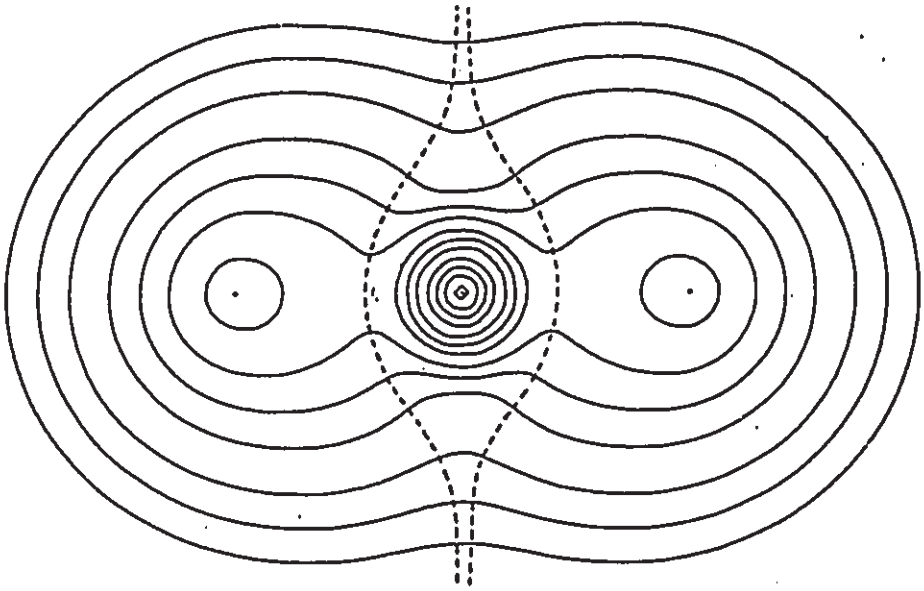

HBeH ($X^1\Sigma^+$)

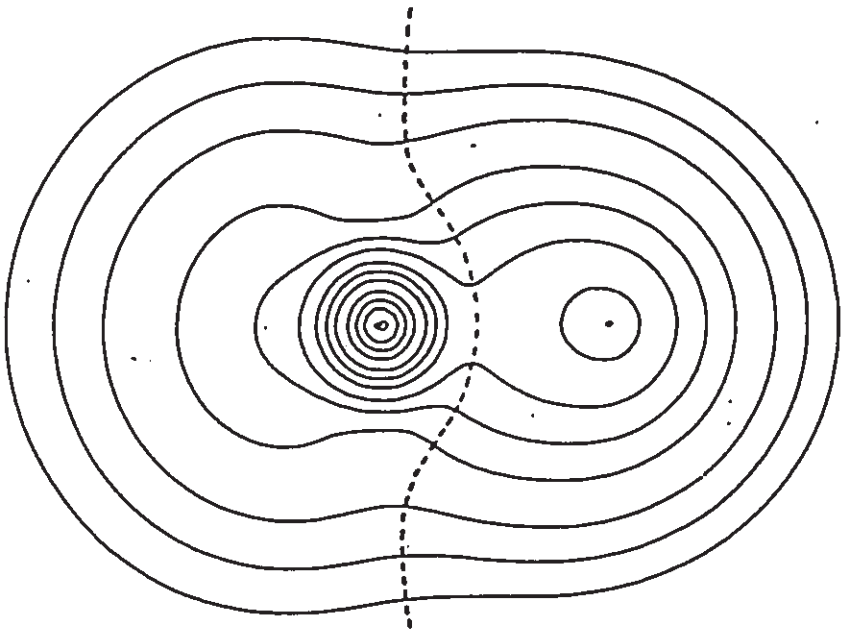

BeH ($X^2\Sigma^+$)

Table 1.6.1. Properties of the Bond Critical Points in Diatomic Molecules (in au).[a]

Sys AB	r_e	r_A	r_B	r_A (Å)	r_B (Å)	r_p[b]		ρ_b	$\nabla^2\rho_b$	$\lambda_1=\lambda_2$	λ_3
HH	1.4000	0.7000	0.7000	2.54	2.54	2.83		0.2728	-1.3784	-0.8917	0.6049
LiH	3.0150	1.3444	1.6706	1.88	3.27	3.68	B	0.0407	0.1571	-0.0619	0.2808
BeH	2.5380	1.0829	1.4551	4.58	2.88	3.54	A	0.0965	0.1638	-0.2032	0.5703
BH	2.3360	1.0015	1.3345	4.34	2.75	3.59	A	0.1843	-0.5847	-0.4622	0.3397
CH	2.1240	1.3584	0.7656	3.86	2.52	3.54	A	0.2787	-1.0389	-0.7572	0.4754
NH	1.9614	1.4227	0.5387	3.51	2.37	3.38	A	0.3384	-1.6034	-1.2399	0.8765
OH	1.8342	1.4509	0.3833	3.23	2.18	3.29	A	0.3756	-2.6482	-1.6968	1.1454
FH	1.7328	1.4648	0.2680	2.97	2.01	3.16	A	0.3884	-4.3872	-2.8015	1.2159
NaH	3.5660	1.8790	1.6870	2.64	3.33	3.72	B	0.0337	0.1320	-0.0394	0.2108
MgH	3.2710	1.6640	1.6070	5.18	3.09	3.92	A	0.0529	0.1844	-0.0695	0.3233
AlH	3.1140	1.5176	1.5964	4.97	3.03	4.13	A	0.0743	0.1883	-0.1054	0.3890
SiH	2.8740	1.3882	1.4858	4.49	2.82	4.34	A	0.1134	0.1330	-0.1686	0.4663
PH	2.7080	1.3238	1.3842	4.16	2.64	4.25	A	0.1590	-0.1142	-0.2222	0.3302
SH	2.5510	1.5482	1.0028	3.86	2.46	4.14	A	0.2128	-0.5663	-0.3732	0.1801
ClH	2.4087	1.6716	0.7371	3.68	2.28	3.99	A	0.2540	-0.7824	-0.6035	0.4247
LiLi	5.0510			2.61	2.61	4.29					
LiBe	5.1662	1.6797	3.4866	3.77	4.59	4.02	A	0.0130	0.0268	-0.0088	0.0439
LiB	4.5000	1.4662	3.0338	1.94	4.49	3.59	B	0.0269	0.0854	-0.0275	0.1404
LiC	3.8000	1.3143	2.4858	1.88	4.07	3.68	B	0.0445	0.2097	-0.0664	0.3424
LiN	3.4000	1.2241	2.1759	1.94	3.65	3.54	B	0.0603	0.3656	-0.1127	0.5910
LiO	3.1840	1.1850	1.9990	1.91	3.54	3.51	B	0.0673	0.4825	-0.1428	0.7881
LiF	2.9550	1.1304	1.8246	1.91	3.12	3.36	B	0.0802	0.7018	-0.1932	1.0882
BeB	4.0000	1.3847	2.6153	4.35	3.89	4.25	B	0.0409	-0.0100	-0.0303	0.0506
BeC	3.5000	1.1819	2.3181	4.17	3.63	4.05	A	0.0580	0.1277	-0.0617	0.2511
BeN	3.2500	1.0999	2.1501	3.65	3.42	3.86	A	0.0758	0.2918	-0.0992	0.4901
BeO	2.5149	0.8944	1.6205	1.50	3.41	3.71	B	0.1842	1.5892	-0.4586	2.5064
BeF	2.5720	0.9268	1.6453	4.58	3.08	3.56	A	0.1535	1.3393	-0.4925	2.3242
BB	3.0050	1.5025	1.5025	3.89	3.89	3.98		0.1250	-0.1983	-0.0998	0.0014
BC	2.6525	0.8898	1.7627	3.89	3.50	3.87	B	0.2037	0.3838		
BN	2.4210	0.8166	1.6044	4.31	3.54	3.74	A	0.3142	0.4378	-1.1563	2.7504
BO	2.2750	0.7765	1.4985	3.95	3.27	3.44	B	0.3194	2.0866	-0.9405	3.9676
BF	2.3910	0.8093	1.5817	4.23	2.99	3.68	A	0.2391	1.5852	-0.9234	3.4319
CC	2.3481			3.45	3.45	3.75					
CN	2.2140	0.7633	1.4507	3.51	3.47	3.48	B	0.4474	0.1547	-0.7565	1.6677
CO	2.1320	0.7228	1.4092	3.77	3.21	3.42	A	0.5101	0.2682	-1.7696	3.8083
CF	2.4020	0.7783	1.6237	3.69	2.96	3.44	A	0.2924	0.6047	-0.7822	2.1681
NN	2.0680	1.0340	1.0340	3.42	3.42	3.42		0.7218	-3.0500	-1.9337	0.8175
NO	2.1747	0.9153	1.2594	3.33	3.14	3.38	A	0.5932	-2.0353	-1.8460	1.2568
NF	2.4890	1.0211	1.4678	3.27	2.88	3.33	A	0.3420	-0.4972	-0.7853	1.0733
OO	2.2820	1.1410	1.1410	3.08	3.08	3.23		0.5513	-1.0127	-1.4730	1.9333
OF	2.4958	1.1698	1.3260	2.94	2.90	3.20	A	0.3692	0.0302	-0.9414	1.9130
FF	2.6800	1.3400	1.3400	2.84	2.84	3.08		0.2945	0.2287	-0.7327	1.6941

[a] Near-Hartree-Fock quality state functions (Cade and Huo 1973, 1974, 1975) are used except for LiBe and BC where 6-311G*//6-311G* is used.

[b] For each system, r_p is the maximum distance perpendicular to the bond axis of a nucleus to the 0.001 au contour of ρ. The letter A or B listed to the immediate right of this value denotes the nucleus of the atom giving the larger r_p value.

Table 1.6.2 Atomic Monopole, Dipole[a] and Quadrupole Moments and Atomic Volumes of Diatomic Molecules.

Sys AB	q(A)	μ(A)	μ(B)	Q_{zz}(A)	Q_{zz}(B)	v(A)	v(B)	v(AB)
HH	0.000	0.095	-0.085	0.759	0.759	60.24	60.24	120.48
LiH	0.912	-0.001	0.389	0.051	1.524	30.53	193.48	224.01
BeH	0.868	1.520	0.571	-2.878	0.885	161.03	137.67	298.70
BH	0.754	1.951	0.493	-1.534	0.352	166.79	95.19	261.98
CH	0.032	0.806	-0.121	-0.008	0.604	169.28	54.61	223.89
NH	-0.323	0.182	-0.176	0.067	0.199	150.14	34.70	184.84
OH	-0.585	-0.225	-0.148	0.065	-0.012	144.43	21.32	165.75
FH	-0.761	-0.453	-0.103	-0.022	-0.078	128.65	12.45	141.10
NaH	0.811	0.018	0.135	0.600	2.529	83.48	189.62	273.10
MgH	0.796	1.701	0.302	-3.159	1.636	255.10	155.18	410.28
AlH	0.825	2.274	0.359	-1.792	0.934	268.18	131.47	399.65
SiH	0.794	1.973	0.427	3.011	1.115	272.52	110.25	382.77
PH	0.578	1.461	0.316	4.800	0.803	251.72	82.44	334.16
SH	0.094	0.587	-0.009	4.445	0.624	249.49	54.76	304.25
ClH	-0.242	-0.007	-0.103	3.666	0.311	231.87	36.97	268.84
LiLi	0.619	0.391	-0.391	0.365	0.365	110.19	110.19	220.38
LiBe	0.464	-0.648	-1.088	1.130	-6.512	161.71	378.98	540.69
LiB	0.761	0.242	1.016	-0.074	-10.646	60.64	326.36	387.00
LiC	0.884	0.044	0.645	-0.040	-4.702	33.57	257.58	291.15
LiN	0.916	0.008	0.408	0.043	-1.721	28.06	204.93	232.99
LiO	0.935	0.010	0.295	0.056	-0.332	26.56	180.34	206.90
LiF	0.938	0.017	0.281	0.061	0.726	25.45	149.30	174.75
BeB	0.438	0.892	0.466	2.732	0.166	234.78	258.41	493.19
BeC	0.853	0.893	0.920	1.333	0.489	184.92	241.82	426.74
BeN	1.236	0.539	1.218	0.801	0.320	124.05	231.63	355.68
BeO	1.694	0.095	1.243	0.110	0.190	32.42	220.08	252.50
BeF	0.945	1.429	0.547	-2.091	0.551	157.06	142.97	300.03
BB	0.000	0.289	-0.289	2.914	2.914	197.51	197.51	395.02
BC	1.041	-1.263	-1.331	0.864	0.536	138.27	204.99	343.26
BN	0.831	2.024	0.544	-1.132	-1.482	160.54	156.08	316.62
BO	1.553	1.219	1.162	-1.075	-0.214	105.48	160.51	265.99
BF	0.934	1.883	0.729	-0.829	0.084	154.99	125.06	280.05
CC	0.000	0.172	-0.172	3.583	3.583	150.20	150.20	300.40
CN	1.123	0.931	0.592	1.513	0.553	104.67	145.90	250.57
CO	1.346	1.701	1.061	-0.463	-0.060	110.18	133.90	244.08
CF	0.780	1.470	0.521	1.087	0.267	125.91	107.65	233.56
NN	0.000	0.590	-0.590	1.492	1.492	115.49	115.49	230.98
NO	0.495	0.990	-0.041	1.594	1.552	117.98	114.84	232.82
NF	0.438	0.876	0.069	1.930	1.205	112.61	98.89	211.50
OO	0.000	0.437	-0.437	1.725	1.725	102.40	102.40	204.80
OF	0.201	0.518	-0.160	1.969	1.553	102.52	96.34	198.86
FF	0.000	0.197	-0.197	1.656	1.656	96.26	96.26	192.52

[a] Directions of the first moments for CO and HF are given in Figure 1.2.5.

Table 1.6.3. Energies of Atoms in Diatomic Molecules.[a]

Sys AB	E(A)	E(B)	E(AB)[b]	Escf	-V/T	Erel(A)[c]	Erel(B)
HH	-0.56681	-0.56681	-1.13382	-1.13363	2.006664	-41.9	-41.9
LiH	-7.38406	-0.62330	-7.98735	-7.98731	1.999500	43.1	-77.4
BeH	-14.38131	-0.77178	-15.15311	-15.15312	2.000250	120.3	-170.6
BH	-24.24362	-0.88788	-25.13150	-25.13137	2.000800	179.1	-243.4
CH	-37.65672	-0.62257	-38.27929	-38.27935	2.000640	20.0	-76.9
NH	-54.48486	-0.49302	-54.97788	-54.97806	2.000570	-52.7	4.4
OH	-75.05461	-0.36609	-75.42070	-75.42083	2.000520	-153.9	84.0
FH	-99.81559	-0.25342	-100.06901	-100.07030	2.000430	-255.0	154.7
NaH	-161.82053	-0.57465	-162.39517	-162.39280	1.999960	24.1	-46.6
MgH	-199.50913	-0.64888	-200.15811	-200.15660	2.000020	66.2	-93.5
AlH	-241.72378	-0.73794	-242.46172	-242.46340	2.000000	85.9	-149.3
SiH	-288.63488	-0.79808	-289.43296	-289.43620	2.000020	137.7	-187.0
PH	-340.51220	-0.78005	-341.29226	-341.29320	2.000070	129.6	-175.7
SH	-397.48442	-0.61527	-398.09968	-398.10150	2.000060	12.8	-72.3
ClH	-459.61614	-0.50064	-460.11677	-460.11030	2.000030	-84.2	-0.4
LiBe	-7.40597	-14.60383	-22.00979	-22.00968	1.999977	16.8	-19.3
LiB	-7.39382	-24.56127	-31.95508	-31.95512	1.999090	24.4	-20.2
LiC	-7.37672	-37.73467	-45.11139	-45.11165	1.998730	35.1	-28.9
LiN	-7.36904	-54.45688	-61.82592	-61.82640	1.998880	40.0	-35.1
LiO	-7.35611	-74.85420	-82.31030	-82.31114	2.000080	49.1	-90.9
LiF	-7.35249	-99.63795	-106.89044	-106.89040	1.999850	50.4	-143.5
BeB	-14.48563	-24.60076	-39.08639	-39.08664	1.999830	54.8	-45.0
BeC	-14.43159	-37.82704	-52.25862	-52.25849	2.000580	88.8	-86.9
BeN	-14.34526	-54.53135	-68.87661	-68.87696	2.002940	142.9	-81.8
BeO	-14.21706	-75.23477	-89.45182	-89.45047	2.001120	223.4	-266.9
BeF	-14.33751	-99.83172	-114.16922	-114.16880	2.000230	147.8	-265.1
BB	-24.54517	-24.54517	-49.09035	-49.09088	1.998890	-10.1	-10.1
BC	-24.13173	-38.18982	-62.32155	-62.32156	2.000160	249.3	-314.5
BN	-24.14386	-54.82325	-78.96711	-78.96701	1.994100	241.7	-265.0
BO	-23.97867	-75.57778	-99.55645	-99.55550	2.000680	345.4	-482.2
BF	-24.10774	-100.05757	-124.16531	-124.16590	2.000410	264.4	-408.8
CN	-37.20466	-55.00901	-92.21368	-92.21342	2.001410	303.7	-381.6
CO	-36.88502	-75.90121	-112.78623	-112.78600	2.001280	504.3	-685.1
CF	-37.24904	-99.96833	-137.21737	-137.21690	1.999600	275.8	-350.8
NN	-54.49588	-54.49588	-108.99176	-108.99280	2.001850	-59.6	-59.6
NO	-54.07897	-75.20561	-129.28458	-129.28370	2.000840	202.0	-248.6
NF	-54.12435	-99.70550	-153.82985	-153.83110	2.000000	173.6	-185.9
OO	-74.83337	-74.83337	-149.66674	-149.66590	2.001630	-15.1	-15.1
OF	-74.66891	-99.52623	-174.19514	-174.19502	1.999840	88.1	-73.4
FF	-99.38513	-99.38513	-198.77026	-198.77010	2.000930	15.2	15.2

[a] All values are in au except the relative energies which are in kcal mol^{-1}.
[b] E(AB) = E(A) + E(B)
[c] $E_{rel}(A) = E(A)_{AB} - E(A)_{A}$.

Table 1.6.4. Classifications of Neutral, Ground-State Diatomic Molecular Charge Distributions

Class I	Class II	Class III	Class IV
LiH ($^1\Sigma$)	BeH ($^2\Sigma$)	BeH ($A^2\pi$)	NO ($^2\pi$)
CH ($^2\pi$)	BH ($^1\Sigma$)	MgH ($A^2\pi$)	NF ($^3\Sigma$)
NH ($^3\Sigma$)	MgH ($^2\Sigma$)		OF ($^2\pi$)
OH ($^2\pi$)	AlH ($^1\Sigma$)		
FH ($^1\Sigma$)	SiH ($^2\pi$)		
NaH ($^1\Sigma$)	PH ($^3\Sigma$)		
SH ($^2\pi$)	LiBe ($^2\Sigma$)		
ClH ($^1\Sigma$)	BeF ($^2\Sigma$)		
LiB ($^1\Sigma$)	BO ($^2\Sigma$)		
LiC ($^2\pi$)	BF ($^1\Sigma$)		
LiN ($^3\Sigma$)	CN ($^2\Sigma$)		
LiO ($^2\pi$)	CO ($^1\Sigma$)		
LiF ($^1\Sigma$)	CF ($^2\pi$)		
BeB ($^2\pi$)			
BeC ($^3\Sigma$)			
BeN ($^2\pi$)			
BeO ($^1\Sigma$)			
BC ($^2\pi$)			
BN ($^3\Sigma$)			

Table 1.6.5. Comparison of Charge and Energies of H atoms in AH and AH_n Systems

Systems	N(H)	ΔN(H)	E(H)	ΔE(H)
BeH;BeH_2	1.868	-0.007	-484	+6
BH;BH_3	1.754	-0.042	-557	+7
CH;CH_4	1.054	+0.008	-407	0
NH;NH_3	0.677	-0.041	-310	+8
OH;OH_2	0.415	-0.022	-230	+9
HgH;HgH_2	1.786	+0.024	-406	-2
AlH;AlH_3	1.825	-0.031	-468	+3
SiH;SiH_4	1.760	-0.037	-509	-3
PH;PH_3	1.629	-0.015	-522	-2
SH;SH_2	1.094	+0.011	-386	-4

a Populations are in au and energies are in kcal mol^{-1}. $\Delta N(H) = N(H)_{AH_n} - N(H)_{AH}$. $\Delta E(H) = E(H)_{AH_n} - E(H)_{AH}$ and E(H) = -314 kcal mol^{-1}.

Table 1.6.6. Electronegativity Schemes for Diatomic Hydrides.

	GAUSSIAN[a]		SLATER[b]		ALLRED[c]	BADER-BEDDALL[d]
Sys	F_A	x_A	F_A	x_A	x	x_A
AH						
LiH	14.08	1.00	13.61	1.00	1.00	-0.91
BeH	3.27	1.44	2.97	1.47	1.57	-0.87
BH	1.07	1.90	1.03	1.92	2.04	-0.75
CH	0.31	2.60	0.32	2.58	2.55	-0.03
NH	0.16	3.08	0.16	3.07	3.04	0.32
OH	0.08	3.62	0.09	3.53	3.44	0.59
FH	0.06	4.00	0.06	4.00	4.00	0.76
NaH	14.18	1.00	14.04	0.99	0.93	-0.81
MgH	4.72	1.32	4.64	1.31	1.31	-0.80
AlH	2.28	1.58	2.30	1.57	1.61	-0.83
SiH	1.15	1.87	1.14	1.87	1.90	-0.79
PH	0.63	2.17	0.64	2.17	2.19	-0.58
SH	0.29	2.64	0.31	2.61	2.58	-0.09
ClH	0.16	3.05	0.17	3.02	3.16	0.24
KH	14.41	0.99			0.82	
CaH	4.35	1.34			1.32	
GaH	1.51	1.75			1.80	
GeH	0.90	1.99			2.01	
AsH	0.59	2.21			2.18	
SeH	0.39	2.46			2.55	
BrH	0.25	2.75			2.96	

[a] Boyd and Edgecombe 1988.
[b] Present work using Slater basis set as opposed to the Gaussian basis set of [a].
[c] Empirical values: Allred 1961.
[d] Bader and Beddall 1973.

Table 1.6.7 Group Electronegativities.[a]

group	x_{group}	N(H)[b]
-MgH	1.33	1.81
-BeH	1.47	1.86
-AlH_2	1.62	1.79
-SiH_3	1.91	1.74
-BH_2	1.93	1.71
-PH_2	2.17	1.63
-CH_2CH_3	2.56	1.08
-CH_3	2.56	1.06
-CH_2OH	2.59	1.05
-CHO	2.60	1.00
-$CHCH_2$	2.61	1.04
-SH	2.63	1.34
-COOH	2.66	0.97
-CCH	2.66	0.88
-CN	2.69	0.78
-NH_2	3.10	0.64
-OH	3.64	0.39
-OCH3	3.70	0.39

[a] The x values are relative to hydrogen and are calculated using the Boyd and Edgecombe method (1988).
[b] The electron population of H is calculated using the theory of atoms in molecules.

Table 1.6.8. Predicted Electron Populations of atom A, Nm(A), Using Bader and Beddall (1973) Method.[a]

Sys AB	Nm(A)	N(A)	%err
LiB	2.842	2.239	26.9
LiC	2.120	2.116	0.2
LiN	2.000	2.084	4.0
LiO	2.000	2.065	3.1
LiF	2.000	2.062	3.0
BeB	3.772	3.562	5.9
BeC	2.328	3.147	26.0
BeN	1.618	2.764	41.5
BeO	1.094	2.306	52.6
BeF	3.000	3.055	1.8
BC	2.834	3.959	28.4
BN	1.769	4.169	57.6
BO	2.322	3.447	32.6
BF	4.000	4.066	1.6
CN	4.935	4.877	1.2
CO	4.766	4.654	2.4
CF	5.207	5.220	0.2
NO	6.476	6.505	0.4
NF	6.562	6.562	0.0
OF	7.824	7.799	0.3
PN	12.297	13.259	7.3
MgO	9.238	10.588	12.8
SiO	11.242	12.383	9.2
NaF	10.000	10.057	0.6
AlF	12.000	12.027	0.2
LiCl	2.000	2.070	3.4
NaCl	10.000	10.089	0.9

[a] State functions using Slater basis sets from Cade and Huo 1973,1974,1975 and McClean and Yoshimine 1968.

CHAPTER 2

THE NATURE, ENERGETICS AND MECHANISM OF HYDROGEN-BOND FORMATION

An enormous amount of research has been directed at the phenomenon of hydrogen bonding because of the importance of hydrogen bonds in nature (reviews include Dyke 1984, Schuster et al 1976, Joesten and Schaad 1974, Vinogradov and Linnell 1971, Pimental and McClellan 1960). In general, the structure and properties of condensed phases are dependent on interactions involving hydrogen bond formation. The structure and solvation properties of macromolecules in biological systems (proteins and nucleic acids for example) are greatly influenced by hydrogen bonding. Atmospheric processes such as the transmission of electromagnetic radiation can be affected by hydrogen-bonded molecules (Carlon and Harden 1980).

Latimer and Rodebush (1920), working in Dr. G. N. Lewis's laboratory, were the first to propose a hydrogen bond: "Water shows tendencies both to add and give up hydrogen, which are nearly balanced. Then a free pair of electrons on one water molecule might be able to exert sufficient force on a hydrogen held by a pair of electrons on another water molecule to bind the two water molecules together. Indeed the liquid may be made up of large aggregates of molecules, continually breaking up and reforming under the influence of thermal agitation. Such an explanation amounts to saying that the hydrogen nucleus held between 2 octets constitutes a weak "bond"." From these observations the definition of the hydrogen bond was developed and

extended and today is given as follows: If a covalently bonded hydrogen atom forms a second bond to another atom, then the second bond is referred to as a hydrogen bond (abbreviated H-bond). Using the notation A-H···B (where A and B are atoms with electronegativity usually greater than that of H), A-H is termed the covalent or normal bond and H···B is termed the weaker or hydrogen bond (Schuster et al 1976). The theory of atoms in molecules allows us to gain a greater understanding of the hydrogen bond as the theory precisely defines the term "bond" and the interactions between atoms. Thus, we rephrase the definition as follows: If a hydrogen atom is bonded to atom A through a shared interaction and is also bonded to atom B through a closed shell interaction, then a hydrogen bond exists between H and B. The notation AH-B where the hyphen represent the hydrogen bond path in the molecular graphs (Figure 2.1.1) is used hereafter. The AH bond path length is less than the H-B bond path length and the value of ρ at the AH bond critical point, in general, is an order of magnitude greater than the value of ρ at the HB bond critical point. To a first approximation then, the AH bond will be stronger (have a greater bond energy) than the HB bond.

As demonstrated in this chapter, the theory of atoms in molecules enables us to describe the nature, energetics and mechanism of hydrogen bond formation and in so doing, account for experimental observations of the properties of hydrogen-bonded complexes. Before we describe the application of this relatively recent theory (Bader 1985, Bader and Nguyen-Dang 1981, Bader et al 1981) to hydrogen-bonded complexes, it is appropriate to briefly review other theoretical

approaches that have been used to study these systems. Pauling (1944) was the first to develop a simple electrostatic model that could qualitatively reproduce trends in observed H-bond energies. Tsubomura (1954) and Coulson (1957) were the first to use perturbation theory to estimate the contribution of different energy components to the H-bond energy. This theory was later refined and is still the most direct way to obtain estimates of the electrostatic, exchange, charge-transfer, polarization and dispersion energy contributions (Basilevsky and Berenfeld 1972, Daudey 1974, Fujimoto et al 1974, Hayes et al 1984). A widely used alternative involves the decomposition of the interaction energy using the Hartree-Fock SCF formalism, as developed by Morokuma and others (Morokuma 1971, Kitaura and Morokuma 1976). Kollman has used this analysis to rationalize geometries and interaction energies of a wide variety of H-bonded complexes (Kollman 1977). However, both the virial theorem and Pauli exclusion principle are violated in this procedure (Janda et al 1977). Mulliken populations (Kollman 1977, Kollman et al 1974, Kollman and Allen 1971), distributed and point multipole analyses (Hurst et al 1986, Kollman 1977, Kollman et al 1974, Kollman and Allen 1971), density difference maps (Benzel and Dykstra 1983), localized molecular orbital (Rudenberg 1975) and HOMO-LUMO descriptions (Janda et al 1977), and charge transfers calculated using the Townes-Dailey model (Legon et al 1981, Townes and Dailey 1948) have also been used in attempts to further the understanding of hydrogen bonding.

Elaborating on the energy decomposition techniques, it is claimed that progress in interpreting hydrogen bonding has been made by

partitioning the hydrogen bond energy into a term arising from the unrelaxed reactants and consisting of the classical electrostatic interaction, quantum mechanical exchange interaction, and a term reflecting the relaxation of the reactants due to intramolecular polarization and intermolecular charge transfer (Krijn and Fiel 1988). However, such an energy decomposition is not unique since it depends on the orbital orthogonalization scheme used. For example, the decomposition method of Morokuma (1971) yields the attractive electrostatic term to be dominant and the smaller repulsive exchange contribution to be mainly cancelled by the relaxation terms, whereas the natural bond orbital analysis of Reed et al (1988) yields the charge transfer term to be dominant. According to Krijn and Fiel (1988), an approach that has drawn little attention until recently, is to discuss hydrogen bonding in terms of some experimentally observable quantity like the electron density distribution. Interpreting chemical bonding in terms of ρ has the advantage of not being intrinsically dependent on certain models utilized for its definition as, for example, many of the current concepts like σ,π bonding and covalency are. Further, according to DFT, ρ is considered to be the fundamental variable to describe the ground state.

No models are employed in the present work. Instead, the theory of atoms in molecules is used to analyze ρ. In Section 2.1, this theory is used to study the nature, mechanics and energetics of gas-phase intermolecular hydrogen-bonded complexes of the type BASE-HF (where BASE = OC, SC, N_2, HCN, H_3N, O_3, SCO, CO_2, N_2O, SO_2, H_2CO, H_2O, HF, H_3P, H_2S, N_2S, H_2CS and HCl). A quantitative description of the

electron redistribution and changes in atomic properties, including electron populations, energies, volumes and moments upon H-bond formation are given by the theory, information which in turn provides a qualitative understanding of the hydrogen bond. A hydrogen bond results from the interaction of two closed-shell systems and the theory quantifies the concept of the mutual penetration of the van der Waals envelopes of the acid and base molecules. The extent of this penetration and the factors which govern it are of great importance in determining the strength of the interaction.

The effects of basis set superposition error and electron correlation are also discussed in this section. In addition, a comparison between BASE-HCl and BASE-HF complexes is made.

In Section 2.2, changes in atomic properties accompanying the formation of hydrogen bonds in the homo and hetero dimers of water and ammonia and in the corresponding protonated species are examined. A water trimer is also studied.

In Section 2.3 the theory is applied to a study of the electron redistribution of formamide upon dimerization to form both cyclic and open H-bonded structures. An important factor governing the changes in the relative stabilities of the atoms on forming the dimers are the opposing flows of σ and π density through conjugated NCO fragments, as measured by the shift in the electron populations into or out of the plane of the nuclei over each of the atomic basins and by the changes in the quadropole moments and ellipticities of the atomic electron distributions.

Section 2.4 deals with the OH-O bonds present in the diformate

anion, hydrated lithium hydroxide and hydrated lithium formate. The H-O hydrogen bond lengths in these complexes and those of Section 2.2 range in values from long to short and the overall trends in the properties of these complexes are discussed.

Section 2.5 examines the effects of a crystal environment on the charge distributions of the complexes of the previous section. The crystal environment is modelled as a set of point charges where the charges are obtained from the theory of atoms in molecules.

2.1 BASE-HF COMPLEXES

Progress in the development of pulsed molecular beam techniques has made it possible to spectroscopically characterize weak gas-phase hydrogen-bonded complexes of the type BASE-HF. A recent review of the experimental procedure has been given by Legon and Millen (1988). These complexes have importance in atmospheric chemistry (Sapse 1983) and femto and pico second chemistry (Scherer et al 1987). The change in the charge distributions of the isolated reactants upon BASE-HF hydrogen bond formation is important from our standpoint as these changes explain experimental results and predict what will occur for those BASE-HF complexes not yet characterized spectroscopically.

Geometries, Structures and Energies of BASE-HF Complexes

Seventy percent of the BASE-HF complexes studied in this work have been characterized experimentally. Of these, the dissociation energies have been measured only for the complexes of HF with HCN, HF and H_2O. To supplement this information, ab initio SCF calculations are performed for the entire set of complexes.

Full geometry optimizations using the 6-31G** basis set have been performed and, in general, they are in good agreement with experiment (Tables 2.1.1 and 2.1.2 and the molecular graphs displayed in Figure 2.1.1). The optimized AB separation (where A is the halide of the acid and B is the base atom participating in the hydrogen bond) is an overestimation of the experimental value in all cases except H_3N

-HF, HF-HF, and ClH-FH where it is a slight underestimation. Typical of 6-31G** calculations, the overestimates range between two and seven percent and are larger for the weaker complexes (Boyd and Choi 1986, 1985). The CA, NA and OA optimized separations range from 3.0 to 3.3, 2.8 to 3.2 and 2.7 to 3.0 A respectively. Considering the floppiness of the weak complexes, the calculated H approach angles to the base (where H denotes the hydrogen-bonded hydrogen) do not differ significantly from experiment with the largest deviation being less than 15° for HF-HF. Most experimental interpretations of rotational spectra assume at least a nearly linear hydrogen bond angle (within 10°) and the theoretical calculations of the experimentally studied complexes agree with this with the exceptions of NNO-HF, H_2CO-HF and HF-HF.

In the interpretation of the experimental spectra it is also assumed that the base geometry will remain relatively unchanged on complex formation. The theoretical results are in agreement with this assumption with the largest change being only 0.008 A in the CS bond of SCO-HF (Legon and Millen 1986). In the systems not yet studied by experiment, the largest change is a decrease of 0.010 A in the CS bond of SC-HF. The base angles change by no more than 1.2°.

Legon and Millen (1986) have calculated the HF bond length increase, δr, from hyperfine coupling constants and have shown in general δr to increase with increasing strength of the hydrogen bond. The 6-31G** δr values exhibit this trend roughly though they are underestimations of the experimental values by as much as fifty percent (Table 2.1.1).

For the hydrogen-bonded complexes, the SCF calculated values of the dissociation energies D_e,

$$D_e = E_{SCF}(BASE) + E_{SCF}(HA) - E_{SCF}(BASE\text{-}HA) \qquad [2.1.1]$$

are given in Table 2.1.1. Scheme I refers to RHF/6-31G**//6-31G** calculations while Scheme II refers to RHF/6-311++G**//6-31G** calculations. The larger basis set (6-311++G**) yields E_{SCF} values larger in magnitude than those calculated using Scheme I. The magnitude of the V/T ratio is smaller for Scheme II. The D_e values range from 6.3 (6.9) kJ mol^{-1} for NN-HF to 49.4 (48.2) kJ mol^{-1} for H_3N-HF (the values in parantheses are Scheme II values). Scheme II does not necessarily give better agreement with experimental dissociation energies than Scheme I.

Secondary minimum energy structures of some of the complexes between BASE and HF are given in Table 2.1.1. In agreement with experiment, Scheme II predicts the cis complex of SO_2 with HF to be the global minimum, predicting it to be 6.5 kJ mol^{-1} more stable than the trans isomer. Scheme I, on the other hand, predicts the trans complex to be the global minimum, 0.8 kJ mol^{-1} more stable than the cis isomer. For the remaining complexes, the predictions of the primary minimum energy structures are the same for Scheme I and Scheme II.

Scheme I (or Scheme II) calculations predict hydrogen fluoride to be the base in the complex between HCl and HF and this is experimentally observed (Janda et al 1977). These same calculations predict that the complex formed between NNS and HF is more stable if it is not hydrogen-bonded (13 of Figure 2.1.1). In fact, the theory of atoms in molecules finds that in the most stable structure F is bonded

to both the central N and S as well as to H. The linear SNN-HF complex is less stable than structure 13 by 11.3 (7.5) kJ mol^{-1}. The H_2CS-HF complex is found to have two hydrogen bonds (14 of Figure 2.1.1) and this accounts for its relatively large stability. Linear HCP-HF is 7.1 (6.7) kJ mol^{-1} less stable than the T-shaped structure 2. Theoretical calculations of the protonation of HCP also favour attack at the carbon (Lohr et al 1984). From previous theoretical calculations (Sapse 1983), the T-shaped NN-HF complex has been found to be less stable than the linear one. The only energy minimum structures we could find for the complexes of OCO and H_2CS with HF were 7 and 14 respectively.

On further examination of Table 2.1.1 one notes that CO-HF is 2.9 (1.1) kJ mol^{-1} less stable than OC-HF. Both of the bent OCO-HF and SCO-HF complexes are only slightly less stable than their linear counterparts and to within 0.1 kJ mol^{-1} have the same D_e values. The H_a approach angle of 164.8° for OCO-HF falls within the 30° range estimated for HF libration about the oxygen in the experimental structure. An analysis of $\nabla^2\rho$ will explain why the energy differences are so small and why the H_a approach angle can be so broad in these cases (Chapter 3).

Test calculations using geometries optimized at the 6-311++G** basis set lower the Scheme II energy by negligible amounts (0.04 kJ mol^{-1}) and have only a small effect on the geometry (bond lengths change by at most 0.006 au). This observation and those of correct structure predictions and smaller virial ratios leads to the decision to use Scheme II exclusively in all remaining calculations in this section (Tables 2.1.3 - 2.1.14 inclusive and Tables 2.1.18 - 2.1.21

inclusive). For consistency, only weak intermolecular, single hydrogen-bonded complexes are examined in the remainder of this section. Dykstra (1988) defines a weak hydrogen-bonded complex as one in which D_e is < 50 kJ mol^{-1}. Thus, all the complexes studied in this section are weak.

The optimized hydrogen bond length B-H does not correlate with D_e, a result hardly surprising considering the diverse set of hydrogen bonds encountered here. Within each group of similar H-bonds, however, in general a decrease in H-bond length with increasing D_e is observed. This observation has also been made for RCN-HA (A=F,Cl) (Boyd and Choi 1986, 1985) and OH-O systems (Section 2.4).

Basis Set Superposition Error

For a given basis, the calculated value of D_e is too large because of the basis set superposition error (BSSE) [Hobza and Zahradnik 1988, Mo' et al 1988, Hobza and Sandorfy 1987, Mayer 1987, Szczesniak and Scheiner 1986, Collins and Gallup 1986, Frisch et al 1986, Gutowski et al 1986, Schwenke and Truhlar 1985, Bachrach and Streitweiser 1984, Kolos 1979, Boys and Bernardi 1970). This error arises from the fact that the basis set used to describe each reactant is larger for the complex than for the isolated molecule because in the complex use can be made of the basis functions centred on the other reactant.

In the function counterpoise method used to correct for BSSE (Boys and Bernardi 1970), the energies of the separated reactants are calculated with the full complement of basis functions used in the

calculation of the complex. To find the proper description of isolated HF for example, means that in addition to the basis functions centred on the acid nuclei, basis functions of the base molecule, called ghost orbitals, are centred at locations relative to the nuclei in HF that they have in the complex.

The full counterpoise corrections to the total energy of the reactants in HF-HF and H_3N-HF are given in Table 2.1.3. It has been argued that the full counterpoise correction overestimates the error and that procedures which use only the polarizing functions or the virtual orbitals for the ghost orbitals reduce the correction [Szczesniak and Scheiner 1986, Collins and Gallup 1986, Frisch et al 1986, Gutowski et al 1986, Schwenke and Truhlar 1985, Bachrach and Streitweiser 1984). Thus the results of Table 2.1.3 are upper bounds to BSSE. In the strongest of the BASE-HF complexes studied, H_3N-HF, for which the correction will be relatively large, the full counterpoise correction to the energies of the base and acid are 2.3 and 1.0 kJ mol^{-1} respectively, compared to the calculated D_e of 46.2 kJ mol^{-1}. In the weaker complex HF-HF the corrections are even smaller. It has been found that the addition of diffuse functions to a basis set can be more important than the addition of polarization functions in the reduction of BSSE (Frisch et al 1986, Schwenke and Truhlar 1985, Bachrach and Streitweiser 1984). The 6-311++G** set, in addition to the set of polarizing functions on each atom, has even larger sets of diffuse functions. Because of this feature the energy corrections are quite small and they will not influence the trends in the calculated values of D_e.

Bachrach and Streitweiser (1884) examined the effect of BSSE on the electron density of the isolated reactants and found the corrections to be small when the basis set contained diffuse functions. In the present work the effects of BSSE on the electron density of the reactants in HF-HF and H_3N-HF are examined (Table 2.1.3). The corrections to the average electron population of an atom Ω, $N(\Omega)$ are small as are the changes in its first moment $\mu(\Omega)$ and volume $v(\Omega)$. The largest of these changes are for nitrogen in H_3N. The values of the charge density and Laplacian of the charge density at the bond critical points $\rho(r_c)$ and $\nabla^2\rho(r_c)$ also change by small amounts. Thus the charge densities calculated from the 6-311++G** basis set are relatively insensitive to the basis set superposition error.

BSSE is important when examining interaction energies in large biological systems where minimal basis sets must be used (Hobza and Sandorfy 1987). Attempts to improve corrections to BSSE in these cases have been made (Mayer 1987).

Topological Analysis of ρ for BASE-HF Complexes

The locations of the (3,-1) critical points in the charge density of the complexes are given in Figure 2.1.1. The values of ρ and of its curvatures at the bond critical point of the hydrogen bond and of the HF bond in the acid are listed in Tables 2.1.4 and 2.1.5.

The values of the charge density at a hydrogen bond critical point, the values listed under $\rho(r_b)$ in Table 2.1.4 are, in general, at least an order of magnitude smaller than those found in shared interactions. These values are typical of closed-shell interactions,

and they are indicative of a relative depletion of charge in the interatomic surface - a consequence of the requirements of the Pauli exclusion principle. In a closed-shell interaction there is little shared concentration of charge. Instead, the charge concentrations and the corresponding regions of excess potential energy are separately localized in the basins of the neighbouring atoms. As a result of this localization, the values of $\nabla^2\rho(r_b)$ are positive and, in general, smaller for the weaker complexes. To illustrate these features, the Laplacian distribution for OC-HF is presented (Figure 2.1.2).

Within each set of H-bonded complexes, where the base atom B is C, N or O, D_e increases with increasing values of $\rho(r_b)$ (with the exception of OOO-HF). Boyd and Choi (1985, 1986) in a study of RCN-HA systems found a strong correlation between $\rho(r_b)$ (and $\nabla^2\rho(r_b)$) and D_e. We find a roughly linear relationship between $\rho(r_b)$ and D_e with the greater scatter being understandable in view of the diverse range of H-bonds studied here (Figure 2.1.3a). Within each set of H-bonds, $\nabla^2\rho(r_b)$ and the magnitudes of the curvatures of ρ increase with D_e.

The values of $\rho(r_b)$ for the secondary structures CO-HF, ONN-HF, and HCl-HF are 0.0095, 0.0089 and 0.0072 au respectively. These values are significantly smaller than those of the corresponding primary structures. The values of $\rho(r_b)$ for the bent secondary structures OCO-HF and SCO-HF are almost identical to those of the primary linear structures and this observation helps explain the very small difference in D_e between the corresponding primary and secondary structures.

The charge distributions of OC, HF and of their hydrogen-bonded complex OC-HF are illustrated in Figure 2.1.2. The positions and

shapes of the interatomic surfaces are also indicated. The surface resulting from the approach of the base atom B to the hydrogen is relatively flat, a characteristic feature of a hydrogen bond interatomic surface. Also indicated for the complex are the bonded radii r_B (shown as r_C) and r_H. These radii are much larger than the bonded radii of a normal B-H bond. The bonded radii for the hydrogen-bonded complexes decrease as D_e increases within each set. The value of r_H is in most cases, only half as large as the value of r_B. The nonbonded radii of the B and H atoms (r_B^o and r_H^o) of the reactants are also indicated in the figure and listed in Table 2.1.6.

The nonbonded radii decrease in value upon the formation of the new interatomic surface to the values of the bonded radii r_B and r_H listed in Table 2.1.4. These changes in radii are listed under the headings $|\Delta r_B^o|$ and $|\Delta r_H^o|$. They provide a direct measure of the extent to which the separate van der Waals envelopes are penetrated upon formation of the hydrogen bond. The sum $|\Delta r_B^o + \Delta r_H^o|$ increases as D_e increases (Figure 2.1.3b). While Figure 2.1.3b displays the general trend between penetration and D_e, the correlation is best within each separate series of molecules where B is C, N or O because of the differing nonbonded radii of these B atoms. In general, the nonbonded charge density on H is penetrated to a lesser extent than is that on B, the exceptions being OCO-HF, SCO-HF and ClH-FH. The third row atoms P, S and Cl are least effective in penetrating the nonbonded density of H. The most effective atoms are N in H_3N and O in H_2CO and H_2O. For the second row atoms, the largest values of $|\Delta r_B^o|$ correlate with the largest values of $|\Delta r_H^o|$. The third row atoms, while less effective in

penetrating H, are themselves relatively soft towards the approach of H. Hydrogen fluoride is a hard acid as a consequence of the contraction of the charge density towards the F nucleus, as reflected in the large extent of charge transfer present in this molecule (Table 2.1.2) and in its relatively small value of r_H^o = 2.04 au (Table 2.1.6). The data in Table 2.1.4 show that the base atom F penetrates H of the softer acid HCl, whose nonbonded radius equals 2.42 au, to a greater extent than it does H of HF. The pair of complexes, HCl-HF and HF-HCl, allow for a comparison of soft and hard bases interacting with hard and soft acids, respectively. The penetration of the soft acid H is more than twice that of the hard H, while the base atoms are penetrated equally by the hard and soft H atoms. The result is that HF-HCl is the energetically favoured complex. The concept of mutual penetration has also been used in a discussion of $[HCN\text{-}NgF]^+$ complexation (where Ng = Kr, Xe) (MacDougall et al 1989).

The secondary structures CO-HF and ONN-HF have mutual penetrations both of only 1.2 au compared to 1.5 and 1.4 au for the respective primary structures. Thus, the concept of penetration can be used to predict which isomer will be more stable. The bent secondary structures OCO-HF and SCO-HF have mutual penetration values the same as for the primary structures and their D_e values are virtually identical.

Also listed in Table 2.1.4 under the headings $\rho^o(r_B)$ and $\rho^o(r_H)$ are the values of ρ in the isolated base and acid molecules at the point of penetration, i.e., at the position determined by the vector corresponding to the bonded radius r_B or r_H. The sum of $\rho^o(r_B)$ and $\rho^o(r_H)$ is close in value to $\rho(r_b)$, the value of the charge density at

the hydrogen bond critical point, being either equal to it to within a few per cent or else slightly smaller in value. This analysis yields a picture of hydrogen bond formation which corresponds to the mutual penetration of the outer diffuse nonbonded densities of the base atom B and of H, with the final density at the bond critical point being equal to or slightly greater than the sum of the unperturbed densities. Unlike a shared interaction, there is not a large increase in charge density at the bond critical point and in the interatomic surface relative to the unperturbed densities. The final density is instead determined primarily by the extent of penetration - the greater the penetration the larger the value of $\rho(\mathbf{r}_b)$ and the stronger the resulting hydrogen bond. To obtain bonds with $D_e > 25$ kJ mol^{-1}, the van der Waals envelope of the H atom must be penetrated by approximately 1 au and the van der Waals envelope of the B atom by a still larger amount. For these penetrations both of the unperturbed densities are in excess of 0.01 au.

The changes induced in the charge distribution of the HF bond are monitored by examining the corresponding changes in the properties of its bond critical point (denoted by the position vector $\mathbf{r}_a$; Table 2.1.5). The formation of each complex results in a decrease in the value of $\rho(\mathbf{r}_a)$ relative to its value of 0.3923 au in the HF monomer (i.e., $\Delta\rho(\mathbf{r}_a)$ is negative), indicating that charge density is removed from the HF bond. Figure 2.1.3c shows that $\rho(\mathbf{r}_a)$ decreases linearly with increasing D_e. These data provide direct evidence that the HF bond is weakened through a loss of charge density upon formation of a hydrogen bond, a result in accord with the increase in length and

decrease in stretching frequency of the AH bond of the acid which is observed to accompany the formation of a hydrogen bond (Legon and Millen 1986, Schuster et al 1976). The value of $\nabla^2\rho(r_a)$ is -3.3685 au for the HF monomer, the negative sign implying a shared interaction. Upon complex formation, the curvatures both perpendicular and parallel to the H-F bond path at r_a decrease in magnitude as D_e increases. This is in contrast to the three curvatures at r_b which all increase in magnitude as D_e increases. The distance from r_a to the proton, the bonded radius r_H, decreases with increasing D_e. Since the HF bond length increases upon complex formation, the bonded radius r_F in general increases with increasing D_e. Thus the weakening and lengthening of the HF bond and the strengthening and shortening of the hydrogen bond as D_e is increased, are reflected in the properties of the charge density at the corresponding bond critical points.

Atomic Properties

The atomic properties $N(\Omega)$, $N_\sigma(\Omega)$, $N_\pi(\Omega)$, $q(\Omega)$, $E(\Omega)$, $V_A(\Omega)$, $V_R(\Omega)$, $V_C(\Omega)$, $\mu(\Omega)$ and $Q(\Omega)$ and their changes upon H-bond formation are described in this section. Because the virial correction factor $|V/T + 1|$ differs widely between systems (Tables 2.1.1 and 2.1.2) the atomic energies between the reactants and complexes cannot be compared in every case. There are however, two systems O_3-HF and SCO-HF where the correction factors are similar enough to permit a meaningful comparison of the changes in the atomic energies on complex formation. Also, the calculated $(V/T + 1)$ ratios correct the energy of a hydrogen atom by less than 1 kJ mol^{-1} and the difference between the largest and

smallest of these corrections amounts to only 0.5 kJ mol^{-1}. Thus the energies of the hydrogen atoms may be compared throughout the complete set of molecules. Only the overall trends in the changes in the total energies of the base and acid molecules in forming the complex, as listed in Table 2.1.7, are discussed.

Isolated Reactants

Table 2.1.8 lists $N(\Omega)$, $|\mu(\Omega)|$ and $v(\Omega)$ for the atoms in the isolated reactants. Quadropole moments for the reactants which form linear BASE-HF complexes are also given ($Q_{zz}(\Omega) = -(1/2)(Q_{xx}(\Omega) + Q_{yy}(\Omega))$. Molecular graphs of the reactants showing the values of $q(\Omega)$ and the directions and magnitudes of $\mu(\Omega)$ have been previously given in Figure 1.2.5. In general, because of the fields created by the transfer of charge from one atom to another, the charge distributions of the atoms become polarized in a direction counter to the direction of charge transfer (Figures 1.2.5 and 2.1.2). In isolated HF for example, 0.75e are transferred from H to F. The fluorine, responding to the net positive electric field exerted upon it by hydrogen, polarizes towards its neighbour, while the latter atom polarizes in the same direction, away from F, in response to the negative field emanating from F.

These atomic moments are essential to the prediction and understanding of molecular dipole moments and their change upon nuclear displacements (Bader et al 1987b). When the donor atom possesses relatively loosely bound, nonbonded charge density, such as C in OC or P or S in their hydrides, the atomic moment can become quite large in

magnitude. This back polarization of the nonbonded density resulting from the charge transfer field is reflected in the values of the nonbonded radii of these atoms. The nonbonded radius of C in OC for example, is larger than the atomic radius of the free C atom by 0.2 au. The large atomic moments on the atoms in OC, particularly that for C accounts for the near zero value for the dipole moment observed for this molecule in spite of a considerable degree of charge transfer (Section 1.5). The value of $|\mu(P)|$ in H_3P is the largest of the atomic moments found in this work. The directions of the dipole moments of H_3P and H_2S are determined by atomic rather than charge transfer moments.

There are only a few exceptions to the rule that the atoms are polarized in a direction counter to the direction of charge transfer. In H_3N the acceptor atom has relatively loosely bound nonbonded density (the N lone pair) and its contribution to the atomic moment of N opposes that arising from the charge transfer field effect. As a result, $\mu(N)$ is small in magnitude and directed away from the hydrogens. (Its value is one-third the magnitude of $|\mu(N)|$ for N in N_2 where there is no charge transfer field opposing the polarization of the nonbonded density.) In contrast, $\mu(O)$ in H_2O is directed towards the hydrogens as determined by the field effect because the nonbonded density on oxygen is more tightly bound and is not concentrated along the axis of the dipole.

In CO_2 only a small amount of charge is transferred from the central to the terminal oxygens and the positive field exerted by this atom is of insufficient strength to counter the moment arising from the

nonbonded density on the terminal oxygens (Figure 1.2.5). The O in NNO, while polarized outwards, is not an exception since both it and the neighbouring nitrogen have net negative charges and are consequently polarized away from one another. The charge density of hydrogen in HCl is polarized counter to the direction of charge transfer but the moment of Cl is oppositely directed. The value of $|\mu(Cl)|$ is however, extremely small, being the smallest of all the nonzero moments listed here.

As a result of these polarization effects, the base atom B that participates in hydrogen bonding is initially polarized away from the incoming hydrogen H of the acid in SC, HCN, SCO, OCO, OSO, H_2CO, H_2O and HF while in the remaining base molecules it is initially polarized towards H.

Changes in Atomic Properties on Hydrogen-Bond Formation

The changes in the populations, energies and volumes of the acid and base molecules upon hydrogen bond formation are given in Table 2.1.7 and the corresponding changes in these same properties, excluding the energies, are given in Table 2.1.9 for the individual atoms.

In all cases there is a transfer of charge from the base to the acid, HF, in agreement with Lewis' generalized definition of an acid and a base as an electron acceptor and donor, respectively. The strongest of the complexes studied here, H_3N-HF, has the greatest number of electrons transferred (0.046e) while the weakest complex, NN-HF has among the least (0.005e). The former complex exhibits the greatest degree of interpenetration of the van der Waals envelopes of the acid and base molecules, and the latter among the least.

The magnitude of the transfer of charge from base to acid is relatively small compared to the changes in the individual atomic charges (Table 2.1.9). There is therefore, a considerable redistribution of charge within the acid and the base. A consequence of this redistribution is a loss of electronic charge from the "tail" of the base (the X group) and a comparable gain in negative charge by the "head" of the acid (the F of HF). For example, in H_3N-HF, 0.078e are lost by X and 0.066e are gained by F. As a result of this charge transfer, across the length of the complex, the dipole moment of the complex is greater than the vector sum of the moments of the isolated reactants, an effect experimentally observed and termed "dipole moment enhancement" (Legon and Millen 1986).

As anticipated on the basis of the above discussion of the decreases in nonbonded radii of B and H, the volumes of these atoms decrease on hydrogen bond formation (Figure 2.1.2). In fact, there is an overall decrease in volume for the entire base fragment and where B is a second-row atom, for the entire acid fragment as well (Table 2.1.7). There is a rough correlation between the decrease in volume upon complexation and increasing D_e.

In general, the acid is stabilized (ΔE(acid) is negative) except when the base contains third-row atoms P, S or Cl. The base is stabilized when B is a third-row atom and in all other cases with the exceptions of OC, NN, HCN, OCO, NNO and H_2CO.

The most important trends are to be found in the changes of the properties of the B, H and F atoms. The changes in the atomic properties of the acid HF are considered first. Fluorine gains charge in all cases, in amounts ranging from 0.012e for the weakest complex NN-HF to 0.066e for the strongest complex H_3N-HF. It acquires charge not only from the base, but also from H since the bond critical point in HF shifts closer to the proton upon complexation (Table 2.1.5). H loses charge in all cases (except in H_3P-HF where $\Delta N(H) \approx 0$) in amounts ranging from 0.002 to 0.024e. In all complexes, the charge gained by F is greater than the charge lost by H and, therefore, ΔN(acid) increases.

The decrease in v(H) ranges between 1.0 and 5.8 au. The increase in v(F) ranges between 0.2 and 3.8 au. v(H) decreases mainly because of the creation of the B-H interatomic surface which removes the outermost charge density from H (and B) (Figure 2.1.2). The

removal of this density is a factor contributing to the change in $\mu(H)$.

Although $|\Delta N(H)|$ increases linearly with D_e within each set, it does not do so overall. However, $\Delta E(H)$ does exhibit such a relationship through the complete series of molecules (Figure 2.1.3d). The nonbonded density on H is penetrated by the base, H loses charge and is consequently destabilized. The linear relationship between $\Delta E(H)$ and D_e emphasizes the importance of the perturbation of the charge distribution of H in hydrogen bonding and in particular it demonstrates again the dependance of D_e on the degree of penetration of the nonbonded density on the H atom. Table 2.1.10 lists the contributions to the changes in potential energy for the H atom. The symbol $V_H(H)$ denotes the potential energy of interaction of the charge density within the basin of the H atom with its own nucleus. Because of the loss of charge by H, the change in this quantity is positive and the effect on the energy of H is destabilizing. The quantity $V_A(H)$, the total attractive potential energy, is the interaction of all the nuclei in the system with the charge density of the H atom. This quantity decreases on the formation of the hydrogen bond and is stabilizing because of the interaction of the nuclei of the base, particularly that of the B atom, with the density of the H atom. The repulsive contributions to the energy of the H atom, the electron-electron and nuclear-nuclear repulsions which are grouped under the heading $V_R(H)$, increase by more than the attractive interactions decrease and overall, the H atom is destabilized. (By the virial theorem, $\Delta E(H) = (1/2)[\Delta V_A(H) + \Delta V_R(H)]$).

In all the systems studied, H undergoes a reduction in

polarization upon H-bond formation. This reduction is primarily the result of the loss of its nonbonded density. The moment $\mu(\Omega)$ is determined by the average value of r over the atomic charge distribution and its value is therefore sensitive to the amount of density relatively far from the nucleus. This counter polarization of the charge density of the hydrogen atom is enhanced when the base atom B is negatively charged as in the complexes with H_3N, H_2CO and H_2O. These three complexes possess the greatest extent of mutual penetration and the three largest values of D_e. In the complexes with OC, H_2S and H_3P, the B atoms are positively charged and consequently, the corresponding $\Delta|\mu(H)|$ values are the smallest of those listed in Table 2.1.9.

We now focus on the atoms of the base molecule XB. Upon hydrogen bond formation, the base molecule loses charge in all instances as does the X group. The B atom gains charge if B is a second-row atom but loses charge if B is a third-row atom. Both B and X decrease in volume and, in general, $|\Delta V(B)| > |\Delta V(X)|$. In general, the greatest volume changes occur for those B atoms with diffuse regions of nonbonded density.

The XB-HF complexes are divided into two categories: those which have the change in the first moment of B directed away from H and those which have this change directed towards H. The bases belonging to the first class are H_3N, H_2O, HF, H_3P, H_2S, HCl, NN, HCN, OC, SC and O_3. Those belonging to the second class all have oxygen as the base atoms B and are SCO, OCO, NNO, OSO and H_2CO. The signs of $\Delta|\mu(B)|$ need not be the same for two bases belonging to one class, since the

original polarization of B may be directed towards H as in H_3N where $\Delta|\mu(N)| < 0$, or away from H as in H_2O where $\Delta|\mu(O)| > 0$ (Figure 1.2.5).

The change in $\mu(B)$ away from H in the first class of complexes is rationalized as follows: The creation of the B-H interatomic surface removes diffuse density from B and this decreases its atomic moment. This effect is most pronounced for those base molecules which initially possess diffuse regions of nonbonded density on the base atom B, such as found in H_3N, H_3P, H_2S, OC and SC. In each complex of the first class, with the exception of $(HF)_2$, the X group loses more charge than H and this, coupled with the fact that the X group is closer to B means that the electric field generated by X is dominant. Thus both effects cause a change in polarization of B away from H.

This back polarization of the density on B leads to an increase in D_e (Table 2.1.11). Within each group of base atoms in this class, one finds a correlation of the magnitude of the change in the polarization of the base atom B away from the proton with the extent of the mutual penetration of both the B and H atoms and hence with D_e. As noted above, the change in the polarization of H is also directed away from the bonded region. In other words, the removal of density from the bonded region resulting from these polarizations facilitates the approach of the two closed-shell systems.

The B atoms of the second class of molecules are oxygen atoms and their nonbonded density is tightly bound. For example, the nonbonded radius of C in OC is much larger than that of O in SCO (Table 2.1.6). The creation of a new O-H interatomic surface upon complexation and the concomitant removal of diffuse density does not

have a large effect on $\mu(O)$ owing to the tightness of the O charge distribution. Therefore, field effects play a dominant role in determining changes in $\mu(O)$. In OCO-HF and OSO-HF, the base atom neighbouring B loses charge but less than that lost by H and the net field is such as to cause the change in $\mu(O)$ to be directed towards H. In SCO-HF, NNO-HF and H_2CO-HF, the base atom neighbouring B gains charge on complexation and the change in $\mu(O)$ is again directed towards H. Since the change in polarization of B is directed towards H in this class of molecules, the extent of mutual penetration of the B and H atoms and the value of D_e increase with a decrease in the value of $|\Delta\mu(B)|$ (Table 2.1.11). The value of D_e increases with a decrease in the extent to which the polarization of B places density in the bonded region. Unlike a shared interaction where charge is accumulated in the bonded region, these interactions are strengthened by polarizations of both B and H which lead to a lessening of charge in this region, thereby facilitating their mutual penetration. While D_e does increase with increasing charge density at the bond critical point, the values of $\rho(r_b)$, which are approximately the sum of the unperturbed densities, increase because of increasing penetration and not because of polarizations of charge into the bonded region. Further evidence of a relation between the polarization of density on B and the extent of penetration is provided by the σ to π promotion of the density on B which, as discussed next, accompanies the formation of a hydrogen bond.

The complexes listed in Table 2.1.12 are linear and one may distinguish between the contributions of the σ and π orbitals to the atomic populations for each of these molecules (Wiberg and Wendolowski

1981). The changes in these contributions, together with the total atomic π population in the complex are given in Table 2.1.12. In each complex, HF has a π population which varies from its unperturbed value of four by only ±0.002e, and there is essentially no direct transfer of π density from the base to the acid. The loss and gain of charge by X and B respectively, is primarily a result of changes in their π populations. In fact, the π charge lost by X is nearly equal to that gained by B and it is possible to refer to a corresponding transfer of π charge from X to B. The π population of the B atoms increase, while their σ populations decrease. This implies that the formation of the hydrogen bond causes a promotion of σ into π density. An exception is found for N in N_2. Only in this molecule, which forms the weakest complex, is there an increase in the σ density of the base atom B. This atom exhibits the smallest penetration of the nonbonded density of the H atom of the acid (Table 2.1.4). Those base atoms showing the largest σ to π promotion, C of SC and N of HCN, also possess the greatest extent of penetration of the nonbonded density of the H atom. The σ to π promotion corresponds to the transfer of nonbonded density on B from a distribution which attains its maximum value on the axis of approach of B to H to one which is a maximum in a torus-like distribution about this axis. This redistribution of charge facilitates the approach of two closed-shell systems and, like the polarizations of B and H discussed above, leads to a greater penetration of their charge distributions and to a stronger hydrogen bond. This same promotion of density out of the plane of the hydrogen bond to a π-like distribution concentrated above and below this plane

has been found to occur for the base atoms in the cyclic formamide dimer (Section 2.3).

The changes in the atomic quadrupole moments reflect the promotion of σ to π density. For the B atom, $\Delta Q_{zz}(B)$ is always positive implying that charge density is removed from along the internuclear axis and becomes more concentrated in a toruslike distribution about the internuclear axis. For a particular B atom (C,N or O), $\Delta Q_{zz}(B)$ increases with increasing $\Delta N_{\pi}(B)$. $\Delta Q_{zz}(H)$ is always positive though the $\Delta N_{\pi}(H)$ values are very small. In general for the X atom $\Delta Q_{zz}(X)$ is negative implying that charge density is removed from the toruslike distribution about the internuclear axis and placed along the internuclear axis. Quadrupole moment changes offer a more physical description of the charge redistribution than the σ to π promotion argument where the rule of electron indistiguishability is violated.

These considerations make the differences in D_e values between complexes understandable, between those of OC and SC, for example. The positively charged carbon in OC possesses a diffuse nonbonded density distribution, but the remaining density of OC is tightly bound and does not undergo significant relaxations on forming the complex. In SC, carbon is negatively charged and more readily polarized, in addition to possessing diffuse nonbonded density (Table 2.1.6). All of the charge relaxations accompanying the formation of the complex are greater for SC than for OC: S transfers nearly four times as much charge as does the more electronegative O and the carbon atom gains more charge in SC than in OC by close to a factor of ten; C in SC is polarized towards

the soft and positively charged S and this is increased on complexation, while C in OC undergoes only a very small change in polarization towards the hard, negatively charged O; the σ to π polarization is greatest for C in SC; $|\Delta Q_{\sigma\pi}(C)|$ is more than twice as great in SC compared to OC. As a consequence of these differences, the mutual penetration of C and H is greater in SC than in OC by 0.34 au and SC forms the stronger hydrogen bond.

Table 2.1.13 summarizes the changes in energy and population of each atom in the complexes with O_3 and SCO which have nearly equal values for D_e. A gain or loss of charge results in a corresponding increase or decrease in the stability of each atom. As noted above, the H atom is destabilized in all systems. The F and B atoms are stabilized in both complexes, more so in the O_3 complex because of greater gains in charge, particularly for the B atom. The change in energy per change in charge for both F and H are of the same order of magnitude for both complexes, but differ by a factor of three for the B atom. The two molecules belong to different classes with regard to the change in polarization of the B atom and both exhibit the least favourable type of change. The polarization of the B atom towards H is essentially unchanged in O_3 while in SCO, it undergoes the largest of the polarizations towards H (Table 2.1.11). Consequently of the two, the penetration of the B atom is greatest in the former complex. In the O_3 complex, both of the remaining atoms in the base lose charge and are destabilized by an amount almost equal to the stabilization energy of the B atom and overall the base fragment is stabilized by only 2.6 kJ mol^{-1}. In the SCO complex, the C atom gains more charge than does

the base atom O and is considerably stabilized. The S atom on the other hand undergoes a loss in charge in excess of that gained by O and C and is destabilized so that the final base fragment is stabilized by 6.3 kJ mol^{-1}.

Dipole Moment Enhancement

Dipole moments of some of the BASE-HF complexes have been measured experimentally (Legon and Millen 1986) and they, along with the theoretically determined values, are listed in Table 2.1.14. The theoretical results overestimate the experimental values of the dipole moment with the exceptions of OC-HF, NNO-HF and H_2CO-HF.

It is experimentally observed that the dipole moment of the complex is always greater than the vector sum of the dipole moments of the isolated reactants and this result is predicted by the theoretical calculations. This dipole moment enhancement (DME) along with the theoretical values are listed in Table 2.1.14. The theoretical values are in fair agreement with experiment. The theory of atoms in molecules demonstrates that the dipole moment enhancement is a result of a loss of charge by the the X group (the tail) of the base and a gain by the F (the head) of the acid (Table 2.1.9). This effective transfer of charge across the length of the complex creates a moment which adds to the head to tail alignment of the base and acid dipoles to yield a moment that is greater than the sum of the reactant dipoles. The competing moment arising from a gain of charge by atom B of the base and a loss of charge by H, is of smaller magnitude since the distance over which this effective charge transfer occurs is much

shorter than the head to tail distance between F and X.

Summary of the Properties of BASE-HF Complexes

It has been claimed that a successful theory of the hydrogen bond has to explain the properties of H-bonded complexes listed below, for which extensive experimental evidence is available (Schuster et al 1976). Each of these observations is followed by its explanation as given by the theory of atoms in molecules.

1. `Molecules forming H-bonds approach much closer than the sums of the van der Waals radii of the nearest atoms would allow.' The theory of atoms in molecules quantifies the concept of the penetration of van der Waals envelopes and relates the extent of penetration to the strength of the hydrogen bond. The basis of this relation lies in the closed-shell nature of the hydrogen bond as characterized by the properties of the charge density at its critical point. The mutual penetration of the outer diffuse nonbonded densities of the B and H atoms is facilitated by their dipolar and quadrupolar polarizations, which remove density from along their axis of approach, to yield a final density in the interatomic surface that is only slightly greater than the sum of the unperturbed densities. The greater the penetration, the larger the value of ρ_b and the stronger the resulting bond.

2. `The dipole moment of the complex is larger than the vectorial addition of the monomer moments.' This so-called dipole moment enhancement is readily accounted for in terms of the changes in the atomic populations as an effective transfer of charge from the tail of

the base to the head of the acid.

3. 'The electron density at H is decreased and so NMR signals are shifted to lower magnetic fields.' Indeed, $\Delta N(H)$ is negative in all hydrogen-bonded complexes studied to date. The accompanying descreening of the proton raises the energy of H in the complex.

4. 'Upon hydrogen bond formation, the H-Y bond of the acid molecule HY is lengthened and its IR stretching frequency is shifted to smaller wave numbers.' Ab initio calculations confirm the elongation of the bond (Table 2.1.1). The redistribution of charge which leads to the weakening of the H-Y bond and the concomitant strengthening of the hydrogen bond are characterized by the properties of the charge density at the corresponding bond critical points.

Electron Correlation in BASE-HF Complexes

A recent investigation of the effects of electron correlation on the topological properties of molecular charge distributions has shown that the number and type of critical points are not changed (Gatti et al 1988). Changes in the properties of ρ at its critical points and in atomic properties change by only a few per cent. While the energies do change by an amount equal to the correlation energy, the trends in energy changes through series of molecules (hydrocarbons and carbenes) and the conclusions based on these trends were found to be unchanged by correlation.

We wish to see if any conclusions made using the RHF/6-311++G**//6-31G** scheme must be altered when electron correlation is incorporated into the description of the charge distribution of the

weak BASE-HF complexes. To this end, we study a weak system OC-HF and a strong system H$_3$N-HF using the MP2/6-311++G**//6-31G** scheme (Scheme III). The symbol MP2 denotes Moller-Plesset (1934) second-order perturbation theory, a widely used scheme to incorporate electron correlation (Hehre et al 1986).

Table 2.1.15 compiles the dissociation energies. Scheme III, like Schemes I and II, predict OCO-HF to be more stable than OC-HF and, in turn, OC-HF to be more stable than CO-HF. Thus, the energy trends are preserved when correlation is included. Also listed in this table are the D_e values for HF-HF, HCN-HF and H_2O-HF because their D_e values have been experimentally determined. Again, the energy trends are preserved. In fact, for HF-HF and H_2O-HF, Scheme III performs the best while for HCN-HF Scheme I still gives the D_e value closest to experiment. The effect of MP2 on the D_e of many hydrogen-bonded complexes has been recently reviewed by Hobza and Zahradnik (1988).

Important from the viewpoint of the theory of atoms in molecules are the changes in the charge distributions of the systems owing to the inclusion of correlation. It is found that the qualitative features of ρ do not change, i.e, the numbers and types of critical points remains unchanged upon MP2 inclusion in both the isolated reactants and the complexes. Table 2.1.16 deals with quantitative changes in the topology of ρ while Table 2.1.17 deals with the changes in atomic properties.

The quantitative changes in ρ are small. They are greater in the stronger complex H$_3$N-HF as compared to the weaker OC-HF complex (Table 2.1.16). In both of these systems the inclusion of MP2 causes a

greater buildup of charge at the H-bond critical point and greater penetration values (as compared to the corresponding Scheme II values). Consistent with these observations are the greater values of D_e for these complexes using Scheme III as compared to Scheme II. As evidenced in the values for r_e, Scheme III causes more charge to be removed from the HF bond than in Scheme II, also consistent with the larger D_e values present in Scheme III.

Examining the changes in the atomic properties of the strongest complex H_3N-HF on going from Scheme II to Scheme III, we note the following: the hydrogen-bonded H gains electrons while F and N lose electrons. Electron correlation causes the polarization of N away from H to increase significantly and this is consistent with the larger D_e value for Scheme III. Both H and N decrease to a greater extent in atomic volume for Scheme III.

To gain a greater understanding of the effect of MP2 correlation on ρ, we examine the changes in the atomic properties on going from Scheme II to Scheme III for the molecules HF, CO and H_3N separately (Table 2.1.17). In all cases, the heavier atom loses electrons. Consistent with this observation is the decrease in the first moment and atomic volume for F in HF and O in CO. Figure 2.1.4. is a plot of the Scheme III minus Scheme II charge density for hydrogen fluoride. Charge is removed from the fluorine basin including its nonbonded region and this is why its first moment is reduced from Scheme II. The H gains charge in its nonbonded region, and consequently, its first moment increases.

BASE-HCl Complexes

In the above BASE-HF study we have varied the base but kept the acid constant. What if we keep the base constant and vary the acid? To answer the question, we examine the linear NN-HCl, OC-HCl, SC-HCl, OCO-HCl, SCO-HCl and HCN-HCl complexes and the near C_{3v} complex H_3N-HCl. Of these, only SC-HCl has not been characterized experimentally.

Geometries and Energies of BASE-HCl Complexes

The RHF/6-311++G**//6-31G** scheme employed in this work overestimates the BCl internuclear distance in the BASE-HCl complexes just as it did for the BASE-HF complexes (Table 2.1.1). The calculated hydrogen bond length is greater in a given BASE-HCl complex than in the corresponding BASE-HF complex by ~10% and the D_e values are smaller by ~50%. Still, the relative ordering of the D_e values is the same for BASE-HCl as for BASE-HF complexes. As the BASE-HCl complexes are weaker than the BASE-HF complexes, it is not surprising that the changes in the base geometry upon BASE-HCl complex formation are smaller than the corresponding changes upon BASE-HF complex formation. While the changes in the HCl bond length are very small for the linear BASE-HCl complexes, this change for H_3N-HCl is relatively large, even larger than that in H_3N-HF.

Topological Analysis of ρ for BASE-HCl Complexes

The values of ρ and of its curvatures at the bond critical point of the hydrogen bond and of the HCl bond in the acid are listed in Tables 2.1.18 and 2.1.19.

Within each set of H-bonded complexes, where the base atom B is C, N or O, D_e increases with increasing values of $\rho(r_b)$ at the H-bond critical point (Table 2.1.18). Overall, there is a roughly linear relationship between $\rho(r_b)$ and D_e just as was found for the BASE-HF complexes. Consistent with the smaller D_e values for the BASE-HCl complexes compared to the BASE-HF complexes, we find that $\rho(r_b)$ is correspondingly small. For the linear complexes, $\rho(r_b)$ is ~25% smaller in BASE-HCl than in BASE-HF.

Within each set of H-bonds of the BASE-HCl systems, $\nabla^2\rho(r_b)$, the magnitudes of the curvatures of ρ, the mutual penetration values and the sum of the unperturbed densities increase with D_e. These values are smaller than the corresponding values found in the BASE-HF complexes. Thus, the description of BASE-HCl complexation emerging from Table 2.1.18 is the same as that for BASE-HF complexation, only in BASE-HCl all the changes are on a smaller scale. There is one exception. The mutual penetration value for H_3N-HCl is 8% larger than the value for H_3N-HF.

The changes in the values of properties evaluated at the HCl bond critical point are given in Table 2.1.19. In general the changes in ρ and $\nabla^2\rho$ parallel the changes in the acid critical point in BASE-HF, but again on a smaller scale. The location of r_a moves progressively to Cl as D_e increases within each set of H-bonds and these shifts are greater than the corresponding shifts to F in the BASE-HF systems.

Changes in Atomic Properties on BASE-HCl Hydrogen Bond Formation

The changes in the populations and volumes of the acid and base molecules upon hydrogen bond formation are given in Table 2.1.20 and the corresponding atomic changes are given in Table 2.1.21.

There is a transfer of charge from the base to the acid in all systems. The strongest of the complexes, H_3N-HCl, has the greatest number of electrons transferred (0.038e) while the weakest complex, NN-HCl has among the least (0.001e). The former complex has the greatest mutual penetration value and the latter the least. The charge transfer from base to acid is smaller in BASE-HCl than BASE-HF complexes. Consequently, the dipole moment enhancements of the linear BASE-HCl complexes are smaller than the corresponding BASE-HF complexes (Table 2.1.14). The RHF/6-311++G**//6-31G** scheme yields DME results closer to experiment for the BASE-HCl complexes than for the BASE-HF complexes.

The volumes of both the base and acid fragments decrease upon H-bond formation with the base fragment becoming more contracted than the acid (with the exception of OCO-HCl). The total volume decrease is smaller than the corresponding decrease for BASE-HF systems.

The most important trends are to be found in the changes of the properties of the B, H and Cl atoms. The acid is discussed first. Chlorine gains electrons in all cases, in amounts ranging from 0.018e for the weakest complex NN-HCl to 0.166e for the strongest complex H_3N-HCl. These gains are greater than the corresponding gains by fluorine in BASE-HF systems and this is rationalized by noting that the charge distribution of Cl in HCl is not as tight as that of F in HF. The softer hydrogen of HCl (as compared to the tight H of HF) loses

charge in all cases in amounts ranging from 0.017e for the weakest complex NN-HCl to 0.128e for the strongest complex H$_3$N-HCl. The tight H of HF does not lose as much electrons upon BASE-HF formation as the soft H of HCl does upon BASE-HCl formation.

The decrease in v(H) for the acidic hydrogen ranges between 1.5 au (NN-HCl) and 14.1 au (H$_3$N-HCl). The large $\Delta v(H)$ value in the strongest complex, H$_3$N-HCl, is the largest value yet observed for H for any hydrogen-bonded complex. This large value is consistent with the large value of $|\Delta r_H^c|$, also the largest value yet observed for H.

Although $|\Delta N(H)|$ increases linearly with D_e within each set of BASE-HCl systems, it does not do so overall. However, in general, $\Delta E(H)$ does increase overall with D_e. These $\Delta E(H)$ values are greater than the corresponding values in BASE-HF systems. The exceptional behavior of the H$_3$N-HCl system is again manifested in the large value of $\Delta E(H) = 175$ kJ mol^{-1}.

Just as with the BASE-HF systems, in all the BASE-HCl systems studied H undergoes a reduction in polarization upon H-bond formation and this reduction becomes greater with increasing D_e. The reductions are also greater than the corresponding reductions in the BASE-HF complexes. In the BASE-HCl complexes, a significant reduction in the polarization of Cl is observed and this reduction increases with increasing D_e. In fact, for the stronger SC-HCl, HCN-HCl and H$_3$N-HCl, the atomic first moment of Cl is directed counter to the direction of charge transfer. This is in contrast to the isolated reactant HCl in which Cl is polarized slightly in the same direction as the charge transfer. While changes in the acid fragment are large between HF and

HCl in the BASE-HF and BASE-HCl complexes respectively, changes in the atomic properties of the constituent atoms of the base upon BASE-HCl formation are very similar to the corresponding changes upon BASE-HF formation. The mechanism of hydrogen bond formation is also the same and the discussion need not be repeated.

Figure 2.1.1

Molecular graphs of nonlinear BASE-HF complexes. These graphs are determined from the charge densities of the complexes. The black dots between atoms denote the positions of the bond critical points of ρ. The hydrogen fluoride bond critical point is close to the proton. Refer to Table 2.1.1 for the numbering scheme and values of geometric parameters.

1

7

12

2

8

13

3

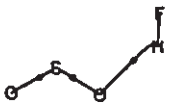

9

14

4

15

5

10

16

6

11

17

Figure 2.1.2

a) Contour maps of the charge distributions of carbon monoxide, hydrogen fluoride and the complex OC-HF are presented. Included are zero flux surfaces, critical points (black dots) and bonded and nonbonded radii. A bonded radius for a given bond is measured from the nucleus to the corresponding bond critical point. A nonbonded radius is measured from the nucleus out to the 0.001 au contour. The innermost contours (those of values greater than 0.8 au) are not shown. b) Contour plot of the Laplacian distribution of OC-HF. Zero flux surfaces and bond critical points (black dots) are included.

a

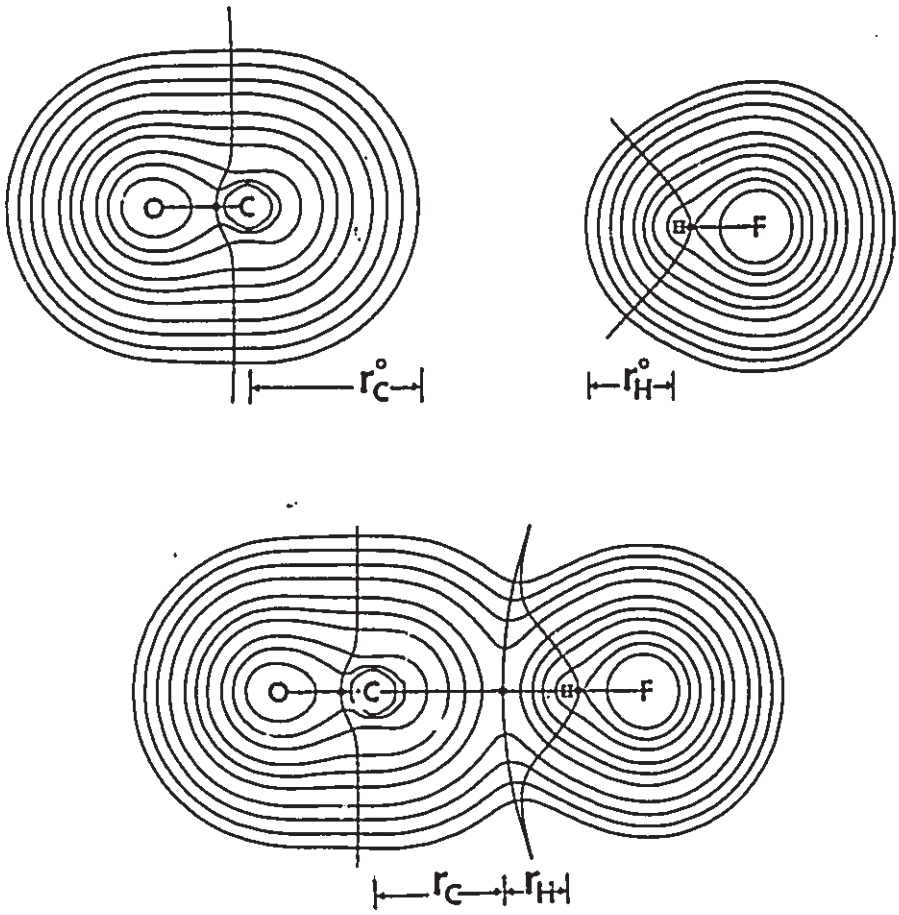

b

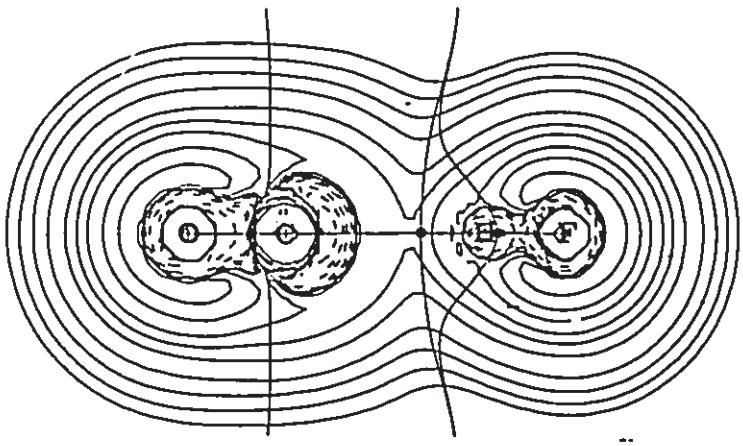

Figure 2.1.3

Relationships between properties of the charge density and D_e (kJ mol^{-1}) for BASE-HF complexes. The data labels (a)-(p) are for complexes (arranged in order of increasing D_e) of HF with the bases N_2 (a), HCl (b), OC (c), O_3 (d), SCO (e), OCO (f), NNO (g), H_3P (h), HF (i), SC (j), OSO (k), H_2S (l), HCN (m), H_2CO (n), H_2O (o) and H_3N (p).

a) Plot of the charge density at the hydrogen bond critical point $\rho(r_b)$ (in au) versus D_e.

b) Plot of the sum of the changes in nonbonded radii of B and H upon hydrogen bond formation, i.e. the mutual penetration $|\Delta r_B^o + \Delta r_H^o|$ (in au) versus D_e.

c) Plot of the decrease in the charge density at the H-F bond critical point $\Delta\rho(r_e)$ (in au) versus D_e.

d) Plot of the increase in the energy of the hydrogen-bonded hydrogen, $\Delta E(H)$ (in kJ mol^{-1}) versus D_e.

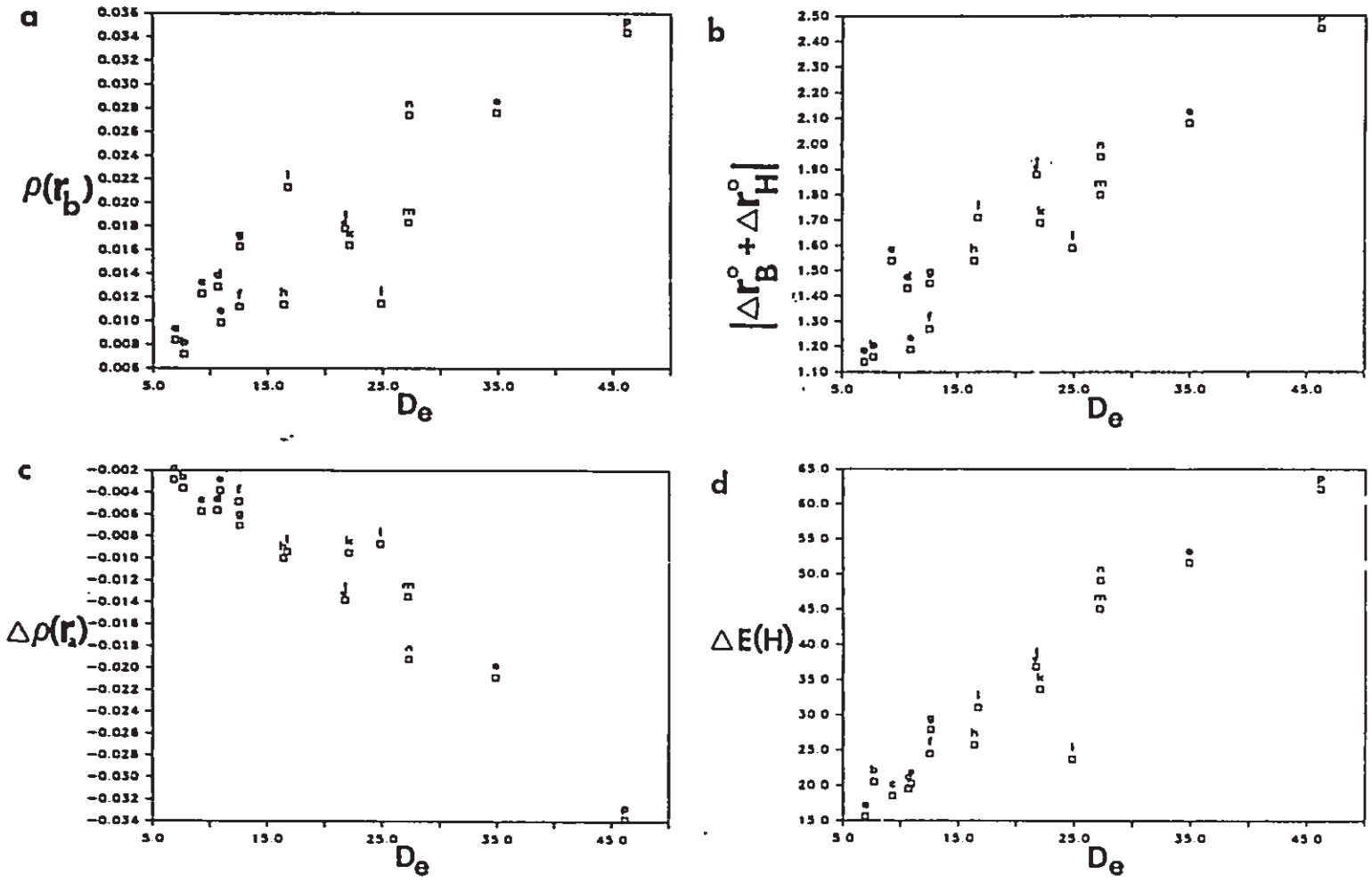
a
$\rho(r_b)$
D_e
b
$|\Delta r_B^o + \Delta r_H^o|$
D_e
c
$\Delta\rho(r_c)$
D_e
d
$\Delta E(H)$
D_e

Figure 2.1.4

Contour map of the MP2 minus Hartree-Fock charge density for hydrogen fluoride. Solid (dashed) contours correspond to regions of charge buildup (removal). The contours for this figure and the other difference density figures in this chapter change in steps of $2x10^n$, $4x10^n$, $8x10^n$ with n beginning at -4 and increasing in steps of unity.

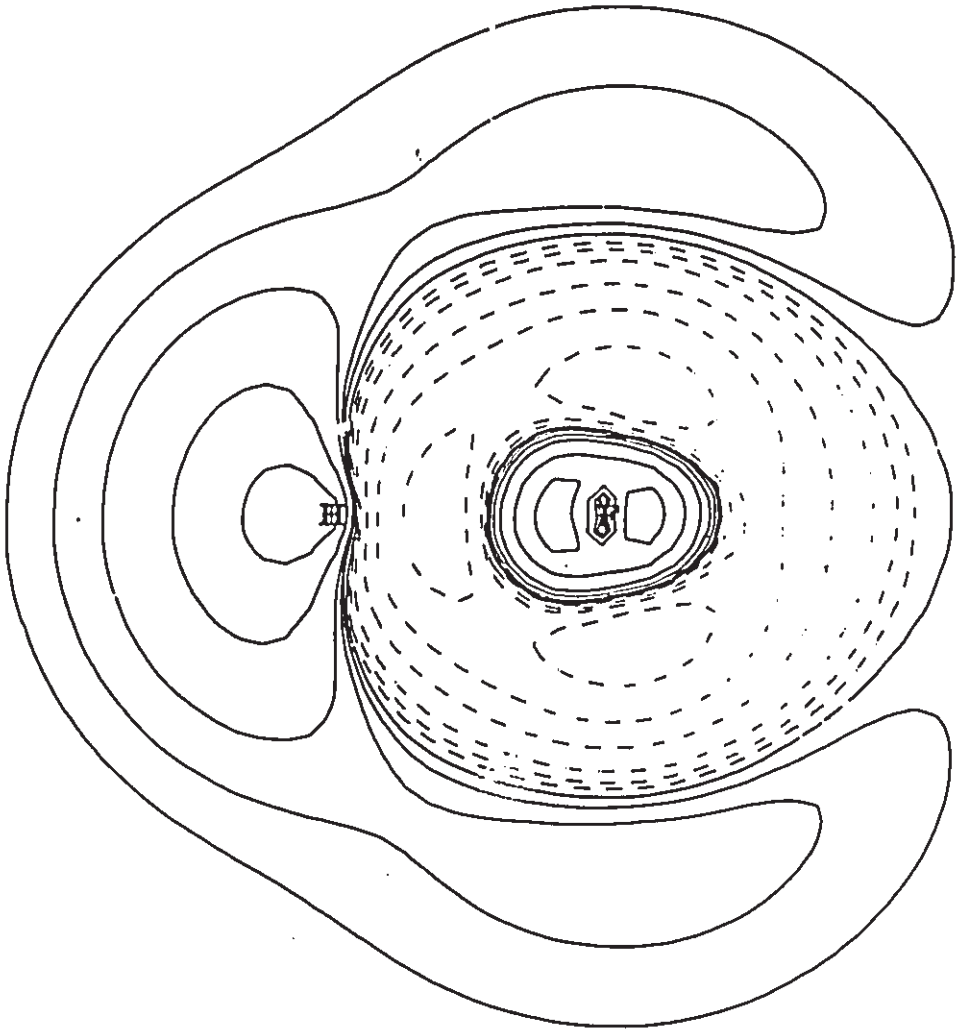

Table 2.1.1. Geometries and Energies of Primary and Secondary BASE-HA Structures.

Struct[a]	Complex	Parameters Optimized[b]	Expt	Escf[c]	-V/T	D_e[d] Calc	D_e[d] Expt	% err
PRIMARY BASE-HF								
linear	NN-HF	NH 2.304		-208.95817	2.0025328	6.3		
		NF 3.205	3.087	-209.02991	2.0005306	6.9		
		NN 1.078 (0.000)						
		HF 0.901 (0.001)	(0.001)					
	OC-HF	CH 2.265		-212.75406	2.0020000	11.7		
		CF 3.168	3.064	-212.82802	2.0004117	9.3		
		OC 1.111 (-0.003)						
		HF 0.903 (0.003)	(0.007)					
	SC-HF	CH 2.138		-535.32470	2.0005378	22.6		
		CF 3.045		-535.40013	2.0000447	21.8		
		SC 1.510 (-0.010)						
		HF 0.907 (0.007)						
	O=CO-HF	OH 2.076	1.91	-287.65049	2.0023493	12.1		
		OF 2.978		-287.74963	2.0003827	12.6		
		O=C 1.139 (-0.004)						
		CO 1.148 (0.003)						
		HF 0.902 (0.002)						
	SCO-HF	OH 2.129	1.94	-610.27583	2.0009730	9.2		
		OF 3.031		-610.37529	2.0001255	10.9		
		SC 1.564 (-0.008)						
		CO 1.136 (0.005)						
		HF 0.902 (0.002)						
	H=CN-HF	NH 2.012		-192.89901	2.0018200	26.8	25.9	3
		NF 2.918	2.804	-192.96537	2.0004383	27.2		5
		H=C 1.060 (0.001)						
		CN 1.131 (-0.002)						
		HF 0.906 (0.006)	(0.014)					
1	NNO-HF	OH 2.093	1.94	-283.69750	2.0024638	15.1		
		OF 2.807		-283.78999	2.0003565	12.6		
		NN 1.089 (-0.003)		-284.65851				
		NO 1.186 (0.007)						
		HF 0.903 (0.003)						
		NOH 104.4	116					
		OHF 135.2	167					

Table 2.1.1 (con'd)

Struct[a]	Complex	Parameters Optimized[b]	Expt	Escf[c]	-V/T	D_e[d] Calc	D_e[d] Expt	% err
2	H-CP-HF	CH 2.547 CF 3.311 HC 1.064 (0.001) CP 1.516 (-0.002) HF 0.902 (0.002) PCH 92.6 HCH 88.6 HCP 178.8 (-1.2) CHF 142.8		-479.12230 -479.19513	2.0006856 2.0000586	10.0 7.0		
3	H_2O-HF	OH_a 1.817 OF 2.724 HO 0.944 (0.001) H_aF 0.910 (0.010) θ 136.7 OH_aF 173.2 HOH_a 115.7 HOH 107.0 (1.0)	2.662 (0.015) 134±8	-176.04975 -176.12008	2.0018684 2.0002109	38.1 34.8	42.7	11 18
4	H_2S-HF	SH_a 2.553 SF 3.453 HS 1.327 (-0.001) H_aF 0.904 (0.004) θ 104.7 SH_aF 173.8 HSH_a 99.9 HSH 94.7 (0.3)	3.249 (0.010) 91	-498.69229 -498.76150	2.0005540 2.0000179	14.6 24.8		
5	H_2N-HF	NH_a 1.837 NF 2.755 HN 1.001 (0.000) H_aF 0.918 (0.018) NH_aF 179.9 HNH_a 111.1 HNH 107.8 (0.2)	2.80	-156.22607 -156.28567	2.0015688 2.0002483	49.4 46.2		
6	H_2P-HF	PH_a 2.625 PF 3.530 HP 1.401 (-0.004) H_aF 0.905 (0.005) PH_aF 179.8 HPH_a 120.3 HPH 96.8 (1.2)	3.311	-442.47184 -442.53770	2.0005644 2.0000361	15.5 16.4		

Table 2.1.1 (con'd)

Struct[a]	Complex	Parameters: Optimized[b]	Expt	Escf[c]	-V/T	D_e[d] Calc	Expt	err
7	O*CO-HF	OH 2.120		-324.27802	2.0024173	13.0		
		OF 3.021		-324.38742	2.0001207	10.7		
		O*O 1.195 (-0.009)						
		CO 1.213 (0.009)						
		HF 0.903 (0.003)						
		COH 114.4						
		OHF 175.5						
		O*CO 118.8 (-0.2)						
8	O*SO-HF	OH 1.983		-647.18820	2.0014332	19.7		
	(cis)	OF 2.887	2.818	-647.22372	2.0000350	22.1		
		O*S 1.411 (-0.003)						
		SO 1.420 (0.006)						
		HF 0.904 (0.004)						
		SOH 140.8	144.9					
		OHF 179.2						
		O*SO 118.3 (-0.5)						
9	O*SO-HF	OH 2.082		-647.18850	2.0014364	20.5		
	(trans)	OF 2.782		-647.29125	2.0000121	15.6		
		O*S 1.412 (-0.002)						
		SO 1.421 (0.007)						
		HF 0.904 (0.004)						
		SOH 107.6						
		OHF 133.6						
		O*SO 117.8 (-1.0)						
10	H_2CO-H_aF	OH_a 1.853	1.784	-213.89432	2.0018460	33.9		
		OF 2.688	2.659	-213.96673	2.0002246	27.3		
		H^cC 1.089 (-0.004)						
		HC 1.089 (-0.004)						
		CO 1.191 (0.007)						
		H_aF 0.910 (0.010)						
		COH_a 105.4	115					
		COF 96.2	109.5					
		OH_aF 151.6						
		H^cCO 121.6 (-0.5)						
		HCO 121.4 (-0.7)						
		H^cCH 117.0 (1.2)						
11	HF*-H_aF	F*H_a 1.850		-200.03289	2.0016114	25.1	19.1	31
		HH_a 2.315		-200.11309	2.0000961	16.7		12
		FH_a 0.904 (0.004)						
		F*F 2.717	2.72					
		F*H_aF 159.6						
		HF*H_a 109.5						
		θ_1[h] 77.1	63±6					
		θ_2[h] 13.7	10±6					

Table 2.1.1 (con'd)

Struct[a]	Complex	Parameters Optimized[b]	Expt	Escf[c]	-V/T	D_e[d] Calc	Expt	err
12	ClH"-FH[h]	ClF 3.328		-560.08393	2.0006569	15.9		
		H"F 2.067	2.12	-560.15288	1.9999626	9.9		
		HH 2.644						
		ClH" 1.268 (0.002)						
		FH 0.902 (0.002)						
		ClH"F 172.4						
		HFH 120.7	130					
13	N"NS-HF[h]	SF 3.328		-606.38954	2.0011810	13.0		
		SH 2.783		-606.48186	2.0001424	9.9		
		NF 2.976						
		NH 2.898						
		N"N 1.083 (-0.003)						
		NS 1.664 (0.012)						
		HF 0.903 (0.003)						
		SFH 46.4						
		NSF 63.2						
14	H_2CS-H_aF[i]	SH_a 2.539		-536.52979	2.0006701	23.4		
		SF 6.186		-536.60146	2.0000421	16.7		
		H^cF 2.488						
		H^cC 1.078 (0.000)						
		HC 1.078 (0.000)						
		CS 1.600 (0.001)						
		H_aF 0.906 (0.006)						
		CSH_a 82.8						
		CSF 72.2						
		SH_aF 138.5						
		CH^cF 75.7						
		H^cCS 121.6 (-0.5)						
		HCS 121.7 (-0.4)						
		H^cCH 116.6 (0.8)						
SECONDARY BASE-HF								
linear	CO-HF	OH 2.156		-212.75296	2.0019852	8.8		
		OF 3.058		-212.82762	2.0004173	8.2		
		CO 1.116 (0.002)						
		HF 0.902 (0.002)						
	ONN"-HF	N"H 2.260		-283.69450	2.0024744	7.1		
		N"F 3.161		-283.78804	2.0003848	7.4		
		N"N 1.092						
		NO 1.172						
		HF 0.901						

Table 2.1.1 (con'd)

Struct[a]	Complex	Parameters Optimized[b]	Expt	Escf[c]	-V/T	D.[d] Calc	Expt err
	SNN=-HF	N=H 2.416 N=F 3.317 N=N 1.086 (0.000) SN 1.639 (-0.013) HF 0.901 (0.001)		-606.38523 -606.47902	2.0012154 2.0001509	1.8 2.4	
linear	H=CP-HF	PH 3.235 PF 4.135 H=C 1.083 (0.000) CP 1.513 (-0.005) HF 0.901 (0.001)		-479.11957 -479.19256	2.0006856 2.0000676	2.9 0.3	
15	O=CO-HF	OH 2.077 OF 2.971 O=C 1.139 (-0.004) CO 1.146 (0.003) HF 0.902 (0.002) COH 164.8 OHF 170.5		-287.65049 -287.74962	2.0023510 2.0003842	12.1 12.5	
16	SCO-HF	OH 2.132 OF 3.025 SC 1.564 (-0.008) CO 1.136 (0.005) HF 0.902 (0.002) COH 165.2 OHF 170.4		-610.27581 -610.37528	2.0009733 2.0001268	9.2 10.9	
17	H=Cl-HF	ClH 2.628 ClF 3.507 H=Cl 1.267 HF 0.902 (0.002) H=ClH 100.1 ClHF 164.9		-560.08085 -560.15204	2.0006174 1.9999700	7.5 7.7	
PRIMARY BASE-HCl							
linear	NN-HCl	NH 2.576 NCl 3.842 NN 1.078 (0.000) HCl 1.266 (0.000)	3.729	-569.01155 -569.07100	2.0010128 2.0001188	3.6 3.5	
	OC-HCl	CH 2.541 CCl 3.809 OC 1.112 (-0.002) HCl 1.268 (0.002)	3.710	-572.80663 -572.86846	2.0008288 2.0000779	6.7 4.1	

Table 2.1.1 (con'd)

Struct[a]	Complex	Parameters Optimized[b]	Expt	Escf[c]	-V/T	Calc	D_e[d] Expt	% err
	SC-HCl	CH 2.358		-895.37598	2.0003783	14.3		
		CCl 3.631		-895.43875	1.9999778	11.8		
		SC 1.513 (-0.007)						
		HCl 1.272 (0.006)						
	O=CO-HCl	OH 2.305		-647.70323	2.0011201	7.4		
		OCl 3.572	3.430	-647.78994	2.0001020	7.1		
		O=C 1.140 (-0.003)						
		CO 1.145 (0.002)						
		HCl 1.267 (0.001)						
	SCO-HCl	OH 2.380		-970.32888	2.0006669	5.4		
		OCl 3.646	3.479	-970.41590	2.0000355	6.2		
		SC 1.566 (-0.006)						
		CO 1.134 (0.003)						
		HCl 1.266 (0.000)						
	H=CN-HCl	NH 2.219		-552.95014	2.0007246	17.8		
		NCl 3.491	3.404	-553.00349	2.0000730	16.0		
		H=C 1.060 (0.001)						
		CN 1.131 (-0.002)						
		HCl 1.272 (0.006)						
C_{3v}	H_3N-H_aCl	NH_a 1.936		-516.27540	2.0005908	35.8		
		NCl 3.230	3.136	-516.32111	1.9999923	27.8		
		HN 1.002 (0.000)						
		H_aCl 1.294 (0.028)						
		NH_aCl 179.8						
		HNH_a 111.1						
		HNH 107.8 (0.2)						

[a] See Figure 2.1.1 for molecular graphs of the nonlinear structures. The linear structures are written so that the base atom, B, participating in the hydrogen bond is linked by a hyphen to the acidic hydrogen, H_a of HA (A=F,CL). Where possible, the subscript a is dropped for simplicity.

[b] 6-31G**; distances in Å and angles in degrees. Geometry changes from 6-31G** optimized monomer geometries are enclosed in parentheses.

[c] Values are in au. The first entry for each complex uses RHF/6-31G**//6-31G** (Scheme I) while the second entry uses RHF/6-311++G**//6-31G** (Scheme II).

[d] Dissociation energies are given in kJ mol^{-1}. The experimental values are from Legon and Millen (1986). The numbers under the % err column are the absolute values of the percent relative errors of the calculated from the experimental dissociation energies.

[e] θ is the obtuse angle between H_a and the base molecular plane.

[f] The non-participating hydrogen nearest the B-H_aF bond.

[g] θ_1 is the acute angle the HF subunit acting as a proton acceptor is bent from the FF axis. θ_2 is the dihedral angle HF-H_aF.

[h] FH is the base.

[i] FH acts both as an acid and a base.

Table 2.1.2. Geometries, Energies and Atomic Charges of Reactants.[a]

BASE	Geometric Parameters	E_{SCF}	-V/T	Ω	q(Ω) I	q(Ω) II
HF	HF 0.900	-100.01169	2.0014313	F	-0.7570	-0.7527
		-100.05336	2.0001316	H	0.7570	0.7526
OC	OC 1.114	-112.73788	2.0024104	C	1.4034	1.3269
		-112.77113	2.0006958	O	-1.4034	-1.3269
SC	SC 1.520	-435.30432	2.0002901	C	-0.8728	-0.8870
		-435.33849	2.0000305	S	0.8728	0.8870
NN	NN 1.078	-108.94395	2.0034006	N	0.0000	0.0000
		-108.97390	2.0008970			
HCN	HC 1.059	-92.87714	2.0020653	N	-1.4794	-1.3454
	CN 1.133	-92.90164	2.0007527	C	1.2869	1.1232
				H	0.1922	0.2222
H_2N	HN 1.001	-56.19554	2.0015700	N	-1.1192	-1.0759
	HNH 107.6	-56.21474	2.0004015	H	0.3731	0.3586
OOO	OO 1.204	-224.26144	2.0027792	O	-0.1080	-0.1088
	OOO 119.0	-224.32989	2.0001389	O_c	0.2126	0.2177
SCO	SC 1.572	-510.26062	2.0008814	O	-1.3476	-1.2743
	CO 1.131	-510.31777	2.0001254	C	0.8601	0.7639
				S	0.4856	0.5104
OCO	OC 1.143	-187.63418	2.0028032	O	-1.3784	-1.2976
		-187.69148	2.0005161	C	2.7567	2.5851
NNO	NN 1.092	-183.68012	2.0029688	O	-0.4118	-0.4247
	NO 1.179	-183.73184	2.0005184	N_c	-0.0847	-0.0158
				N	0.4966	0.4404
OSO	OS 1.414	-547.16900	2.0013984	O	-1.3941	-1.3311
	OSO 118.8	-547.23195	2.0000016	S	2.7884	2.6621
H_2CO	HC 1.093	-113.86974	2.0020973	O	-1.2972	-1.2403
	CO 1.184	-113.90298	2.0004179	C	1.3631	1.2453
	HCO 122.1			H	-0.0331	-0.0025
	HCH 115.8					
H_2O	HO 0.943	-76.02362	2.0020960	O	-1.2389	-1.2234
	HOH 106.0	-76.05344	2.0002526	H	0.6194	0.6117
H_3P	HP 1.405	-342.45419	2.0003433	P	1.8449	1.8799
	HPH 95.6	-342.47810	2.0000060	H	-0.6139	-0.6266
HCP	HC 1.063	-379.10670	2.0004179	C	-1.4558	-1.4666
	CP 1.518	-379.13909	2.0000807	P	1.3476	1.3261
				H	0.1083	0.1412
H_2S	HS 1.328	-398.67503	2.0003439	S	0.4879	0.6736
	HSH 94.4	-398.69868	1.9999924	H	-0.2440	-0.3368
NNS	NN 1.086	-506.37286	2.0011098	N	0.3367	0.3407
	NS 1.652	-506.42473	2.0001592	N_c	-0.5536	-0.5473
				S	0.2171	0.2066
SCS	SC 1.544	-832.88408	2.0004506	C	-1.3554	-1.3572
		-832.93967	2.0000220	S	0.6777	0.6786
H_2CS	HC 1.078	-436.50924	2.0004172	S	0.5220	0.5155
	CS 1.599	-436.54172	2.0000572	C	-0.5693	-0.6178
	HCS 122.1			H	0.0239	0.0512
	HCH 117.4					

Table 2.1.2 (con'd)

HCl	HCl 1.266	-460.06621	2.0004374	Cl	-0.2329	-0.2771
		-460.09575	1.9999364	H	0.2329	0.2771

[a] Internuclear separations are in A and angles are in degrees. Energies and atomic charges are in atomic units. The subscript c denotes the central atom.

Table 2.1.3. Absolute Values of Full Counterpoise Corrections (cc) to Energies and Charge Densities of the Reactants HF and H_3N in HF-HF and H_3N-HF.[a]

cc to	Complex: HF-HF		Complex: H_3N-HF	
	base	acid	base	acid
energy	1.0	0.7	2.3	1.0
N(A)	-	0.001	-	0.000
N(H)	-	0.001	-	0.000
N(B)	0.000	-	0.006	-
N(H′)	0.000	-	0.002	-
$\lvert\mu(A)\rvert$	-	0.007	-	0.007
$\lvert\mu(H)\rvert$	-	0.001	-	0.001
$\lvert\mu(B)\rvert$	0.008	-	0.041	-
$\lvert\mu(H')\rvert$	0.000	-	0.001	-
v(A)	-	0.78	-	0.55
v(H)	-	0.13	-	0.12
v(B)	0.33	-	1.92	-
v(H′)	0.06	-	0.01	-
$\rho(r_c)$	0.004	0.005	0.000	0.000
$\nabla^2\rho(r_c)$	0.060	0.076	0.002	0.007

[a] The 6-311++G** energy corrections are given in kJ mol^{-1}. The remaining values are given in au. The fluorine of the acid, the hydrogen-bonded hydrogen and the base atom participating in the H-bond are labelled A, H and B respectively. The remaining hydrogens not participating in the H-bond are labelled H′.

Table 2.1.4. Hydrogen Bond Critical Point Analysis of BASE-HF Complexes.[a]

XB-HF	$\rho(r_b)$	$\nabla^2\rho(r_b)$	$\lambda_1(r_b)$	$\lambda_2(r_b)$	$\lambda_3(r_b)$	r_B	r_H	$\lvert\Delta r_B^{\circ}\rvert$	$\lvert\Delta r_H^{\circ}\rvert$
OC-HF	0.0123	0.0500	-0.0132	-0.0132	0.0764	2.8682	1.4118	0.91	0.63
SC-HF	0.0178	0.0851	-0.0210	-0.0210	0.1071	2.7440	1.2861	1.14	0.74
NN-HF	0.0084	0.0406	-0.0086	-0.0086	0.0578	2.8456	1.5083	0.81	0.53
HCN-HF	0.0183	0.0851	-0.0234	-0.0234	0.1319	2.5525	1.2497	1.01	0.79
H_3N-HF	0.0344	0.1132	-0.0521	-0.0521	0.2174	2.4033	1.0678	1.48	0.97
OCO-HF	0.0129	0.0617	-0.0158	-0.0149	0.0924	2.6410	1.3665	0.78	0.67
SCO-HF	0.0099	0.0568	-0.0107	-0.0107	0.0782	2.5941	1.4290	0.58	0.81
OCO-HF	0.0112	0.0654	-0.0125	-0.0125	0.0904	2.5352	1.3874	0.62	0.65
NNO-HF	0.0163	0.0708	-0.0199	-0.0190	0.1097	2.5190	1.4672	0.88	0.57
OSO-HF	0.0164	0.0864	-0.0208	-0.0203	0.1275	2.4762	1.2735	0.92	0.77
H_2CO-HF	0.0274	0.1178	-0.0407	-0.0396	0.1979	2.3328	1.1771	1.09	0.86
H_2O-HF	0.0276	0.1270	-0.0425	-0.0399	0.2094	2.3215	1.1149	1.16	0.92
HF-HF	0.0213	0.1113	-0.0313	-0.0296	0.1722	2.2872	1.2199	0.89	0.82
H_3P-HF	0.0114	0.0332	-0.0104	-0.0104	0.0540	3.4761	1.4842	0.98	0.56
H_2S-HF	0.0115	0.0380	-0.0113	-0.0110	0.0603	3.3569	1.4679	1.02	0.57
HCl-HF	0.0072	0.0294	-0.0067	-0.0062	0.0423	3.3547	1.6173	0.74	0.42
HF-HCl	0.0147	0.0621	-0.0180	-0.0170	0.0971	2.4524	1.4564	0.73	0.96

XB-HF	$\rho^o(r_B)$	$\rho^o(r_H)$	$\rho^o(r_B) + \rho^o(r_H)$
OC-HF	0.0063	0.0051	0.0114
SC-HF	0.0093	0.0072	0.0165
NN-HF	0.0042	0.0039	0.0081
HCN-HF	0.0094	0.0083	0.0177
H_3N-HF	0.0187	0.0148	0.0335
OCO-HF	0.0068	0.0059	0.0127
SCO-HF	0.0048	0.0049	0.0097
OCO-HF	0.0055	0.0055	0.0110
NNO-HF	0.0085	0.0079	0.0164
OSO-HF	0.0087	0.0078	0.0165
H_2CO-HF	0.0140	0.0130	0.0270
H_2O-HF	0.0151	0.0130	0.0281
HF-HF	0.0114	0.0105	0.0219
H_3P-HF	0.0061	0.0042	0.0103
H_2S-HF	0.0062	0.0044	0.0106
HCl-HF	0.0039	0.0032	0.0071
HF-HCl	0.0072	0.0085	0.0157

[a] All values are in au. The bond critical point of the B-H hydrogen bond is denoted r_b.

Table 2.1.5. HF Bond Critical Point Analysis of BASE-HF Complexes.[a]

XB-HF	$\Delta\rho(r_a)$	$\Delta\nabla^2\rho(r_a)$	$\lambda_1(r_a)$	$\lambda_2(r_a)$	$\lambda_3(r_a)$	Δr_F	Δr_h
OC-HF	-0.0057	-0.0123	-2.8110	-2.8110	2.2402	0.0086	-0.0040
SC-HF	-0.0138	0.0240	-2.7811	-2.7811	2.2167	0.0186	-0.0067
NN-HF	-0.0028	-0.0319	-2.8225	-2.8225	2.2436	0.0050	-0.0035
HCN-HF	-0.0135	-0.0145	-2.8029	-2.8029	2.2218	0.0189	-0.0081
H_3N-HF	-0.0338	0.2091	-2.6486	-2.6486	2.1368	0.0425	-0.0089
OCO-HF	-0.0056	-0.0178	-2.8137	-2.8137	2.2401	0.0084	-0.0041
SCO-HF	-0.0038	-0.0374	-2.8268	-2.8268	2.2467	0.0063	-0.0040
OCO-HF	-0.0048	-0.0357	-2.8245	-2.8245	2.2438	0.0076	-0.0044
NNO-HF	-0.0070	-0.0186	-2.8124	-2.8119	2.2362	0.0104	-0.0049
OSO-HF	-0.0095	-0.0205	-2.8114	-2.8114	2.2328	0.0137	-0.0063
H_2CO-HF	-0.0192	0.0509	-2.7567	-2.7566	2.1947	0.0257	-0.0081
H_2O-HF	-0.0208	0.0580	-2.7524	-2.7522	2.1931	0.0276	-0.0086
HF-HF	-0.0094	-0.0170	-2.8103	-2.8102	2.2340	0.0138	-0.0061
H_3P-HF	-0.0100	-0.0293	-2.7822	-2.7822	2.2242	0.0131	-0.0042
H_2S-HF	-0.0087	0.0181	-2.7897	-2.7896	2.2279	0.0116	-0.0041
HCl-HF	-0.0036	-0.0025	-2.8056	-2.8055	2.2391	0.0052	-0.0022
HF-HCl[b]	-0.0011	-0.0186	-0.6524	-0.6523	0.4693	0.0243	-0.0185

[a] All values are in au. The bond critical point of the HF bond is denoted r_a. For isolated hydrogen fluoride $\rho(r_a) = 0.3923$ au, $\nabla^2\rho(r_a) = -3.3695$ au, $r_F = 1.4441$ au and $r_h = 0.2576$ au. Changes refer to the complex minus isolated reactant values.

[b] HCl is the proton donor in this primary energy minimum complex, and so, r_a is between H and Cl of HCl here.

Table 2.1.6. Nonbonded Radii (out to the 0.001 au charge density contour) of Isolated Bases and Acids.[a]

Base XB	r_B	Acid	r_H
HF	3.18	HF	2.04
OC	3.78	H_2O	2.22
SC	3.88	H_3N	2.40
NN	3.46	HCl	2.42
HCN	3.56	H_2S	2.56
H_3N	3.88	H_3P	2.80
OCO	3.40	HCN	2.30
SCO	3.18	H_2CO	2.60
OCO	3.16		
NNO	3.40		
OSO	3.40		
H_2CO	3.42		
H_2O	3.48		
H_3P	4.46		
H_2S	4.38		
HCl	4.09		

[a] All values are in au. The results are obtained from Restricted Hartree-Fock/6-311++G**//6-31G** calculations.

Table 2.1.7. Changes in the Acid and Base Fragments of BASE-HF Complexes.[a]

Complex	ΔN	ΔE	Δν
OC-HF			
acid	0.0163	-89.0	-0.29
base	-0.0164	79.6	-6.89
SC-HF			
acid	0.0284	8.5	-0.28
base	-0.0285	-30.4	-11.93
NN-HF			
acid	0.0046	-112.9	-0.47
base	-0.0047	105.9	-9.03
HCN-HF			
acid	0.0170	-87.6	-2.50
base	-0.0171	60.3	-10.18
H_3N-HF			
acid	0.0457	-42.6	-2.64
base	-0.0460	-3.6	-16.54
OCO-HF			
acid	0.0081	-8.2	-1.28
base	-0.0081	-2.6	-3.20
SCO-HF			
acid	0.0026	-4.7	-1.43
base	-0.0026	-6.3	-9.19
OCO-HF			
acid	0.0044	-70.2	-2.24
base	-0.0046	57.6	-3.68
NNO-HF			
acid	0.0085	-80.9	-2.58
base	-0.0087	68.2	-10.35
OSO-HF			
acid	0.0093	18.2	-2.60
base	-0.0095	-40.4	-5.26
H_2CO-HF			
acid	0.0230	-49.4	-4.24
base	-0.0230	22.0	-12.11
H_2O-HF			
acid	0.0231	-30.0	-3.40
base	-0.0232	-5.0	-11.76
HF-HF			
acid	0.0083	-6.9	-3.73
base	-0.0084	-10.0	-5.42
H_3P-HF			
acid	0.0328	15.2	2.63
base	-0.0330	-31.6	-10.28
H_2S-HF			
acid	0.0266	19.5	2.37
base	-0.0267	-44.4	-10.69
HCl-HF			
acid	0.0124	44.3	3.49
base	-0.0125	-52.1	-2.74

Table 2.1.7. (con'd)

Complex	ΔN	ΔE	Δv
HF-HCl			
acid	-0.0028	-35.9	-5.32
base	0.0026	25.9	-2.36

[a] All results are in au except ΔE values which are in kJ mol^{-1}.

Table 2.1.8. Atomic Properties of Isolated Reactants.[a]

Reactant	Ω	N(Ω)	|μ(Ω)|[b]	v(Ω)	Q_{zz}(Ω)
HF	F	9.7527	0.373	128.26	0.050
	H	0.2474	0.109	13.02	-0.080
OC	C	4.6731	1.718	112.74	-0.288
	O	9.3269	0.984	139.47	-0.052
SC	C	6.8870	0.438	174.89	-1.610
	S	15.1130	1.494	206.61	5.702
NN	N	7.0000	0.646	129.75	1.444
HCN	N	8.3454	0.786	168.77	0.368
	C	4.8768	1.134	84.96	2.332
	H	0.7778	0.114	38.62	0.366
H_3N	N	8.0759	0.208	138.41	
	H	0.6414	0.189	31.96	
OOO	O	8.1088	0.580	112.12	
	O	7.7823	0.433	71.90	
SCO	O	9.2743	0.825	137.44	0.123
	C	5.2361	2.006	75.71	0.514
	S	15.4896	1.252	224.81	7.615
OCO	O	9.2976	0.789	137.38	0.329
	C	3.4049	0.000	27.56	1.588
NNO	O	8.4247	0.419	118.31	
	N	7.0158	0.790	75.77	
	N	6.5596	1.150	119.72	
OSO	O	9.3311	0.681	133.72	
	S	13.3379	2.021	112.70	
H_2CO	O	9.2403	0.597	137.74	
	C	4.7547	0.912	58.71	
	H	1.0025	0.122	49.85	
H_2O	O	9.2234	0.243	147.39	
	H	0.3883	0.158	20.15	
H_3P	P	13.1201	2.361	145.86	
	H	1.6266	0.358	77.97	
H_2S	S	15.3264	1.461	207.21	
	H	1.3368	0.201	60.25	
HCl	Cl	17.2771	0.035	237.01	
	H	0.7229	0.135	37.93	

[a] All values are in au. The base atom that participates in the H-bond is listed first, followed by the next nearest base atom and the remaining nonequivalent base atoms.
[b] See Figure 1.2.5 for directions of moments.

Table 2.1.9. Changes in Atomic Properties of BASE-HF Complexes.

Complex	Q	ΔN(Q)	Δ|μ(Q)|	Δv(Q)	ΔQzz(Q)
OC-HF	F	0.0209	0.001	2.16	-0.007
	H	-0.0046	-0.008	-2.45	0.056
	C	0.0059	-0.007	-5.20	0.220
	O	-0.0223	0.014	-1.69	-0.043
SC-HF	F	0.0380	-0.002	3.45	-0.016
	H	-0.0096	-0.011	-3.74	0.070
	C	0.0543	0.057	-8.50	0.493
	S	-0.0828	-0.004	-3.43	-0.180
NN-HF	F	0.0121	0.001	1.09	-0.012
	H	-0.0075	-0.010	-1.56	0.048
	N	0.0424	0.000	-3.99	0.070
	N	-0.0471	0.002	-5.04	-0.037
HCN-HF	F	0.0376	-0.006	2.36	-0.028
	H	-0.0206	-0.019	-4.86	0.069
	N	0.0388	0.014	-8.18	0.220
	C	-0.0355	0.012	-0.52	-0.226
	H	-0.0204	-0.002	-1.48	-0.017
H3N-HF	F	0.0659	-0.016	3.20	
	H	-0.0202	-0.022	-5.84	
	N	0.0317	-0.095	-12.53	
	H	-0.0259	-0.009	-1.32	
	H	-0.0257	-0.009	-1.32	
	H	-0.0261	-0.009	-1.37	
OCO-HF	F	0.0189	0.001	2.12	
	H	-0.0108	-0.014	-3.40	
	O	0.0488	-0.001	-1.81	
	O	-0.0129	-0.008	-0.45	
	O	-0.0440	-0.011	-0.94	
SCO-HF	F	0.0158	-0.002	1.47	-0.022
	H	-0.0132	-0.015	-2.90	0.055
	O	0.0250	-0.047	-2.87	0.091
	C	0.0304	0.021	-0.12	0.026
	S	-0.0580	0.001	-6.20	-0.192
OCO-HF	F	0.0177	-0.002	1.30	-0.024
	H	-0.0133	-0.015	-3.54	0.064
	O	0.0202	-0.041	-2.19	0.082
	C	-0.0119	0.005	-0.83	-0.032
	O	-0.0129	0.023	-0.66	-0.048
NNO-HF	F	0.0230	0.000	0.17	
	H	-0.0145	-0.013	-2.75	
	O	0.0273	0.016	-3.21	
	N	0.0088	0.000	0.38	
	N	-0.0448	-0.012	-7.52	
OSO-HF	F	0.0281	-0.004	1.98	
	H	-0.0188	-0.020	-4.58	
	O	0.0261	-0.016	-2.91	
	S	-0.0182	-0.015	-1.12	
	O	-0.0174	0.022	-1.23	

Table 2.1.9 (con'd)

Complex	Ω	ΔN(Ω)	Δ|μ(Ω)|	Δv(Ω)
H_2CO-HF	F	0.0455	-0.008	0.77
	H	-0.0225	-0.021	-5.01
	O	0.0180	-0.018	-8.18
	C	0.0279	0.016	0.09
	H	-0.0432	-0.006	-2.75
	H	-0.0257	-0.004	-1.27
H_2O-HF	F	0.0475	-0.009	2.43
	H	-0.0244	-0.025	-5.83
	O	0.0251	0.052	-9.86
	H	-0.0241	-0.011	-0.95
	H	-0.0242	-0.011	-0.95
HF-HF	F	0.0288	-0.004	1.19
	H	-0.0205	-0.022	-4.92
	F	0.0059	0.000	-4.40
	H	-0.0143	-0.008	-1.02
H_3P-HF	F	0.0316	0.006	3.83
	H	0.0012	0.001	-1.20
	P	-0.0179	-0.059	-8.45
	H	-0.0050	0.019	-0.64
	H	-0.0051	0.019	-0.62
	H	-0.0050	0.019	-0.57
H_2S-HF	F	0.0285	0.006	3.38
	H	-0.0019	-0.003	-1.01
	S	-0.0141	-0.016	-8.51
	H	-0.0064	-0.008	-1.08
	H	-0.0062	-0.008	-1.10
HCl-HF	F	0.0141	0.003	2.28
	H	-0.0017	0.001	1.21
	Cl	0.0051	-0.012	-1.43
	H	-0.0176	-0.003	-1.31
HF-HCl	Cl	0.0534	-0.022	2.89
	H	-0.0562	-0.038	-8.21
	F	0.0123	-0.002	-1.70
	H	-0.0097	-0.005	-0.66

[a] All values are in au. For all complexes the F of HF is listed first (except in HF-HCl), followed by the H-bonded H, the base atom B participating in the hydrogen bond, the next nearest base atom, and the remaining base atoms.

Table 2.1.10. Attractive (A) and Repulsive (R) Contributions to the Changes in Potential Energy for H in BASE-HF Complexes.[a]

Complex	$\Delta V_H(H)$	$\Delta V_A(H)$	$\Delta V_R(H)$	$\Delta E(H)$	$\Delta N(H)$
OC-HF	29.2	-1743.7	1780.8	18.6	-0.0046
SC-HF	60.1	-2364.8	2438.4	36.8	-0.0096
NN-HF	28.3	-1740.6	1772.0	15.6	-0.0075
HCN-HF	85.8	-1616.1	1706.2	45.0	-0.0206
H_3N-HF	110.7	-1385.0	1509.2	62.1	-0.0202
OCO-HF	40.4	-3192.4	3231.5	19.5	-0.0108
SCO-HF	43.1	-2935.5	2976.0	20.2	-0.0132
OCO-HF	47.2	-2467.6	2516.6	24.5	-0.0133
NNO-HF	54.3	-2647.2	2703.1	27.9	-0.0145
OSO-HF	69.8	-3559.1	3626.4	33.6	-0.0188
H_2CO-HF	95.9	-2142.5	2240.7	49.1	-0.0225
H_2O-HF	102.9	-1411.4	1514.7	51.6	-0.0244
HF-HF	70.0	-1557.7	1619.7	31.0	-0.0205
H_3P-HF	30.1	-2395.2	2446.5	25.7	0.0012
H_2S-HF	16.4	-2637.9	2685.4	23.7	-0.0019
HCl-HF	-8.7	-2747.8	2788.8	20.5	-0.0017
HF-HCl	128.5	-3437.7	3548.4	55.4	-0.0562

[a] Energy values are in kJ mol^{-1}.

Table 2.1.11. Correlation of D_e with Changes in Atomic Properties (in au).

Class I	D_e	Δr_B^o	$\lvert\Delta\mu(B)\rvert$	Δr_H^o	$\lvert\Delta\mu(H)\rvert$	$\lvert\Delta r_B^o + \Delta r_H^o\rvert$
XB	kJ/mol					
OC	9.3	0.81	0.007	0.63	0.008	1.54
SC	21.8	1.14	0.057	0.74	0.001	1.88
NN	6.9	0.61	0.000	0.53	0.010	1.14
HCN	27.2	1.01	0.014	0.79	0.019	1.80
H_3N	46.1	1.48	0.095	0.97	0.022	2.45
OOO	10.7	0.76	0.001	0.67	0.014	1.43
H_2O	34.9	1.16	0.052	0.92	0.025	2.08
Class II						
SCO	10.9	0.58	0.047	0.61	0.015	1.19
OCO	12.6	0.62	0.041	0.65	0.015	1.27
NNO	12.6	0.88	0.016	0.57	0.016	1.45
OSO	22.1	0.92	0.016	0.77	0.016	1.69
H_2CO	27.3	1.09	0.018	0.86	0.018	1.95

Table 2.1.12. Changes in the Contributions of the σ and π Orbitals to the Atomic Populations in Linear BASE-HF Complexes and Changes in $Q_{zz}(\Omega)$ (in au).

Complex		F	H	B	X1[a]	X2[a]
NN-HF	$\Delta N_\sigma(\Omega)$	0.012	-0.008	0.006	-0.012	
	$\Delta N_\pi(\Omega)$	0.000	0.000	0.036	-0.035	
	$N_\pi(\Omega)$	3.987	0.012	2.036	1.965	
	$\Delta Q_{zz}(\Omega)$	-0.012	0.048	0.070	-0.037	
OC-HF	$\Delta N_\sigma(\Omega)$	0.022	-0.004	-0.008	-0.009	
	$\Delta N_\pi(\Omega)$	-0.001	-0.001	0.015	-0.013	
	$N_\pi(\Omega)$	3.986	0.012	0.565	3.437	
	$\Delta Q_{zz}(\Omega)$	-0.007	0.056	0.220	-0.043	
SCO-HF	$\Delta N_\sigma(\Omega)$	0.016	-0.013	-0.003	0.005	-0.004
	$\Delta N_\pi(\Omega)$	0.000	0.000	0.028	0.025	-0.054
	$N_\pi(\Omega)$	3.988	0.013	3.583	1.395	7.022
	$\Delta Q_{zz}(\Omega)$	-0.022	0.055	0.091	0.026	-0.192
OCO-HF	$\Delta N_\sigma(\Omega)$	0.018	-0.014	-0.001	-0.006	0.002
	$\Delta N_\pi(\Omega)$	0.000	0.001	0.021	-0.006	-0.015
	$N_\pi(\Omega)$	3.988	0.014	3.659	0.716	3.623
	$\Delta Q_{zz}(\Omega)$	-0.024	0.064	0.082	-0.032	-0.048
SC-HF	$\Delta N_\sigma(\Omega)$	0.039	-0.009	-0.012	-0.019	
	$\Delta N_\pi(\Omega)$	-0.001	-0.001	0.066	-0.064	
	$N_\pi(\Omega)$	3.986	0.012	1.494	6.508	
	$\Delta Q_{zz}(\Omega)$	-0.016	0.070	0.483	-0.190	
HCN-HF	$\Delta N_\sigma(\Omega)$	0.038	-0.020	-0.009	0.008	-0.017
	$\Delta N_\pi(\Omega)$	0.000	-0.001	0.048	-0.044	-0.003
	$N_\pi(\Omega)$	3.987	0.012	2.790	1.185	0.026
	$\Delta Q_{zz}(\Omega)$	-0.028	0.069	0.220	-0.226	-0.017

[a] X1 denotes the nearest base atom to atom B of the base and X2 denotes the remaining base atom.

Table 2.1.13. Changes in Atomic Populations and Energies for O_3-HF and SCO-HF.[a]

Complex	Ω	ΔN(Ω) au	ΔE(Ω) kJ mol^{-1}
OOO-HF	F	0.019	-27.7
	H	-0.011	19.5
	O	0.049	-44.6
	O	-0.013	18.9
	O	-0.044	23.1
SCO-HF	F	0.016	-25.0
	H	-0.013	20.2
	O	0.025	-7.2
	C	0.030	-48.2
	S	-0.058	49.1

[a] The F of HF is listed first, followed by the hydrogen-bonded H, the base atom B participating in the hydrogen bond, the next nearest base atom, and the remaining base atoms.

Table 2.1.14. Dipole Moments and Dipole Moment Enhancements for BASE-HA Complexes.[a]

Complex	μ		DME	
	calc	expt	calc	expt
OC-HF	2.2534	2.3520	0.45	0.55
SC-HF	4.5327		1.89	
NN-HF	2.3992		0.37	0.36
HCN-HF	6.0653	5.6100	0.75	0.80
H3N-HF	4.5912		0.79	
OCO-HF	3.2952		0.40	
SCO-HF	3.2291	3.2085	0.80	0.84
OCO-HF	2.6131	2.2465	0.58	0.60
NNO-HF	1.9510	2.0700	0.19	0.50
OSO-HF	4.8352		0.54	
H2CO-HF	3.7189	4.0060	0.62	0.86
H2O-HF	4.3314	4.0730	0.39	0.68
HF-HF	3.1410	2.9900	0.24	0.60
H3P-HF	3.5317		0.65	
H2S-HF	3.1029	2.6239	0.92	0.78
HCl-HF	2.6462		0.07	
HF-HCl	3.2000	2.4085	0.29	0.14
OC-HCl	1.5347	1.5200	0.34	0.39
SC-HCl	3.8086		1.76	
NN-HCl	1.6847	1.2442	0.25	0.25
HCN-HCl	5.4420	4.8170	0.73	0.94
H3N-HCl	4.3095		1.11	
SCO-HCl	2.4077		0.58	
OCO-HCl	1.8945	1.4509	0.46	0.45

[a] All values are in debyes. The magnitude of the molecular dipole moment is denoted μ and the dipole moment enhancement is denoted DME. The experimental results are from Legon and Millen (1986).

Table 2.1.15. Effect of Electron Correlation on Dissociation Energies of BASE-HF Complexes.[a]

Complex	D_e (kJ mol^{-1}) Scheme				%error in D_e Scheme		
	I	II	III	exp't[b]	I	II	III
HF-HF	25.1	16.7	18.7	19.1	31	12	2
HCN-HF	26.8	27.2	29.4	25.9	3	5	14
H_2O-HF	38.1	34.8	39.4	42.7	11	18	8
OC-HF	11.7	9.3	13.8				
CO-HF	8.8	8.2	6.3				
H_3N-HF	49.4	46.2	53.8				

[a] Schemes I, II and III refer to the following respective methods of calculation: RHF/6-31G**//6-31G**, RHF/6-311++G**//6-31G** and MP2/6-311++G**//6-31G**.
[b] Legon and Millen (1986).

Table 2.1.16. Effect of Electron Correlation on the Properties of the Hydrogen Bond Critical Point (r_b) and HF bond critical point (r_a) in OC-HF and H$_3$N-HF.[a]

	$\rho(r_b)$	$\nabla^2\rho(r_b)$	$\lvert\Delta r_B^o\rvert$	$\lvert\Delta r_H^o\rvert$
OC-HF	0.0007	-0.0026	0.03	0.04
H$_3$N-HF	0.0019	-0.0087	0.08	0.05

	$\Delta\rho(r_a)$	$\Delta\nabla^2\rho(r_a)$	Δr_F	Δr_h
OC-HF	0.0003	0.0160	-0.0003	0.0003
H$_3$N-HF	0.0035	0.0397	-0.0039	0.0038

[a] The values listed are the changes in the given property due to correlation, that is, Scheme III minus Scheme II values.

Table 2.1.17. Effect of Electron Correlation on Atomic Properties of the Constituent Atoms in HF, OC, H_3N and H_3N-HF.[a]

		Scheme III values			Scheme III - Scheme II		
System	Ω	N(Ω)	μ(Ω)	v(Ω)	ΔN(Ω)	Δ|μ(Ω)|	Δv(Ω)
HF	F	9.7200	0.332	128.11	-0.0327	-0.041	-0.15
	H	0.2800	0.127	16.34	0.0326	0.018	3.32
OC	C	4.8746	1.677	120.66	0.2015	-0.041	7.92
	O	9.1254	0.826	138.22	-0.2015	-0.158	-1.25
H_3N	N	8.0597	0.225	143.53	-0.0162	0.017	5.12
	H	0.6468	0.200	33.07	0.0054	0.011	1.11
H_3N-HF[b]	F	9.7832	0.313	133.40	-0.0354	-0.044	1.94
	H	0.2720	0.104	9.00	0.0448	0.017	5.84
	N	8.0820	0.103	127.11	-0.0256	-0.010	1.13
	H	0.6209	0.189	31.76	0.0054	0.009	1.12
Differences in atomic properties upon complexation.							
H_3N-HF[b]	F	0.0632	-0.019	5.29	-0.0027	-0.003	2.09
	H	-0.0080	-0.023	-7.34	0.0122	-0.001	-1.50
	N	0.0223	-0.122	-16.42	-0.0094	-0.027	-3.89
	H	-0.0259	-0.011	-1.31	0.0000	-0.002	0.01

[a] All values are in au.

[b] The F of HF is listed first followed by the H-bonded H, the base atom B participating in the hydrogen bond and the next nearest base atom.

Table 2.1.18. Hydrogen Bond Critical Point Analysis of BASE-HCl Complexes.*

XB-HCl	$\rho(r_b)$	$\nabla^2\rho(r_b)$	$\lambda_1(r_b)$	$\lambda_2(r_b)$	$\lambda_3(r_b)$	r_B	r_H	$\lvert\Delta r_B^o\rvert$	$\lvert\Delta r_H^o\rvert$
OC-HCl	0.0085	0.0259	-0.0075	-0.0075	0.0409	3.0605	1.7414	0.72	0.68
SC-HCl	0.0131	0.0400	-0.0128	-0.0128	0.0655	2.9040	1.5522	0.98	0.67
NN-HCl	0.0062	0.0204	-0.0055	-0.0055	0.0313	3.0028	1.8655	0.46	0.55
HCN-HCl	0.0136	0.0519	-0.0143	-0.0143	0.0805	2.6977	1.4863	0.86	0.92
H_3N-HCl	0.0306	0.0876	-0.0413	-0.0413	0.1702	2.4618	1.1975	1.42	1.22
SCO-HCl	0.0073	0.0293	-0.0067	-0.0067	0.0428	2.7422	1.7555	0.44	0.66
OCO-HCl	0.0085	0.0356	-0.0080	-0.0080	0.0516	2.6716	1.8850	0.49	0.74

XB-HCl	$\rho^o(r_B)$	$\rho^o(r_H)$	$\rho^o(r_B) + \rho^o(r_H)$
OC-HCl	0.0043	0.0044	0.0087
SC-HCl	0.0068	0.0068	0.0136
NN-HCl	0.0029	0.0034	0.0063
HCN-HCl	0.0068	0.0077	0.0145
H_3N-HCl	0.0167	0.0159	0.0326
SCO-HCl	0.0033	0.0043	0.0076
OCO-HCl	0.0039	0.0050	0.0089

* All values are in au and are calculated using Scheme II. The bond critical point of the B-H hydrogen bond is denoted r_b.

Table 2.1.19. HCl Bond Critical Point Analysis of BASE-HCl Complexes.[a]

XB-HCl	$\Delta\rho(r_a)$	$\Delta\nabla^2\rho(r_a)$	$\lambda_1(r_a)$	$\lambda_2(r_a)$	$\lambda_3(r_a)$	Δr_{Cl}	Δr_H
OC-HCl	-0.0006	-0.0086	-0.6452	-0.6452	0.4651	0.0141	-0.0103
SC-HCl	-0.0036	-0.0101	-0.6498	-0.6498	0.4726	0.0363	-0.0231
NN-HCl	0.0000	-0.0074	-0.6430	-0.6430	0.4618	0.0077	-0.0064
HCN-HCl	-0.0032	-0.0177	-0.6539	-0.6539	0.4733	0.0378	-0.0261
H_3N-HCl	-0.0170	0.0223	-0.6375	-0.6375	0.4805	0.1038	-0.0505
SCO-HCl	-0.0001	-0.0116	-0.6464	-0.6464	0.4643	0.0111	-0.0084
OCO-HCl	-0.0002	-0.0134	-0.6478	-0.6478	0.4655	0.0137	-0.0113

[a] All values are in au. The bond critical point of the HCl bond is denoted r_a. For isolated hydrogen chloride $\rho(r_a)$ = 0.2581 au, $\nabla^2\rho(r_a)$ = -0.8168 au, r_{Cl} = 1.7091 au and r_H = 0.6824 au. Changes represent complex minus isolated reactant values.

Table 2.1.20. Changes in the Acid and Base Fragments of BASE-HCl Complexes.[a]

Complex	ΔN	Δv
OC-HCl		
acid	0.0075	-1.87
base	-0.0080	-2.14
SC-HCl		
acid	0.0161	-2.67
base	-0.0157	-6.69
NN-HCl		
acid	0.0009	-1.44
base	-0.0007	-3.74
HCN-HCl		
acid	0.0070	-3.42
base	-0.0070	-7.43
H$_3$N-HCl		
acid	0.0376	-1.25
base	-0.0375	-14.68
SCO-HCl		
acid	0.0001	-3.59
base	-0.0002	-3.95
OCO-HCl		
acid	0.0002	-3.84
base	-0.0002	-0.69

[a] All results are in au.

Table 2.1.21. Changes in Atomic Properties of BASE-HCl Complexes.[a]

Complex	Ω	ΔN(Ω)	Δ|μ(Ω)|	Δv(Ω)	ΔQzz(Ω)	ΔE(H)[b]
OC-HCl	Cl	0.0300	-0.031	0.67	-0.091	
	H	-0.0225	-0.015	-2.54	0.085	28.80
	C	0.0061	-0.005	-1.51	0.181	
	O	-0.0141	0.008	-0.63	-0.021	
SC-HCl	Cl	0.0685	0.057	3.13	-0.234	
	H	-0.0524	-0.022	-5.80	0.116	72.45
	C	0.0421	0.040	-5.35	0.426	
	S	-0.0578	-0.003	-1.34	-0.138	
NN-HCl	Cl	0.0178	-0.021	0.04	-0.061	
	H	-0.0169	-0.015	-1.48	0.080	18.24
	N	0.0275	0.003	-3.69	0.059	
	N	-0.0282	0.000	-0.05	-0.025	
HCN-HCl	Cl	0.0752	0.057	4.01	-0.274	
	H	-0.0682	-0.032	-7.43	0.097	82.06
	N	0.0324	0.005	-5.72	0.183	
	C	-0.0248	0.008	-0.37	-0.161	
	H	-0.0146	-0.001	-1.34	-0.012	
H3N-HCl	Cl	0.1660	0.059	12.82		
	H	-0.1284	-0.045	-14.07		174.68
	N	0.0298	-0.092	-11.34		
	H	-0.0224	-0.008	-1.07		
	H	-0.0224	-0.008	-1.14		
	H	-0.0225	-0.008	-1.13		
SCO-HCl	Cl	0.0270	-0.024	-0.36	-0.068	
	H	-0.0269	-0.023	-3.23	0.091	28.69
	O	0.0191	-0.034	-0.17	0.063	
	C	0.0195	0.014	0.57	0.010	
	S	-0.0388	0.005	-4.35	-0.146	
OCO-HCl	Cl	0.0346	-0.028	0.43	-0.092	
	H	-0.0344	-0.027	-4.27	0.093	33.76
	O	0.0167	-0.032	-0.73	0.059	
	C	-0.0083	0.004	-0.20	-0.018	
	O	-0.0086	0.016	0.24	-0.032	

[a] All values are in au. For all complexes the Cl of HCl is listed first, followed by the hydrogen-bonded H, the base atom B participating in the hydrogen bond, the next nearest base atom and the remaining base atoms.

[b] This value represents the energy of the hydrogen-bonded hydrogen in the complex minus the value of the energy of the hydrogen in isolated hydrogen chloride.

2.2 HYDROGEN BONDING IN NEUTRAL AND CHARGED WATER AND AMMONIA DIMERS

In this section we see if the description of the nature, energetics and mechanism of BASE-HA hydrogen-bond formation can be extended to both larger and stronger hydrogen-bonded complexes, namely the water dimer, the ammonia dimer, the mixed water-ammonia complex and the corresponding protonated species. Strong hydrogen bonds are of interest because of their role in mediating acid-base equilibria (Bell 1973), proton transfer (Caldin and Gold 1975), and solvation (Jones and Arnett 1974).

Energies and Geometries of the Complexes

The pertinent energies and geometries of the complexes are presented in Table 2.2.1 and the molecular graphs are presented in Figure 2.2.1. Table 2.2.2 lists the fully optimized geometries (6-31G**) in terms of cartesian coordinates. The symbols A and B refer to the oxygen or nitrogen atom of the acid or base molecule and H to the atom shared in the hydrogen bond. The energy surface of the ammonia dimer is extremely flat with only a small difference in energy (less than 0.1 kcal mol^{-1}) between a linear C_s geometry reported here and a nearly cyclic structure (Buckingham et al 1988). The atomic properties of the two structures are very similar.

The heavy atom distances r(AB) and the H-bond lengths r(H-B) do not decrease in a linear fashion with increasing D_e. Still, the

weakest complex, the ammonia dimer, has the largest values for r(AB) and r(H-B) and the strongest complex, the hydronium ion-water complex, has the smallest. With the exception of the ammonia dimer, $\Delta r(AH)$ increases with increasing D_e. We have previously seen that $\Delta r(AH)$ increases with increasing D_e for the BASE-HF complexes. In general, the H-bonds are nearly linear ($\angle AHB > 170^o$).

Topology of the Charge Distributions

The values of the charge density at the hydrogen bond critical point r_b are small and positive, characteristic of a closed-shell interaction, and parallel the increase in H-bond strength (Table 2.2.3). The corresponding value of the Laplacian is positive in all cases except for the complex between the hydronium ion and water. Examination of Table 2.2.3 and Figure 2.2.2 shows that as the hydrogen bond energy increases, the critical point of the H-bond moves progressively closer to the zero contour encompassing the valence shell of charge concentration in the Laplacian distribution of the acid (i.e. r_H decreases as D_e increases). In the H_2OH^+-OH_2 system the critical point lies just inside this contour. It is noteworthy that $\nabla^2\rho(r_b)$ for this system using the RHF/DZP//DZP scheme (Dunning 1970) is slightly positive (0.0212 au).

The penetration values listed in Table 2.2.3 do increase with increasing D_e just as they did for the BASE-HA complexes. There is a much better correlation between penetration and D_e than between hydrogen bond length and D_e. The sum of the unperturbed densities, $\rho^o(r_B) + \rho^o(r_H)$, is nearly equal to the value of $\rho(r_b)$. For example,

the sum is 0.0190 for the water dimer and 0.1080 for the hydronium ion-water complex.

Turning to the properties of the AH bond critical point, denoted r_a, we see that $\Delta\rho(r_a)$ becomes more negative as D_e increases. More electron density is removed from the AH bond and placed in the H-B region as D_e increases. For the neutral complexes, $\Delta\nabla^2\rho(r_a)$ is negative implying that of the charge density left in the AH bond, more is concentrated at r_a in the complex than at r_a in the isolated reactant. For the cationic species, the reverse is true and this helps explain the greater stability of these systems.

Atomic Properties

The energies of hydrogen bond formation and the individual atomic contributions to these energy changes are given in Table 2.2.4. The strongest H-bond for the neutral systems is found in the mixed complex with H_2O being a stronger acid than NH_3. The mixed cationic complex is NH_4^+-H_2O but the strongest cationic complex is that between the hydronium ion and water.

In general, the acid molecule is stabilized upon H-bond formation and this stabilization is greater in magnitude than the stabilization (or destabilization) of the corresponding base molecule. Only in the two strongest complexes, H_3NH^+-NH_3 and H_2OH^+-OH_2, are both the acid and base stabilized.

Of the atoms which participate in the hydrogen bond, A,H and B, we note that the H atom is always destabilized though the destabilization does not correlate with D_e. (The virial correction

factors are sufficiently close between complex and isolated reactants to allow meaningful energy comparisons). The A atom is stabilized with the exception of the oxygen in the hydronium ion-water complex and the B atom is always stabilized. The stabilization of B dominates the energy changes for the cationic systems and this effect is greatest in the strongest of these interactions.

The formation of a hydrogen bond in the neutral and charged complexes is accompanied by a transfer of charge from the base to the acid with the magnitude of transfer paralleling the increase in D_e (Table 2.2.5). The magnitude of this transfer is relatively small compared to the changes in the individual atomic charges for the neutral complexes, a fact previously observed for the BASE-HA complexes. Therefore, there is a considerable redistribution of charge within the acid and the base. The hydrogen-bonded atom H of the acid undergoes a loss of charge larger than or comparable to the total charge transferred from base to acid, the only exception being for H in the hydronium ion complex. This latter behaviour is understandable since there is a large net positive charge already present on the hydrogens of the free hydronium ion. Upon complexation, the largest fraction of the electronic charge increase on the H_nA fragment of the acid resides on the A atom in the neutral systems and on the nonparticipating hydrogens H_n in the cationic systems.

The net negative charge on the B atom of the base BH_m increases in magnitude upon complexation by an amount which, in general, is greater than the total electronic charge lost by the base. Thus the m hydrogen atoms of the base undergo both intra- and intermolecular

charge transfer, transferring charge to the B atom of the base as well as to the acid.

There is a decrease in the molecular volumes of both reactants upon hydrogen bond formation (Table 2.2.5). The magnitude of the total decrease parallels the strength of interaction (Figure 2.2.3). The two sets of nearly linear data points lead to energy changes per unit change in volume of 0.5 and 1.4 kcal/au for the neutral and cationic complexes respectively. The largest atomic decreases in volume are for the H atom of the acid and the B atom of the base, a result of the formation of a new interatomic surface between these two atoms. This surface is much flatter than that for a normal OH or NH bond (Figure 2.2.2). The decrease in the H atom volume is relatively small for the hydronium ion-water complex because of the very contracted nature of the charge density in the hydronium ion. The magnitude of the atomic volume decrease for B increases with the strength of the hydrogen bond. The A atom increases slightly in volume upon complexation with the exception of the hydronium ion-water complex.

Changes in the atomic properties of a water trimer wherein a single water molecule provides both acidic hydrogens (Tables 2.2.1, 2.2.2 and Figure 2.2.1) are given in Tables 2.2.4 and 2.2.5. The formation of the water dimer results in an energy lowering of 5.5 kcal mol^{-1} and the formation of a second hydrogen bond lowers the energy by another 3.9 kcal mol^{-1}. The energy and volume decrease on dimer formation are both ~60% of that observed for the formation of the trimer. Each H atom of the acid undergoes a loss of electrons and volume on hydrogen bonding, greater than two-thirds of that found in

the formation of the dimer. The base oxygen atoms B undergo increases in electronic charge and decreases in energy almost identical with those found for the formation of the dimer. The decreases in their volumes are about three-quarters as great. The increases in charge, stability and volume found for the oxygen atom of the acid are almost twice as large as those found for the dimer.

It is found that for all seven systems examined in this section, the hydrogen-bonded atom H undergoes a decrease in electronic charge, stability and volume upon complexation. The B atom of the base also decreases in volume but increases in electronic charge and stability. In general, the A atom increases in charge and volume but decreases in stability. The charge and energy changes for the H and B atoms are consistent with an ionic interaction. The substantial initial net charges on H and B are further increased and the accompanying polarizations of the base and acid molecules are in a direction counter to the direction of this apparent charge transfer. The charge transferred to B lowers the energy of the system and is the major source of stability in the tightly bound systems. It is the same transfer of charge to atom B which binds both nuclei in an ionic system in the electrostatic interpretation of binding using the Hellmann-Feynman theorem.

In this section we have looked at NH-N, NH-O, OH-N and OH-O hydrogen bonds in both neutral and cationic small complexes. In the following section we examine the NH-O hydrogen bond in a larger, neutral, conjugated system, the formamide dimer, and in Section 2.4. we study OH-O bonds in larger, anionic systems.

Figure 2.2.1

Molecular graphs of hydrogen-bonded complexes H_nAH-BH_m (A=N,O; B=N,O). Bond critical points are indicated by black dots.

1) H_2NH-NH_3; 2) $HOH-OH_2$; 3) $HOH-NH_3$; 4) $H_3NH^+-OH_2$; 5) $H_3NH^+-NH_3$ 6) $H_2OH^+-OH_2$ 7) H_2O trimer.

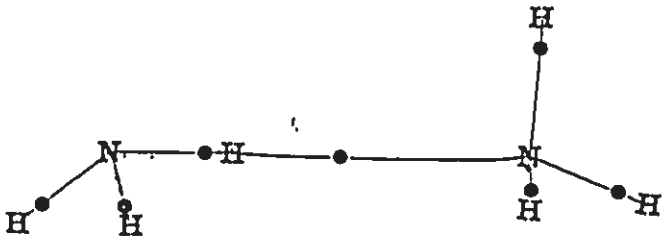

1

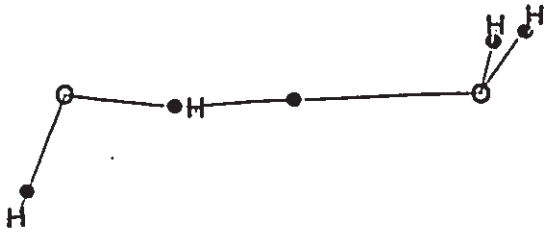

2

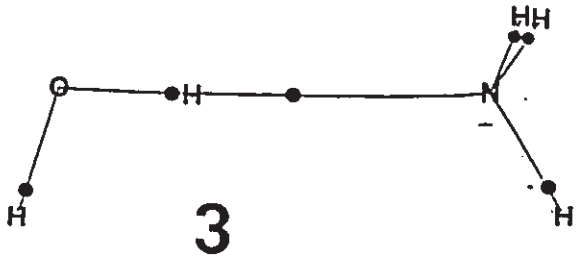

3

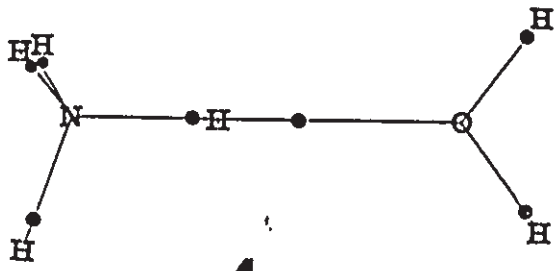

4

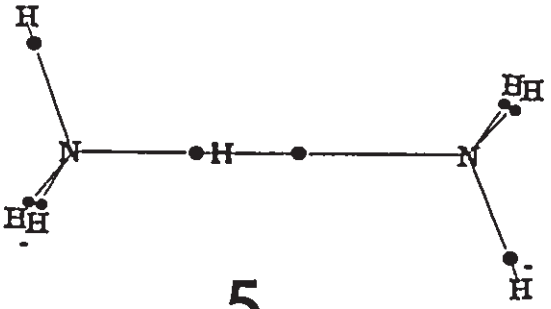

5

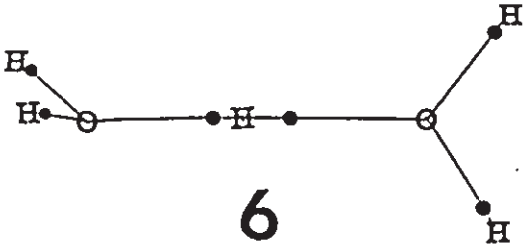

6

7

Figure 2.2.2

Contour maps of $\nabla^2\rho$ for HOH-OH$_2$ (a) and H$_2$OH$^+$-OH$_2$ (b). The out-of-plane hydrogens of the base in (a) and of the acid in (b) are indicated. The zero flux surfaces, bond paths and bond critical points (black dots) are shown. The critical point of the hydrogen bond in the charged complex is found just inside the zero contour encompassing the proton.

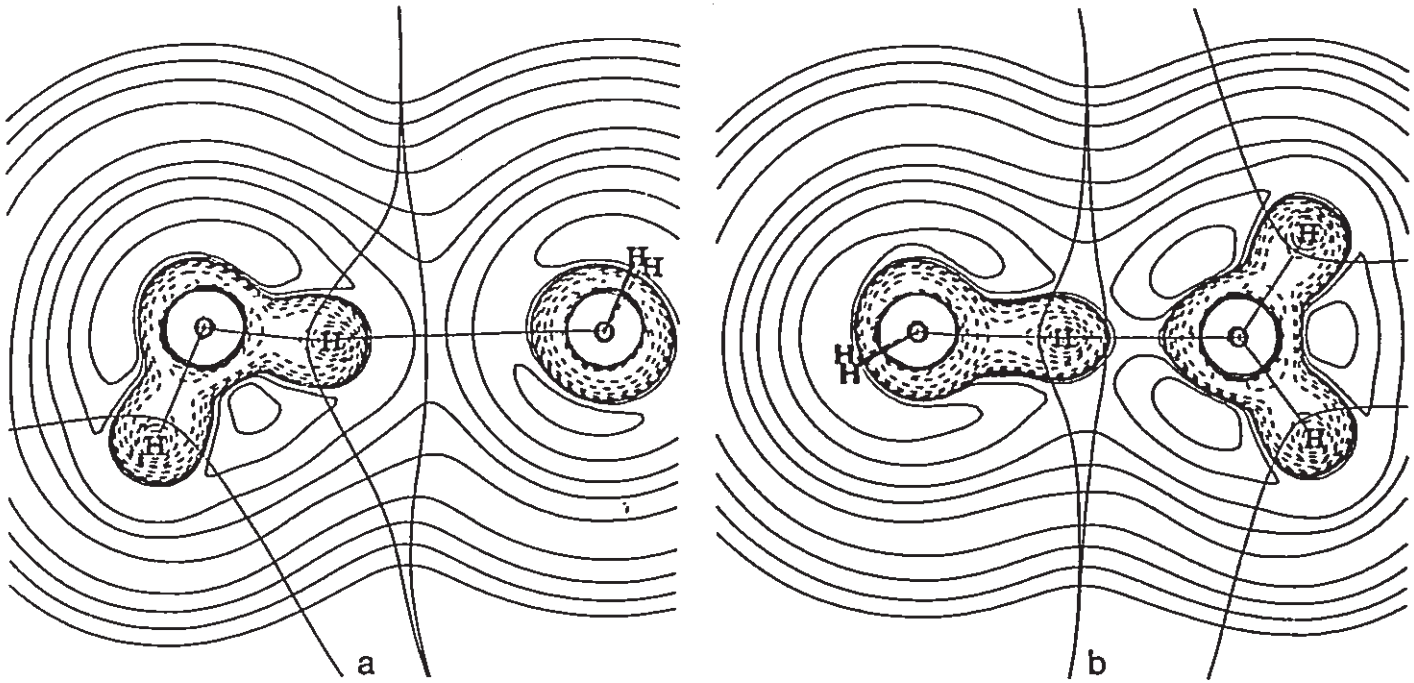
a
b

Figure 2.2.3

Plots of Δv versus ΔE for the dimers listed in Table 2.2.1. The volume changes, v(dimer) - v(monomers) in the upper curves are determined using the 0.002 au envelope while those in the lower curves are determined using the 0.001 au envelope of the charge density.

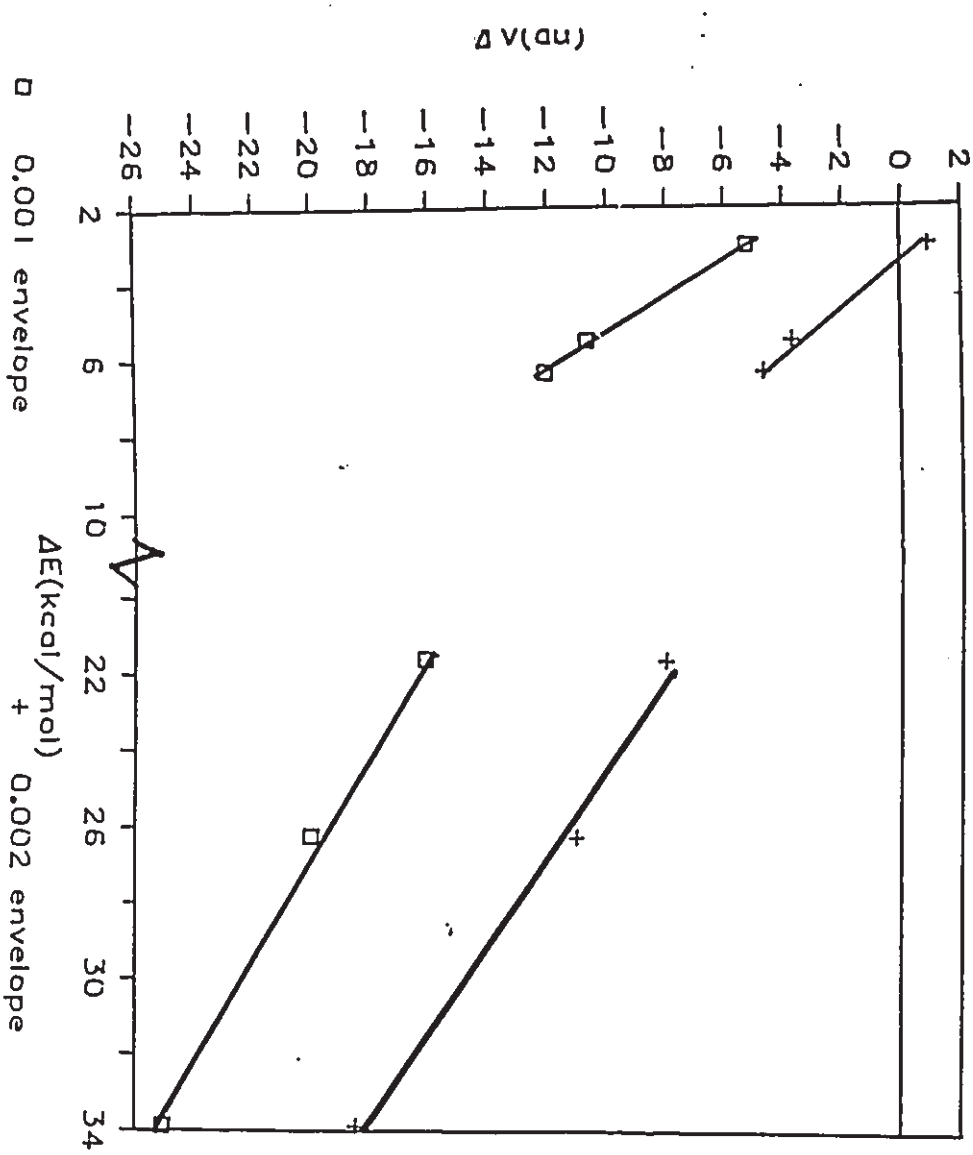
Δν(nD)
2
0
−2
−4
−6
−8
−10
−12
−14
−16
−18
−20
−22
−24
−26
2
6
10
22
26
30
34
ΔE(kcal/mol)
□ 0.001 envelope
+ 0.002 envelope

Table 2.2.1. Geometries[a] for the Hydrogen-Bonded Complexes of Water and Ammonia and Their Corresponding Protonated Species, 6-31G**//6-31G**.

HnAH-BHm	-Escf[b]	-V/T	r(AB)	r(H-B)	r(AH)	Δr(AH)	r(BX)[c]	Δr(BX)
H_2NH-NH_3	112.39589	2.0016512	6.482	4.583	1.889	0.033	1.892	0.028
HOH-OH_2	152.05606	2.0022209	5.633	3.850	1.791	0.008	1.784	0.002
HOH-NH_3	132.22931	2.0019374	5.768	3.972	1.797	0.015	1.892	0.028
H_3NH^+-OH_2	132.60346	2.0024576	5.203	3.248	1.955	0.043	1.788	0.006
H_3NH^+-NH_3	112.78284	2.0022083	5.274	3.263	2.010	0.098	1.899	0.036
H_2OH^+-OH_2	152.38793	2.0028610	4.525	2.494	2.042	0.225	1.792	0.010
H_2O trimer[d]	228.08595	2.0022498	5.669	4.019	1.786	0.004	1.785	0.003
			5.732	3.997	1.788	0.006	1.783	0.001

HnAH-BHm	∠AHB	∠XBH
H_2NH-NH_3	180.0	95.1
HOH-OH_2	171.3	108.6
HOH-NH_3	177.6	120.2
H_3NH^+-OH_2	179.9	126.6
H_3NH^+-NH_3	180.0	112.5
H_2OH^+-OH_2	177.3	126.3
H_2O trimer[d]	153.1	93.0
	163.2	113.2

[a] All values are in au except the internuclear angles which are in degrees.
[b] The 6-31G**//6-31G** energies and virial ratios of the monomers NH_3 and H_2O are given in Table 2.1.2 while those of NH_4^+ and H_3O^+ are -56.54553, 2.0022912 and -76.31032, 2.0030016 respectively
[c] The hydrogen nucleus in the base fragment closest to the B nucleus in the base is denoted X.
[d] The hydrogen bond with the shorter OO distance is listed first here and in the remaining tables in this section.

Table 2.2.2. Fully Optimized 6-31G** Geometries of the Complexes Displayed in Figure 2.2.1.

System	Atom	Cartesian Coordinates (au)		
HnAH-BHm	Name	x	y	z
H_2NH-NH_3	N	0.06880	3.38472	0.00000
	H	0.06880	1.48800	0.00000
	N	0.06880	-3.11103	0.00000
	H	1.95306	-3.27993	0.00000
	H	-0.58780	-4.01282	1.52746
	H	-0.58780	-4.01282	-1.52746
	H	-0.90477	3.95089	1.52075
	H	-0.90477	3.95089	-1.52075
$HOH-OH_2$	O	0.00000	0.00000	0.00000
	O	0.00000	0.00000	5.63327
	H	1.67102	0.00000	6.24931
	H	0.13662	0.00000	3.84790
	H	-0.92490	1.42836	-0.53728
	H	-0.92382	-1.42812	-0.53762
$HOH-NH_3$	O	0.00000	0.00000	0.00000
	H	0.00000	0.00000	1.79656
	H	1.71290	0.00000	-0.48664
	N	-0.16842	0.00000	5.76520
	H	1.42500	-0.00066	6.78462
	H	-1.16757	1.52813	6.25989
	H	-1.16873	-1.52721	6.26038
$H_3NH^+-OH_2$	O	0.00000	0.00000	0.00000
	H	0.00000	0.00000	3.24812
	N	0.00414	0.00000	5.20305
	H	1.79916	0.00000	5.84711
	H	-0.88967	1.55474	5.85175
	H	-0.88957	-1.55485	5.85164
	H	1.43991	0.00001	-1.06049
	H	-1.43197	0.00001	-1.07126
$H_3NH^+-NH_3$	N	0.00000	0.00000	0.00000
	H	0.00000	0.00000	2.01043
	N	0.00000	0.00000	5.27386
	H	1.78979	0.00000	-0.65492
	H	-0.89489	-1.55000	-0.65492
	H	-0.89489	1.55000	-0.65492
	H	-1.75199	0.00000	5.99946
	H	0.87749	-1.51986	5.99946
	H	0.87749	1.51986	5.99946

Table 2.2.2 (con'd)

System HnAH-BHm	Atom Name	Cartesian Coordinates (au) x	y	z
H_2OH^+-OH_2	O	0.00000	0.00000	0.00000
	H	1.49730	0.00000	0.99888
	H	-1.49850	-0.02410	0.99690
	H	-0.00671	1.07654	-1.73454
	O	-0.01332	2.27844	-3.90856
	H	-0.00560	4.05522	-4.13877
	H	-0.03084	1.44755	-5.49686
H_2O trimer	O	0.00000	0.00000	0.00000
	O	0.00000	0.00000	5.66909
	H	1.46857	0.00000	6.68908
	H	0.57324	0.00000	3.97787
	H	-1.07440	1.42373	0.05961
	H	-1.07687	-1.42186	0.05963
	O	5.26953	0.00000	7.92450
	H	6.18028	-1.44207	7.40502
	H	6.19320	1.41519	7.35617

Table 2.2.3. Critical Point Data for the Hydrogen-Bonded Complexes of Water and Ammonia and Their Corresponding Protonated Species, 6-31G**//6-31G**.[a]

HnAH-BHm	$\rho(r_b)$	$\nabla^2\rho(r_b)$	r_B	r_H	$\lvert\Delta r_B^o\rvert$	$\lvert\Delta r_H^o\rvert$	$\lvert\Delta r_B^o+\Delta r_H^o\rvert$	$\Delta\rho(r_a)$	$\Delta\nabla^2\rho(r_a)$
H_2NH-NH_3	0.0122	0.0337	2.93	1.66	0.78	0.68	1.46	-0.0024	-0.0302
HOH-OH_2	0.0199	0.0624	2.52	1.34	0.83	0.85	1.68	-0.0087	-0.0905
HOH-NH_3	0.0214	0.0581	2.85	1.32	1.06	0.87	1.93	-0.0137	-0.0934
H_3NH^+-OH_2	0.0387	0.1370	2.20	1.05	1.15	1.05	2.20	-0.0277	0.1417
H_3NH^+-NH_3	0.0507	0.1084	2.27	0.99	1.44	1.11	2.55	-0.0559	0.3809
H_2OH^+-OH_2	0.1109	-0.0110	1.88	0.61	1.44	1.31	2.75	-0.1275	1.7300
H_2O trimer	0.0174	0.0539	2.58	1.44	0.77	0.75	1.52	-0.0042	-0.0462
	0.0170	0.0536	2.58	1.42	0.77	0.77	1.54	-0.0070	-0.0731

HnAH-BHm	Δr_A	Δr_B
H_2NH-NH_3	0.0315	-0.0262
HOH-OH_2	0.0235	-0.0151
HOH-NH_3	0.0332	-0.0188
H_3NH^+-OH_2	0.0743	-0.0313
H_3NH^+-NH_3	0.1280	-0.0295
H_2OH^+-OH_2	0.1843	0.0406
H_2O trimer	0.0119	0.0185

[a] All values are in au. The H-B critical point (i.e. the hydrogen bond critical point is denoted r_b) and the AH bond critical point is denoted r_a.

Table 2.2.4. Hydrogen Bond Energies and Their Atomic Contributions for Complexes of Water and Ammonia and Their Corresponding Protonated Species, 6-31G**//6-31G**.

HnAH-BHm	ΔE[a]	ΔE(acid)	ΔE(base)	ΔE(A)	ΔE(H)	ΔE(B)
H_2NH-NH_3	-3.0	-5.3	2.3	-14.8	20.9	-7.1
HOH-OH_2	-5.5	-10.6	5.0	-23.5	16.4	-7.5
HOH-NH_3	-6.4	2.7	-9.2	-12.4	21.4	-28.7
H_3NH^+-OH_2	-21.5	-27.2	5.7	-31.4	33.5	-38.8
H_3NH^+-NH_3	-26.2	-21.5	-4.4	-23.2	42.6	-75.7
H_2OH^+-OH_2	-33.8	-15.0	-18.9	4.8	13.7	-93.4
H_2O trimer	-9.5	-15.1	3.7	-37.0	8.1	-7.5
			1.8		13.8	-7.5

[a] ΔE is the difference in the calculated SCF total energies (complex minus isolated reactants in kcal mol^{-1}). ΔE(acid) and ΔE(base) are the sums of the changes in the corresponding atomic energies as determined by numerical integration. The symbols A and B refer to the oxygen or nitrogen atom of the acid or base molecule and H refers to the atom shared in the hydrogen bond.

Table 2.2.5. Volume and Average Electron Population Changes for Complexes of Water and Ammonia and Their Corresponding Protonated Species, 6-31G**//6-31G**.[a]

HnAH-BHm	Δv	Δv (acid)	Δv (base)	ΔN(acid)= -ΔN(base)	Δv(A)	Δv(H)	Δv(B)	ΔN(A)	ΔN(H)	ΔN(B)
H_2NH-NH_3	-5.17	-2.64	-2.53	0.009	0.82	-5.32	-1.57	0.032	-0.061	0.015
HOH-OH_2	-10.65	-4.97	-5.67	0.012	1.18	-6.48	-3.90	0.045	-0.043	0.017
HOH-NH_3	-12.06	-4.64	-7.43	0.022	1.55	-6.80	-4.57	0.054	-0.047	0.035
H_3NH^+-OH_2	-15.11	-4.85	-11.16	0.033	1.44	-9.78	-4.85	0.040	-0.083	0.072
H_3NH^+-NH_3	-19.97	-1.95	-18.01	0.081	2.08	-9.07	-7.59	0.050	-0.080	0.124
H_2OH^+-OH_2	-25.06	-5.20	-19.86	0.096	-1.46	-6.18	-9.96	0.036	-0.009	0.079
H_2O trimer	-17.41	-8.32	-4.50	0.018	2.11	-4.81	-2.99	0.077	-0.022	0.016
			-4.58			-5.62	-3.21		-0.037	0.015

[a] All values are in au. The average electron populations and volumes in the protonated monomers are: N(N) = 8.236, v(N) = 115.0, N(H) = 0.441, v(H) = 21.5 in NH_4^+; N(O) = 9.300, v(O) = 124.2, N(H) = 0.233, v(H) = 11.8 in H_3O^+. In the neutral monomers they are: N(N) = 8.190, v(N) = 134.1, N(H) = 0.627, v(H) = 130.8 in NH_3; N(O) = 9.239, v(O) = 136.9, N(H) = 0.381, v(H) = 19.1 in H_2O.

2.3 HYDROGEN BONDING IN FORMAMIDE DIMERS

One of the two kinds of hydrogen bonds found in DNA base pairs, the -CO-HN- bond, occurs in the cyclic and open formamide dimers. These dimers can serve as simple models of the hydrogen bond structure found in DNA (Wojcik et al 1983). In light of recent theoretical studies of hydrogen bonding in DNA base pairs (Hobza and Sandorfy 1987, Clementi et al 1986, del Bene 1983), the present work shows how the theory of atoms in molecules explains the mechanics of hydrogen bond formation at the atomic level. The extra stability associated with the formation of the cyclic dimer is determined by comparing its atomic properties with those of the open dimer which has only a single hydrogen bond.

Molecular Structure, Geometry and Energy

The energies and geometrical parameters are given in Table 2.3.1. Molecular graphs of the formamide monomer and the cyclic and open formamide dimers are presented in Figure 2.3.1. The open dimer is constrained to have the "trans" geometry illustrated in this figure to prevent its closure to the cyclic form. Otherwise its geometry is fully optimized. The two dimers and the DNA base pairs possess a plane of symmetry. The cyclic dimer is slightly more than twice as stable as its open form, the energy changes on dimer formation being -27.6 and -25.5 kJ mol^{-1} per hydrogen bond respectively.

Geometry changes for the molecules participating in the

hydrogen bonds are small, the NH_b bond length (where H_b is the H-bonded hydrogen) increasing by only 0.014 Å upon formation of the cyclic dimer, for example.

The values of ρ and $\nabla^2\rho$ at a bond critical point r_c, of the dimers are given in Table 2.3.2 together with the changes from the monomer values. The relatively low values of $\rho(r_c)$ together with the positive values for $\nabla^2\rho(r_c)$ for the hydrogen bond critical points are typical of closed shell interactions while the larger values of ρ and negative values for $\nabla^2\rho$ as found for the N-H and C-H bonds are typical of shared interactions. The value of $\rho(r_c)$ for hydrogen bonds has been shown to increase along with an increase in the hydrogen bond strength (Sections 2.1 and 2.2) and indeed, the value is greater for the cyclic than for the open dimer. Correspondingly, the changes in the values of $\rho(r_c)$, negative for the neighbouring N-H_b and C-O bonds and positive for the C-N bonds, are twice as large for the cyclic dimer than for the open dimer.

The values of $|\Delta r_B^o + \Delta r_H^o|$ where B is the base atom (oxygen) participating in the hydrogen bond and H is the corresponding hydrogen, are 2.02 and 1.77 au for the cyclic and open dimers respectively. Thus, as observed in the previous sections of this chapter, the strength of the hydrogen bond increases with increasing mutual penetration.

A study of the ellipticities along the bond paths shows that there are substantial reorganizations of electronic charge within the basins of the N and O atoms which correspond to a transfer of out-of-plane density into the plane of the molecule for the N atom, and

to the reverse of this for oxygen (Cheeseman et al 1988). These changes are shown to correlate with the changes in the π populations of the N and O atoms as well as the changes in the quadropole moments.

Atomic Properties

The atomic populations, energies, volumes and quadropole moments for the formamide monomer are given in Table 2.3.3, together with the changes in these properties encountered in the formation of the cyclic and open dimers. The net charges on the atoms are also listed. In formamide the C atom loses charge mainly to both the N and O atoms and C has a substantial net positive charge. The N atom withdraws charge from the two neighbouring H atoms as well as from C and it has the largest net negative charge. Of these two hydrogens, the one syn to oxygen has the largest positive charge and it forms the hydrogen bond in the cyclic dimer. In all complexes studied in this thesis, the hydrogen of largest positive charge and of smallest atomic volume, participates in the H-bond. The H atom bonded to C has a small negative charge and the less contracted nature of its charge distribution compared to that of the amide hydrogens (Figure 2.3.1) is reflected in its volume being approximately twice as great.

The cyclic dimer is discussed first. Essentially all the changes in population, energy, volume and quadropole moments are restricted to the atoms of the NH_b-O fragments. Denoting N and O as the acid and base atoms respectively, H_b loses charge to both and the acid atom gains more charge than does the base atom. The volume decrease accompanying the formation of the two H-bonds in the cyclic

dimer is 26.8 au, nearly all of which results from the formation of the new interatomic surfaces between the H_b and O atoms. The volumes of the N atoms increase slightly as a result of their increased populations.

The values of -V/T for the monomer and dimer are very similar (Table 2.3.1), and so, the values of $\Delta E(\Omega)$ will be meaningful. The substantial loss of charge by the hydrogen causes its energy to increase. While both the acid and base atoms gain charge as in the water and ammonia dimers (Section 2.2), unlike these latter non-conjugated systems, only the acid atom is stabilized and it is this stabilization which is responsible for the overall energy decrease accompanying the formation of the hydrogen bonds. The differing behaviour of the O and N atoms with respect to an increased electron population is attributed to the accompanying changes in their σ to π population ratios. The π population of the O atom increases and this increase is greater than the charge transferred to this atom. Thus in addition to the charge transferred to its π population, there is an accompanying promotion of 0.017e from its σ to its π system and the O atom is destabilized. The N atom on the other hand undergoes a decrease in its π population and hence the total increase in its σ population is the interatomic charge transfer plus the π to σ polarization, or 0.102e. The C atom, while losing a small amount of charge, undergoes a π to σ polarization which is five times greater than its loss of charge and there is a small stabilizing energy change for this atom.

The polarization changes are paralleled by the $\Delta Q_{zz}(\Omega)$ values.

If $\Delta Q_{zz}(\Omega)$ is negative, more charge will be concentrated above and below the molecular plane meaning a greater amount of π density. Thus, oxygen has a large negative value for $\Delta Q_{zz}(O)$ since it has gained π density while nitrogen has a large positive value of $\Delta Q_{zz}(N)$ since it has lost π density. The largest changes in $N_\pi(\Omega)$ correlate with the largest changes in $Q_{zz}(\Omega)$.

The positive charge on the H of the acid (Table 2.3.3) increases via a polarization of its charge density away from the negatively charged base atom which results in a sigma charge transfer from H to N. The negative charge on the base atom O is increased and there is an accompanying smaller transfer of charge to its π system. The O atom is polarized towards C but because of the polarization of its density towards H in the dimer the magnitude of the first moment of the charge distribution of the O atom is reduced to 0.63 au from its value of 0.70 au in the monomer. Thus the positively charged H atom and the negatively charged O atom are polarized in a direction counter to the direction of charge transfer from acid to base, characteristic of an ionic interaction.

The changes in the charge densities of the NCO fragments correspond to opposing flows of σ and π charge, and these flows, together with the loss of charge by H, dominate the energy changes. Sigma density is maximally concentrated in the plane of the nuclei and is bound more tightly by the nuclear-electron attractive force than is π density which has a node in this plane. An atom which experiences a net gain in its σ over its π population, whether its total population increases or decreases, is stabilized, (the N and C atoms), while one

which experiences a net loss in its σ relative to its π population is destablized even though its total population is increased, albeit by a lesser amount (the O atom).

The patterns of change in the atomic properties for the formation of the open dimer are the same for corresponding atoms as for the formation of the cyclic dimer, but are in general, of reduced magnitude. The increase in the π population of the oxygen atom of the base is only one-half as great as in the cyclic case and more nearly equal to the charge transferred to this atom. The near balance in charge gain and charge promotion results in a near zero energy change for the oxygen atom. The N atom of the base and the O atom of the acid imitate on a smaller scale, the changes in charge, in σ-π polarizations and in energy for the O and N atoms directly involved in the H-bond formation. Thus, the formation of the first hydrogen bond changes the system in such a way as to facilitate the formation of a second such bond.

Figure 2.3.1

Molecular graphs of formamide, the cyclic and the open dimer superimposed on contour maps of the electronic charge density. Included are zero flux surfaces and bond critical points (black dots).

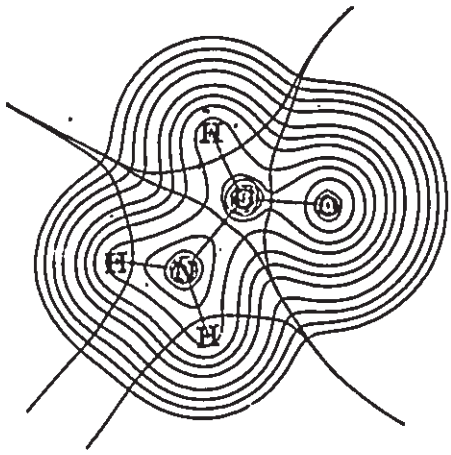
H
H
N
O
H

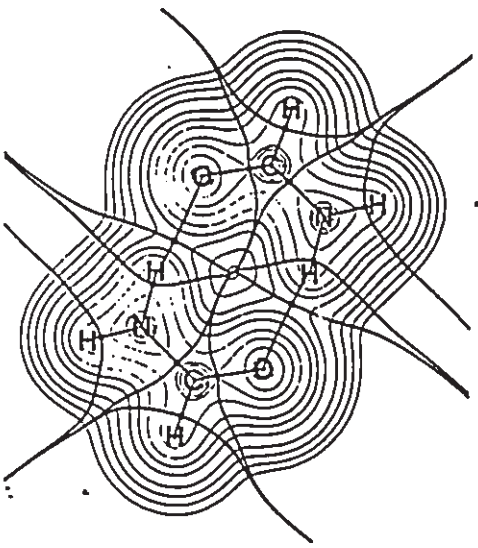
H
O
C
N
H
H
H
N
C
O
H

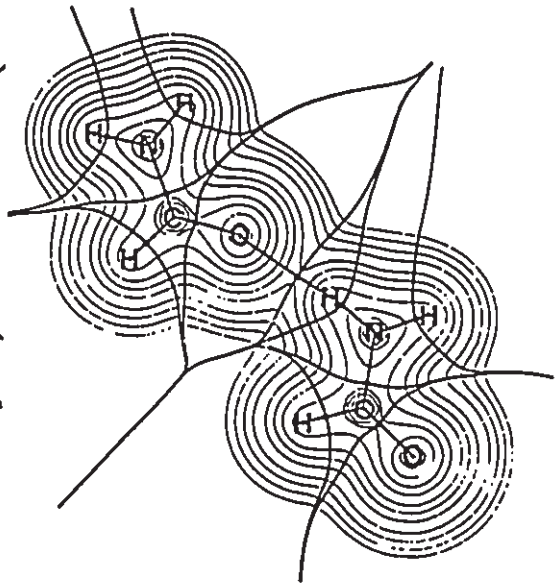
H
H
N
C
O
H
H
N
H
H
O

Table 2.3.1. Calculated Equilibrium Geometries for Formamide and its Dimers.[a]

Parameter	Monomer	Cyclic dimer	Open dimer	
			acid	base
CO	1.216	1.230	1.221	1.221
CN	1.347	1.328	1.338	1.338
CH_c	1.081	1.080	1.082	1.078
NH_s	0.992	1.006[b]	0.992	0.993
NH_a	0.989	0.990	0.997[b]	0.990
OH_b	-	1.903	1.959	
NO	-	2.898	2.851	
COH_b	-	125.4	161.1	
NH_bO	-	169.2	173.3	
NCO	124.7	125.1	125.6	124.4
NCH_c	113.8	115.0	113.3	114.3
H_cCO	121.5	119.9	121.0	121.3
CNH_s	119.5	120.3	119.1	119.7
CNH_a	121.9	120.9	121.5	121.9
H_aNH_s	118.6	118.8	119.4	118.5
SCF Energy	-168.93953	-337.89992	-337.88881	
-V/T	2.0024672	2.0024996	2.0024472	

[a] Geometrical distances and angles are in angstroms and degrees. Energies (RHF/6-31G**//4-31G) are in au. The subscripts s and a denote the hydrogens which are syn and anti to the keto oxygen respectively. The subscripts b and c denote the hydrogen-bonded hydrogen and the hydrogen bonded to carbon respectively.
[b] Geometrical distance to the hydrogen-bonded hydrogen.

Table 2.3.2. Values of the Charge Density and Laplacian of the Charge Density at Bond Critical points of Formamide Dimers.[a]

Dimer	Bond	$\rho(r_c)$		$\nabla^2\rho(r_c)$	
cyclic	CO	0.4025	(-0.0132)	0.0204	(-0.1260)
	CN	0.3485	(0.0161)	-0.8271	(-0.0562)
	NH_b	0.3445	(-0.0160)	-1.9800	(0.0387)
	OH_b	0.0265		0.0882	
	NH	0.3648	(0.0007)	-2.0328	(-0.0042)
	CH	0.3084	(0.0011)	-1.2815	(-0.0099)
open					
acid:	CO	0.4111	(-0.0046)	0.0959	(-0.0506)
	CN	0.3416	(0.0082)	-0.8043	(-0.0334)
	NH_b	0.3561	(-0.0081)	-2.0244	(0.0042)
	OH_b	0.0205		0.0773	
base:	CO	0.4096	(-0.0061)	0.0999	(-0.0465)
	CN	0.3404	(0.0070)	-0.7850	(-0.0141)

[a] All values are in au. Numbers in parentheses represent the change from the monomer value. H_b denotes the hydrogen-bonded hydrogen.

Table 2.3.3. Average Electron Populations, Energies, Volumes and Quadrupole Moments of Formamide and Changes upon Dimerization.[a]

Monomer	Ω	N(Ω)	E(Ω)	v(Ω)	N_π(Ω)	Q_{zz}(Ω)	q(Ω)
	O	9.3703	-75.58890	131.39	1.706	-0.314	-1.370
	N	8.4805	-55.25862	120.67	1.846	-2.365	-1.480
	C	4.0525	-36.57949	36.65	0.398	-1.218	1.948
	H_s	0.5247	-0.42062	25.28	0.018	-0.018	0.475
	H_a	0.5424	-0.43344	25.92	0.018	-0.018	0.458
	H_c	1.0294	-0.65851	50.36	0.016	-0.314	-0.029
	total	23.9998	-168.93958	390.27	4.000		
	SCF		-168.93953				
Dimers[b]							
	Ω	ΔN(Ω)	ΔE(Ω)	Δv(Ω)	ΔN_π(Ω)	ΔQ_{zz}(Ω)	q(Ω)
cyclic	O	0.0291	35.6	-4.64	0.046	-0.151	-1.399
	N	0.0724	-200.4	2.41	-0.030	0.234	-1.553
	C	-0.0020	-10.0	-0.87	-0.010	0.036	1.950
	H_b	-0.1048	160.2	-10.46	-0.004	-0.034	0.580
	H_a	0.0077	-13.0	0.38	-0.001	-0.006	0.450
	H_c	-0.0025	-0.4	-0.22	-0.001	-0.002	-0.027
	total	-0.0002	-56.1	-26.80	0.001		
	SCF		-54.8				
open							
acid:	O	0.0151	21.8	0.60	0.016	-0.023	-1.385
	N	0.0522	-128.4	1.46	-0.012	0.107	-1.533
	C	-0.0065	10.5	-0.55	-0.002	-0.002	1.854
	H_b	-0.0826	116.7	-8.63	-0.004	-0.030	0.540
	H_s	0.0189	-29.3	1.22	0.002	-0.005	0.456
	H_c	0.0123	-14.2	0.57	0.000	-0.012	-0.042
base:	O	0.0213	3.3	-2.58	0.024	-0.083	-1.392
	N	0.0057	-43.9	-0.13	-0.008	0.067	-1.486
	C	0.0005	-9.6	-0.14	-0.012	0.058	1.947
	H_s	-0.0082	12.1	-0.43	-0.002	0.000	0.484
	H_a	-0.0110	16.3	-0.58	0.000	0.000	0.469
	H_c	-0.0182	18.4	-1.00	-0.002	0.007	-0.011
	total	-0.0005	-26.4	-10.19	0.000		
	SCF		-25.5				

[a] All values are in au except energy changes which are in kJ mol^{-1}. The subscripts s and a denote the hydrogens which are syn and anti to the keto oxygen respectively. The subscripts b and c denote the hydrogen-bonded hydrogen and the hydrogen bonded to carbon respectively.

[b] Atomic property changes are given by subtracting the monomer values from the corresponding dimer values.

2.4 ANIONIC, CATIONIC AND NEUTRAL COMPLEXES CONTAINING OH-O BONDS

In Section 2.2 neutral and cationic complexes containing AH-B bonds (where A = O, N and B = O, N) were examined to gain insight into hydrogen bonding. In the present section, we explore the OH-O hydrogen bond in more detail and in a larger variety of systems, including anionic complexes.

Complexes of varying H-O hydrogen bond lengths are considered including the water dimer (structure 1), the monohydrated formate anion (2), the diformate anion (3), the hydroxide ion water complex [HOH-OH]- (4) and the hydronium ion water complex (5) (Figure 2.4.1). The geometries of these complexes are fully optimized in a crystal field free environment using both the 6-31G** and DZP (Dunning 1970) basis sets. The only exception is for 2 in which a partial optimization is performed (intermolecular angles are constrained to within two degrees of the experimental angles in the lithium formate crystal). We wish to compare singly hydrogen-bonded systems but a full geometry optimization of 2 would result in a doubly hydrogen-bonded ring structure. Properties of the resulting charge distributions are discussed with emphasis on the topological properties of the charge density ρ and the atomic properties of the atoms in the complex and their changes from those in the isolated reactants. Comparisons with other types of H-bonds that have been studied in this chapter are made.

Geometries and Energies of Complexes Containing OH-O Bonds

To within 8°, the hydrogen bond angles (∠AHB) are linear for all five complexes studied (Table 2.4.1 and 2.4.2). The H-bond length (BH) decreases and AH increases as D_e increases. The H-bond length varies over a much greater range than the AH length. Also, the lengthening of AH from the isolated acid increases with increasing D_e, an observation also made for the BASE-HF complexes (Section 2.1). Structure 1 is said to possess a long H-bond, 2 possesses an H-bond medium in length and structures 3-5 possess short H-bonds (Joswig et al 1982). In fact, the crystal structure of 3 contains one of the shortest OH-O bond ever observed (Section 2.5). There are only small differences between the geometrical parameters optimized at the 6-31G** basis set as compared to the DZP basis set. The values of D_e are slightly larger at the 6-31G** level. It is noteworthy that the dissociation energies of the complex of water and its conjugate base and of water and its conjugate acid are quite similar. Though it is useful to compare the 6-31G** to the DZP results, emphasis is placed on the DZP results since the DZP basis set is larger, describing both the core and valence shells more fully, especially for the anionic complexes. Also the DZP basis set yields -V/T ratios closer to two (Table 2.4.1). Thus, hereafter unless otherwise noted it is the DZP results that are referred to in this section.

Topology of the Charge Distributions of Complexes 1 - 5

The values of the charge density at the hydrogen bond critical point, the values listed under $\rho(r_b)$ in Table 2.4.3 are, in general, at

least five times smaller than those found in shared interactions present in the given system. The values of $\rho(r_b)$ increase monotonically with D_e. In contrast to the BASE-HF complexes, we find the positive value of $\nabla^2\rho(r_b)$ to decrease among the short, strong H-bonded systems 3-5 while the magnitudes of the curvatures of ρ increase with D_e. Thus, in the strong H-bonded complexes, at least to some extent charge is accumulating in a region perpendicular to the B-H bond axis between the B and H nuclei at the expense of charge concentrated parallel to the B-H bond axis.

As D_e increases and the BH separation decreases, the critical point of the H-bond moves progressively closer to the zero contour encompassing the valence shell of charge concentration of the Laplacian distribution of the acid. In **5** the critical point lies just outside this contour, and so, $\nabla^2\rho(r_b)$ is still positive. As seen in Section 2.4.2 , the same point lies just inside this contour in the 6-31G** result, and so, $\nabla^2\rho(r_b)$ is very slightly negative and the bond has some of the characteristics of a shared interaction.

In general, the sum $|\Delta r_B^o + \Delta r_H^o|$ increases as D_e increases. The largest values of $|\Delta r_B^o|$ correlate with the largest values of $|\Delta r_H^o|$ and H is always less penetrated than B.

The sum of $\rho^o(r_B)$ and $\rho^o(r_H)$ is close in value to $\rho(r_b)$, the value of the charge density at the hydrogen bond critical point. To obtain complexes with $D_e > 5$ kcal mol^{-1}, the van der Waals envelope of the H atom must be penetrated by ≈ 1.2 au and that of the B atom by a still larger amount. For these penetrations, the sums of the unperturbed densities are in excess of 0.04 au.

The changes induced in the charge distribution of the AH bond are monitored by examining the corresponding changes in the properties of its bond critical point (denoted by the position vector $\mathbf{r}_a$; Table 2.4.3). The formation of each complex results in a decrease in the value of $\rho(\mathbf{r}_a)$ relative to its value in the isolated acid reactant (i.e., $\Delta\rho(\mathbf{r}_a)$ is negative), indicating that charge density is removed from the AH bond. The magnitude of this change increases linearly with increasing D_e. Upon complex formation, $\nabla^2\rho(\mathbf{r}_a)$ decreases in magnitude as do the curvatures both perpendicular and parallel to the AH bond path and, in general, these changes increase in magnitude with increasing D_e, a reflection of the increasing removal of charge from the AH bond.

Critical point information for the remaining bonds in each complex is given in Table 2.4.3. In general, the changes in properties associated with these bond critical points upon complexation are smaller than the changes in the AH bond.

Atomic Properties

Table 2.4.5 lists $q(\Omega)$, $N(\Omega)$, $|\mu(\Omega)|$ and $v(\Omega)$ for the atoms in the isolated reactants. The most negatively charged atoms are the equivalent oxygens in the formate anion and the most positively charged are the hydrogens in the hydronium ion. Along with having the least number of electrons, these hydrogens have the smallest magnitude for $E(\Omega)$, $|\mu(\Omega)|$ and $v(\Omega)$.

In both the isolated reactants and complexes, atomic charge densities are polarized counter to the direction of net charge

transfer. Consequently, the B atom is polarized away from the incoming H which is, in turn, polarized towards B. Polarization changes of B and H upon H-bond formation are discussed shortly.

The changes in the populations, energies and volumes of the acid and base molecule upon H-bond formation are given in Table 2.4.6 and the corresponding changes in these same properties are given in Table 2.4.7 for the individual atoms.

In all cases there is a transfer of charge from the base to the acid. The strongest systems, the complexes of water with its conjugate acid and base, have the greatest number of electrons transferred while the weakest complex, the water dimer, has the least.

The magnitude of transfer of charge from base to acid, in general, is relatively small compared to the changes in the individual atomic charges (Table 2.4.7). The hydrogen-bonded hydrogen, H, as always, loses charge upon complexation. This atom undergoes a loss of charge larger than the charge transferred from base to acid, the only exception being found for H in **5**. This latter behaviour is understandable in view of the large net positive charge already present on the hydrogens of the free hydronium ion. The A atom, as always, gains electrons and, in general, the charge gained by A is greater than the charge lost by H. The remaining atoms in the acid fragment of the complex gain charge (with the exception of carbon in the formic acid fragment of **3**) and for the neutral and negatively charged structures, **1**-**4**, their gain is less than that of A. In **5** their gain is greater than that in A.

Upon H-bond formation, the base molecule loses charge in all

instances as does the X group (where hereafter X refers to the base atoms not participating in the H-bond). The B atom gains electrons if the complex is neutral or positively charged but loses otherwise (Table 2.4.7). A loss of electronic charge from the X group and a gain in electronic charge by A and the acidic atoms not participating in the H-bond causes dipole moment enhancement, an effect discussed in Section 2.1.

We now focus our attention on the energy changes accompanying H-bond formation. The dominant feature is the large stabilization and destabilization of the base and acid fragments respectively in the anionic complexes 3 and 4 (Table 2.4.6). The magnitude of the energy changes are smaller for the remaining complexes and in contrast to 3 and 4, the acid is stabilized.

Turning to individual atomic energy changes, $\Delta E(H)$ is positive in all the systems. The nonbonded density on H is penetrated by the base, H loses charge and is consequently destabilized. In general, $\Delta E(H)$ increases with increasing D_e. Only $\Delta E(H)$ for 5 deviates greatly from this relationship, a consequence of the tightness of the charge density of H in this complex.

The B atom is stabilized in all cases (except 2 where its energy change is near zero) and accounts for the greatest fraction of the stabilization in 4 and 5. The A atom is stabilized in all cases except 4.

In general, there is a decrease in the molecular volumes of both reactants upon formation of a hydrogen bond. The entire base fragment decreases in volume by a greater amount than the entire acid

fragment. The largest atomic decreases in volume are for H and B, a result of the decreases of the respective nonbonded radii owing to the formation of a new interatomic surface between these two atoms. The A atom slightly increases in volume.

Changes in atomic polarizations are greater for the charged than the neutral complexes. In all five complexes, H undergoes a reduction in polarization upon H-bond formation (Table 2.4.7). This reduction is primarily the result of the loss of the nonbonded density of H. This counter polarization of the charge density of H is enhanced when the base atom that will participate in the H-bond is negatively charged. The base oxygens in the formate and hydroxide ions bear the greatest negative charges and, indeed, the reduction of $\mu(H)$ is greatest for structures 3 and 4. Further, it has been shown in this chapter that the greater the extent of mutual pentration, the greater the reduction in $\mu(H)$. Here, 3 and 4 exhibit the greatest extent of mutual penetration, and so, this observation still is valid. The magnitudes of $\Delta|\mu(H)|$ are the largest of all the atoms in each of the five complexes.

To discuss the changes in $\mu(B)$ in the OH-O complexes, it is convenient to divide them into two categories: those which have the change in the first moment of B directed away from H, 1 and 4, and those which have this change directed towards H, 2, 3 and 5.

The change in $\mu(B)$ away from H in the first class of complexes is rationalized as follows: the creation of the B-H interatomic surface removes diffuse density from B and this decreases its atomic moment. This effect is more pronounced for 4 since 4 initially possesses more

diffuse regions of nonbonded density on B than 1. Although the X group loses only half as much charge as H, the X group is closer to B and so the net field effect caused by the electric fields generated by X and H is relatively small. As is evident for this first class of complexes and the first class of BASE-HF complexes, a correlation exists between the magnitude of B's change in polarization away from H with the extent of mutual penetration of both the B and H atoms and hence with D_e. The change in the polarization of H is also directed away from the hydrogen-bonded region. Therefore, the removal of density from the bonded region resulting from these polarizations facilitates the approach of the two closed-shell systems. In the second class of the OH-O and BASE-HF complexes, the field effects play a more dominant role and the change in $\mu(B)$ is directed towards H. In general for this second class, D_e increases with a decrease in the extent to which the polarization of B places density in the H-bonded region and indeed, of the OH-O systems, 5, the strongest complex, has the smallest polarization of B into the H-bonded region.

Graphical Summary of Properties of Hydrogen-Bonded Complexes

In this chapter, systems containing the following types of hydrogen bonds have been considered (B-HA): C-HF, N-HF, O-HF, F-HF, P-HF, S-HF, Cl-HF, C-HCl, N-HCl, O-HCl, F-HCl, N-HN, N-HO, OH-N and OH-O. Figure 2.4.2 and Table 2.4.8 summarize the global trends of various properties associated with the charge redistribution. The correlations are best within the same type of hydrogen-bond in all of the graphs.

Figure 2.4.1

Molecular graphs of complexes of varying H-O hydrogen bond lengths are displayed: water dimer (1), the monohydrated formate anion (2), the diformate anion (3), the hydroxide ion water complex [HOH-OH]- (4) and the hydronium ion water complex (5).

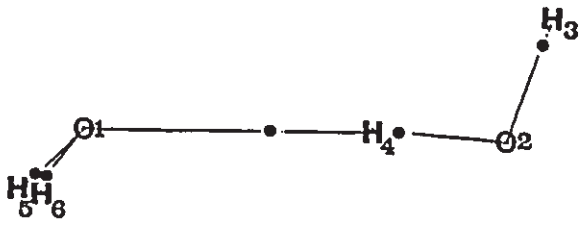

1

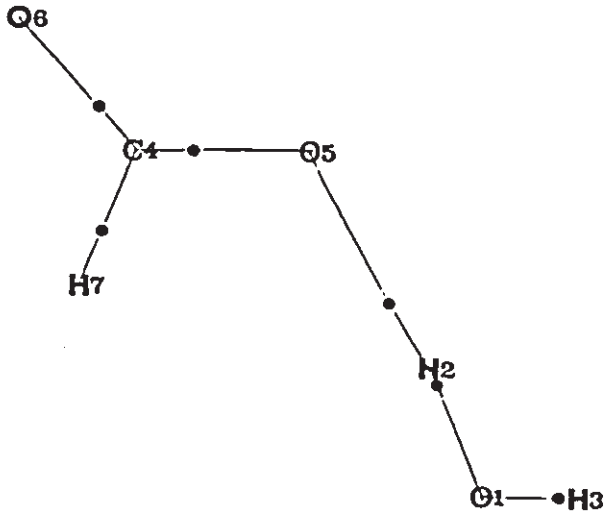

2

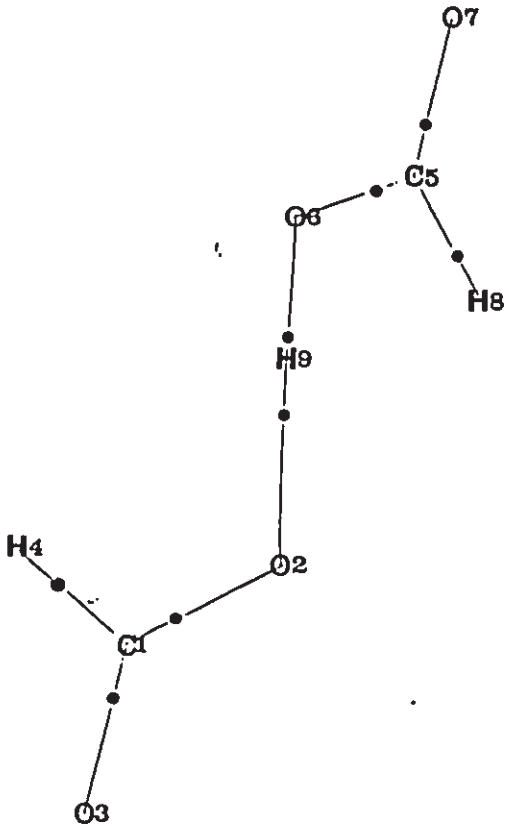

3

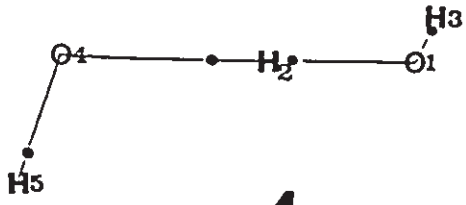

4

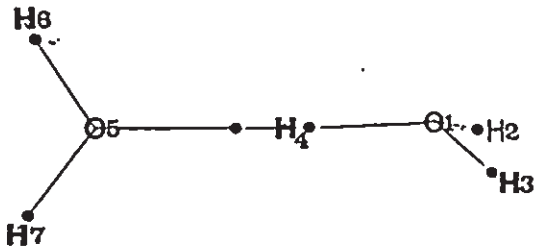

5

Figure 2.4.2

Relationships between properties of the charge density and D_e (kJ mol^{-1}) for hydrogen-bonded complexes considered in this chapter. Values for these plots are summarized in Table 2.4.5. The B-HF and B-HCl complexes are calculated using RHF/6-311++G**//6-31G**, N-HN, N-HO and O-HN using RHF/6-31G**//6-31G** (except for O-HN in the open formamide dimer which uses RHF/6-31G**//4-31G), and O-HO complexes are calculated using RHF/DZP//DZP.

a) Plot of the charge density at the hydrogen bond critical point $\rho(r_b)$ (in au) versus D_e. The correlation coefficient is 0.959.

b) Plot of the sum of the changes in nonbonded radii of B and H upon hydrogen bond formation, i.e. the mutual penetration $|\Delta r_B^o + \Delta r_H^o|$ (in au) versus D_e. The correlation coefficient is 0.857.

c) Plot of the decrease in the charge density at the H-A bond critical point $\Delta\rho(r_a)$ (in au) versus D_e. The correlation coefficent is -0.956.

d) Plot of the increase in the energy of the hydrogen-bonded hydrogen, $\Delta E(H)$ (in kJ mol^{-1}) versus D_e. The correlation coefficient is 0.772.

a

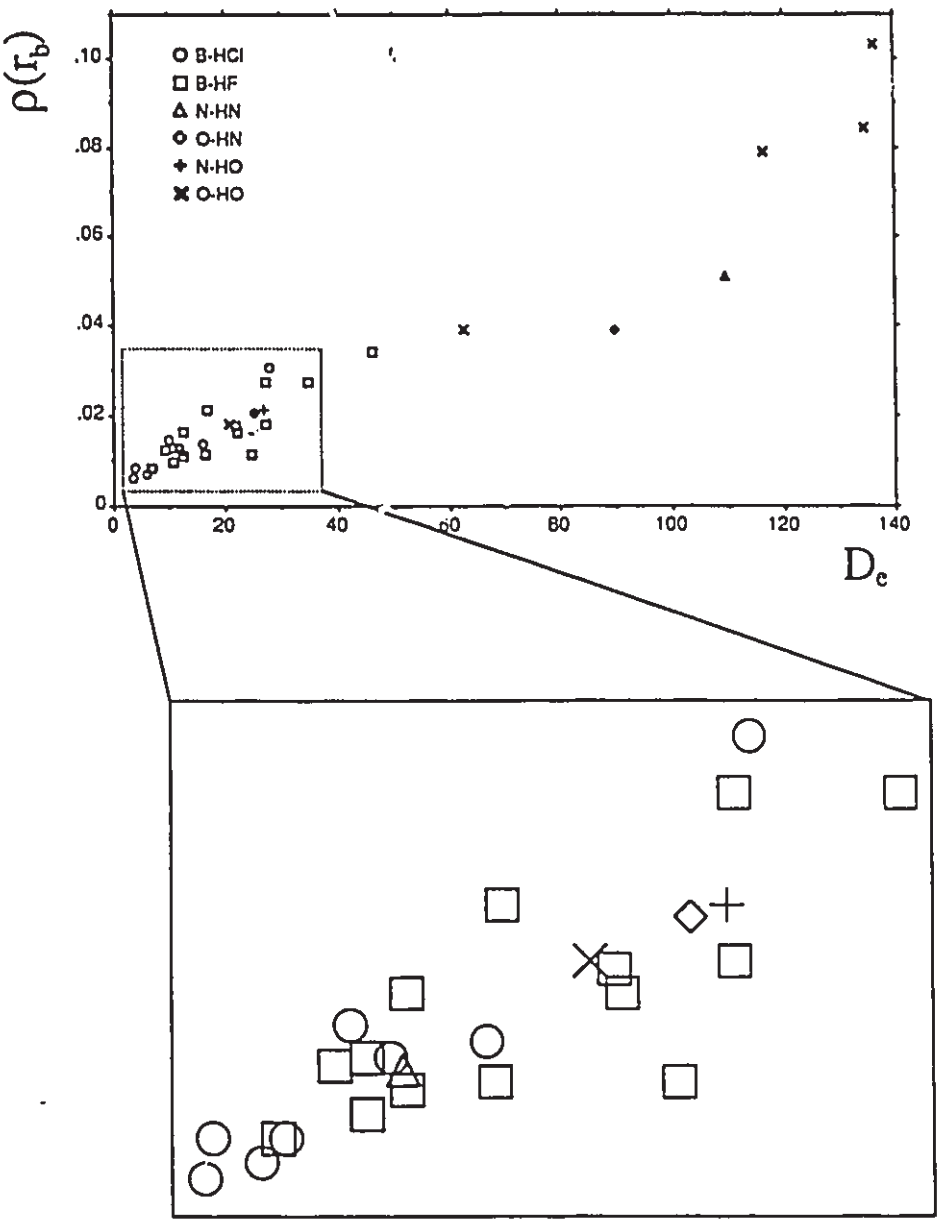
ρ(r_b)
.10
.08
.06
.04
.02
0
B-HCl
B-HF
N-HN
O-HN
N-HO
O-HO
0
20
40
60
80
100
120
140
D_e

b

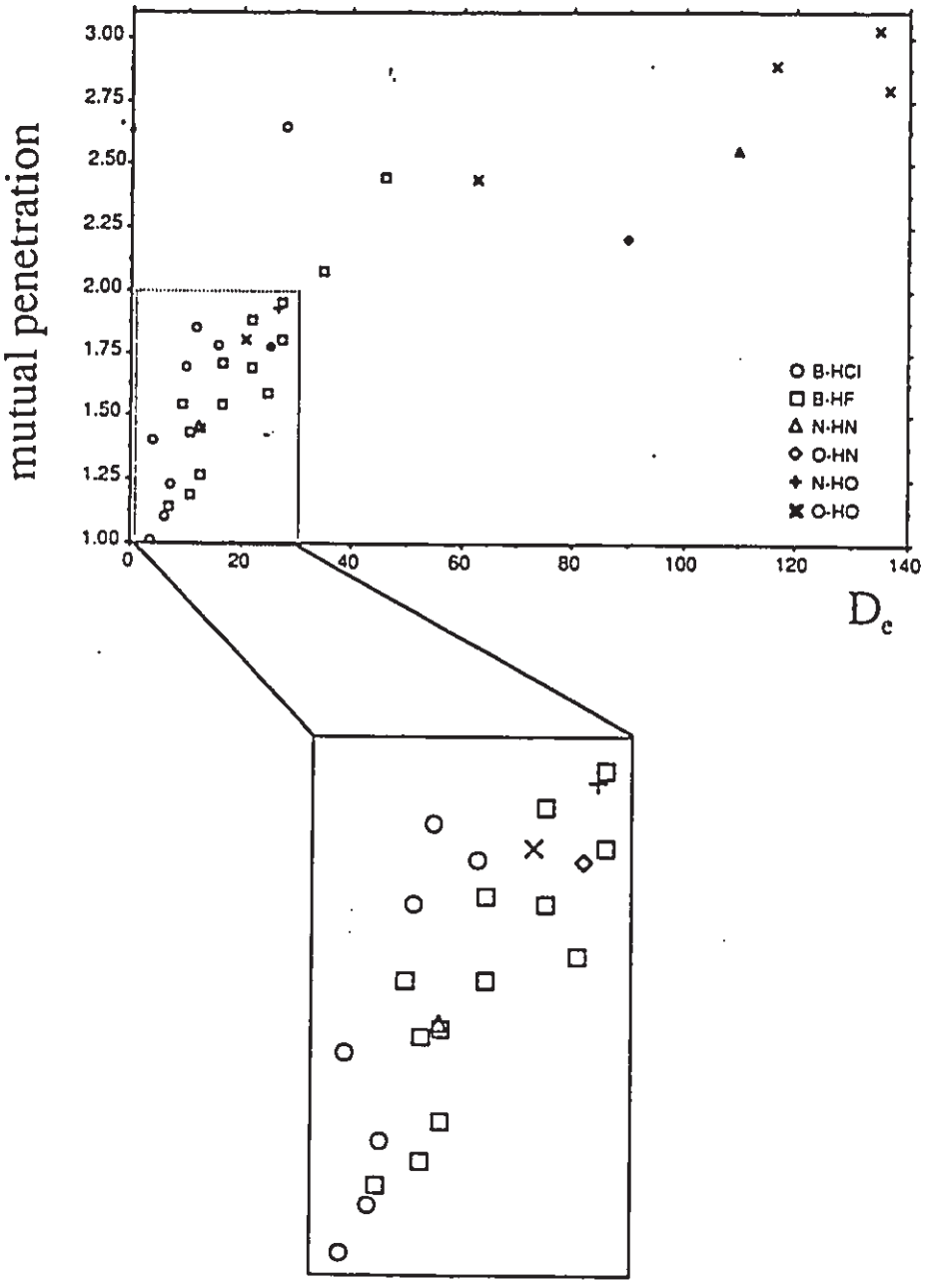
mutual penetration
3.00
2.75
2.50
2.25
2.00
1.75
1.50
1.25
1.00
0
20
40
60
80
100
120
140
D_e
B-HCl
B-HF
N-HN
O-HN
N-HO
O-HO

c

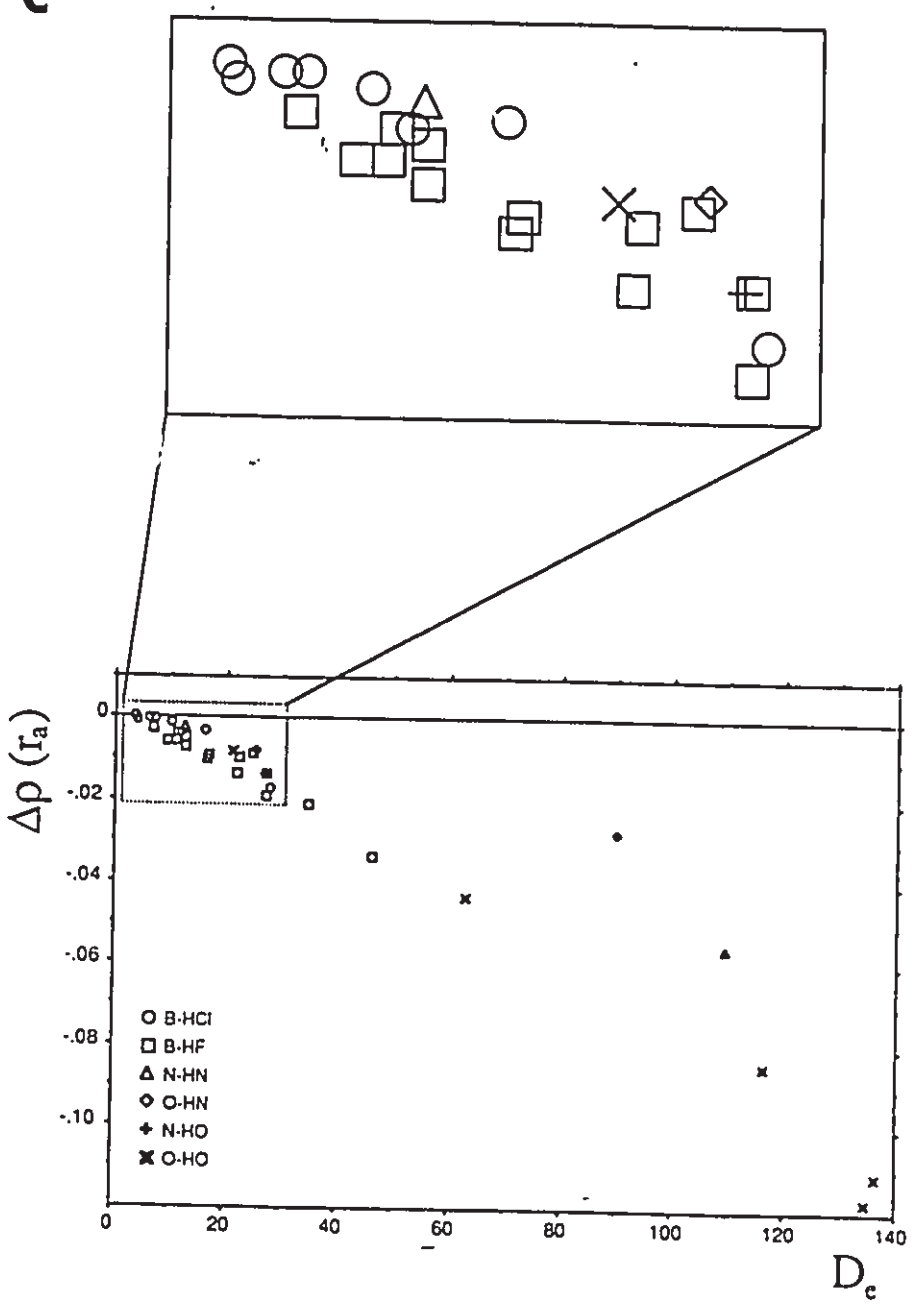
Δρ (r_a)
0
-.02
-.04
-.06
-.08
-.10
B-HCl
B-HF
N-HN
O-HN
N-HO
O-HO
0
20
40
60
80
100
120
140
D_e

d

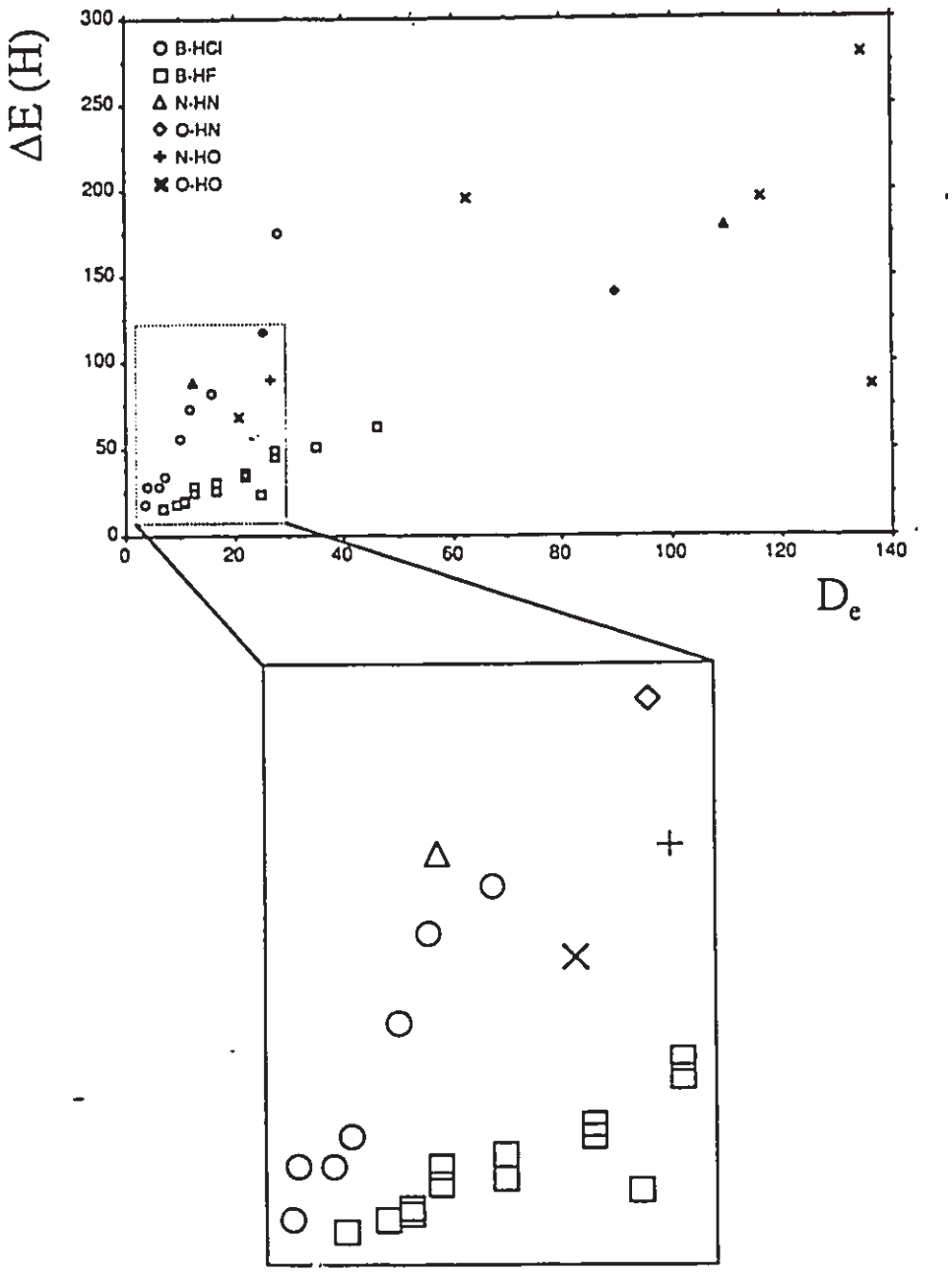
ΔE (H)
300
250
200
150
100
50
0
B-HCl
B-HF
N-HN
O-HN
N-HO
O-HO
0
20
40
60
80
100
120
140
D_e

Table 2.4.1. Fully Optimized Geometries and Energies of Crystal-Free Complexes Containing OH-O Bonds.[a]

Complex	Label	Parameter	Method of Calculation 6-31G**//6-31G**	DZP//DZP
$(H_2O)_2$	1	O1O2	5.6333	5.6428
		O1H4	3.8503	3.8534
		O2H4	1.7906 (0.0085)	1.7925 (0.0089)
		O1H5	1.7845 (0.0024)	1.7854 (0.0018)
		O1H6	1.7838 (0.0017)	1.7854 (0.0018)
		O2H3	1.7810 (-0.0011)	1.7824 (-0.0012)
		O1H4O2	173.59	175.85
		H5O1H4	108.62	113.45
		H6O1H4	108.64	113.45
		H5O1H6	106.36 (0.40)	106.84 (0.14)
		H3O2H4	105.86 (-0.10)	106.50 (-0.20)
		Escf	-152.05606	-152.10170
		-V/T	2.00222091	1.99968102
		D_e	5.53	5.04
[HOH-OC(OH)]-	2	O1O5		5.0895
		O1H2		1.8373 (0.0537)
		O1H3		1.7794 (-0.0042)
		O5H2		3.2699
		C4O5		2.3594 (0.0224)
		C4O6		2.3209 (-0.0161)
		C4H7		2.1052 (-0.0158)
		H2O1H3		107.01 (0.31)
		H2O5C4		118.81
		O5C4O6		129.55 (-1.22)
		O5C4H7		114.72 (0.10)
		O6C4H7		115.72 (1.10)
		O1H2O5		173.46
		Escf		-264.30825
		-V/T		2.00020131
		D_e		15.05
$[H(HCOO)_2]$-	3	O2O6	4.7178	4.6973
		O2H9	2.8192	2.7794
		O6H9	1.9091 (0.1156)	1.9202 (0.1251)
		C1O2	2.3724 (0.0456)	2.3812 (0.0442)
		C1O3	2.2939 (-0.0329)	2.3022 (-0.0348)
		C1H4	2.1039 (-0.0301)	2.0978 (-0.0232)
		C5O6	2.4422 (-0.0551)	2.4428 (-0.0522)
		C5O7	2.2598 (0.0345)	2.2684 (0.0283)
		C5H8	2.0658 (0.0154)	2.0677 (0.0170)
		O2H9O6	172.21	176.34
		C1O2H9	119.98	115.26
		O2C1O3	128.84 (-2.14)	129.03 (-1.74)
		O2C1H4	114.38 (-0.13)	114.15 (-0.47)
		O3C1H4	116.77 (2.26)	116.82 (2.20)

Table 2.4.1. (con'd)

	3	C5O6H9	109.90 (1.00)	111.21 (2.07)
		O6C5O7	125.29 (0.49)	125.44 (0.53)
		O6C5H8	113.47 (2.95)	113.72 (3.20)
		O7C5H8	121.24 (-3.44)	120.84 (-3.73)
		E_{SCF}	-377.00107	-377.09646
		-V/T	2.00196582	2.00020461
		D_e	29.08	27.75
[HOH-OH]-	4	O1O4	4.7259	4.7155
		O4H2	2.7615	2.7500
		O1H2	1.9717 (0.1896)	1.9702 (0.1866)
		O4H5	1.7944 (-0.0163)	1.7921 (-0.0116)
		O1H3	1.7831 (0.0010)	1.7834 (-0.0002)
		O1H2O4	173.55	174.74
		H2O4H5	102.59	107.92
		H3O1H2	101.17 (-4.79)	102.97 (-3.73)
		E_{SCF}	-151.41267	-151.47014
		-V/T	2.00106597	1.99894445
		D_e	35.38	32.25
$[H_5O_2]+$	5	O1O5	4.5242	4.5553
		O5H4	2.4841	2.5418
		O1H4	2.0415 (0.2249)	2.0150 (0.1970)
		O5H6	1.7916 (0.0095)	1.7943 (0.0107)
		O5H7	1.7926 (0.0105)	1.7953 (0.0117)
		O1H2	1.8000 (-0.0166)	1.8030 (-0.0150)
		O1H3	1.8000 (-0.0166)	1.8030 (-0.0150)
		O5H4O1	177.11	177.22
		H4O5H6	126.32	126.65
		H4O5H7	123.45	123.56
		H6O5H7	110.23 (4.27)	109.80 (3.10)
		H2O1H4	118.31 (3.57)	117.65 (2.96)
		H3O1H4	118.35 (3.61)	117.70 (3.01)
		H2O1H3	112.65 (-2.09)	112.75 (-1.94)
		E_{SCF}	-152.38794	-152.42850
		-V/T	2.00276475	1.99984049
		D_e	33.88	32.59

[a] Distances and E_{SCF} are in atomic units, angles are in degrees and D_e is in kcal mol^{-1}. All complexes are of C_1 symmetry and their molecular graphs are displayed in Figure 2.4.1. Differences (complex minus isolated reactants) are given in parentheses.

Table 2.4.2. Summary of Pertinent Geometrical Parameters for the Hydrogen-Bonded Complexes Containing an OH-O Bond, DZP//DZP.

System	Label	D_e	r(AB)	r(H-B)	r(AH)	Δr(AH)	r(BX)[b]	Δr(BX)	∠AHB
HOH-OH_2	1	5.0	5.6333	3.8534	1.7925	0.0089	1.7854	0.0018	175.8
HOH-OCO(H)$^-$	2	15.0	5.0995	3.2699	1.8373	0.0537	1.7784	-0.0042	173.5
(H)OCOH-OCO(H)$^-$	3	27.8	4.6973	2.7794	1.9202	0.1251	2.3812	0.0442	176.3
HOH-OH$^-$	4	32.2	4.7155	2.7500	1.9702	0.1868	1.7921	-0.0116	174.7
H_2OH^+-OH_2	5	32.6	4.5553	2.5418	2.0150	0.1970	1.7943	0.0107	177.2

System	Label	∠XBH
HOH-OH_2	1	113.4
HOH-OCO(H)$^-$	2	118.8
(H)OCOH-OCO(H)$^-$	3	115.3
HOH-OH$^-$	4	107.9
H_2OH^+-OH_2	5	126.6

[a] All values are in au except the internuclear angles which are in degrees and D_e which is in kcal mol^{-1}.
[b] The hydrogen nucleus in the base fragment closest to the B nucleus in the base is denoted X.

Table 2.4.3. Properties of the Bond Critical Points of OH-O Complexes, DZP//DZP.*

	αβ	ρ	∇²ρ	r_α	r_β
1	O1H4	0.0184	0.0702	2.5161	1.3374
	O2H4	0.3743 (-0.0084)	-2.2490 (-0.0636)	1.4557 (0.0218)	0.3369 (-0.0130)
	O1H5	0.3804 (-0.0023)	-2.2036 (-0.0182)	1.4393 (0.0054)	0.3462 (-0.0037)
	O1H6	0.3804 (-0.0023)	-2.2036 (-0.0182)	1.4393 (0.0054)	0.3462 (-0.0037)
	O2H3	0.3835 (0.0008)	-2.1647 (0.0207)	1.4300 (-0.0039)	0.3525 (0.0026)
2	O5H2	0.0394	0.1389	2.2416	1.0294
	O1H2	0.3392 (-0.0435)	-2.1690 (0.0164)	1.5169 (0.0830)	0.3206 (-0.0293)
	C4O5	0.3766 (-0.0107)	-0.1717 (-0.0650)	0.7771 (0.0071)	1.5823 (0.0153)
	C4O6	0.3943 (0.0070)	-0.0476 (0.0591)	0.7649 (-0.0051)	1.5560 (-0.0110)
	C4H7	0.2819 (0.0078)	-1.0946 (-0.0612)	1.2777 (0.0017)	0.8274 (-0.0307)
	O1H3	0.3864 (0.0037)	-2.1083 (0.0771)	1.4181 (-0.0158)	0.3613 (0.0114)
3	O2H9	0.0781	0.1520	1.6995	0.7806
	O6H9	0.2908 (-0.0847)	-1.7227 (0.5195)	1.5947 (0.1407)	0.3256 (-0.0156)
	C1O2	0.3671 (-0.0202)	-0.2179 (-0.1112)	0.7835 (0.0135)	1.5977 (0.0307)
	C1O3	0.4028 (0.0155)	0.0119 (0.1186)	0.7598 (-0.0102)	1.5425 (-0.0245)
	C1H4	0.2857 (0.0116)	-1.1246 (-0.0912)	1.2797 (0.0057)	0.8182 (-0.0287)
	C5O6	0.3395 (0.0272)	-0.2359 (-0.0495)	0.7974 (-0.0123)	1.6458 (-0.0474)
	C5O7	0.4185 (-0.0132)	0.1444 (-0.1601)	0.7506 (0.0084)	1.5180 (0.0198)
	C5H8	0.3013 (-0.0075)	-1.2680 (0.2353)	1.3020 (-0.0153)	0.7656 (0.0321)
4	O4H2	0.0848	0.1233	1.9946	0.7558
	O1H2	0.2651 (-0.1176)	-1.4314 (0.7540)	1.6338 (0.1999)	0.3365 (-0.0134)
	O4H5	0.3762 (0.0076)	-1.8444 (-0.1211)	1.4005 (0.0083)	0.3916 (-0.0200)
	O1H3	0.3844 (0.0017)	-2.0198 (0.1656)	1.4116 (-0.0223)	0.3718 (0.0219)
5	O5H4	0.1031	0.0212	1.8983	0.6435
	O1H4	0.2353 (-0.1109)	-1.2001 (1.2429)	1.6758 (0.1673)	0.3393 (0.0297)
	O5H6	0.3661 (-0.0166)	-2.3027 (-0.1173)	1.4663 (0.0324)	0.3280 (-0.0219)
	O5H7	0.3654 (-0.0173)	-2.3026 (-0.1172)	1.4677 (0.0338)	0.3276 (-0.0223)
	O1H2	0.3589 (0.0127)	-2.3804 (0.0626)	1.4837 (0.0498)	0.3194 (-0.0305)
	O1H3	0.3589 (0.0127)	-2.3806 (0.0624)	1.4837 (0.0498)	0.3194 (-0.0305)

* All values are in au. Differences from isolated reactant values are enclosed in parentheses. Values for the hydrogen bond critical point are listed first, followed by those for the AH bond critical point, the BX bond critical point, the remaining base bond critical points and finally the remaining acid bond critical points.

Table 2.4.4. H-bond critical point analysis in complexes containing OH-O bonds, DZP//DZP.*

System	$\rho(r_b)$	$\nabla^2\rho(r_b)$	r(BH)	$\lvert\Delta r_B^o\rvert$	$\lvert\Delta r_H^o\rvert$	$\lvert\Delta r_B^o + \Delta r_H^o\rvert$	$\rho^o(r_B)$	$\rho^o(r_H)$	$\rho^o(r_B)+\rho^o(r_H)$
1	0.0184	0.0702	3.8534	0.934	0.863	1.797	0.0086	0.0100	0.0186
2	0.0394	0.1383	3.2924	1.268	1.171	2.439	0.0188	0.0223	0.0411
3	0.0781	0.1520	2.7784	1.510	1.379	2.889	0.0364	0.0414	0.0778
4	0.0848	0.1233	2.7500	1.585	1.444	3.029	0.0397	0.0490	0.0887
5	0.1031	0.0212	2.5418	1.482	1.306	2.788	0.0491	0.0512	0.1003

* All values are in au. The H-bond critical point is denoted r_b.

Table 2.4.5. Atomic Properties of Isolated Reactants, DZP//DZP.[a]

Reactant	Ω	q(Ω)	N(Ω)	E(Ω)	|μ(Ω)|	v(Ω)
H2O	O	-1.2287	9.2287	-75.34653	0.264	140.58
	H	0.6144	0.3856	-0.35014	0.152	19.72
HCOO-	O	-1.4932	9.4932	-75.61658	0.526	145.44
	C	2.1623	3.8377	-36.31020	0.670	31.76
	H	-0.1759	1.1759	-0.68464	0.134	58.36
HCOOH	H	0.6501	0.3499	-0.32711	0.136	17.80
	O	-1.3189	9.3189	-75.68194	0.377	122.09
	C	1.9997	4.0003	-36.46341	0.839	36.02
	O	-1.3765	9.3765	-75.72604	0.724	137.36
	H	0.0448	0.9548	-0.61640	0.109	46.93
OH-	O	-1.4181	9.4181	-74.92276	0.064	169.63
	H	0.4181	0.5819	-0.44914	0.245	31.24
H3O+	O	-1.2652	9.2652	-75.57578	0.245	125.29
	H	0.7551	0.2449	-0.25132	0.090	12.55

[a] All values are in au. Only nonequivalent atoms are listed and the atoms that will participate in the H-bond are listed first for each molecule. The values of E_{SCF} and -V/T for H_2O, $HCOO^-$, HCOOH, OH^- and H_3O^+ are -76.04683, 1.99959599, -188.23744, 2.00016918, -188.81480, 2.00033237, -75.37191. 1.99758554 and-76.32974, 1.99995146 respectively.

Table 2.4.6. Changes in the Acid and Base Fragments of Complexes Containing OH-O bonds.[a]

Complex	ΔN	ΔE	Δν
1			
acid	0.011	-3.14	-3.23
base	-0.011	-1.86	-5.15
2			
acid	0.039	-8.36	-2.88
base	-0.039	-6.40	-12.94
3			
acid	0.075	34.61	-4.59
base	-0.075	-62.04	-18.86
4			
acid	0.092	66.54	0.28
base	-0.092	-98.51	-17.15
5			
acid	0.086	-17.06	-3.25
base	-0.086	-15.35	-19.94

[a] All results are in au except ΔE values which are in kcal mol^{-1}.

Table 2.4.7. Changes in Atomic Properties of Complexes Containing OH-O bonds.[a]

Complex	Ω	ΔN(Ω)	ΔE(Ω)	Δ|μ(Ω)|	Δv(Ω)
1	O	0.0433	-15.84	0.002	2.72
	H	-0.0416	16.22	-0.031	-6.29
	O	0.0159	-12.94	0.008	-3.54
	H	-0.0133	5.54	-0.006	-0.80
	H	-0.0133	5.54	-0.006	-0.81
	H	0.0096	-3.52	0.005	0.31
2	O	0.0975	-39.33	-0.014	6.32
	H	-0.1004	46.72	-0.060	-11.05
	O	-0.0096	0.47	-0.039	-10.08
	C	0.0255	-11.58	0.019	0.68
	O	-0.0149	-1.83	0.026	-1.14
	H	-0.0397	6.54	-0.010	-2.40
	H	0.0416	-15.75	0.020	1.85
3	O	0.1178	-50.24	0.030	3.27
	H	-0.0958	46.69	-0.074	-11.77
	O	-0.0222	-22.82	-0.072	-13.82
	C	0.0407	-27.47	0.031	0.96
	O	-0.0363	-21.38	0.060	-2.57
	H	-0.0580	9.63	-0.014	-3.43
	C	-0.0471	26.03	-0.045	-1.41
	O	0.0394	28.54	-0.075	2.99
	H	0.0611	-16.41	0.000	2.33
4	O	0.1420	26.58	-0.074	9.11
	H	-0.1261	66.75	-0.092	-12.76
	O	-0.0342	-115.33	0.045	-14.22
	H	-0.0571	16.82	-0.024	-2.93
	H	0.0758	-26.79	0.037	3.93
5	O	0.0472	-6.85	-0.051	1.65
	H	-0.0257	20.67	-0.051	-7.14
	O	0.0757	-83.38	-0.030	-10.54
	H	-0.0796	33.64	-0.036	-4.67
	H	-0.0816	34.39	-0.036	-4.73
	H	0.0321	-15.44	0.014	1.12
	H	0.0321	-15.44	0.014	1.12

[a] All values are in au except ΔE(Ω) which is in kcal mol^{-1}. For all complexes the A of acid is listed first, followed by the H-bonded H, the base atom B participating in the hydrogen bond, the next nearest base atom, the remaining base atoms and finally the remaining acid atoms.

Table 2.4.8 Relationships Between Properties of the Charge Density and D_e for Hydrogen-Bonded Complexes in this Chapter.

Base-HA	D_e*	$\rho(r_b)$	mut pen	$\Delta\rho(r_a)$	$\Delta E(H)$*
NN-HCl	3.5	.0062	1.01	0.0000	18.2
OC-HCl	4.1	.0085	1.40	-.0006	28.9
SCO-HCl	6.2	.0073	1.10	-.0001	28.7
NN-HF	6.9	.0084	1.14	-.0028	15.6
OCO-HCl	7.1	.0085	1.23	-.0002	33.8
OC-HF	9.3	.0123	1.54	-.0057	18.6
HF-HCl	9.9	.0147	1.69	-.0011	55.4
OOO-HF	10.7	.0129	1.43	-.0056	19.5
SCO-HF	10.9	.0099	1.19	-.0038	20.2
SC-HCl	11.8	.0131	1.85	-.0036	72.4
OCO-HF	12.6	.0112	1.27	-.0048	24.5
H_3N-HNH_2	12.6	.0122	1.46	-.0024	87.4
NNO-HF	12.6	.0163	1.45	-.0070	27.9
HCN-HCl	16.0	.0136	1.78	-.0032	82.1
H_3P-HF	16.4	.0114	1.54	-.0100	25.7
HF-HF	16.7	.0213	1.71	-.0094	31.0
H_2O-HOH	20.9	.0184	1.80	-.0084	67.9
SC-HF	21.8	.0178	1.88	-.0138	36.8
OSO-HF	22.1	.0164	1.69	-.0095	33.6
H_2S-HF	24.8	.0115	1.59	-.0087	23.7
(H_2N)HCO-HNH(COH)	25.5	.0205	1.77	-.0081	116.7
H_3N-HOH	26.8	.0214	1.93	-.0137	89.5
HCN-HF	27.2	.0183	1.80	-.0135	45.0
H_2CO-HF	27.3	.0274	1.95	-.0192	49.1
H_3N-HCl	27.9	.0306	2.64	-.0170	174.7
H2O-HF	34.8	.0276	2.08	-.0208	51.6
H_3N-HF	46.2	.0344	2.45	-.0338	62.1
[HOCO-HOH]$^-$	62.8	.0394	2.44	-.0435	195.5
[H_2O-HNH_3]$^+$	90.0	.0387	2.20	-.0277	140.2
[H_3N-HNH_3]$^+$	109.6	.0507	2.55	-.0559	178.2
[HOCO-HOCO(H)]$^-$	116.3	.0791	2.89	-.0847	195.4
[HO-HOH]$^-$	134.7	.0848	3.03	-.1176	279.3
[H_2O-HOH_2]$^+$	136.4	.1031	2.79	-.1109	86.5

*kJ mol^{-1}

2.5 THE EFFECTS OF A CRYSTAL ENVIRONMENT ON THE ANIONIC OH-O COMPLEXES

In Section 2.4, the anionic complexes $(H)OCOH\text{-}OCO(H)^-$, $HOH\text{-}OH^-$ and $HOH\text{-}OCO(H)^-$ were examined using the RHF/DZP//DZP scheme in the absence of any crystal field. In the present section, we wish to see what happens to the charge density when these complexes are placed in the crystal environments of $KH(HCOO)_2$, $(LiOH)_2 \cdot H_2O$ and the system of $[Li(HCOO)] \cdot H_2O$ with two nearest neighbour water molecules, respectively. These crystal systems, all containing at least one OH-O hydrogen bond are labelled **1**, **2** and **3** respectively. Species **1** has a very short H-bond (H-O = 2.3990 au) while species **2** and **3** have medium range H-bonds (see Table 2.5.1 and Figure 2.5.1).

The theory of atoms in molecules first is used to examine the charge density of **1**, **2**, and **3** at their experimental crystal geometries (1 and 3: Hermansson et al 1983, 2: Hermansson and Lunell 1982) but without explicitly modelling a crystal field. This allows us to see how the crystal experimental geometry (as compared to the optimized geometry) affects ρ. Then we use various point charge models to simulate the crystal fields and thus are able to see how the crystal field affects ρ and functions of ρ. Both the theory of atoms in molecules and double difference density plots are used in this vein.

The questions of interest include the following:

1) What is the nature of the interaction between the atoms in the complex? Is the H-bond a closed-shell interaction as it was in the

previous sections of this chapter or does it become a shared interaction when in a crystal environment?

2) Does a shorter H-bond mean more ρ in the H-bond region?

3) Can the value of ρ at the bond critical points be used to predict a bond order and bond strength in these systems (for CO bonds for example)?

4) How do the point charge crystal fields affect ρ, $\nabla^2\rho$ and the atomic properties of the constituent atoms? Are the changes from a field free situation at the same experimental geometry large? Can the crystal field effects rationalize the asymmetry of the H-bond in 1?

Method of Calculation

i) $KH(HCOO)_2$

RHF/DZP//experimental crystal geometry calculations are performed first for the crystal-field free diformate anion. The charge density resulting from this is analyzed using the theory of atoms in molecules and the values are listed in Tables 2.5.1 - 2.5.3 under the scheme denoted "free". Secondly, the same level of calculation is used to compute the charge density of the anion placed in a crystal with the crystal described by point charges. The point charges are positioned at the atomic coordinates determined by neutron diffraction out to a distance of about 15A for Schemes A to C and further out from the central anion for Scheme D. The same number of point charges are used for Schemes A to C (500) but 8200 are used for Scheme D.

The SCF calculations associated with Schemes A-D are done according to the following procedure (I thank Kersti Hermansson at

Uppsala for helping with these calculations):

(a) A crystal-field free diformate anion calculation is performed.

(b) The resulting Mulliken charges are positioned at the appropriate lattice points. The cluster, i.e. the $H(HCOO)_2^-$ ion plus the point charges, is electrically neutral. The potassium ions are assigned net charges of +1.

(c) The one-electron integrals are recalculated.

(d) A new SCF calculation in the crystal field created by the surrounding point charges is performed.

Steps (b)-(d) are repeated until a self-consistent set of point charges is obtained with the criterion for self consistency being a difference of $< 0.001e$.

(e) The charge density resulting from the self-consistent set of Mulliken point charges is analyzed using the theory of atoms in molecules. The corresponding data are listed under Scheme A and Scheme D in the Tables 2.5.2 -2.5.3. This is the only place in the thesis where Mulliken charges have been used and only to facilitate a comparison with the work of Taurian et al (1987).

(f) The net charges, as calculated using the theory of atoms in molecules, arising from Scheme A are placed at the appropriate lattice points and a new ρ is calculated. This new ρ is analyzed using the theory and the results are listed under Scheme B.

(g) The process is repeated till self-consistency is achieved. The results for the analysis of this final ρ are listed under Scheme C.

ii) Structures 2 and 3

The procedure is similar to that in i) but only the "free"

results and the results of Schemes A and B are given. As opposed to i), here the Li atom is an explicit part of the molecule and not modelled as a point charge. For 2, 918 point charges are used and for 3, 2700 point charges are used.

Geometries

The structures of the complexes are displayed as molecular graphs in Figure 2.5.1 and the geometrical parameters are given in Table 2.5.1.

i) The H-bond in $H(HCOO)_2^-$ is one of the shortest observed of all OH-O complexes. It is not symmetric. The internuclear separations O2H9 and O6H9 are 2.3990 and 2.2055 au respectively. Thus, the atoms C1, O2, O3 and H4 constitute the formate group while the atoms C5, O6, O7, H8 and H9 constitute the formic acid group. This identification will also be made apparent when the values of ρ and $\nabla^2\rho$ in the O6H9-O2 region of the anion are examined. The C1O2O3H4 and C5O6O7H8 groups are structurally similar. For example, C1O2 differs from C5O6 by only 0.0028 au and C1O3 differs from C5O7 by only 0.0178 au. Each group is nearly planar though they are twisted relative to each other. Table 2.5.1 lists the changes from the optimized DZP geometry of the free anion (given in Table 2.4.1). The biggest changes are in the hydrogen-bonded region. The crystal forces the H9-O2 bond to contract by 0.380 au while the O6H9 bond expands by 0.2853 au. These geometry changes have important consequences on the topology of ρ in this region. The H9-O2 bond now has some of the characteristics of a shared interaction ($\nabla^2\rho(\mathbf{r}_b)$ is negative) whereas in the free optimized structure it is still

closed-shell (Table 2.4.3).

ii) A water molecule intervenes between the lithium cations and the hydroxide anions in the crystal structure. The O5H8-O3 hydrogen bond is then between the water molecule acting as an acid and OH- acting as a base. The O5H9-O4 hydrogen bond is, of course, equivalent. The H-bond is not symmetric as O5H8 = 1.8936 au and H8-O3 = 3.1820 au. The hydrogen bond length is 0.7830 au longer than that of 1 and falls into the medium length H-bond class.

iii) The shortest of the three OH-O bonds here is between water acting as an acid and the formate anion acting as a base. The H2-O5 separation is 3.292 au and falls into the medium range H-bond category. The water-water H-bonds are appreciably longer (H10-O1 is 3.683 au as is the equivalent H3-O12) and these fall into the long-range category. An unexpected feature of this system is the very long H-bond between H7 of the formate group and O8 of a neighbouring water. The existance of this bond path causes a seven-member ring structure to form.

iv) The partially optimized structure HOH-OH- (intermolecular angles are constrained to a degree of experimental values) differs from the corresponding structure at the experimental geometry. In the former complex, the H-bond length is appreciably shorter and the AH bond length is longer. The energy difference between the partially and fully optimized structure (Section 2.4) is only 0.31 kcal mol^{-1} while the difference between the partially optimized and experimental structure is also small (3.6 kcal mol^{-1}). An examination of the geometry differences between 2 and 4 (Table 2.5.1) shows that the

parameters of the partially optimized structure are very similar to those of the fully optimized structure, a fact not surprising considering the small energy differences. In the crystal system 2 the two OH bondlengths in water are equivalent due to symmetry but for 4 they are not. The OH bond in the acid water in 2 is longer than that of the nonparticipating OH bond in 4 because in 2 this bond makes up part of the H-bond while in 4 it does not (see the square bracketed values in Table 2.5.1).

v) The partially optimized structure 5 differs slightly from the corresponding structure at the experimental geometry in that both the AH and BH lengths are shorter for 5. The energy difference between 5 partially optimized and 5 at the experimental geometry is 326.4 kcal mol^{-1}. Note that a full geometry optimization would produce a cyclic structure with the water acting as a two proton donor.

Topology of 1

a) The hydrogen bond

The H-B hydrogen bond of the free diformate anion (DZP//DZP) is an example of a closed shell interaction since ρ at the hydrogen bond critical point, $\rho(r_b)$, is small and the sign of $\nabla^2\rho(r_b)$ is positive (Table 2.4.3 and Figure 2.5.2d). In the present case (DZP//experimental crystal geometry: Scheme "free") $\rho(r_b)$ is larger by 0.0605 au and $\nabla^2\rho(r_b)$ is negative for the now very short H-bond, and so, the H-bond has some of the characteristics of a shared interaction (Table 2.5.2 and Figure 2.5.2). The geometry of the crystal forces the H-bond in the diformate anion to be much shorter than it is for the

fully optimized case and this constraint causes charge density to accumulate between O2 and H9. The distances from r_b to O2 and H9, that is the bonded radii of B and H respectively, are shorter for DZP//experimental geometry than DZP//DZP (Table 2.5.2) again because the H-bond length is shorter in the former.

The AH bond length (i.e. O6H9) is significantly larger at the experimental geometry as compared to DZP//DZP. Consequently, the charge density at the AH bond critical point, $\rho(r_a)$, is smaller (by 0.10 au) at the experimental geometry as is the magnitude of $\nabla^2\rho(r_a)$. Thus there is less charge accumulated between O6 and H9 in the experimental case.

b) The remaining bonds in 1

Comparing the values of ρ at the bond critical points in the experimental geometry to the optimized DZP geometry, the changes are all at least three times smaller than those that occur in the H-bonded region. Thus, the H-bonded region is most sensitive to the change from optimized to experimental geometry. The value of $\rho(r_c)$ decreases in all cases except C1H4 and C5O6. The changes in $\nabla^2\rho$ are also smaller than those in the H-bonded region. Contrary to the DZP//DZP case, where $\nabla^2\rho(r_c)$ was positive in some of the bonds, in the experimental case $\nabla^2\rho(r_c)$ is always negative. Thus, in this constrained system each interaction between two neighbouring atoms is classified as a shared interaction.

Concentrating now solely on the experimental structure, we see how the values of ρ and $\nabla^2\rho$ reflect the similarity between the C1O2O3H4 and C5O6O7H8 groups. The bond critical points in C1H4 and C5H8 yield

very similar values (Table 2.5.2) as do C102 with C506 and C103 with C507. Figure 2.5.2. displays the similarities in the ρ and $\nabla^2\rho$ fields between the acid and base planes.

Since, in general, the bond order and strength of the bond increase with increasing value of $\rho(r_b)$, the C103 and C507 bonds will be stronger and have a larger bond order than C102 and C506. In accordance with classical valence theory and deformation density maps (Taurian et al 1987), the C103 and C507 bonds will have more double bond character than the other carbon-oxygen bonds.

Atomic Properties of 1

a) The formic acid fragment and the formate anion fragment of 1

The atomic properties N(Ω), K(Ω) and μ(Ω) are listed in Table 2.5.3. On summing up the N(Ω) values for the formic acid and formate group, we see that 0.175e have been transferred from the formate to the formic acid group. This is close to Taurian et al's (1987) value of 0.10e obtained by Mulliken population analysis. Thus, as always, electrons are transferred from base to acid. q(Ω) calculated using the theory of atoms in molecules is larger in magnitude than the corresponding Mulliken charges. K(formic acid group) is greater in magnitude than K(formate group), and so, the formic acid group in 1 has a lower energy than the formate group.

b) The O6H9-O2 fragment of 1

The smallest value of N(Ω) is N(H9) = 0.270 e. Because of this electron deficiency, both K(H9) and $|\mu(H9)|$ are the smallest of all the atoms.

As is the case for all OH-O fragments, both the more electronegative atoms to which H9 bonds (O2 and O6) are negatively charged. It so happens that O2 and O6 bear almost an equal charge and these charges are the largest in magnitude of all the atoms in 1. The energies of O2 and O6 are of greater magnitude than the remaining oxygens while the magnitude of the atomic first moments for O2 and O6 are smaller.

c) The remaining atoms of 1

The remaining oxygens have very similar values for their atomic properties. The same is true for H4 and H8 which are both slightly negatively charged. The carbons also exhibit very similar values for their atomic properties. They are positively charged and have the largest values for $|\mu(\Omega)|$. Therefore, the similarity between the formic acid and formate groups in 1 is reflected once again, this time through the atomic properties.

Crystal Field Effects on 1

a) Influence on the topology of the charge density of 1

The charge density is perturbed when an array of point charges used to model a crystal field is applied. As is seen in Table 2.5.2, the perturbations are not as great as those that arise due to a change in geometry from DZP//DZP to DZP/experimental. (Of course, the crystal effect is manifested to its greatest extent by the fact that we now look at experimental geometry). Still, the bond critical points shift slightly in position from those in the experimental case to those in the experimental case with the point-charge field simulation included.

For Schemes A and D, the greatest changes are in the C1-H4 and C5-H8 terminal bonds. The greatest changes in $\rho(r_a)$ parallel these. For both these schemes and also Schemes B and C, we see that the changes of the charge density in the H-bonded region are among the smallest. In Schemes B and C the greatest change in $\rho(r_a)$ is for the C5O6 bond.

In general, the changes due to Schemes B and C are similar and of the same sign. This observation is used to justify the application of only Schemes A and B in a study of 2 and 3 (vide infra). The changes due to B (or C) as compared to A are not necessarily of the same sign.

Scheme C is deemed a better model than B because in C there exists a self-consistent set of $q(\Omega)$ (as determined by the theory of atoms in molecules). In Scheme A there exists a self-consistent set of $q(\Omega)$ as determined by Mulliken population analysis.

With this in mind, we show the rearrangement of electron density caused by the modelled crystal field in terms of double difference density countour maps. In these maps (Figure 2.5.3) the charge density of a free $H(HCOO)_2^-$ ion (in the geometry of the crystal) is subtracted from the density calculated in the crystal. Both the affect of Scheme A and Scheme C on ρ are displayed and compared. These maps supplement the information obtained from examining the differences in ρ at bond critical points (Table 2.5.2) because the maps show the differences in charge density for a whole range of points (in a specified plane).

Figure 2.5.3a displays the double difference density in the acid plane (i.e. the C5O6O7H8 plane). Looking at the left diagram

first, we note the following effects of the crystal field on the charge density: There are weak positive contours outside O7 in agreement with Taurian et al's (1987) picture. Charge has shifted into the C5H8 bond. Recall that this observation is also reflected in the data in Table 2.5.2 which shows that the increase in $\rho(r_a)$ in the C5H8 bond (of 0.005 au) is among the largest. Taurian et al's plots also reflect this buildup. Also in agreement with Taurian et al, we see the shift of charge density away from the nonbonding regions of the hydrogen atoms. The Scheme C field effect (right diagram of Figure 2.5.3a) is similar to the A field effect except for the C field there is an even greater removal of charge density from H8 and a greater buildup of charge in the C5H8 bonding region.

The left diagram of Figure 2.5.3b gives the A-"free" results for the base plane. This diagram is quite similar to Taurian et al's except the removal of charge density from the O2H9 region is even more pronounced. We see the shift of electron density away from the nonbonded region of H4, a large buildup in the C1H4 bond (in agreement with Table 2.5.2), and the weak contours outside the oxygens. Thus the features of the base plane plots are very similar to those of the acid plane plots, an observation that by now is not surprising. In Figure 2.5.3b (right) we do not see very much charge removal from the immediate vicinity of H9. Indeed, the value of ρ at the H-bond remains essentially unchanged from the "free case".

In Figure 2.5.3c (left) we look at the A minus "free" results in the H-bonded plane. As in the other planes there is charge buildup in the far nonbonded regions of the oxygens and removal of nonbonded

charge density from the terminal hydrogens. Along the H-bond, in the immediate vicinity of O2 there is a build-up of charge because of the crystal effects. Closer to H8 along this same bond, charge has been removed. In the O6H8 bond the reverse situation occurs. In Figure 2.5.3c (right), O2 and O6 look more similar. They both have charge depleted near themselves along their respective bond axes with H8. H8 itself has a very slight build-up of charge immediately around it along the above mentioned bond axes.

b) Influence on the atomic properties of 1

Taurian et al use a scheme very much like Scheme A but they stop at the Mulliken charges. They do not consider the theory of atoms in molecules. They say that there is a shift in negative charge from the central part of the anion to the O3 and O7 ends, and that this is a consequence of the distribution of K^+ ions in the crystal. Indeed, the K^+ ions are closest to the central anion and they also bear the greatest Mulliken charges. In our Scheme A, O3 gains the most electrons and O7 also gains electrons. However, only in Scheme D do both O3 and O7 gain the most electrons as compared to the other atoms. In Schemes B and C, O7 actually loses electrons and the O3 changes are small. Why does O7 not gain electrons? Granted, the K^+ ions are closest to the central anion. But they do not have the greatest charges as determined from the theory of atoms in molecules. For example, the carbons have a charge of $\approx +2$. Therefore, the entire crystal field must be taken into account when examining charge reaarangements due to crystal fields as both the magnitude of the charge and distance it is away from the central anion are important.

In Schemes A and D, the H-bonded atoms (O6, H9 and O2) are, in general, changed the least (as reflected in the changes of $N(\Omega)$, $K(\Omega)$ and $|\mu(\Omega)|$) while the terminal atoms are in general changed the most. A division like this cannot be made in Schemes B and C but it is worthwhile to note that in all schemes the H-bonded hydrogen is least affected by the crystal field. The charge density of H9 is very tightly held so the changes in the three properties listed in Table 2.5.3 due to crystal fields will be small.

Taurian et al state that the crystal field affects the two formate groups unsymmetrically. They say that the formate group of the formic acid (i.e. the C5O6O7H8 group) retains the same charge when placed in a crystal field. For Schemes A to D inclusive, we agree with this observation. Further, they find that the formate ion group (i.e. the C1O2O3H4 group) acquires an additional 0.02 electrons due to the crystal field, and that these electrons are taken from H9. In Schemes A and D we find that this group acquires an additional 0.01 electrons but in Schemes B and C the gain is insignificant.

In Taurian et al's Scheme and our Scheme A and D, since the crystal field causes electrons to flow from the acid to the base, the positive electrostatic field due to the K^+ ions is stronger in the base fragment. The repulsive field for a positive charge thus is also stronger from the base than from the acid side. Consequently, H9 is displaced towards O6 and, therefore, the H-bond is not symmetrical.

Although the changes in the charge density due to crystal effects for 1 are small, they are not negligible. In fact, in 2 and 3 they are much more pronounced.

Topological Analysis of the Charge Density of 2

We look at the "free" situation first for $(LiOH)_2 \cdot H_2O$. We need only look at the O5H8-O3 hydrogen bond since the other one is equivalent. In the H-bond the value of $\rho(r_c)$ is 0.0512 au (Table 2.5.2). This value is more than twice as small as that found for the H-bond of 1. In addition, $\nabla^2\rho(r_c)$ is positive for the H-bond in 2 and so we have a closed shell interaction between H8 and O3 (Figure 2.5.4). Thus, the longer H-bond in 2 has less of a charge buildup than 1 and is an example of a closed-shell rather than a shared interaction. In Section 2.4, $\rho(r_c)$ in the H-bond is slightly greater for [HOH-OH]- than the diformate anion (DZP//DZP) while at the experimental geometries, the opposite conclusion is reached. Both the absolute values of $\rho(r_c)$ and $\nabla^2\rho(r_c)$ in the O5H8 bond in 2 are larger than the corresponding (but longer) AH bond in 1.

b) The remaining bonds of 2

The value of $\rho(r_c)$ for O3H6 is the largest of all the bonds of 2 and $\nabla^2\rho(r_c)$ is negative. The long Li1O5 bond is an example of a closed shell interaction because $\nabla^2\rho(r_c)$ is positive and $\rho(r_c)$ is small (even smaller than that for the H-bond).

c) Changes in topology of the charge density of 2 from free [HOH-OH]-: Looking first at the changes of 2 from that of the free isolated [HOH-OH]- (herafter called the "naked" species) at the same experimental geometry we note the following (from Table 2.5.2): $\rho(r_c)$ is greater in 2 than in the naked species for the BH and XB bonds but smaller for the remaining bonds that can be compared. The greatest

changes are for the acid water OH bonds. The r_α and r_β changes are also greater for these bonds, and so, the bond critical point shifts the most in these bonds on going from naked to 2, a result not surprising considering that the main differences between the structure of 2 and naked are the Li atoms bonded to the water oxygen and the O4H7 group bonded to H9 of water in 2. These additional atoms in 2 will thus affect the water molecule more than they will the BX and the hydrogen bond in the naked structure.

The changes in the values of $\rho(r_\alpha)$ of 2 from the naked structure (partially optimized geometry) are, in general, of opposite sign to those mentioned in the previous paragraph. However, as is the case with 2 minus the naked structure (experimental geometry), the difference here is greatest for the water OH bond not participating in the H-bond in the naked structure.

Atomic Properties of 2

a) The H-bonded atoms O5, HC and O3 of 2

Just as in 1, H8 bears the greatest positive charge (of the hydrogens) and is bonded to the two greatest negatively charged atoms O3 and O5 ("free" results of Table 2.5.3). The magnitudes of the charges are greater than those for the A, B and H atoms of 1.

b) The remaining atoms of 2

The X atoms H6 and H7 are positively charged and have greater absolute values for both K(H) and $|\mu(H)|$ than H8 or H9. The Li atoms each donate almost an entire electron to the acidic water; q(Li) = 0.9630e so the conventional representation of Li in this system as Li^+

is a good one. The representation of the base group OH as OH^- is not quite as good since q(O3H6) = -0.8786e only. One can think of electrons flowing from both these groups to the central acid water. Electrons are transferred from base to acid as we saw in 1. Note the very small value of $|\mu(Li)|$. This is because the Li is behaving as a hard very nonpolarizable Li^+ cation.

c) Changes in atomic properties of 2 from free [HOH-OH]-

The changes of 2 from the naked at experimental geometry and naked at partially optimized geometry are similar (Table 2.5.3), and so, we will treat them together. Only O5 of 2 gains electrons. This is obviously because of the presence of lithium in 2. Indeed, $\Delta N(O5)$ is at least an order of magnitude larger than any of the other population changes. Note that $\Delta K(O5)$ is positive but $\Delta K(\Omega)$ is negative for the remaining atoms. Also note that the magnitude of $\Delta|\mu(O5)|$ is the largest. In short, the important effect of going from the naked case to 2 is the flow of charge density to the central oxygen, that is, O5 of the acid.

Crystal Field Effects on 2

a)Influence on the topology of the charge density of 2

It has been established through a study of the crystal effects on 1 that no important new information is garnered from using Scheme C instead of Scheme B. Thus, only the results of Schemes A and B have been determined.

The perturbations arising from the point charges are, in general, of similar magnitudes to those that arise just from a change

of geometry, and so, the crystal field effects are more important in 2 than in 1. Scheme A minus free values and corresponding Scheme B minus free values have the same sign for each property of each bond, a result not observed in 1. The largest changes in $\rho(r_c)$ for both schemes is for the AH bond and the smallest is for the Li1O5 bond. Only in the AH bond does $\rho(r_c)$ increase. For $\nabla^2\rho(r_c)$, the largest changes are for the BX bond. Also, the critical point shifts are largest for the BX bond. Thus the effect of the crystal field generated using either scheme is felt most in the BX and AH bond and not nearly as much in the actual hydrogen bond BH. In 1 the crystal effects on the hydrogen bond are also small.

Double difference density plots in the H-bonded plane are displayed in Figure 2.5.5. We observe the following:

1) The left map (A-free) is remarkably similar to the right map (B-free). Granted the net (Mulliken) charges of the atoms used to model the crystal fields in Scheme A are different (lower in magnitude) than those used to model the crystal fields in Scheme B (calculated using the theory of atoms in molecules). But because the field we are modelling is symmetric, it seems that the magnitudes of the charges are not so important. In 1 we have an asymmetric field and so there are larger differences (Figure 2.5.3).

2) In both maps we observe a charge buildup near the H-bonded hydrogen (H8 or H9) due to the crystal effects. There also exist regions of smaller charge removal between this H and the two oxygens to which it is bonded. There are also regions of charge buildup near O5 towards a lithium and a weaker buildup in the far nonbonded region of O3.

b) Influence on the atomic properties of 2

For the acid fragment, the changes due to geometry are greater than the direct point charge crystal effects but for the base fragment the reverse is true (for both schemes). It should be noted that the differences in all the atomic properties arising from Scheme A and Scheme B are of the same sign and of similar magnitude, just as was the case for the critical point analysis. The effect of either scheme is to remove electrons from O5, H6 and Li1 and to give electrons to O3 and H8. O3 gains the most electrons and H6 loses the most electrons. The $\Delta K(\Omega)$ values parallel these changes. O3 gains more electrons than H6 loses, and so, the OH base fragment gains electrons while the acid fragment loses electrons because of the effect of the crystal field.

Topological Analysis of the Charge Density of 3

a) The OH-O hydrogen bonds

From Table 2.5.1 and Figure 2.5.1 we see that the H-bond between the formate group and the central water, H2O5 is shorter than that between the central water and the neighboring waters H1OO1 and H3O12. The value of $\rho(r_c)$ for the shorter of the three bonds is twice as great than in the other two water water H-bonds (see "free" values in Table 2.5.2). However, the value of $\rho(r_c)$ for H2O5 is not as large as the shorter H-bond in 2 which, in turn, is not as large as the shorter H-bond in 1. Thus, it can be concluded that in OH-O complexes, the shorter the HO internuclear distance, the greater the value of the corresponding $\rho(r_c)$ and presumably, the stronger the H-bond. In 3, the value of $\nabla^2\rho(r_c)$ is positive in each H-bond so each H-bond exhibits a

closed-shell interaction (Figure 2.5.6). The values for H1001 and H3012 are very similar and would be even more similar were it not for the fact that a weak H-bond exists between H7 and O8.

The O1H2 bond has a smaller value of $\rho(r_c)$ than the O1H3 and O8H10 bonds because O1 and H2 make up part of the shortest and strongest H-bond in the system, that between the formate group and the central water. Charge density is accumulated in the H2O5 bonded region at the expense of charge density in the O1H2 bond. Also, the O1H2 bond is longer than the O1H3 and O8H10 bonds.

b) The C4H7-O8 hydrogen bond

The existance of this bond is unexpected. A hydrogen bond with C and O as the heavy atoms is rare. In fact, in **3**, the C is positively charged and H7 is negatively charged (Table 2.5.3). Nevertheless, this is a very long and very weak H-bond with the value of $\rho(r_c)$ being only 0.0029 au and $\nabla^2\rho(r_c)$ being only 0.0106 au. Because of this bond a ring structure is formed and thus also a ring critical point whose properties are listed in Table 2.5.2. The C4H7 bond in **3** is very similar to the terminal CH bonds in **1**.

c) The remaining bonds in **3**

Looking first at the formate group, we see that the value of $\rho(r_c)$ is greater in C4O6 than in C4O5 (Table 2.5.2). Thus C4O6 has more double bond character than C4O5, a fact previously observed in **1**. Note that C4O6 does not have as much double bond character as the terminal CO bonds in **1** nor does C4O5 have as much single bond character. The O1Li11 bond in **3** is a very long bond with a value of $\rho(r_c)$ comparable to the water-water H-bonds. The O1Li11 bond is an

example of a closed-shell interaction just as was the LiO interaction in 2. Indeed, the data for these two bonds are remarkably similar. The terminal O8H9, O12H13 and O12H1 bonds are all similar.

c) Changes in the charge density of 3 from naked [HOH-OCOH]-

In the naked structure 5 missing are the Li and the two nearest neighbour water molecules. We first examine the differences in the properties of ρ in the bonds that can be compared using the naked species at the crystal experimental geometry. In the H-bond, H2O5, we see that on going from naked to 3, $\rho(r_c)$ has increased by a very small amount and $\nabla^2\rho(r_c)$ has decreased by a small amount. In all the remaining bonds with the exception of C4-O6, $\rho(r_c)$ decreases with the greatest decreases being in the O1H2 and O1H3 bonds. This seems reasonable since O5 of the central water acquires a coordination number of four in the crystal and H3 aquires a coordination number of two. The coordination number of H2 remains at two. Thus, the two neighbouring waters must withdraw charge density from the central water so that they can bond to it. Indeed, the shifts in critical points for O1H2 and O1H3 are among the largest. The formate group is too far away from the Li and nearest neighbour waters to be appreciably affected by their presence and so the changes in the properties of their bonds are smaller than for the central water.

We now look at the differences between 3 and the naked structure 5 at its partially optimized geometry. For the central water atoms, the changes are all of the same sign as they were when the naked at experimental geometry was used but this is not the case in the formate group. $\rho(r_c)$ for the H2-O5 bond increases very slightly and

$\rho(r_c)$ for O1-H2 and O1-H3 decrease with their change being the largest of any of the bonds. The reasons for this have been given in the previous paragraph. $\rho(r_c)$ for the C4-O5 and C4-H7 bonds increase while the value for C4O6 decreases.

Atomic Properties of 3

a) The atoms constituting the H-bonds

If the formate group is initially treated as an isolated 24 electron system, then when brought into the crystal structure of 3, 0.0617e are transferred from this base to the remainder of the system (Table 2.5.3). This is less than the number of electrons transferred from the formate group to the acid in 1 (0.10e).

The shortest H-bond is examined first. It is interesting that H2 is the most positively charged of the hydrogens and that O1 and O5 are the most negatively charged oxygens, seen in the other systems as well. H2 has the lowest K(H) and $|\mu(H)|$. Thus, H2 can be thought of as being "harder" than the other hydrogens.

As previously mentioned, in C4H7-O8 the carbon is positively charged and the hydrogen is negatively charged. Still, a weak H-bond is formed. H7 is more negatively charged here than are either of the terminal hydrogens of 1.

b) The remaining atoms of 3

H13 and H1 have similar values but the terminal H9 has a greater value for N(H). Li loses slightly more charge here than it lost in 2. The "doubly bonded oxygen", O6, has almost the same charge here as it does in 1.

c) Changes in atomic properties of 3 from naked [HOH-OCOH]-

Looking first at the changes from the naked species at experimental geometry, we note the following: i) The greatest change in both N(Ω) and K(Ω) is for O1. This is reasonable because it is the environment around O1 that undergoes the greatest perturbation when the naked species is placed in a crystal. H3 and H2 experience among the next greatest changes which is also reasonable. The changes in the formate group are smaller (with the exception of ΔN(O6)), again because this group does not feel the Li and nearest neighbour water effect as greatly as the central water does. These observations also hold when we examine the 3 minus naked at partially optimized geometry results (Table 2.5.3).

Crystal Field Effects on 3

a)Influence on the topology of the charge density of 3

The perturbations arising from the point charges are similar in magnitude than those that arise just from a change of geometry or structure, and so, the direct crystal field effects are more important in 3 than in 1. Scheme A minus free values and corresponding Scheme B minus free values, in general, have the same sign for each property of each bond, a result observed in 2 but not observed in 1. The largest changes in $\rho(r_c)$ for both schemes is for the "dominant" AH bond (that is, the O1H2 bond) and the smallest (next to the extremely weak H7O8 bond) is for the O1H10 hydrogen bond. The critical point shifts are largest for the C4H7 bond. Note that as usual, the actual H-bonds are not affected greatly by the crystal fields, nor are the values for the

ring critical point.

Double difference density plots in the H-bonded planes O1H2O5, O1H10O8 and also in the O6C4O5 plane are displayed in Figure 2.5.7. The top map (A-free) is remarkably similar to the bottom map (B-free) in all three planes. Thus the essential changes are qualitatively the same and the observations we make below hold for either scheme:

a) In the O1H2O5 plane, we see charge buildup near H2 and also in the immediate vicinity of O5 along the H2O5 bond axis. We see charge removal near the midpoint of this bond. Near O1, along the O1H2 bond axis, we see charge removal. In the nonbonded region of O5 we see charge buildup.

b) In the O1H10O8 plane, we see charge removal near H10 and also in the oxygen regions which do not participate in this bond. There are charge build-up regions near the midpoint of the O1H10 and O8H10 bonds.

c) In the O6C4O5 plane (H7 is almost in this plane also), there is mostly charge removal in the C4O5 and C4O6 bonds but there is charge buildup in the C4H7 bond. These features are similar to those in Figure 2.5.4 for structure **1**.

In all three planes, we see charge buildup around H2. We also see charge removal from H10 in Figures 2.5.7a and 2.5.7b. Obviously, the crystal fields affect the various H-bonded hydrogens differently.

b) Influence on the atomic properties of **3**

With the exception of O5, the differences in all the atomic properties arising from Scheme A and Scheme B are of the same sign and of similar magnitude, just as was the case for the critical point analysis. The effect of either scheme is to remove electrons from O1,

H7, H10, H9, H13, H1, and Li11 and give electrons to H2, C4, O6, O8, H3, and O12. O8 and O12 gain the most electrons while H7 and the terminal hydrogens lose the most electrons. The $\Delta K(\Omega)$ values parallel these changes. Thus, it is the neigbouring two water groups that are most sensitive to the crystal field in terms of changes in atomic properties. The oxygens in these groups gain just slightly more electrons than their respective hydrogens lose. The central water group also loses electrons while the formate group gains electrons. The H-bonded hydrogens have $\Delta N(H)$ values of the smallest magnitude. The fact that the H-bonded hydrogens are not affected much by crystal fields has also been observed for 1 and 2. In summary, the atoms that are positioned in the exterior part of the system are affected greatest by the crystal fields with respect to atomic properties.

Conclusions Regarding Crystal Field Effects on Structures 1, 2 and 3

We address the questions proposed in the Introduction:

1) In general, the H-bond is an example of a closed-shell interaction. But in very short H-bonds, arising from crystal forces, we can have an H-bond with $\nabla^2\rho(r_c)$ being negative, and so, the H-bond will exhibit some of the characteristics of a shared interaction (Figure 2.5.2).

2) For the H-bonds present in 1, 2, and 3, the value of $\rho(r_c)$ for the H-bond increases and the value of $\rho(r_c)$ for the AH bond decreases as the H-bond decreases in length.

3) We have used the value of $\rho(r_c)$ to predict which bonds will have

more "double bond character" and we are in agreement with Taurian et al for 1. We have also explained the reasons for the H-bond in 1 to be asymmetric.

4) We have examined the effect of crystal fields on 1, 2, and 3 and have found the effect due to point charges to be smallest for 1.

Figure 2.5.1

Molecular graphs of anionic and neutral complexes containing OH-O bonds.

1) the diformate anion in $KH(HCOO)_2$

2) $(LiOH)_2 \cdot H_2O$

3) $[Li(HCOO)] \cdot H_2O$ with two nearest neighbour water molecules

4) HOH-OH-

5) [HOH-OCOH]-

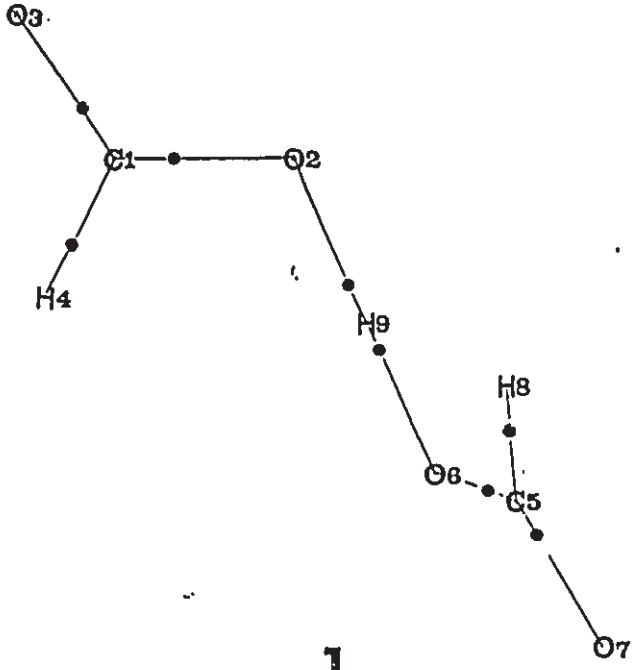

1

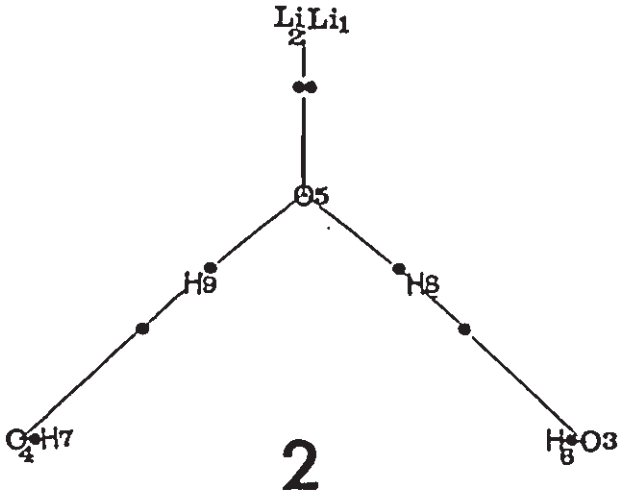

2

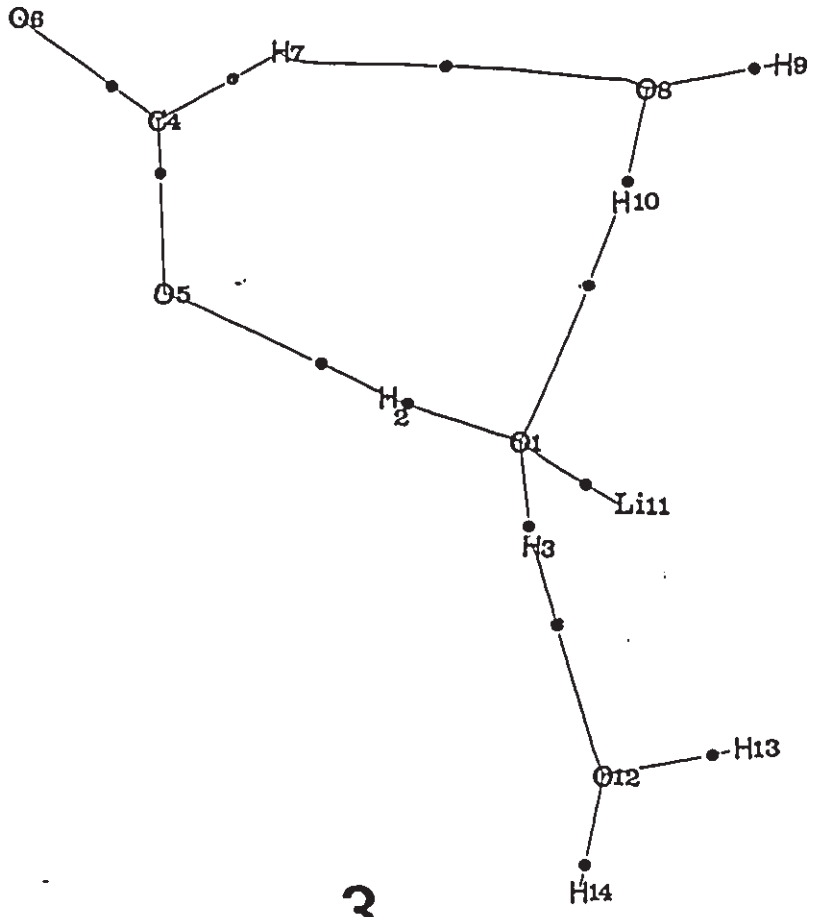

3

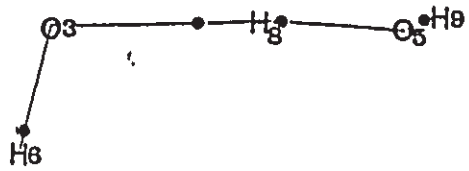

4

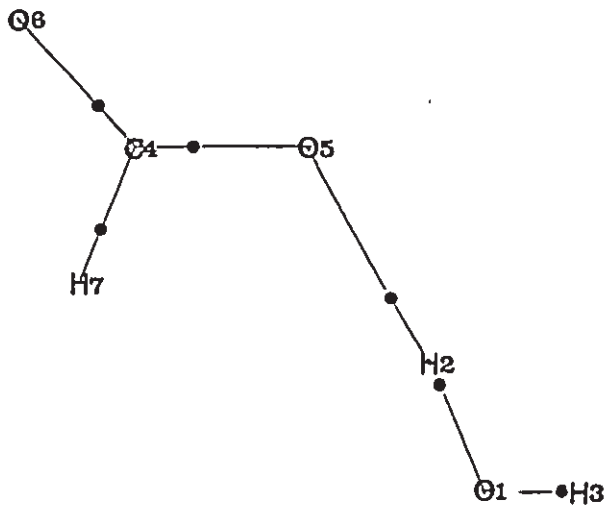

5

Figure 2.5.2

Contour maps of ρ (left) and $\nabla^2\rho$ (right) for the diformate anion in the experimental crystal geometry of $KH(HCOO)_2$. Zero flux surfaces, bond paths and bond critical points (black dots) are included.

a) Maps for the acid plane C5O6O7H8

b) Maps for the base plane C1O2O3H4

c) Maps for the hydrogen-bonded plane O2H9O6

d) $\nabla^2\rho$ map for the hydrogen-bonded plane O2H9O6 but at optimized, as opposed to experimental geometry (i.e. RHF/DZP//DZP rather than RHF/DZP//experimental crystal geometry).

a

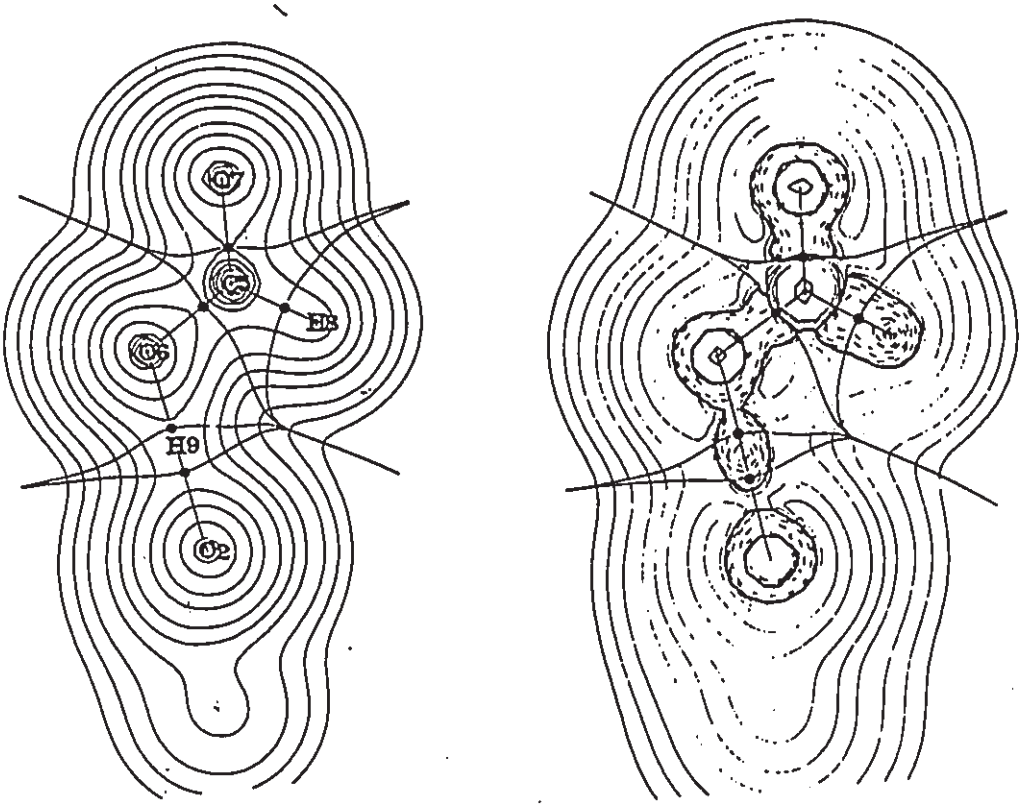

b

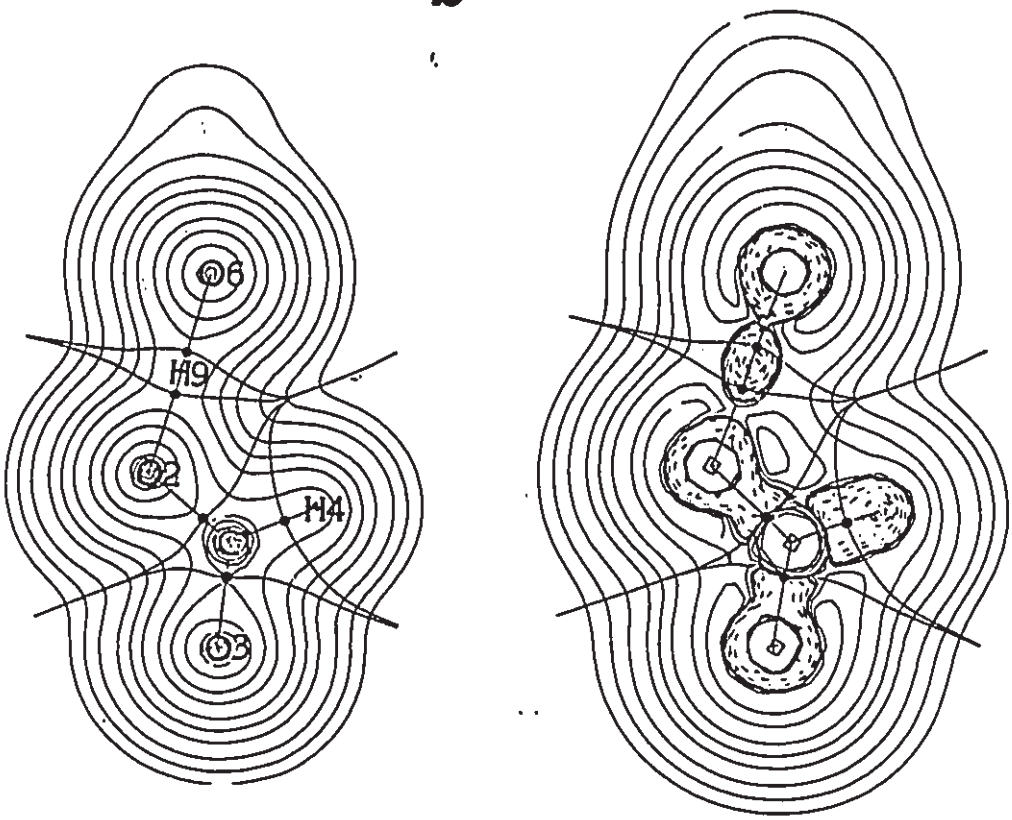

C

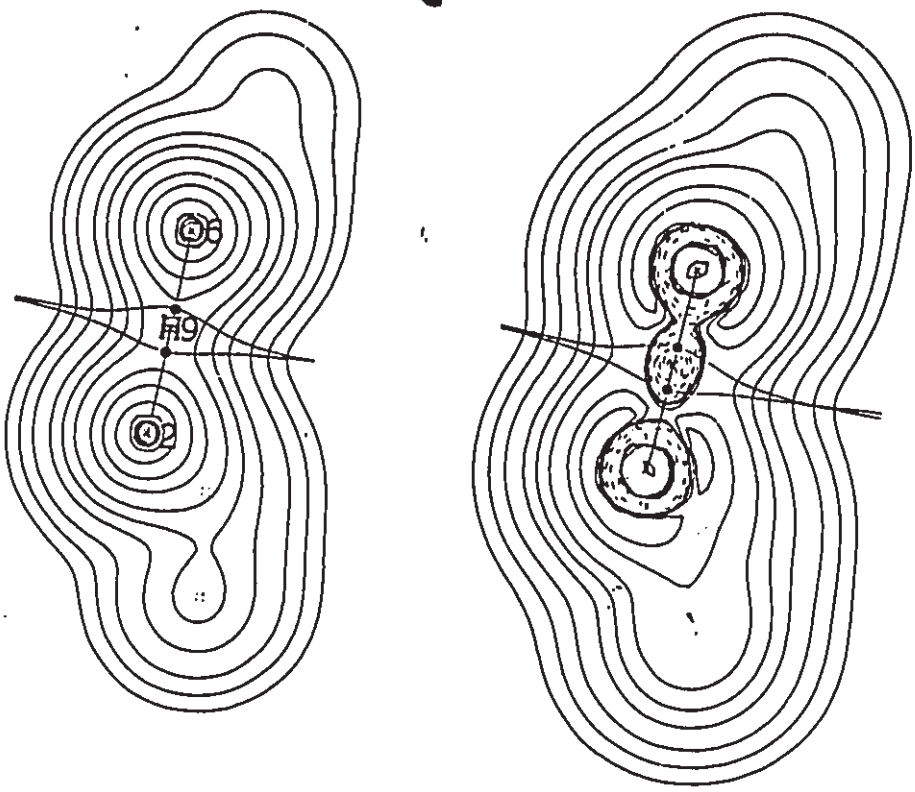

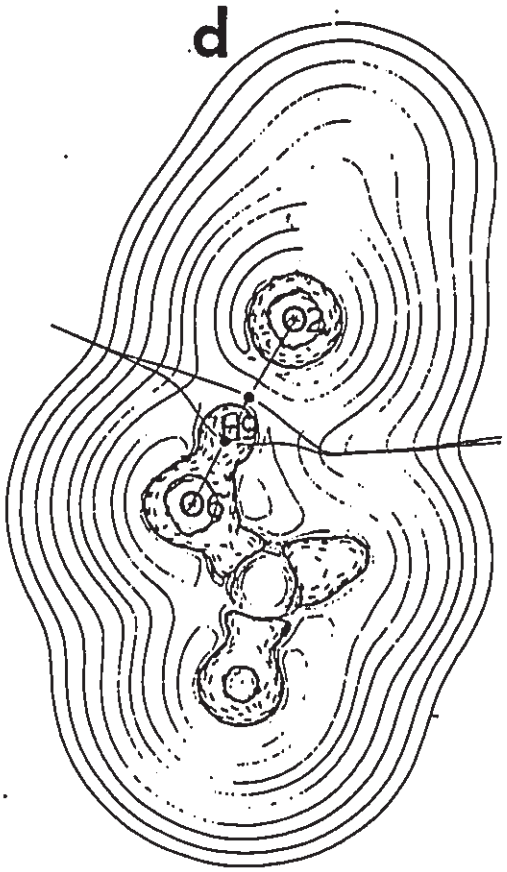
d
O2
Hg
O6

Figure 2.5.3

Double difference density contour maps for the diformate anion in the experimental crystal geometry of $KH(HCOO)_2$. The left diagrams are for the Scheme A minus field free case and the right diagrams are for the Scheme C minus field free case. Solid contours correspond to regions of charge buildup (Scheme A (or C) minus field free case at a given point is positive) and dashed contours correspond to regions of charge removal.

a) Maps for the acid plane C5O6O7H8

b) Maps for the base plane C1O2O3H4

c) Maps for the hydrogen-bonded plane O2H9O6

a

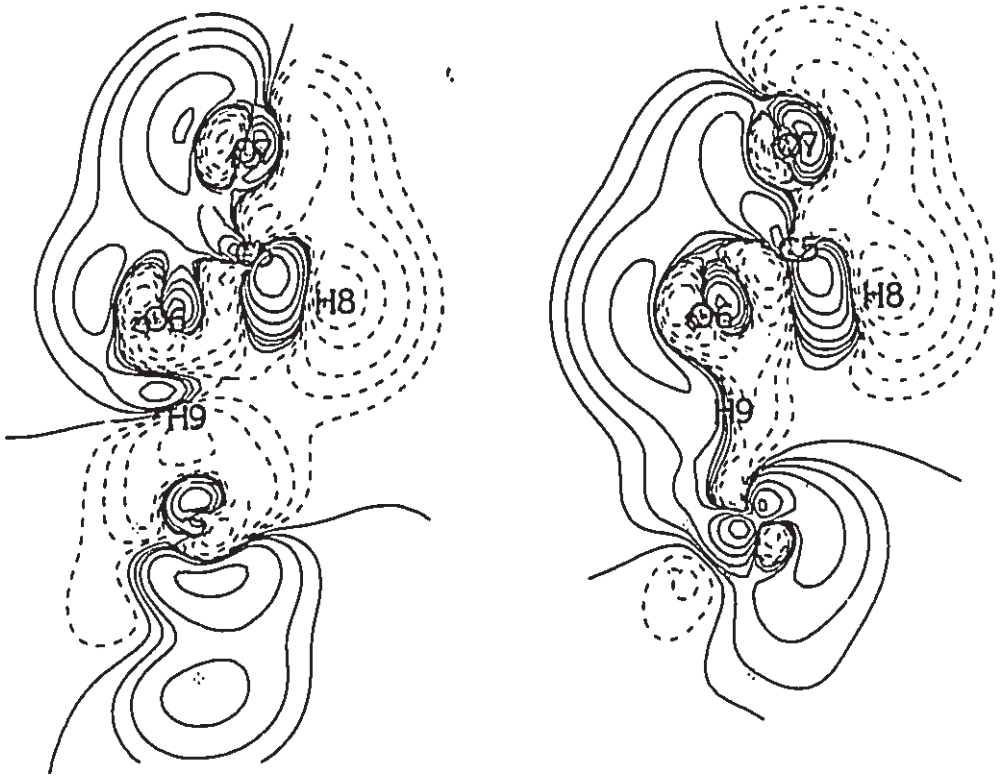

b

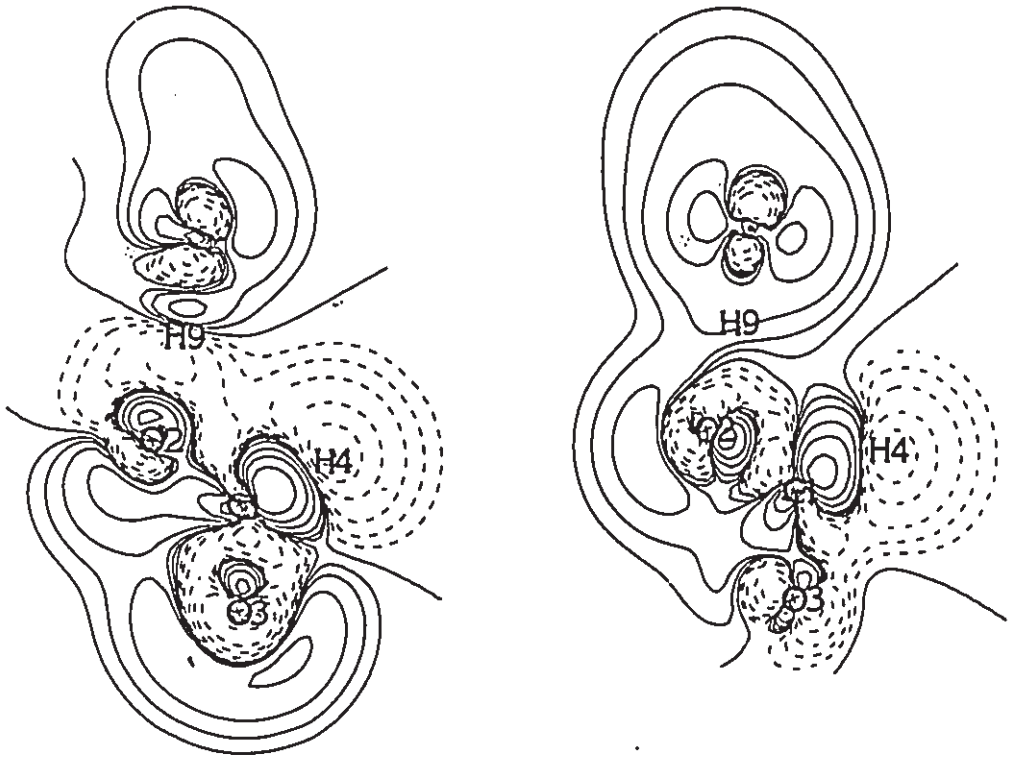

C

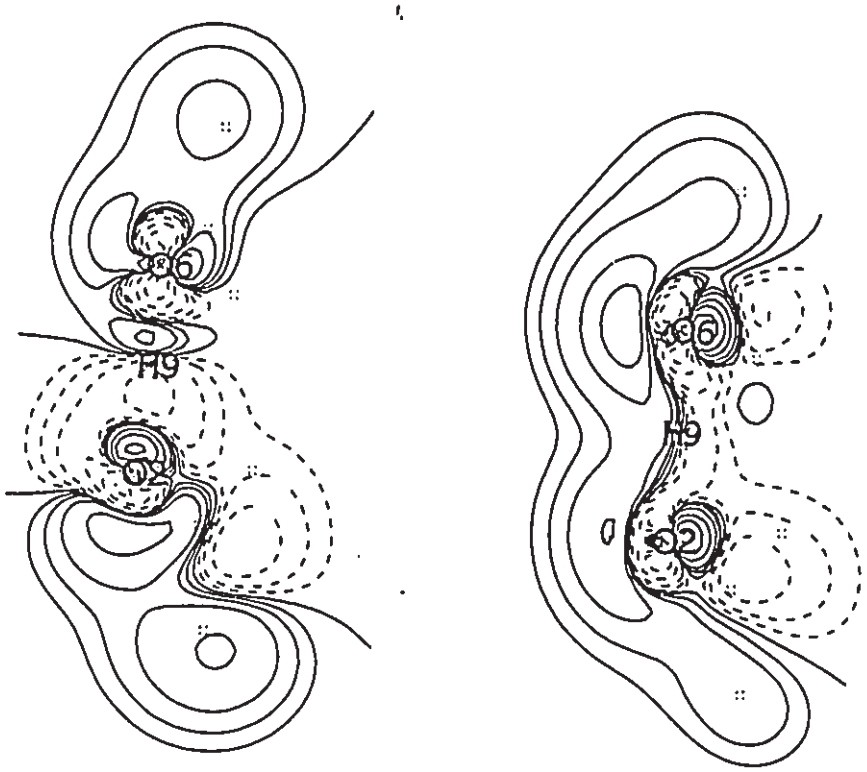

Figure 2.5.4

Contour maps of ρ (left) and $\nabla^2\rho$ (right) for the hydrogen-bonded plane O5H8O3 in $(LiOH)_2 \cdot H_2O$.

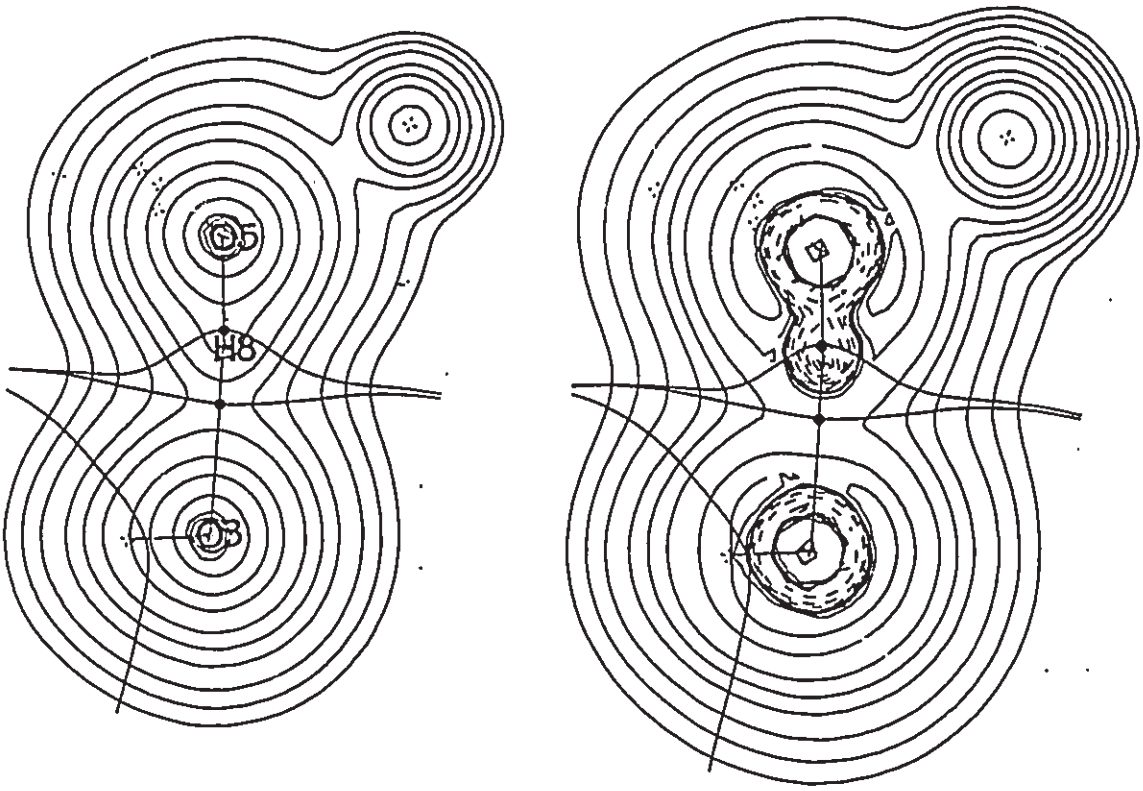
C5
H8
C3

Figure 2.5.5

Double difference density contour maps for the hydrogen-bonded plane O5H8O3 in $(LiOH)_2 \cdot H_2O$. The left diagram is for the Scheme A minus field free case and the right diagram is for the Scheme B minus field free case. Solid contours correspond to regions of charge buildup (Scheme A (or B) minus field free case at a given point is positive) and dashed contours correspond to regions of charge removal.

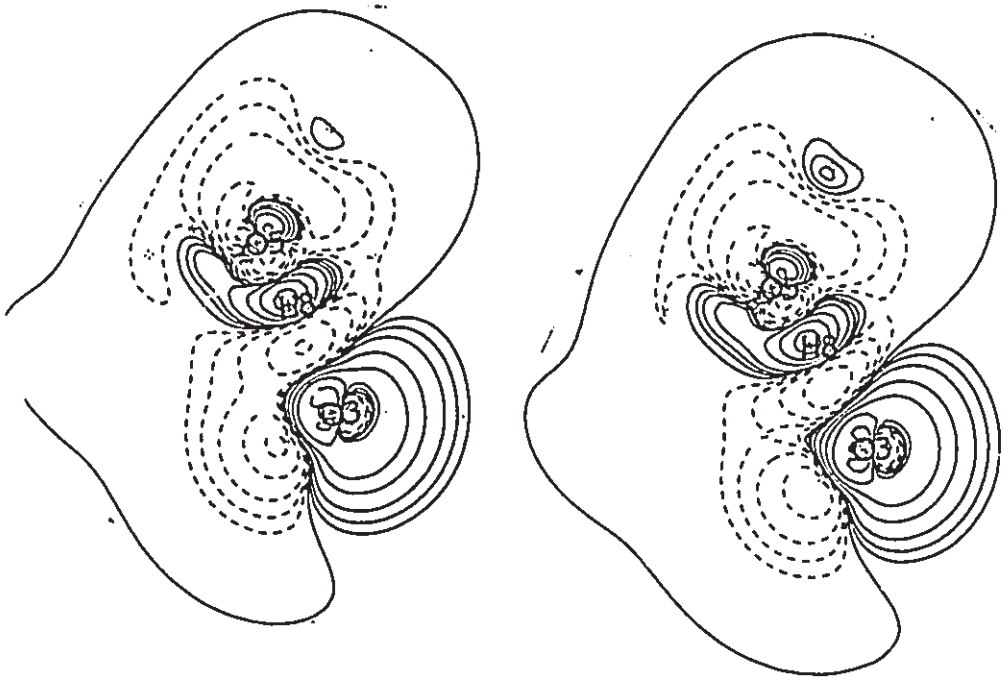
H8
C3
H8
C3

Figure 2.5.6

Contour maps of ρ (left) and $\nabla^2\rho$ (right) for the system [Li(HCOO)]·H_2O with two nearest neighbour water molecules.

a) Maps for the H-bonded plane O1H2O5

b) Maps for the O6C4O5 plane.

a

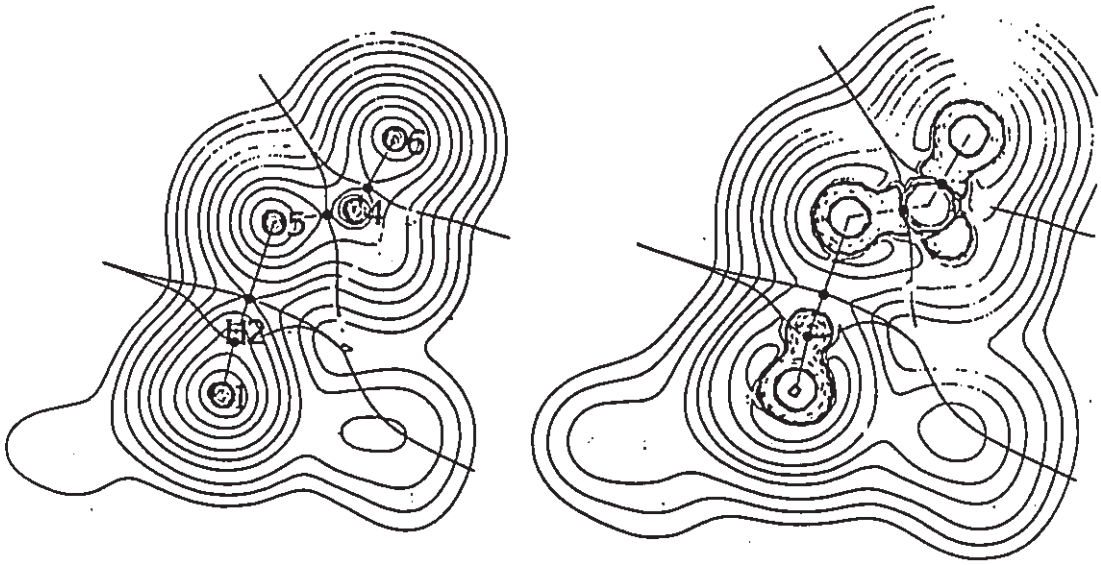

b

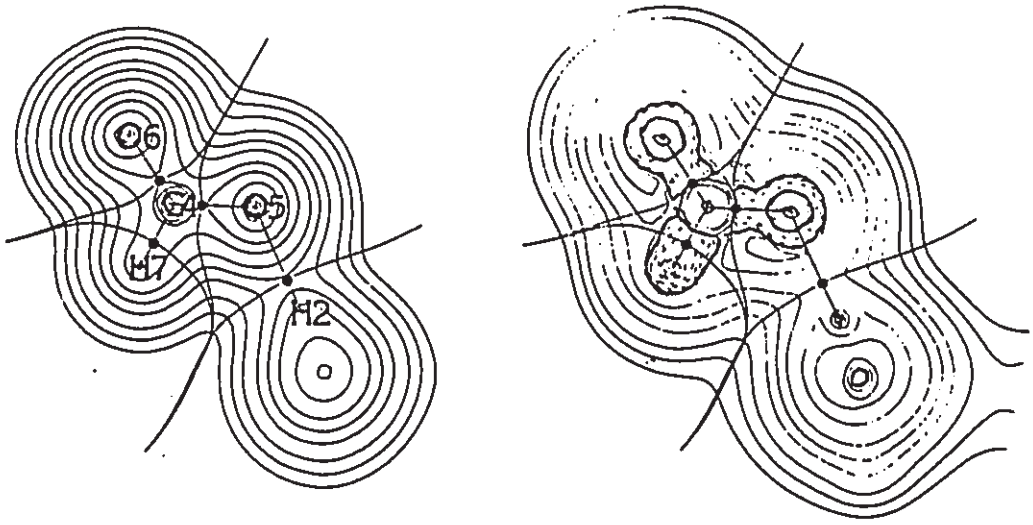

Figure 2.5.7

Double difference density contour maps for the system [Li(HCOO)]·H_2O with two nearest neighbour water molecules. The top diagrams are for the Scheme A minus field free case and the bottom diagrams are for the Scheme B minus field free case. Solid contours correspond to regions of charge buildup (Scheme A (or B) minus field free case at a given point is positive) and dashed contours correspond to regions of charge removal.

a) Maps for the H-bonded plane O1H2O5

b) Maps for the H-bonded plane O1H1O8

c) Maps for the plane O6C4O5


a
O5
H2
O1
O5
H2
O1

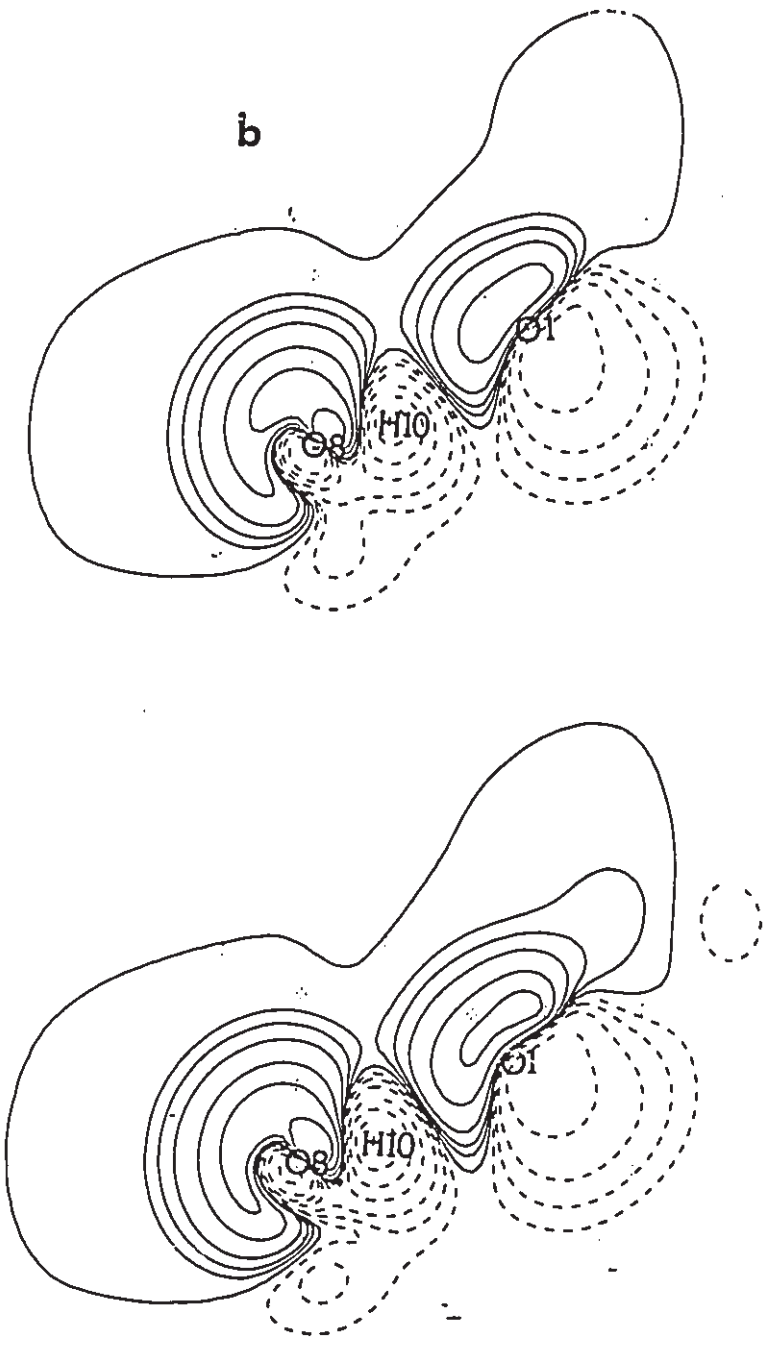
b
O1
O8
H10
O1
O8
H10

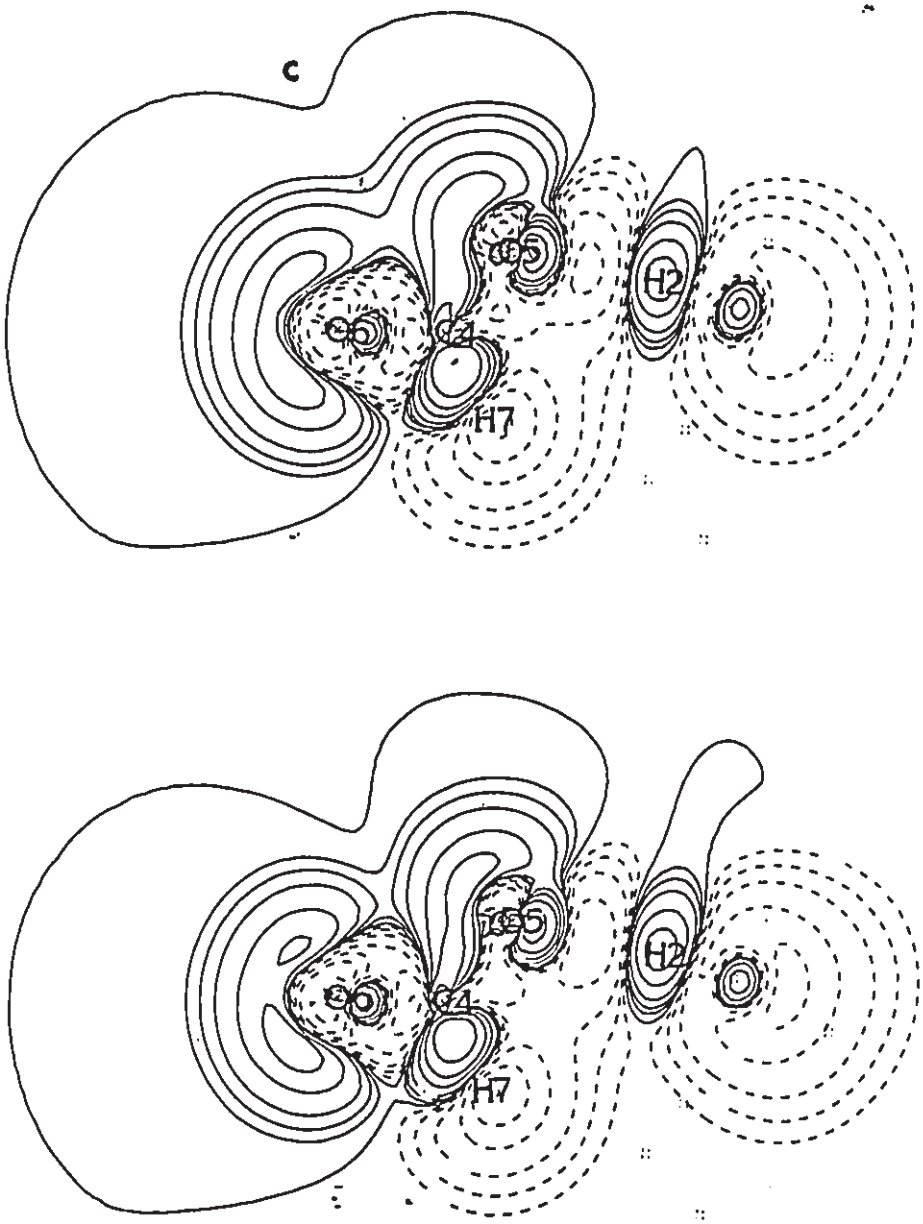
C
C5
H2
C6
C4
H7
C5
H2
C6
C4
H7

Table 2.5.1. Experimental Geometries of the OH-O Complexes 1, 2 and 3 in the Crystalline State and Partially Optimized DZP Geometries of 4 and 5.[a]

Complex	Parameter	Expt'l geometry
1		
$[H(HCOO)_2]^-$	O2O6	4.6045 (-0.0928)
in $KH(HCOO)_2$	O2H9	2.3990 (-0.3804)
	O6H9	2.2055 (0.2853)
	C1O2	2.4083 (0.0271)
	C1O3	2.3340 (0.0318)
	C1H4	2.0736 (-0.0242)
	C5O6	2.4111 (-0.0317)
	C5O7	2.3162 (0.0478)
	C5H8	2.0742 (0.0065)
	O2H9O6	179.32 (2.98)
	C1O2H9	119.47 (4.21)
	O2C1O3	124.33 (-4.70)
	O2C1H4	116.51 (2.36)
	O3C1H4	119.16 (2.34)
	C5O6H9	112.33 (1.12)
	O6C5O7	124.36 (-1.08)
	O6C5H8	115.60 (1.88)
	O7C5H8	120.04 (0.80)
2		
$[Li(OH)]_2 \cdot H_2O$	O3O5	5.0707 (0.3533,0.3552)
	O3H8	3.1820 (0.4319,0.4320)
	O5H8	1.8936 (-0.0797,-0.0766) [0.1113,0.1102]
	O3H6	1.7972 (0.0030,0.0051)
	Li1O5	3.7452
	O3H8O5	174.79 (0.64,0.05)
	H6O3H8	96.39 (-10.03,-11.53)
	H8O5H9	104.28 (-0.38,1.31)
	Li1O5H8	103.55
3		
$[Li(HCOO)] \cdot H_2O$ plus $2H_2O$	O5O1	5.1290 (0.0295)
	O5H2	3.2924 (0.0225)
	O1H2	1.8439 (0.0066)
	C4O5	2.3487 (-0.0107)
	C4O6	2.3561 (0.0352)
	C4H7	2.0536 (-0.0516)
	H7O8	5.8046
	O8H9	1.8439
	O8H10	1.8228
	O1O8	5.4731
	O1H10	3.6834
	O12H3	3.6834
	O1Li11	3.7406
	O1H3	1.8228 (0.0434)
	O1O12	5.4731
	O12H13	1.8439

Table 2.5.1 (con'd)

Complex	Parameter	Expt'l geometry
3 (con'd)	O12H14	1.8228
	O5H2O1	173.63 (0.17)
	H2O5C4	116.60 (-2.21)
	O5C4O6	125.53 (-4.02)
	O5C4H7	117.16 (2.44)
	O6C4H7	117.30 (1.58)
	C4H7O8	117.11
	H7O8H9	140.00
	H7O8H10	69.23
	H9O8H10	107.84
	O1H10O8	166.64
	H2O1H10	94.06
	Li11O1H10	112.26
	Li11O1H3	111.77
	H2O1H3	107.84 (0.83)
	O12H3O1	166.64
	H3O12H13	94.06
	H3O12H14	113.15
	H13O12H14	107.84
		partial opt'n
4	O3O5	4.7174
[HOH-OH]-	O3H8	2.7501
	O5H8	1.9733
	O3H6	1.7942
	O5H9	1.7823
	H8O5H9	104.66
	O5H8O3	174.15
	H6O3H8	106.42
5	O1O5	5.0995
[HOH-OCOH]-	O1H2	1.8373
	O1H3	1.7794
	H2O5	3.2699
	C4O5	2.3594
	C4O6	2.3209
	C4H7	2.1052
	H2O1H3	107.01
	H2O5C4	118.81
	O5C4O6	129.55
	O5C4H7	114.72
	O6C4H7	115.72
	O1H2O5	173.46

[a] Internuclear separations are in au and bond angles are in degrees. In structure **1** the values in parantheses are the experimental minus the DZP fully optimized geometries (Table 2.4.1) while in structure **2** they are the experimental minus the partially and fully

Table 2.5.1. (con'd)
optimized DZP geometries of 4 respectively (where the partially optimized structure of 4 is explicitly given further on in this table and the results for the fully optimized structure of 4 are given in Table 2.4.1). The square bracketed values refer to the now nonequivalent nonparticipating OH bond in the acid. In structure 3 the values in parentheses are the experimental minus the partially optimized DZP geometry of 5.

Table 2.5.2. Crystal Field Effects on the Charge Distributions of OH-O Complexes: a Bond Critical Point Analysis.[a]

Bond αβ sys1	Scheme	$\rho(r_c)$	$\nabla^2\rho(r_c)$	r_α	r_β
O2-H9	free	0.1396 (.0605)	-0.2616 (-.4136)	1.8477 (-.1518)	0.5517 (-.2289)
	A	0.1367 (-.0029)	-0.2370 (.0246)	1.8471 (-.0006)	0.5522 (.0005)
	B	0.1408 (.0010)	-0.2648 (-.0032)	1.8464 (-.0013)	0.5528 (.0011)
	C	0.1397 (.0001)	-0.2579 (.0037)	1.8468 (-.0011)	0.5527 (.0010)
	D	0.1369 (-.0027)	-0.2431 (.0185)	1.8486 (.0009)	0.5515 (-.0002)
O6-H9	free	0.1864 (-.1044)	-0.6582 (1.0645)	1.7728 (.1781)	0.4331 (.1075)
	A	0.1871 (.0007)	-0.6810 (-.0228)	1.7752 (.0024)	0.4306 (-.0025)
	B	0.1867 (.0003)	-0.6512 (.0070)	1.7711 (-.0017)	0.4346 (.0015)
	C	0.1869 (.0005)	-0.6584 (-.0002)	1.7720 (-.0008)	0.4337 (.0006)
	D	0.1864 (.0000)	-0.6741 (-.0159)	1.7757 (.0029)	0.4302 (-.0029)
C1-O2	free	0.3562 (-.0109)	-0.2620 (-.0441)	0.7805 (.0070)	1.6179 (.0202)
	A	0.3579 (.0017)	-0.2936 (-.0316)	0.7910 (.0005)	1.6172 (-.0007)
	B	0.3512 (-.0050)	-0.1518 (.1102)	0.7864 (-.0041)	1.6219 (.0040)
	C	0.3522 (-.0040)	-0.1720 (.0900)	0.7870 (-.0035)	1.6213 (.0034)
	D	0.3559 (-.0003)	-0.2769 (-.0149)	0.7909 (.0004)	1.6199 (.0020)
C1-O3	free	0.3923 (-.0105)	-0.1637 (-.1758)	0.7718 (.0120)	1.5622 (.0197)
	A	0.3873 (-.0050)	-0.0809 (.0828)	0.7680 (-.0038)	1.5660 (.0038)
	B	0.3939 (.0016)	-0.2009 (-.0372)	0.7728 (.0010)	1.5613 (-.0009)
	C	0.3928 (.0005)	-0.1828 (-.0191)	0.7719 (.0001)	1.5622 (.0000)
	D	0.3882 (-.0041)	-0.0977 (.0660)	0.7686 (-.0032)	1.5655 (.0033)
C1-H4	free	0.2958 (.0101)	-1.2139 (-.0893)	1.2835 (.0038)	0.7901 (-.0281)
	A	0.3026 (.0068)	-1.3027 (-.0888)	1.3327 (.0492)	0.7409 (-.0492)
	B	0.2991 (.0033)	-1.2557 (-.0418)	1.3089 (.0254)	0.7651 (-.0250)
	C	0.3004 (.0046)	-1.2735 (-.0596)	1.3188 (.0353)	0.7551 (-.0350)
	D	0.3018 (.0060)	-1.3013 (-.0874)	1.3416 (.0581)	0.7359 (-.0542)
C5-O6	free	0.3535 (.0140)	-0.2240 (.0119)	0.7895 (-.0079)	1.6219 (-.0239)
	A	0.3501 (-.0034)	-0.1400 (.0840)	0.7862 (-.0033)	1.6250 (.0031)
	B	0.3416 (-.0119)	0.0413 (.2653)	0.7818 (-.0077)	1.6295 (.0076)
	C	0.3422 (-.0113)	0.0291 (.2531)	0.7819 (-.0076)	1.6293 (.0074)
	D	0.3539 (.0004)	-0.2278 (-.0038)	0.7891 (-.0004)	1.6222 (.0003)
C5-O7	free	0.3994 (-.0191)	-0.0949 (-.2393)	0.7662 (.0156)	1.5501 (.0321)
	A	0.3970 (-.0024)	-0.0609 (.0340)	0.7652 (-.0010)	1.5513 (.0012)
	B	0.4033 (.0039)	-0.1506 (-.0557)	0.7690 (.0028)	1.5477 (-.0024)
	C	0.4023 (.0029)	-0.1400 (-.0451)	0.7684 (.0022)	1.5484 (-.0017)
	D	0.3950 (-.0044)	-0.0226 (.0723)	0.7636 (-.0026)	1.5526 (.0027)
C5-H8	free	0.2969 (-.0044)	-1.2269 (.0411)	1.2931 (-.0089)	0.7811 (.0155)
	A	0.3019 (.0050)	-1.3010 (-.0741)	1.3384 (.0453)	0.7360 (-.0451)
	B	0.2991 (.0022)	-1.2680 (-.0411)	1.3278 (.0347)	0.7470 (-.0341)
	C	0.3006 (.0037)	-1.2915 (-.0646)	1.3398 (.0467)	0.7349 (-.0462)
	D	0.3022 (.0053)	-1.2988 (-.0719)	1.3338 (.0407)	0.7405 (-.0406)

Table 2.5.2 (con'd)

Bond αβ	Scheme	$\rho(r_\alpha)$	$\nabla^2\rho(r_\alpha)$	r_α	r_β
sys2					
O3-H8	free	0.0512 (.0023) {-.0337}	0.1059 (-.0258) {-.0147}	2.2407 (.0146) {.2447}	0.9415 (-.0146) {.1869}
	A	0.0474 (-.0038)	0.1324 (.0265)	2.2286 (-.0121)	0.9534 (.0119)
	B	0.0482 (-.0030)	0.1318 (.0259)	2.2293 (-.0114)	0.9527 (.0112)
O5-H8	free	0.2888 (-.0153) {.0254} [-.0440] {-.0962}	-1.9115 (-.0007) {-.4953} [-.2491] {.1087}	1.5885 (.0143) {-.0479} [.1072] {.1784}	0.3050 (-.0144) {-.0319} [-.1072] {-.0672}
	A	0.2890 (.0102)	-1.8958 (.0157)	1.5764 (-.0121)	0.3171 (.0121)
	B	0.2895 (.0107)	-1.8821 (.0294)	1.5752 (-.0133)	0.3184 (.0134)
O3-H6	free	0.3741 (.0005) {-.0010}	-1.8388 (-.0308) {-.0013}	1.4062 (.0055) {.0043}	0.3910 (-.0055) {-.0013}
	A	0.3688 (-.0053)	-2.0838 (-.2452)	1.4503 (.0441)	0.3470 (-.0440)
	B	0.3656 (-.0085)	-2.1039 (-.2653)	1.4557 (.0495)	0.3416 (-.0494)
Li1-O5	free	0.0256	0.2067	1.3900	2.3554
	A	0.0248 (-.0008)	0.2041 (-.0026)	1.3949 (.0049)	2.3505 (-.0049)
	B	0.0247 (-.0009)	0.2037 (-.0030)	1.3959 (.0059)	2.3496 (-.0058)
sys3					
O5-H2	free	0.0401 (.0014) {.0007}	0.1181 (-.0158) {-.0208}	2.2830 (.0260) {.0414}	1.0106 (-.0256) {-.0188}
	A	0.0373 (-.0028)	0.1377 (.0196)	2.2518 (-.0312)	1.0418 (.0312)
	B	0.0382 (-.0019)	0.1370 (.0189)	2.2541 (-.0289)	1.0393 (.0287)
O1-H2	free	0.3212 (-.0146) {-.0180}	-2.2738 (-.1451) {-.1048}	1.5435 (.0216) {.0266}	0.3004 (-.0218) {-.0202}
	A	0.3365 (.0153)	-2.1084 (.1654)	1.5188 (-.0247)	0.3252 (.0248)
	B	0.3368 (.0156)	-2.1014 (.1724)	1.5183 (-.0252)	0.3257 (.0253)
C4-O5	free	0.3778 (-.0028) {.0012}	-0.0628 (.0534) {.1089}	0.7712 (-.0015) {-.0059}	1.5778 (.0017) {-.0047}
	A	0.3804 (.0026)	-0.1146 (-.0518)	0.7721 (.0009)	1.5767 (-.0009)
	B	0.3793 (.0015)	-0.0987 (-.0359)	0.7718 (.0006)	1.5769 (-.0007)
C4-O6	free	0.3843 (.0025) {-.0100}	-0.2583 (-.0506) {-.2107}	0.7796 (.0022) {.0147}	1.5765 (-.0022) {.0205}
	A	0.3735 (-.0108)	-0.0495 (.2088)	0.7720 (-.0076)	1.5841 (.0076)
	B	0.3760 (-.0083)	-0.1004 (.1579)	0.7737 (-.0059)	1.5824 (.0059)
C4-H7	free	0.2982 (-.0001) {.0163}	-1.2216 (.0011) {-.1270}	1.2351 (-.0008) {-.0426}	0.8186 (.0008) {-.0088}
	A	0.3074 (.0092)	-1.3276 (-.1060)	1.2988 (.0637)	0.7548 (-.0638)
	B	0.3055 (.0073)	-1.3026 (-.0810)	1.2850 (.0499)	0.7686 (-.0500)
O8-H7	free	0.0029	0.0106	3.2459	2.5590
	A	0.0027 (-.0002)	0.0106 (.0000)	3.3003 (.0544)	2.5063 (-.0527)
	B	0.0028 (-.0001)	0.0109 (.0003)	3.2963 (.0504)	2.5111 (-.0479)
O1Li1	free	0.0251	0.2075	2.3498	1.3911
	A	0.0234 (-.0017)	0.2022 (-.0053)	2.3396 (-.0102)	1.4012 (.0101)
	B	0.0229 (-.0022)	0.2001 (-.0074)	2.3356 (-.0142)	1.4052 (.0141)

Table 2.5.2 (con'd)

Bond αβ	Scheme	$\rho(r_c)$	$\nabla^2\rho(r_c)$	r_α	r_β
O1-H3	free	0.3520 (-.0121) {-.0344}	-2.1378 (-.2182) {-.0295}	1.4891 (.0428) {.0710}	0.3337 (-.0429) {-.0278}
	A	0.3528 (.0008)	-2.1445 (-.0067)	1.4891 (.0000)	0.3338 (.0001)
	B	0.3544 (.0024)	-2.1279 (.0099)	1.4862 (-.0029)	0.3367 (.0030)
O1-H10	free	0.0229	0.0887	2.4236	1.2606
	A	0.0229 (.0000)	0.0857 (-.0030)	2.4469 (.0233)	1.2375 (-.0231)
	B	0.0231 (.0002)	0.0842 (-.0045)	2.4567 (.0331)	1.2278 (-.0328)
O8-H10	free	0.3605	-2.0681	1.4736	0.3495
	A	0.3531 (-.0074)	-2.1586 (-.0925)	1.4803 (.0167)	0.3326 (-.0169)
	B	0.3499 (-.0106)	-2.1964 (-.1303)	1.4963 (.0227)	0.3268 (-.0228)
O8-H9	free	0.3542	-1.8768	1.4659	0.3782
	A	0.3443 (-.0099)	-2.0226 (-.1458)	1.4997 (.0338)	0.3444 (-.0338)
	B	0.3409 (-.0133)	-2.1035 (-.2267)	1.5111 (.0452)	0.3329 (-.0453)
O12-H3	free	0.0227	0.0863	2.4436	1.2420
	A	0.0228 (.0001)	0.0862 (-.0001)	2.4454 (.0018)	1.2394 (-.0026)
	B	0.0232 (.0005)	0.0864 (.0001)	2.4452 (.0016)	1.2392 (-.0028)
O12H13	free	0.3523	-1.9238	1.4768	0.3673
	A	0.3431 (-.0092)	-2.0569 (-.1331)	1.5044 (.0276)	0.3396 (-.0277)
	B	0.3392 (-.0131)	-2.1296 (-.2058)	1.5149 (.0381)	0.3290 (-.0383)
O12H14	free	0.3614	-2.0244	1.4655	0.3575
	A	0.3549 (-.0065)	-2.1204 (-.0960)	1.4832 (.0177)	0.3397 (-.0178)
	B	0.3509 (-.0105)	-2.1965 (-.1721)	1.4938 (.0283)	0.3291 (-.0284)
ring	free	0.0020	0.0099		
	A	0.0018 (-.0002)	0.0096 (-.0003)		
	B	0.0019 (-.0001)	0.0098 (-.0001)		

[a] All values are in au. Where possible, for each system, results for the BH bond are listed first, followed by those for the AH bond, the BX bond, the remaining bonds in the base fragment and finally the remaining bonds in the acid fragment. Scheme "free" refers to the crystal structure calculated at the experimental crystal geometry using the DZP basis set but without any point charges included. Schemes A, B, C and D refer to the various point charge crystal field models and are described in the text. In structure 1 the differences are listed as follows: the values in parentheses besides each "free" value are the "free" minus the fully optimized DZP results (Table 2.4.3). The values in parentheses besides each Scheme A,B,C and D value are those respective values minus the "free" value (that is DZP//experimental geometry). In structure 2 the differences are listed as follows: the values in parentheses besides each "free" value are the "free" value minus the "naked" (at expt'l geometry) results while the curly bracketed values under each of these are the corresponding "free" value minus the "naked" (at partially optimized geometry) results. The values in square brackets refer to the now nonequivalent nonparticipating hydrogen of the acid. The values in parentheses besides each scheme A and B are those respective values minus the "free" value. The differences are listed in the same way for structure 3 as for structure 2 except there are no square bracketed values for 3.

Table 2.5.3. Crystal Field Effects on the Charge Distributions of OH-O Complexes: Atomic Properties and Their Changes.[a]

Atom sys1	Scheme	N(Ω)	K(Ω)	|μ(Ω)|
O6	free	9.443 (.006)	75.68573 (-38.14)	0.423 (.016)
	A	9.467 (.024)	75.69330 (4.75)	0.392 (-.031)
	B	9.526 (.083)	75.73765 (32.58)	0.302 (-.121)
	C	9.521 (.078)	75.73214 (29.12)	0.309 (-.114)
	D	9.438 (-.005)	75.67328 (-7.81)	0.429 (.006)
H9	free	0.270 (.016)	0.24817 (-2.81)	0.018 (-.044)
	A	0.264 (-.006)	0.24465 (-2.21)	0.019 (.001)
	B	0.274 (.004)	0.25080 (1.65)	0.019 (.001)
	C	0.272 (.002)	0.24947 (.82)	0.019 (.001)
	D	0.263 (-.007)	0.24379 (-2.75)	0.018 (.000)
O2	free	9.441 (-.030)	75.64348 (3.76)	0.432 (-.022)
	A	9.438 (-.003)	75.63222 (-7.05)	0.453 (.021)
	B	9.482 (.041)	75.66672 (14.60)	0.387 (-.045)
	C	9.478 (.037)	75.66336 (12.49)	0.397 (-.035)
	D	9.447 (.006)	75.63227 (-7.02)	0.441 (.009)
C1	free	3.950 (.072)	36.38950 (26.96)	0.748 (.047)
	A	3.977 (.027)	36.40347 (8.77)	0.840 (.092)
	B	3.972 (.022)	36.40340 (8.72)	0.796 (.048)
	C	3.980 (.030)	36.40918 (12.35)	0.816 (.068)
	D	3.990 (.040)	36.41014 (12.95)	0.854 (.106)
O3	free	9.419 (-.038)	75.56048 (-46.87)	0.587 (.001)
	A	9.510 (.091)	75.59976 (24.65)	0.499 (-.088)
	B	9.407 (-.012)	75.55016 (-6.48)	0.600 (.013)
	C	9.428 (.009)	75.56112 (.40)	0.583 (-.004)
	D	9.500 (.081)	75.59629 (22.47)	0.513 (-.074)
H4	free	1.064 (-.054)	0.66058 (-11.65)	0.111 (-.009)
	A	0.961 (-.103)	0.61582 (-28.09)	0.109 (-.002)
	B	1.011 (-.053)	0.63699 (-14.80)	0.114 (.003)
	C	0.989 (-.075)	0.62763 (-20.68)	0.112 (.001)
	D	0.948 (-.013)	0.60835 (-32.77)	0.109 (-.002)
C5	free	3.953 (.000)	36.39858 (-9.98)	0.767 (-.027)
	A	3.992 (.039)	36.42155 (14.41)	0.854 (.087)
	B	4.030 (.077)	36.45474 (35.24)	0.837 (.070)
	C	4.034 (.081)	36.45612 (36.11)	0.860 (.093)
	D	3.978 (.025)	36.41076 (7.64)	0.848 (.081)
O7	free	9.415 (-.001)	75.58511 (-50.18)	0.606 (-.043)
	A	9.442 (.027)	75.58788 (1.74)	0.574 (-.932)
	B	9.328 (-.087)	75.53850 (-29.25)	0.698 (.092)
	C	9.354 (-.061)	75.55059 (-21.66)	0.680 (.074)
	D	9.478 (.063)	75.60604 (13.13)	0.530 (-.076)
H8	free	1.044 (.028)	0.65191 (5.98)	0.110 (.002)
	A	0.949 (-.095)	0.60868 (-27.13)	0.110 (.000)
	B	0.971 (-.073)	0.61633 (-22.33)	0.115 (.005)
	C	0.945 (-.099)	0.60530 (-29.25)	0.114 (.004)
	D	0.958 (-.086)	0.61406 (-23.75)	0.108 (-.002)

Table 2.5.3 (con'd)

Atom	Scheme	N(Ω)		K(Ω)		|μ(Ω)|	
sys2							
O5	free	9.6679	(.3484)	75.56667	(171.92)	0.037	(-.196)
			{.2979}		{115.29}		{-.154}
	A	9.6352	(-.0327)	75.51234	(-34.09)	0.299	(.262)
	B	9.6029	(-.0650)	75.51320	(-33.55)	0.109	(.072)
H8	free	0.2552	(-.0144)	0.22745	(-14.72)	0.087	(.002)
			{-.0042}		{-9.74}		{.027}
			[-.2262]		[-97.96]		[-.096]
			{-.2088}		{-104.99}		{-.103}
	A	0.2622	(.0070)	0.24145	(8.78)	0.084	(-.003)
	B	0.2657	(.0105)	0.24426	(10.55)	0.085	(-.002)
O3	free	9.3563	(-.0344)	75.08856	(-25.76)	0.193	(.103)
			{-.0259}		{-58.80}		{.090}
	A	9.5161	(.1598)	75.15230	(40.00)	0.312	(.119)
	B	9.5516	(.1953)	75.17392	(53.56)	0.213	(.020)
H6	free	0.5223	(-.0171)	0.41915	(-6.43)	0.225	(-.003)
			{-.0031}		{-2.14}		{.004}
	A	0.3707	(-.1516)	0.33339	(-53.82)	0.153	(-.072)
	B	0.3524	(-.1699)	0.32167	(-61.17)	0.143	(-.082)
Li1	free	2.0370		7.28118		0.010	
	A	2.0274	(-.0096)	7.27363	(-4.74)	0.002	(-.008)
	B	2.0266	(-.0104)	7.27267	(-5.34)	0.004	(-.006)
sys3							
O1	free	9.4754	(.1583)	75.50010	(87.61)	0.250	(.001)
			{.1492}		{57.34}		{.000}
	A	9.4071	(-.0683)	75.46884	(-19.62)	0.263	(.013)
	B	9.4016	(-.0738)	75.46673	(-20.94)	0.278	(.028)
H2	free	0.2489	(-.0373)	0.23924	(-22.31)	0.085	(-.007)
			{-.0363}		{-22.87}		{-.007}
	A	0.2910	(.0421)	0.27608	(23.12)	0.096	(.011)
	B	0.2935	(.0446)	0.27823	(24.47)	0.095	(.010)
O5	free	9.4977	(.0145)	75.62876	(-3.10)	0.445	(-.043)
			{.0141}		{8.41}		{-.042}
	A	9.4949	(-.0028)	75.62411	(-2.92)	0.481	(.036)
	B	9.4999	(.0022)	75.62975	(.62)	0.456	(.011)
C4	free	3.8806	(.0050)	36.35929	(3.87)	0.674	(-.004)
			{.0174}		{19.37}		{-.015}
	A	3.9232	(.0426)	36.37427	(9.40)	0.787	(.113)
	B	3.9139	(.0333)	36.36854	(5.80)	0.766	(.092)
O6	free	9.4203	(-.0433)	75.53109	(-16.57)	0.580	(.036)
			{-.0576}		{-55.17}		{.008}
	A	9.5470	(.1267)	75.57942	(30.33)	0.394	(-.166)
	B	9.5188	(.0985)	75.56952	(24.12)	0.431	(-.129)
H7	free	1.1397	(.0024)	0.70046	(-.44)	0.121	(.010)
			{.0035}		{10.20}		{-.003}
	A	1.0046	(-.1351)	0.64188	(-36.76)	0.109	(-.012)
	B	1.0327	(-.1070)	0.65467	(-28.73)	0.108	(-.013)

Table 2.5.3 (con'd)

Atom	Scheme	N(Ω)	K(Ω)	|μ(Ω)|
O8	free	9.2337	75.30500	0.290
	A	9.3839 (.1502)	75.36802 (39.54)	0.238 (-.052)
	B	9.4309 (.1972)	75.39270 (55.03)	0.236 (-.054)
H10	free	0.3580	0.33008	0.121
	A	0.3156 (-.0424)	0.29811 (-20.06)	0.109 (-.012)
	B	0.3017 (-.0563)	0.28749 (-26.72)	0.106 (-.015)
H9	free	0.4227	0.36064	0.164
	A	0.3213 (-.1014)	0.29719 (-39.82)	0.122 (-.042)
	B	0.2914 (-.1313)	0.27679 (-52.62)	0.111 (-.053)
H3	free	0.3159 (-.1205)	0.29780 (-46.56)	0.109 (-.063)
		{-.1113}	{-48.59}	{-.063}
	A	0.3167 (.0008)	0.29878 (0.61)	0.110 (.001)
	B	0.3258 (.0099)	0.30476 (4.37)	0.113 (.004)
O12	free	9.2150	75.30128	0.297
	A	9.3492 (.1342)	75.36035 (37.06)	0.259 (-.038)
	B	9.4034 (.1884)	75.38969 (55.47)	0.257 (-.040)
H13	free	0.3898	0.34115	0.151
	A	0.3092 (-.0806)	0.28931 (-32.53)	0.118 (-.033)
	B	0.2821 (-.1077)	0.27027 (-44.48)	0.107 (-.044)
H14	free	0.3768	0.33718	0.147
	A	0.3232 (-.0536)	0.30256 (-21.72)	0.124 (-.023)
	B	0.2948 (-.0820)	0.28284 (-34.10)	0.112 (-.035)
Li11	free	2.0295	7.27450	0.004
	A	2.0205 (-.0090)	7.26493 (-6.00)	0.007 (.003)
	B	2.0187 (-.0108)	7.26247 (-7.55)	0.008 (.004)

[a] All values are in au except the energy changes which are in kcal mol^{-1}. Where possible, the acidic atom participating in the H-bond is listed first, followed by the H-bonded hydrogen, the base atom participating in the H-bond, the next nearest base atom, the remaining base atom, and finally the remaining acid atoms. Scheme "free" refers to the crystal structure calculated at the experimental crystal geometry using the DZP basis set but without any point charges included. Schemes A, B, C and D refer to the various point charge crystal field models and are described in the text. In structure 1 the differences are listed as follows: the values in parentheses besides each "free" value are the "free" minus the fully optimized DZP results. The values in parentheses besides each Scheme A,B,C and D value are those respective values minus the "free" (that is DZP//experimental geometry) value. In structure 2 the differences are listed as follows: the values in parentheses besides each "free" value are the "free" value minus the "naked" (at expt'l geometry) results while the curly bracketed values under each of these are the corresponding "free" value minus the "naked" (at partially optimized geometry) results. The values in square brackets refer to the now nonequivalent non-participating hydrogen of the acid. The values in parentheses besides each scheme A and B are those respective values minus the "free" value. The differences are listed in the same way for structure 3 as for structure 2 except there are no square bracketed values for 3.

CHAPTER 3

PREDICTIONS OF SITES OF ELECTROPHILIC AND NUCLEOPHILIC ATTACK USING THE LAPLACIAN OF THE CHARGE DENSITY

Section 1.3 details the topology of $\nabla^2\rho$ and its properties. In this chapter we use $\nabla^2\rho$ to predict the sites of electrophilic attack in BASE-HF and other hydrogen-bonded complexes (Section 3.1) and to predict the sites of nucleophilic attack in acrolein, acrylic acid, acrylonitrile and methacrylic acid (Section 3.2).

3.1. ELECTROPHILIC ATTACK IN BASE-HF COMPLEXES

In this section, the Laplacian of the charge density, $\nabla^2\rho$, is used to predict the molecular structures (i.e. the arrangement of bonds) and geometries of the BASE-HF complexes studied in Chapter 2. The electrophilic hydrogen H_a of the acid HF will seek the most electron-rich region in the base. In general, the topology of the $\nabla^2\rho$ field yields unambiguously and quantitatively the location of this region. It is shown that the use of the Laplacian in this manner is superior to the Legon-Millen (LM) rules (Legon and Millen 1987) for predicting the angle of attachment in hydrogen-bond formation. For example, the Laplacian predicts the linear structure SCO-HF in agreement with ab initio and experimental results while the LM rules, which are based on the hybridization model, predict a bent structure with a CO-H angle of 120°. Further, the LM rules cannot distinguish between nonbonded pairs and could not be used to determine the site of electrophilic attack in, say, NNO or OSO. An analysis of the Laplacian, however, predicts electrophilic attack at O in agreement with experiment. In general, the $\nabla^2\rho$ method is also superior to the Brobjer-Murrell (BM) (1982) distributed point charge model which, for example, predicts ONN-HF to be more stable than the primary experimental structure NNO-HF. A quantitative parameterized electrostatic model using point multipoles embedded in hard van der Waals spheres devised by Buckingham and Fowler (BF) (1985) has met with much success. The $\nabla^2\rho$ method of predicting approach angles has the

advantage of being parameter-free as it is determined solely by the system's charge distribution. In addition, an analysis of $\nabla^2\rho$ predicts not only the sites of electrophilic attack but nucleophilic attack as well.

Predictions based on the Laplacian must be tested directly against the ab initio results (Table 2.1.1 and Table 3.1.1) as it is the theoretical charge densities that are analyzed in this work. The values of the bonded and nonbonded maxima of $-\nabla^2\rho$ are listed in Table 3.1.1. In H_2CO, for example, the nonbonded O maxima have a value of 7.10 au while the bonded maxima adjacent to O and C respectively in the C-O bond have values of only 3.12 and 1.57 au. In only two bases, H_2S and HCP, is a bonded maximum larger than all of the nonbonded maxima and in HCP this bonded maximum found on carbon serves as the site of electrophilic attack in hydrogen bond formation.

The maxima in the VSCC of an atom increase in magnitude (Table 3.1.1) and decrease in distance from the nucleus on traversing a row of the periodic table from left to right. The average distances for C, N, O and F are 0.50, 0.42, 0.36 and 0.30 A and 0.76, 0.68 and 0.62 A respectively for P, S, and Cl.

Use of the Laplacian for Structure and Geometry Predictions

According to the properties of $\nabla^2\rho$, the BASE-HF hydrogen-bonded complexes will form as a result of a region of charge concentration in the base interacting with a region of charge depletion in HF. There is a (3,+3) critical point, a local minimum in $-\nabla^2\rho$, located 0.38 A from the proton in HF with a magnitude of 0.21 au collinear with the HF bond

axis. This region of charge depletion in the valence shell of H_a will be directed at a maximum in the VSCC of B. It must be decided which maxima in the VSCC of B will be the most readily attacked thereby yielding the most stable structure. The nonbonded maximum of largest magnitude (the most electron-rich region) in the base is predicted to be the site of electrophilic attack and the approach of H_a will be such as to align the (3,+3) minimum in the valence shell of H_a with the chosen (3,-3) maximum of the base.

In Table 3.1.1 we list the angle MBX formed by the line drawn from the chosen nonbonded maximum M to the nucleus of the base atom B on which it resides and the line drawn from the B nucleus to the neighbouring base nucleus X. This MBX angle is compared with the corresponding calculated equilibrium angle H_a-BX. The changes in magnitude and position of M upon formation of the complex are found to be small. The value of $-\nabla^2\rho(r_c)$, distance from M to the B nucleus and MBX angle never change by more than 0.4 au, 0.01 A and 2° respectively.

The first set of molecules in Table 3.1.1 all possess maxima which mimic in number and kind the nonbonded pairs of the Lewis model. For the HF dimer, the MBX angle is 6.7° smaller than the ab initio results. In the complexes of H_2O, H_2CO and NNO with HF the predicted angles differ from the ab initio results by only 2.7, 0.9 and 1.3° respectively. The complexes H_3N-HF and H_3P-HF are predicted to have C_{3v} symmetry while NN-HF and HCN-HF are predicted to be linear in agreement with both ab initio and experimental results. The N-HF and P-HF angles are 180° in the C_{3v} species. The difference between the

values of MBX and H_a-BX for H_2S-HF is 10.2°, the largest difference in this first set. Using larger basis sets (6-311G**,6-311++G**) gives a difference of 8.9° and 7.3°, respectively. As long as polarization functions are present, the qualitative features of the $\nabla^2\rho$ field are independent of basis set and, as observed here, there are only minor quantitative differences.

The second set of molecules in Table 3.1.1 contains OCO and SCO. Laplacian relief plots for the molecular planes of NNO, SCO and OCO are displayed in Figure 3.1.1. In NNO, H_a will attack nonbonded maxima in the VSCC of O rather than the smaller nonbonded maximum in the VSCC of the terminal N. The Laplacian prediction of a bent NNO-HF structure is in excellent agreement with ab initio results (Table 3.1.1). The LM rules also predict a bent structure though the prediction is only qualitative. Contrary to the Lewis model, the oxygen in SCO exhibits only a single nonbonded maxima (collinear with the molecular axis). This maxima is the largest in magnitude, and so, the $\nabla^2\rho$ method predicts a linear SCO-HF complex in agreement with ab initio and experimental results. The LM rules, based on the Lewis model, predict a bent structure. In OCO, the nonbonded charge concentration forms a torus about the molecular axis. The value of $-\nabla^2\rho(r_c)$ for the torus is 4.74 au and the MBX angle is 149.3°. In addition, there is a saddle point at the centre of the torus (collinear with the molecule) whose value of $-\nabla^2\rho(r_c)$ is 4.72 au. Since the difference in the magnitude of the Laplacian between these critical points is extremely small (and, hence, since the rate of change of the curvatures of the Hessian matrix of $-\nabla^2\rho$ is extremely gradual), the

incoming H_a can equally attack any part of the region of oxygen nonbonded charge concentration forming an H_a-BX angle between 149.3° and 180°. The effects of this broad region of charge concentration are seen in Table 2.1.1 where the secondary structure ($\angle H_a$-BX = 164.8°) is to within 0.1 of a kJ mol^{-1} as stable as the linear structure. The predicted MBX angles nearly fall within the error limits of the experimental H_a-BX angle (180 ± 30°).

The third set of molecules in Table 3.1.1 contains SO_2 and O_3. We predict electrophilic attack at the oxygen nonbonded maxima in SO_2 since they are largest in magnitude and this is in agreement with both ab initio and experimental results. However, the difference in magnitude between these nonbonded maxima is very small (the cis nonbonded maximum is greater than the trans by only 0.15 au) making it difficult to predict whether H_a will attack the cis or trans nonbonded maximum. Thus, both MBX angles are listed and they are both underestimations of the 6-31G** angles. The value of 145° for the experimental angle has been explained as a result of the tunnelling of the HF subunit between the two nonequivalent lone-pair sites on O (Fillery-Travis and Legon 1986). Such a motion is controlled by an asymmetric, double-minimum potential energy function. If the cis conformer is lower in energy than the trans conformer, the observed angle would be closer to the cis than the trans angle and the cis lone-pair would be more basic than the trans lone-pair.

The nonbonded maximum on the central oxygen in ozone is largest in magnitude yet the primary ab initio structure has H_a attacking a terminal O nonbonded maximum (7 of Figure 2.1.1). The difference in

magnitude of $-\nabla^2\rho(r_c)$ is slightly more than 1 au. Note that OCO-HF is one of the weaker complexes studied and, next to SCO-HF, it has the longest O-H hydrogen bond length (Table 2.1.1). Therefore, long-range electrostatic effects could play an important role in determining the primary structure if significant atomic charges are present. The terminal oxygens in ozone have relatively large negative charges (q(O) = -0.11 au; Table 2.1.2) and this could account for the fact that the positively charged H_a (q(H) = +0.76 au) will attack a terminal oxygen rather than the central oxygen which has a positive charge of +0.22 au.

The fourth set of molecules in Table 3.1.1 contains SC and CO. The magnitude of the C nonbonded maximum is the largest in SC, and so, the structure SC-HF is predicted in agreement with ab initio results. However, it is the O nonbonded maximum which is largest in magnitude in CO, and so, relying solely on the $\nabla^2\rho$ magnitude argument, we would predict the structure CO-HF. This structure is less stable than OC-HF by 0.7 kcal mol^{-1}. It should be noted that in CO the concentration on O is large in magnitude and tightly bound, while that on C is of smaller magnitude and more spread out both radially and laterally (Figure 3.1.2). HOMO (5σ) is strongly localized in the nonbonded region of C, and so, the nonbonded charge concentration on C is the least tightly bound and most diffuse of the charge concentrations in CO. The LUMO in HF has mostly protonic 2s character and is cylindrically distributed about the HF bond axis. It has been shown that the requirements of the frontier orbital model correspond physically to aligning regions of charge concentration (HOMO) with regions of charge depletion (LUMO) in the reacting atoms (Bader and

MacDougall 1985). The structure OC-HF can be rationalized in this way. The Buckingham-Fowler model also predicts the experimental structure OC-HF.

The remaining molecules in the fifth set in Table 3.1.1 form complexes with HF with unusual structures. For thioformaldehyde, we predict H_a to attack the nonbonded sulfur maxima and, indeed, an S-H_a bond is present in the optimized structure **14** (Figure 2.1.1). However, the MBX angle is 25.2° less than 6-31G** results. This difference can be rationalized in terms of a second hydrogen bond, which the molecular graph shows to be present, between H-C and F. The H_2CS hydrogens are indeed acidic (q(H) = +0.02), and so, hydrogen bond formation with F is possible.

The three-membered ring structure in the NNS - HF complex **13** is unexpected. A Laplacian analysis predicts a linear SNN-HF structure which is calculated to be 11.3 kJ mol^{-1} less stable than the ring structure 13. In the ring structure, H_a is aligned with a diffuse nonbonded charge concentration in S yet no H_a-S bond is formed. A bond between S and F may be predicted using electrostatic arguments but the N-F bond in the ring structure is difficult to explain.

Complexes of HF with HCl have been examined and the structure ClH-FH is more stable both theoretically (by 8 kJ mol^{-1}) and experimentally. This raises an important question. Why is HF not the base in other complexes where an acidic hydrogen is present, such as in H_2O-HF, H_3N-HF and HCN-HF? Firstly, the H in HF is the most protonic (it has the largest positive net charge; q(H) = +0.76 au) and we have seen that the most protonic H will always form the hydrogen bond.

Secondly, from the local virial theorem, a region of charge concentration corresponds with a region of excess potential energy. The value of $-\nabla^2\rho(r_c)$ is greatest for nonbonded maxima on F (11.66 au) implying that the electrons concentrated there are in the deepest possible potential energy well and that these regions will be the most difficult to polarize in a long-range interaction. An incoming acidic hydrogen must be of sufficient electrophilic strength to perturb this concentration so that the virial theorem can again be satisfied on hydrogen bond formation. Certainly the net charge on the acidic hydrogen contributes to its electrophilic strength. It is observed that the acidic hydrogens in H_2O, H_3N and HCN (of net charges q(H) = +0.62, +0.37 and +0.19 au respectively) cannot interact strongly enough with the electrons concentrated in the F nonbonded maxima to form primary structures. Rather, the strongly electrophilic H of HF will interact with nonbonded maxima on O or N where the electrons are not so tightly concentrated and more easily polarizable. It is also observed that the primary structures have a larger difference in q(Ω) between the acidic hydrogen and the base atom it attacks than in the secondary structures.

The H of HCl (q(H) = +0.23 au) is less protonic than the H in HF and the Cl nonbonded maxima ($-\nabla^2\rho(r_c)$ = 0.85 au) is much smaller than the F nonbonded maxima. The observation of a primary structure in which HCl acts as the proton donor suggests that the Cl maxima are too small to attract the H of HF. The nonbonded maxima in H_2S and H_3P are also small but the possibility of HF acting as a base in these complexes is slight since there are no acidic hydrogens in H_2S and H_3P,

i.e., q(H) is negative in these bases. The BF model also predicts the HF-HCl structure.

The final entry in Table 3.1.1 gives data for HCP. Since there is only one nonbonded maximum, we would predict the linear structure HCP-HF. Ab initio results show that this is 7.1 kJ mol^{-1} less stable than the T-shaped structure 2 where H_a is bonded to carbon. Thus, only in this case, where the magnitude of the C bonded maximum is 5.6 times that of the nonbonded maximum on P, is the attachment of H_a to the base via a bonded maximum. Further, electrostatic arguments suggest that an H_a-C bond should form as C is the only negatively charged atom in HCP (q(C) = -0.46 au).

Prediction of the Structures and Geometries of BASE-HCl Complexes

Table 3.1.2 gives the predicted structures and geometries of some BASE-HCl complexes. Since the $\nabla^2\rho$ method is based on the properties of the isolated base, the MBX angle for H_2CO, for example, is the same whether formaldehyde is the base in H_2CO-HCl or H_2CO-HF. In agreement with ab initio and experimental results (where available), the $\nabla^2\rho$ method correctly predicts the structures and geometries of the linear complexes SC-HCl, NN-HCl, HCN-HCl, OCO-HCl and SCO-HCl and also the C_{3v} complexes H_3N-HCl and H_3P-HCl. Obviously, as was the case for the complex between CO and HF, the $\nabla^2\rho$ method predicts the linear structure CO-HCl to be the primary minimum energy structure when, in fact, OC-HCl is found to be more stable both by ab initio calculations (by 1.4 kJ mol^{-1}; Scheme I) and experimentally.

For the angular complexes H_2O-HCl and H_2S-HCl, we find the difference between ∠MBX and ∠H_aBX to be 10° on average. The difference in angles for HF-HCl is the largest of the complexes studied. However, the geometry and structure of the hydrogen chloride dimer is predicted accurately by the $\nabla^2\rho$ method. What is most important is that in the vast majority of cases the $\nabla^2\rho$ method performs well in predicting the structure and geometry of BASE-HA complexes (A=F,Cl).

Predictions for Complexes Containing AH-B Bonds (A=N,O;B=N,O)

The fully optimized 6-31G** geometries of these primary minimum energy structures have been given in Tables 2.2.1 and 2.4.1. The $\nabla^2\rho$ method works best for [HOH-OH]$^-$ where the difference between ∠MBX and ∠H_aBX is only 2.4°. It does not work well for the strong cationic complexes [H_3NH-OH_2]$^+$ and [H_2OH-OH_2]$^+$. Rather than the acidic hydrogen attacking one of the two equivalent nonbonded maxima on the VSCC of O in the base H_2O, the acidic hydrogen attacks the saddle point between these nonbonded maxima. Then the three atoms in the base fragment of the complex and the hydrogen-bonded hydrogen are all in approximately the same plane. A more extensive study of cationic hydrogen-bonded complexes is necessary to determine whether [H_3NH-OH_2]$^+$ and [H_2OH-OH_2]$^+$ are anomolous in their behaviour or whether all cationic complexes (with water as the base) will have the hydrogen-bonded hydrogen sample equally the two nonbonded regions of charge concentration on the basic oxygen and hence attack the saddle point in $\nabla^2\rho$ between them.

Effect of Basis Set and Electron Correlation on Predictions

Using $\nabla^2\rho$

Table 3.1.4 gives a $\nabla^2\rho$ analysis for four bases using RHF/6-31G**//6-31G**, RHF/6-311++G**//6-31G** and MP2/6-311++G**//6-31G** (labelled Schemes I, II and III respectively). The structure prediction using the $\nabla^2\rho$ method does not change with basis set. The geometry prediction changes slightly, the agreement with experiment increasing from Schemes I to III. As previously mentioned, as long as polarization functions are included, even if we incorporate Coulomb correlation (as we do in Scheme III), the qualitative features of the $\nabla^2\rho$ method are independent of basis set and there are only minor quantitative differences.

In each of the bases, the nonbonded maxima decrease in magnitude on going from Scheme I to III. Thus the inclusion of MP2 electron correlation increases the tendency of electrons to avoid each other and, consequently, the magnitude of the nonbonded lumps decrease. The bonded lumps nearest the largest nonbonded lumps increase in magnitude in NNO, OCO and OC while the next nearest bonded lumps decrease in magnitude on going from Scheme I to III. In fact in OCO and OC, the C-O bonded lumps, which are small in magnitude in Scheme I, actually disappear in Schemes II and III as they are flattened out by these larger basis sets. The O-N and O-C bonded lumps become more concentrated as the neighbouring nonbonded and bonded lumps become less concentrated. The magnitude of the cage critical point near the proton collinear with the HF axis is changed only slightly on going from Scheme I to III.

Summary

Properties of the Laplacian of the charge density are used to predict the structures and geometries of BASE-HA complexes (A=F,Cl). These predictions are in good agreement with the ab initio and experimental results. What sets the $\nabla^2\rho$ method apart from the electrostatic models is that it uses a property of the system, its Laplacian distribution, that is determined directly in terms of the charge density. It is parameter-free, basis-set independent and applicable to other generalized Lewis acid-base reactions. The Laplacian of ρ and its critical points are easily and quickly determined requiring no more time than the calculation of ρ itself and its critical points. The HOMO/LUMO method proposed by Klemperer and co-workers, who have raised objections to the electrostatic models, predicts the most stable BASE-HF complex to be one in which maximum overlap occurs between the base HOMO and the acid LUMO (Baiocchi et al 1983, Dyke 1984). Accordingly, OCO-HF, SCO-HF and NNO-HF all should have bent structures. The fact that this is true only for the latter of these molecules leads to the conclusion that the charge distribution around the oxygen atom does not follow this simple MO picture (Janda et al 1977). The existence of charge concentrations on the other hand, as defined independently of any model by the Laplacian distribution, leads to predictions in good agreement with experiment for all three cases.

Figure 3.1.1

Laplacian relief plots in the molecular plane for NNO, SCO and OCO. The core or first quantum shell of each atom exhibits a spike-like charge concentration at the nucleus surrounded by a deep region of charge depletion.

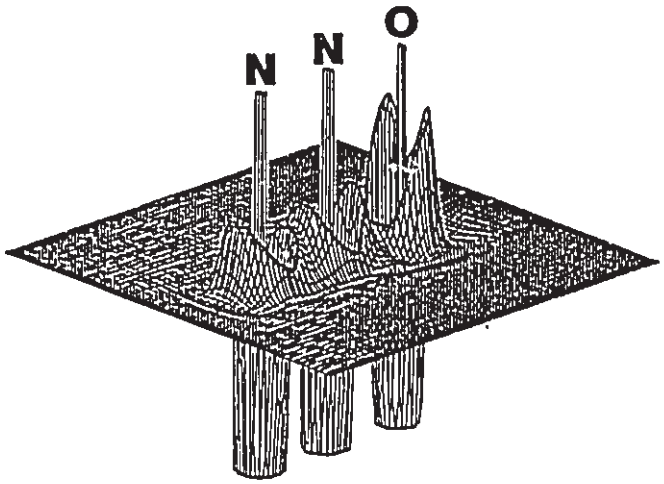
N
N
O

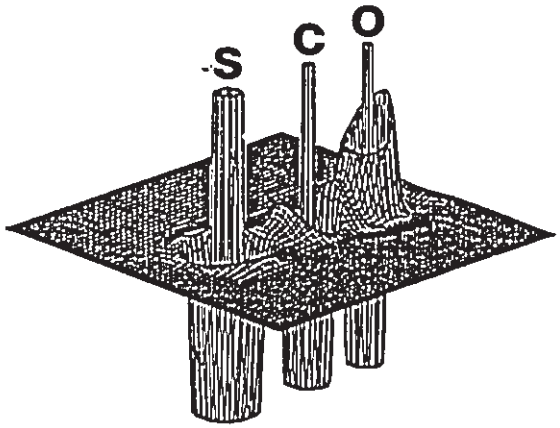
S
C
O

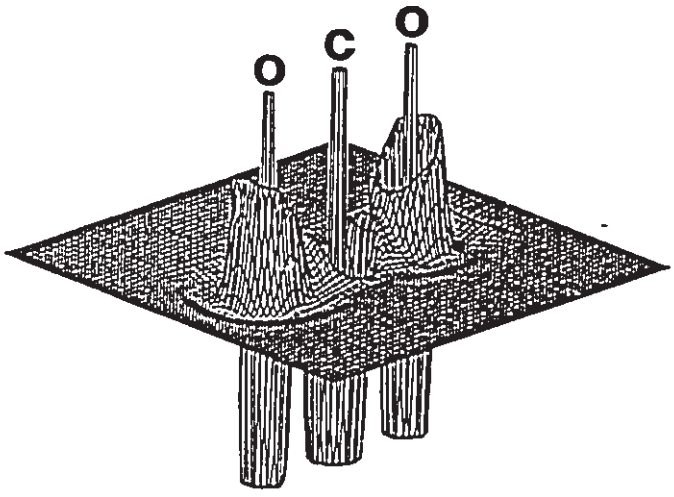
O
C
O

Figure 3.1.2

Laplacian relief plot for carbon monoxide. The curvature in $\nabla^2\rho$ parallel to the bond axis, λ_3, is much smaller for the carbon nonbonded region of charge concentration implying that this region is much more diffuse than the oxygen nonbonded region of charge concentration.

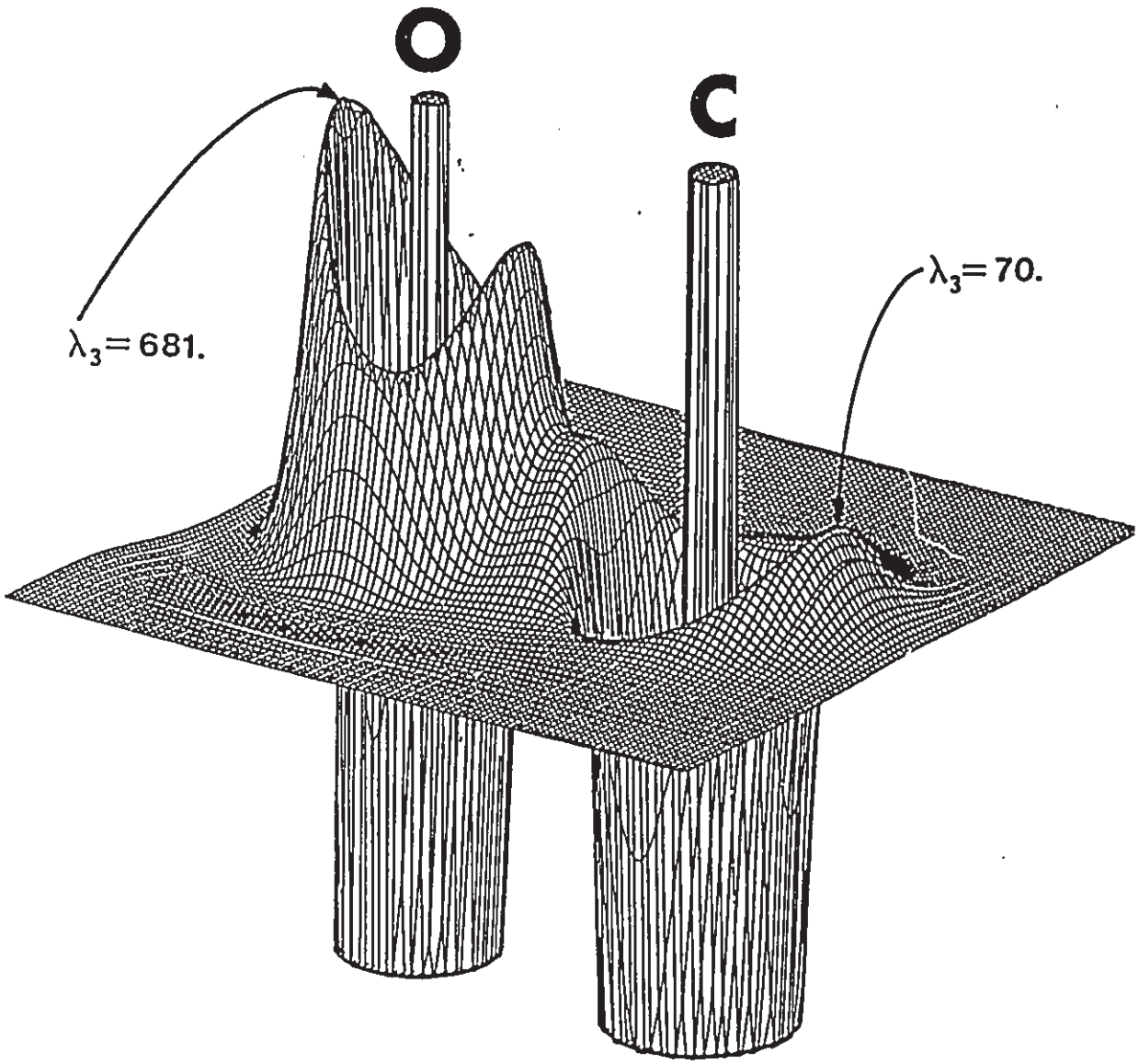
O
C
$\lambda_3 = 681.$
$\lambda_3 = 70.$

Table 3.1.1 Predicted Structures and Geometries of BASE-HF Complexes Using the Laplacian of the Charge Density.

Base	Maxima		$\nabla^2\rho$ prediction	$\angle$HeBX[a]			
	Type[a]	$-\nabla^2\rho(r_c)$	and HBX angle[b]	6-31G**	Expt'l	BF[d]	BH[e]
HF	n,F	11.66	100.8	109.5	110±7	108.0	112.0
H_2O	n,O	6.62	134.0[f]	136.7	134±6	120.0	108.0
	b,O-H	2.69					
H_2CO	n,O	7.10	106.3	105.4	115	113.0	
	b,O-C	3.12					
	b,C-O	1.57					
	b,C-H	1.46					
NNO	n,O	5.63	103.1	104.4	116		ONN-HF
	b,O-N	0.86					
	b,N-O	2.69					
	b,N_α-N	2.70					
	b,N-N_α	1.68					
	n,N	2.90					
H_3N	n,N	3.21	C_{3v}[g]	111.1[h]	C_{3v}[g]	C_{3v}[g]	C_{3v}[g]
	b,N-H	1.91					
NN	n,N	3.58	180.0	180.0	180	180.0	180.0
	b,N-N	3.35					
HCN	n,N	3.42	180.0	180.0	180	180.0	180.0
	b,N-C	2.74					
	b,C-H	1.48					
H_2S	n,S	0.56	114.9[f]	104.7	91	88.0	87.0
	b,H-S	0.68					
H_3P	n,P	0.32	C_{3v}[g]	120.3[h]	C_{3v}[g]	C_{3v}[g]	C_{3v}[g]
OCO	n,O	4.74	149.3	180.0	180±30		
	b,O-C	2.41					
	b,C-O	1.59					
SCO	n,O	5.34	180.0	180.0	180		
	b,O-C	3.19					
	b,C-O	1.67					
	b,C-S	1.37					
	n,S	0.38					
OOO	n,O_α	10.14	120.5				
	n,O trans	9.07	96.6				
	n,O cis	9.04	100.6	114.4			
OSO	n,O cis	5.81	115.7	140.8	145		
	n,O trans	5.66	95.1	107.6		118	
	n,S	0.82					
OC	n,O[i]	6.23	180.0				180.0
	n,C	1.45		180.0	180	180.0	
	b,O-C	4.72					
	b,C-O	1.92					
SC	n,C	1.52	180.0				
	b,C-S	1.53					
	n,S	0.28					

Table 3.1.1 (con'd)

Base	Maxima Type[a]	$-\nabla^2\rho(r_c)$	$\nabla^2\rho$ prediction and HBX angle[b]	$\angle H_aBX^c$ 6-31G**	Expt'l	BF[d]	BH[e]
H_2CS	n,S	0.59	108.0	82.8			
	b,C-S	1.15					
	b,C-H	1.45					
NNS	n,N[i]	3.35	180.0				
	b,N	2.62					
	b,N_c	2.94					
	b,N-S	2.91					
	n,S	0.50					
HCl	n,Cl[i]	0.85	103.6	100.1			
	b,H-Cl	0.87					
HCP	n,P[i]	0.20	180.0				
	b,C-P	1.11					
	b,C-H	1.45					

[a] The maximum in $-\nabla^2\rho$ is characterized as nonbonded (n) or bonded (b) in the VSCC of the atom listed immediately to the right of the "n" or "b" symbol. The nonbonded maximum of largest magnitude (the maximum H_a is predicted to attack) is listed first in each molecule. The subscript "c" denotes the central atom.

[b] The Laplacian prediction is given by listing the angle the chosen maximum in $-\nabla^2\rho$ (H) makes with the base (B) and the nearest neighbouring base atom (X). The RHF/6-31G**//6-31G** scheme is used.

[c] The equilibrium angle formed between the electrophilic hydrogen in HF with B and X is labelled $\angle H_aBX$.

[d] Buckingham-Fowler model (1985).

[e] Brobjer-Murrell model (1982).

[f] $\angle HBX$ is the obtuse angle between H, B, and the molecular plane of the base.

[g] The entry C_{3v} denotes a complex with a linear hydrogen bond ($\angle BH_aF$ = 180°) and C_{3v} symmetry.

[h] $\angle H_aNH$ or $\angle H_aPH$

[i] Attack at this nonbonded maximum forms a secondary structure.

Table 3.1.2. Predicted Structures and Geometries of BASE-HCl Complexes.

BASE	$\nabla^2\rho$ prediction and ∠MBX	∠HaBX 6-31G**	Exp't
HF	100.8	120.7	130
H_2O	134.0	145.8	---
H_2CO	106.3	120.2	---
H_3N	C_{3v}	C_{3v}	C_{3v}
NN	180.0	180.0	180.0
HCN	180.0	180.0	180.0
H_2S	114.9	106.6	93.8
H_3P	C_{3v}	C_{3v}	C_{3v}
OCO	180.0	180.0	180.0
SCO	180.0	180.0	180.0
OC	180.0	180.0	180.0
SC	180.0	180.0	180.0
HCl	103.8	105.0	---

Table 3.1.3. Predicted Structures and Geometries of Complexes Containing NH-N, NH-O, OH-N and OH-O Bonds.

Base	∠MBX	Complex YAH-BXZ	∠HaBX
H_3N	111.3	H_2NH-NH_3	118.5
		HOH-NH_3	108.5
		$[H_3NH$-$NH_3]^+$	112.5
H_2O	134.0	HOH-OH_2	122.2
		$[H_3NH$-$OH_2]^+$	179.9
		$[H_2OH$-$OH_2]^+$	178.6
$[HO]^-$	100.2	$[HOH$-$OH]^-$	102.6
$[(H)OCO]^-$	106.1	$[(H)OCOH$-$OCO(H)]^-$	120.0

Table 3.1.4 Effect of Basis Set and Electron Correlation on the Predicted Structures and Geometries of Hydrogen-Bonded Complexes Using $\nabla^2\rho$.

BASE	Maxima type	$-\nabla^2\rho(r_c)$ I	II	III	$\nabla^2\rho$ Prediction and LMBX I	II	III	Exp't
HF	n, F	11.66	9.27	8.93	100.8	103.0	103.1	110 ± 7
	c, H	-0.21	-0.23	-0.22				
NNO	n, O	5.63	4.77	4.40	103.1	103.1	105.8	116
	b, O-N	0.86	1.12	1.38				
	b, N-O	2.89	2.67	1.94				
	b, N_c-N	2.70	2.60	2.33				
	b, N-N_c	1.88	n/a	n/a				
	n, N	2.90	2.62	2.13				
H_3N	n, N	3.21	2.67	2.48	C_{3v}	C_{3v}	C_{3v}	C_{3v}
	b, N-H	1.91	1.95	1.89				
OC	n, O	6.23	5.14	4.97	180.0	180.0	180.0	180
	n, C	1.45	1.46	1.24	180.0	180.0	180.0	180
	b, O-C	4.72	4.81	4.88				
	b, C-O	1.92	n/a	n/a				

3.2. NUCLEOPHILIC ATTACK IN COMPLEXES WITH ACTIVATED DOUBLE BONDS

The reactivities of activated double bonds toward nucleophilic attack are directly correlated with the electron withdrawing tendency of the group linked to the double bond (Rappoport 1981, Patai and Rappoport 1964). The commonly accepted explanation for this correlation is based on the ability of the electron withdrawing group to stabilize the negative charge formed on the carbon adjacent to the site of nucleophilic attack. In one type of nucleophilic attack at an activated double bond, the Michael addition reaction, the formation of such an intermediate carbanion is followed by a protonation that leads to stable adducts. It has been proposed that congeners of acrylic acid, which contain a double bond activated by an electron withdrawing group, may add to biopolymers by the Michael reaction (Eder et a. 1982). For example, acrylonitrile (ACN) and acrylamide (ACA) have been demonstrated to add to DNA in vitro (Solomon et al 1985, 1984), possibly following the mechanism of a Michael addition reaction. The addition of a nucleophile (fluoride anion) to the activated double bonds of acrylic acid (AA) and methacrylic acid (MAA) was studied recently as a model for such a reaction with DNA (Osman et al 1988). Analysis of the potential energy surfaces for these reactions and of the energy terms calculated for the various stages indicated the scurce of the difference in the reactivities of AA and MAA; it showed that this difference depends mainly on the properties of the isolated species. The reactivity characteristics evidenced in the molecular

electrostatic potential (MEP) maps and in the Mulliken atomic charges in the isolated species suggested a basis for the difference in the reactivities of the two molecules, in agreement with the calculated potential energy surfaces. The favorable agreement between these results from simulations of the nucleophilic attack and the experimental findings showing the lower biological activity of MAA derivatives compared to AA derivatives, supports the hypothesis that Michael addition in biological systems is a likely mechanism for the toxicity of derivatives of acrylates (Osman et al 1988, Moore et al 1988). It also underscores the power of molecular properties as predictors of reactivity.

In the present work the reactivities of a series of such activated double bonds, including those found in AA, MAA, ACN and acrolein (ACR), toward a nucleophile in a Michael addition reaction are predicted on the basis of properties of the above isolated molecules expressed in the Laplacian of the calculated charge distribution. The Laplacian determines regions of local charge concentration and depletion and correspondingly determines sites susceptible to electrophilic or nucleophilic attack. The Laplacian determines the relative susceptibility to attack in a generalized acid-base reaction and also predicts the relative geometry of approach of the acid and base molecules. Further, unlike the MEP maps considered for AA and MAA in the previous work (Osman et al 1988) the Laplacian is quickly and easily calculated once a description of the charge density has been obtained (for example, from an SCF calculation). Examples are known where atomic charges do not determine reaction sites (Bader and Chang

1989, Carroll et al 1988) but the predictions given by $\nabla^2\rho$ are correct. Motivated by these advantages, the results of the $\nabla^2\rho$ analysis are used to predict the order of reactivities of the four molecules in the Michael addition reaction and also the approach angles of the nucleophile. To relate such results to the frame of the previous analysis (Osman et al 1988), the present work also examines the changes in atomic properties of the reactants AA and MAA upon interaction with F^- in the simulated Michael addition.

Restricted Hartree-Fock calculations of the isolated molecular species were performed with the 6-31G//6-31G, 6-31G**//6-31G and 6-31++G//6-31++G schemes (denoted schemes a to c respectively). The four molecules ACR, AA, ACN and MAA are very nearly planar and for simplicity will be assumed planar. Complexes of AA and MAA with F- were calculated using scheme c.

Reference to relief and contour maps of $\nabla^2\rho$ for ACR (Figures 3.2.1 and 3.2.2) indicates that the radial curvature of $-\nabla^2\rho$ is negative for the VSCC of C1 of ACR and that this atom still possesses a surface in which $-\nabla^2\rho$ is a maximum in all radial directions from the carbon nucleus. The two regions of charge depletion on C1 above and below the molecular plane, however, exhibit (3,+1) critical points in $-\nabla^2\rho$. Thus, the remaining two curvatures are positive, $-\nabla^2\rho$ is a minimum in the surface of charge concentration, and charge is locally depleted in the vicnity of these two critical points.

Analysis of $\nabla^2\rho$ in the Isolated Reactants

The (3,+1) critical points of $\nabla^2\rho$ displayed in Figures 3.2.1

and 3.2.2 correlate with centers of nucleophilic attack. These (3,+1) critical points on C1 in all four molecules form angles with the C1C2 bond axis (denoted MC1C2 in Table 3.2.1) of approximately 115°. Thus a nucleophile is predicted to approach C1 from above or below the molecular plane along a path forming an angle of ~115° with the C1C2 bond axis. This prediction agrees favorably with the ab initio calculations of the potential energy surface given by Osman et al (1988) where ∠FC1C2 is 114.4° and 114.5° for the stable carbanions of AA and MAA with F^- respectively. What is most important is that the Laplacian predicts an off angle approach to C1 by a simple determination of the position of a particular critical point in the Laplacian, with no recourse to the calculation of the potential energy surface.

The region of largest nonbonded charge concentration in the nucleophile (e.g. the maxima in $-\nabla^2\rho$ in the VSCC of the fluoride anion or the VSCC of nitrogen in NH_3) aligns with the region of largest charge depletion in the electrophile (C1). The greater the charge depletion, the more susceptible C1 is to nucleophilic attack. The extent of charge depletion is measured by the value of the minimum in $-\nabla^2\rho$ in the VSCC of C1. For the molecules calculated here, these values (Table 3.2.1) show that the order of decreasing reactivity to nucleophilic attack (and Michael addition) is: ACR > AA > ACN > MAA. This prediction is in agreement with experimentally determined activation energies for nucleophilic attack by amines (Morton and Landfield 1952) and also accounts for the greater biological activity of AA derivatives compared to MAA derivatives.

Atomic Properties

The atomic average of the charge of an atom in a molecule q(Ω) is given in Tables 3.2.1 and 3.2.2. The values of q(C1) and q((CH2)1), where the latter symbol denotes the sum of the charges on C1 and the two hydrogens bonded to it, do not parallel the reactivities (Table 3.2.1). Thus, the net charge on the electrophilic group of the Michael addition is not a good predictor of the reactivity of C1 to nucleophilic attack: as q(C1) and q((CH2)1) become more positive, the molecule does not become more susceptible to nucleophilic attack.

Changes in atomic charges and energies upon complex formation are reported in Table 3.2.2 for the addition of the fluoride anion to the activated double bond in AA and MAA. The course of the addition of F- to AA and MAA is very similar. A stable hydrogen-bonded complex is formed (Scheme I of Osman et al 1988) as an intermediate. Further approach of F- to C1 raises the energy of this complex until it reaches a transition state (TS). From this TS the system moves down the potential energy surface to produce a stable carbanion (SC). The only significant difference between the potential energy curves for AA and MAA is in the relative energies of the TS and SC systems from the separated reactants. The TS of the F- addition to MAA is -7.00 kcal mol^{-1} relative to the separated reactants compared to an energy of -10.15 kcal mol^{-1} for AA; the SC is -10.18 kcal mol^{-1} for MAA compared to -13.87 kcal mol^{-1} for AA. Thus, the presence of a methyl group on C2 in MAA causes a reduction in the stabilization of TS and SC by about 3 kcal mol^{-1} compared to the separated molecules. This result is

consistent with both the lower stability of carbanions formed from MAA and a slower rate of nucleophilic addition to methacrylates compared to acrylates.

In general, the results in Table 3.2.2 show that the changes incurred in the atoms upon forming the TS continue in the same direction as the SC is formed. We can therefore restrict our discussion hereafter to the differences in $q(\Omega)$ and $E(\Omega)$ between SC and the isolated reactants. For both stable carbanions, the following observations are made: Both F- and C1 lose electrons and the $|\Delta q(\Omega)|$ values are largest for these atoms. The remaining atoms all gain charge. Most of the charge is gained by the electron withdrawing group COOH. The magnitudes of Δq are similar for the two carbanions except in the activated double bond. The gain of electrons in C2 of AAF- is small but more than twice that in C2 of MAAF-. The change in charge is large on C1, which loses 0.51e more upon AAF- formation than upon MAAF- formation.

The energy changes in the atoms of the complexes, $\Delta E(\Omega)$, are fairly similar for AAF- and MAAF-. The fluoride anion, the hydrogens, the COOH and CH_3 groups are stabilized while the carbons of the activated double bond are destabilized upon carbanion formation. The fluoride anion is stabilized the most (Table 3.2.2), and the difference in $\Delta E(\Omega)$ values between AAF- and MAAF- is greatest for F^- and COOH (compare columns 5 and 7 of Table 3.2.2). The C1 is destabilized the most, more than eight and thirteen times than the destabilization of C2 in AAF- and MAAF-, respectively. A factor contributing to this large destabilization is the larger magnitude of $\Delta q(C1)$, the largest change

in atomic charge of all atoms in the carbanions.

Summary

An incoming nucleophile, such as NH_3 or F^-, initially aligns its largest region of charge concentration with the largest region of charge depletion in the valence shell of the electrophile (C1). The nucleophile is predicted to approach C1 from above or below the molecular plane along a path forming an angle of ~115° with the C1C2 bond axis. This prediction, based on the properties of $\nabla^2\rho$ agrees favourably with ab initio results (Osman et al 1988). The degree of reactivity of C1 to nucleophilic attack is predictable from the relative size of the regions of charge depletion in C1, expressed in the values of $\nabla^2\rho$ at the corresponding critical point. From these criteria, the predicted order of reactivities (from most to least reactive) is ACR > AA > ACN > MAA. These results are in accord with experiment (Morton and Landfield 1952). The calculated atomic properties provide a quantitative description of AAF^- and $MAAF^-$ carbanion formation. Because C1 has a larger region of charge depletion in AA than MAA, one might expect F^- to donate more electronic charge to AA than to MAA. This is not the case. The $\Delta q(F^-)$ values are nearly identical for both reactions. However, F^- is more stabilized by AA than by MAA (by 10.9 kcal mol^{-1}) consonant with the larger positive environment in AA generated by the larger charge depletion on C1. Thus, it appears that the stabilization of the incoming nucleophile is related to the size of the region of charge depletion on the attacked atom.

Figure 3.2.1

Relief maps of $-\nabla^2\rho$ for the acrolein molecule in the plane containing the nuclei (top) and in the perpendicular plane along the C1C2 axis (bottom). The largest valence-shell charge concentrations are found in the nonbonded region of the oxygen atom. While C1 exhibits a shell of charge concentration (both planes show a "lip" around the inner shell region of charge depletion), $\nabla^2\rho$ is actually positive over much of this shell in the perpendicular plane, i.e., only the curvature of $-\nabla^2\rho$ along a radial line out from the C1 nucleus is negative, and the two curvatures tangent to the surface are positive. The core, or first quantum shell, of each atom exhibits a spike-like charge concentration at the nucleus surrounded by a deep region of charge depletion. The arrow in the bottom diagram denotes the site of nucleophilic attack at C1. The charge density is generated using scheme b.

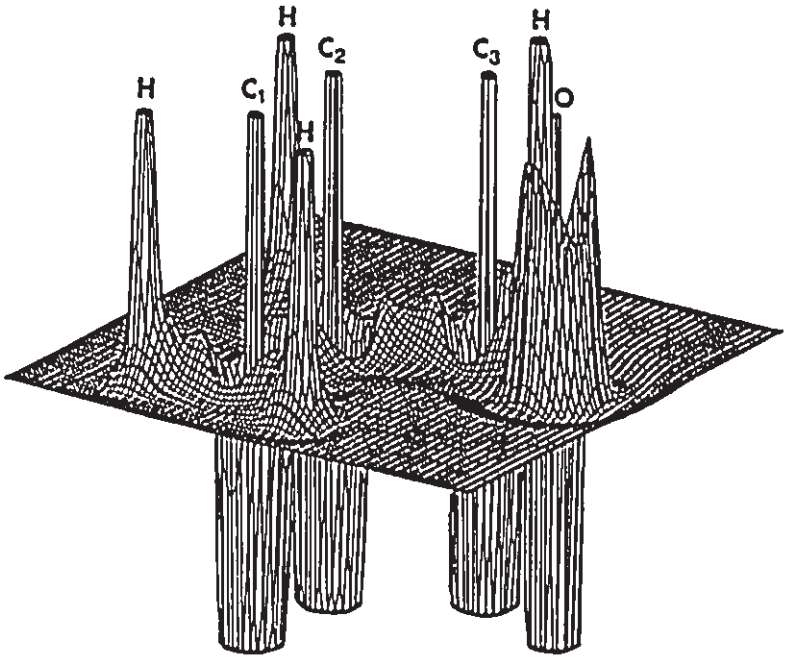
H
C1
H
C2
H
C3
H
O

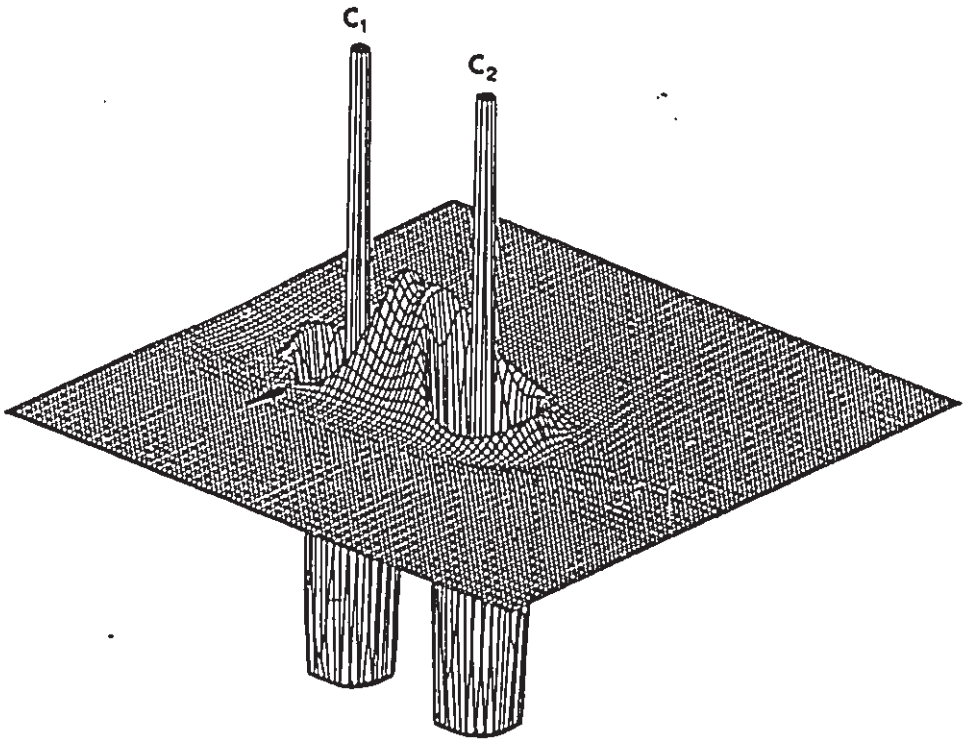
C1
C2

Figure 3.2.2. Contour plots of the Laplacian for two planes of acrolein, one being the plane containing the nuclei (top), and the other a plane perpendicular to this and along the C1C2 axis (bottom). The positions of the bonded and nonbonded charge concentrations are denoted by solid squares. The lower diagram shows the two (3,+1) critical points (denoted by solid triangles) which determine the sites of nucleophilic attack at C1.

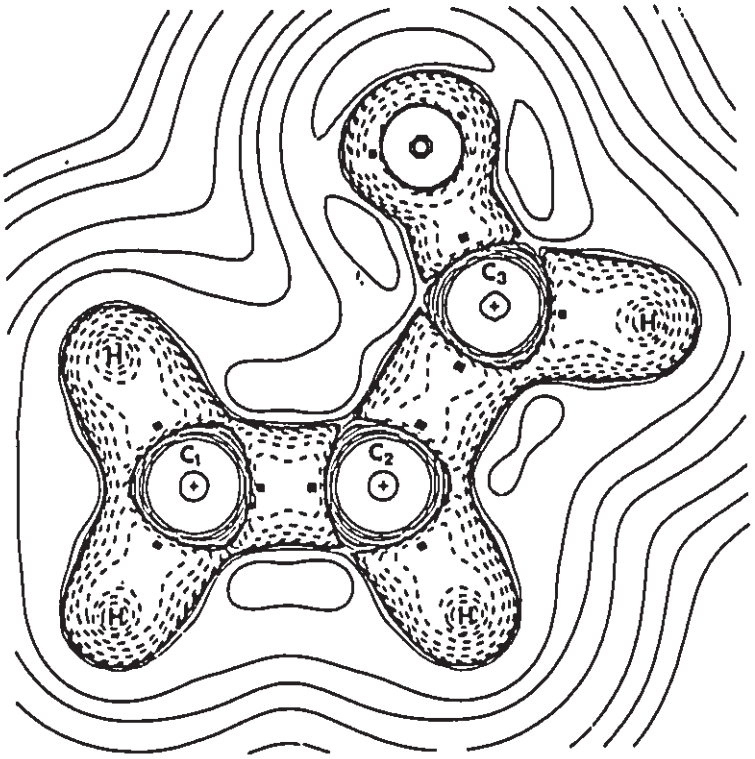
C3
H
H
C1
C2
H
H

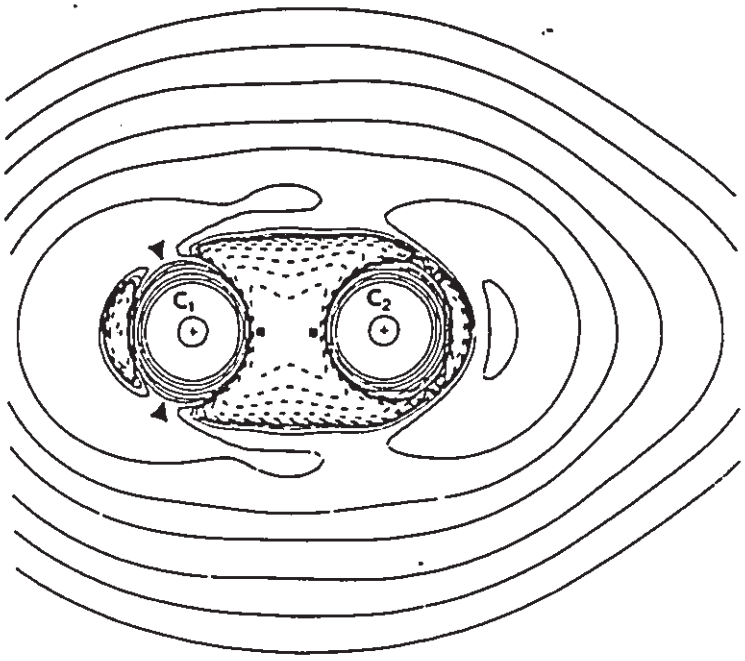
C1
C2

Table 3.2.1 Properties of the Laplacian of the Charge Density for the Isolated Reactants.[a]

Molecule	∠ MC1C2	$10^3\lvert\nabla^2\rho\rvert$[b]	E_a	q(C1)	q((CH2)1)
ACR	113.7	95.2	3.7	0.082	0.093
AA	114.2	92.7	6.2	0.092	0.101
ACN	115.1	82.0	7.4	0.145	0.153
MAA	115.8	75.5	-	0.086	0.078

[a] Results are from Scheme b calculations. Angles are in degrees. All other values are in au except the experimental activation energy of amine addition, E_a, which is in kcal mol^{-1}.

[b] These are the absolute values of $\nabla^2\rho$ evaluated at the extrema of the local regions of charge depletion, M, in the VSCC of C1. To the number of significant figures reported here, the two nearly equivalent M in the VSCC of C1 in each reactant have identical values for $10^3\lvert\nabla^2\rho\rvert$ and the MC1C2 angle.

Table 3.2.2 Atomic Properties and Their Changes for Complexes of AA and MAA with F^-.[a]

		Isolated Reactants		Complexes			
		AA	MAA	AAF^-		$MAAF^-$	
Prop	Ω[b]			TS	SC	TS	SC
q(Ω)	F^-	-1.000	-1.000	0.141	0.305	0.160	0.309
	C1	0.044	0.024	0.250	0.419	0.277	0.368
	C2	0.002	-0.018	-0.062	-0.099	-0.028	-0.045
	$(H_2)1$	0.101	0.085	-0.017	-0.120	-0.016	-0.131
	(H)2	0.054	N/A	-0.062	-0.084	N/A	N/A
	$(CH_3)2$	N/A	0.120	N/A	N/A	-0.126	-0.163
	COOH	-0.201	-0.211	-0.250	-0.421	-0.267	-0.338
E(Ω)	F^-	-99.4174	-99.4174	-23.86	-99.35	-16.71	-88.43
	C1	-37.8037	-37.8070	85.22	160.08	90.61	160.39
	C2	-37.8728	-37.8783	6.28	19.45	4.90	12.55
	$(H_2)1$	-1.2082	-1.2149	-24.41	-53.96	-25.41	-62.29
	(H)2	-0.6031	N/A	-12.93	-15.75	N/A	N/A
	$(CH_3)2$	N/A	-39.6342	N/A	N/A	-19.43	-19.70
	COOH	-188.0544	-188.0314	-40.53	-24.23	-40.51	-12.70
Total		-265.5422	-304.5658	-10.23	-13.76	-6.55	-10.18

[a] For the isolated reactants AA and MAA, q(Ω) and E(Ω) values are listed in au. For the complexes the changes in these values are listed (complex minus reactant) and the energy changes are in kcal mol^{-1}. The E_{SCF} (in au) and -V/T values for AA, MAA, F^-, AAF^- (TS and SC), and $MAAF^-$ (TS and SC) are -265.54244 and 1.99997115, -304.56591 and 1.99974552, -99.41738 and 2.00061525, -364.97598 and 2.00025903, -364.98192 and 2.00020189, -403.99445 and 2.00007034, and -403.99951 and 2.00001908 respectively. The values of ΔE_{SCF} (=E_{SCF}(complex)-E_{SCF}(reactants)) in kcal mol^{-1} for AAF^- (TS and SC) and $MAAF^-$ (TS and SC) are -10.14, -13.86, -7.00 and -10.18 respectively.

[b] The symbols $(H_2)1$, (H)2, $(CH_3)2$ and COOH refer to the sum of the atomic properties for the two hydrogens bonded to C1, the atomic properties of the hydrogen bonded to C2 in the acrylic acid systems, the sum of the atomic properties for the three hydrogens and one carbon comprising the methyl group in the methacrylic acid systems, and the sum of the atomic properties of the atoms comprising the carboxylic acid group in all systems, respectively.

CHAPTER 4

SHARED INTERACTIONS: PROPERTIES OF COMPLEXES CONTAINING NN BONDS

The hydrogen bond is an example of a closed-shell interaction and it has been examined in Chapters 2 and 3. In the present chapter we use the theory of atoms in molecules to study the shared interactions between two neighbouring nitrogen atoms in a variety of complexes. The physical properties, synthetic chemistry and industrial applications involved with compounds containing NN bonds is reviewed in Greenwood and Earnshaw (1984).

In Section 4.1 a bond order for NN bonds, n, is defined in terms of the value of the charge density at the NN bond critical point, ρ_b. Similar studies have been done for CC, CN, CO, OO and RCN-HX bonds (Bader et al 1983, Kraka 1984, Boyd and Choi 1986,1985). Values of the NN bond energies based on the properties of the NN interatomic surface are given in Section 4.2.

4.1. PROPERTIES OF COMPOUNDS CONTAINING NN BONDS: BOND ORDERS

RHF/6-31++G**//6-31++G** calculations are performed for all complexes containing NN bonds in this chapter. The cis-forms of N_2H_2, N_2O_2, and N_2F_2 are found to be 7.76, 2.87, and 1.51 kcal mol^{-1} less stable than the respective trans-forms and the N_3H isomer with the nitrogens collinear is found to be 0.65 kcal mol^{-1} less stable than structure 3 (Figure 4.1.1). Experimentally, the cis-form of N_2O_2 and the N_3H isomer with the nitrogens collinear are the most stable observed species.

Among other quantities, Table 4.1.1 lists the calculated and experimental internuclear separations, R_e and R_e^{expt} respectively, as well as the bond path length R_b. R_b is $\geq R_e$ in all cases because the bond path need not be straight. Indeed, for highly geometrically strained systems such as N_4 and diazirine, interior R_b values are substantially greater than their corresponding R_e values.

In general, R_e is slightly less than R_e^{expt} with the greater deviations being for the oxides and fluorides. Calculated and experimental bond angles, α_c and α_e respectively (Table 4.1.2) are in fairly good agreement. The bond path angle, α_b, the limiting value of the angle subtended at a nucleus by two bond paths, deviates greatest from the calculated bond angle in the ring compounds. The difference between these two quantities, $\Delta\alpha = \alpha_b - \alpha_c$, provides a measure of the degree of relaxation of the charge density away from the geometrical constraints imposed by the nuclear framework.

Bond Properties of Compounds Containing NN Bonds

Bond orders

In general for NN bonds, R_e and R_b decrease as ρ_b increases (Table 4.1.1). If NN bonds in N_2H_4, N_2H_2 and N_2 are assigned (Lewis) bond orders n=1,2,3 then the simplest relationship between n and ρ_b that yields a good fit is of the form of a straight line. Linear regression yields the equation

$$n = 5.254667\rho_b - 0.728398 \qquad [4.1.1]$$

with a correlation coefficient of 0.999982. For the CC bond in hydrocarbons, the best fit is an exponential one (Bader et al 1983). This empirical bond order is only meant to provide a convenient measure of the extent to which electronic charge is accumulated between pairs of bonded nuclei relative to a set of standard values. Next to the NN bond in the nitrogen molecule, the N1N3 bonds in N_3H and N_3F have the highest bond orders with n = 2.53-2.55. The NN bond in N_2O and in diazomethane 8 have the next highest bond orders of 2.50 and 2.47 respectively. The clustering of n values around 2.5 is consistent with the resonance structure description of these complexes. The NN bond in diazirine 10 has n = 2.12 which is smaller in value than the n of its acyclic isomer 8. Indeed, the formal bond order of the NN bond in diazirine is 2. The n value in tetrahedral N_4 is slightly greater than those in cyclic N_3H_3 and diaziridine although all these NN bonds have formal bond orders of 1. The n values in N_2F_2 and N_2F_4 are larger than the corresponding values for N_2H_2 and N_2H_4. At the NN bond critical point, there is both more charge density (ρ_b values) and a greater concentration of charge density ($\nabla^2\rho_b$ values) for the dinitrogen

fluorides over the dinitrogen hydrides. The dinitrogen oxides exhibit the smallest n values implying that these complexes have the least amount of charge concentrated at the NN bond critical point.

The bond order calculated in this manner decreases with increasing R_b (Figure 4.1.2). The equation of the line is

$$n = -2.349R_b + 7.393 \qquad [4.1.2]$$

The ordering of n values for NN bonds calculated by Jug (1978) using the maximum bond order method is the same as that of the present work.

While the values of ρ_b for the NH bonds exhibit a much smaller variation (they are all formally of order 1) two observations can be made: 1) In general, the value of ρ_b is slightly greater in the compounds containing at least two nitrogens as compared to the NH bond in ammonia. 2) The largest values of ρ_b are for cyclic N_3H_3 and diaziridine. The greater values of ρ_b in cyclic molecules also has been observed in CH bonds of hydrocarbons.

The value of ρ_b in the NF bond increases with increasing number of fluorines in the molecule but the same cannot be said for the value of ρ_b in the NO bond.

Bond ellipticity

In a bond in a molecule with cylindrical symmetry, such as those in N_2, N_2O and C_2H_2, the bond ellipticities are zero. The ellipticities of the NN bonds in N_2, N_2H_2 and N_2H_4 are 0.00, 0.20 and 0.00 respectively. The major axis of the ellipticity for N_2H_2 and for the large ellipticities in the N1N2 bond in N_3H and N_3F are perpendicular to the plane of the nuclei as anticipated for molecules

with π-bonds. In diazirine it is also perpendicular while in diaziridine it is in the plane of the ring. The larger NN ellipticity in N_2F_2 (the major axis is perpendicular to the molecular plane) over N_2F_4 emphasizes the π-character of the former.

The ellipticities in the NH bonds are all small. The NO ellipticities are all about 0.1 in value (except in N_2O where it is zero). In N_2F_4 and N_3F, the NF bond ellipticities are about 0.2 while in N_2F_2 it is only 0.1. The NC bond ellipticities are quite large. In 9 the major axis is perpendicular to the molecular plane while in 10 and 11 it is in the plane of the ring.

Laplacian of the charge density

When $\nabla^2\rho_b < 0$ and is large in magnitude, perpendicular contractions of ρ dominate the interaction and electronic charge is concentrated between the nuclei along the bond path. The result is a sharing of electronic charge between the atoms as is found in covalent or polar bonds. This sharing is observed in all the bonds in all the complexes studied in the present work (with the exception of the CN bond in 9). According to the local virial theorem, these bonds achieve their stability through the lowering of the potential energy of the electronic charge that is concentrated between the nuclei and shared by both atoms. In general, for a particular set of bonds, the value of $\nabla^2\rho_b$ parallels ρ_b in its behaviour, becoming more negative as the value of ρ_b increases.

Comparisons with isoelectronic hydrocarbons

Bond orders and ellipticities have been determined for hydrocarbons. The CC bond orders (Table 4.1.1) are calculated from the expression

$$n = \exp\{A(\rho_b - B)\} \qquad [4.1.3]$$

where A and B are constants (Bader et al 1983). These values have been shown to be relatively basis set independant. Therefore meaningful comparisons can be made between the nitrogen-containing compounds calculated using the 6-31++G**//6-31++G** scheme and the respective isoelectronic hydrocarbons calculated using the 6-31G*//6-31G* scheme. These systems, dealt with in turn, are (N_2, C_2H_2), (N_2H_2, C_2H_4), (N_2H_4, C_2H_6), (diazomethane, diazirine and cyclopropene), (N_3H_3, C_3H_6) and (N_4, C_4H_4).

N_2 and C_2H_2 are both of formal bond order 3 and their calculated bond orders are close to this value. The magnitudes of ρ_b and $\nabla^2\rho_b$ are greater in N_2 implying that the NN bond in N_2 is stronger than the longer CC bond in C_2H_2.

N_2H_2 and C_2H_4 are both of formal bond order 2 and their calculated bond orders are close to this value. Again, as in the above paragraph, the magnitudes of ρ_b and $\nabla^2\rho_b$ are greater for the NN bond implying that this bond is stronger than the longer CC bond in ethylene. The CC bond ellipticity in ethylene is over twice as large as the NN bond ellipticity in N_2H_2 suggesting that ethylene has more π-character.

N_2H_4 and C_2H_6 are both of formal bond order 1 and their calculated bond orders reflect this. The same observations made in the above two paragraphs apply here as well.

Comparing the NN bond in the ring structure diazirine to the formally double CC bond in cyclopropene reveals the following: the calculated bond orders are both close to 2. The magnitudes of ρ_b and $\nabla^2\rho_b$ for the shorter NN bond are greater than those for the CC bond. As is the case in the diimine ethylene comparison, the ellipticity is greater for the CC bond. The NN bond in acyclic diazomethane has a bond order of ≈2.5 and the magnitudes of ρ_b and $\nabla^2\rho_b$ are even greater than those in diazirine.

The general observations made in the comparison of NN and CC bonds in isoelectronic systems hold true in a comparison of the tetrahedral molecules N_4 and C_4H_4, those being that the bond orders are very similar, the values of ρ_b and $\nabla^2\rho_b$ are larger in magnitude for the NN bond and the NN bond is shorter. However, in this pair, the NN bond ellipticity, although small, is more than twice as large as the CC bond in tetrahedrane.

Atomic Properties

Values of N(Ω), E(Ω) and v(Ω) are given in Table 4.1.3. An examination of the electron populations reveals the following: 1) For the hydrides, q(N) is always negative except for N3 of N_3H. It is most negative in ammonia. The values of q(N) in NH_3, N_2H_4 and N_2H_2 are -1.1663, -0.7635 and -0.3787 respectively. Thus, in these complexes approximately 0.4e are transferred from each H to a neighbouring N. This observation also holds in N_4H_4. 2) For the oxides, q(N) is always positive except for N1 of N_2O. Each oxygen bonded to a neighbouring N withdraws electrons from it and q(O) ranges between -1.4

to -1.5. 3) For the fluorides, q(N) is always positive except for N1 of N_3F and q(F) ≈ -0.4 in all complexes. 4) q(C) is positively charged in 9, 10 and 11.

In general, the magnitude of E(N) increases as N(N) increases. The nitrogen with the greatest positive charge (in N_2O_4) is the least stable of all the nitrogens while the greatest negatively charged N (in NH_3) is the most stable. In terms of relative stabilities to E(N) in N_2, N is stabilized in N_2H_2 and even more stabilized in N_2H_4, but it is greatly destabilized in the higher oxides and fluorides. The relative destabilization of N in N_4 is in accord with this species not being observed experimentally.

The v(N) values are largest in NH_3 and N_2 where a large diffuse region of nonbonded charge concentration exists. The smallest v(N) values are for the nitrogens in N_2O_4. These nitrogens have among the highest positive charges of the systems studied.

Figure 4.1.1

Molecular graphs of complexes containing NN bonds. Included are bond critical points (black dots). Refer to Tables 4.1.1 and 4.1.2 for the numbering scheme and values of geometric parameters.

1

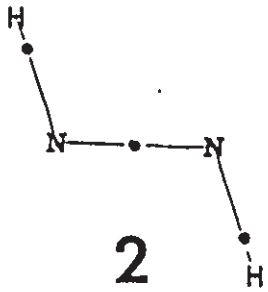

2

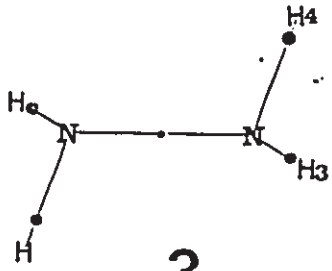

3

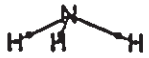

4

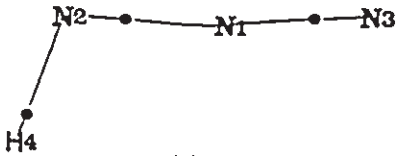

5

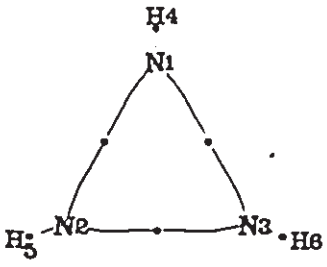

6

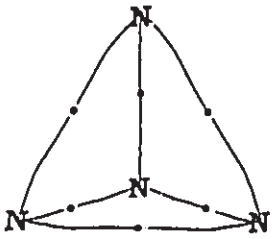

7

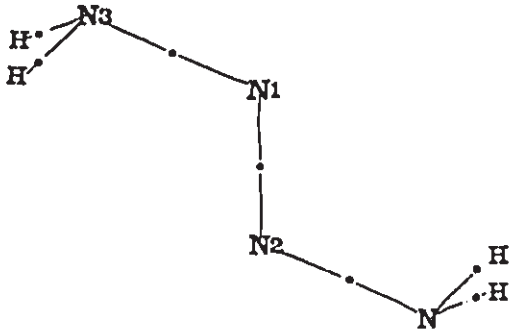

8

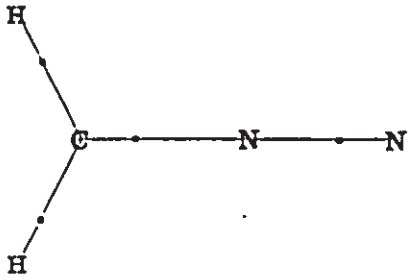

9

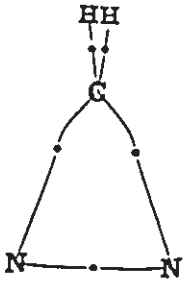

10

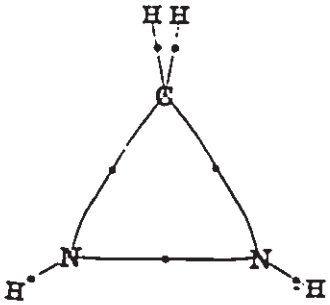

11

12

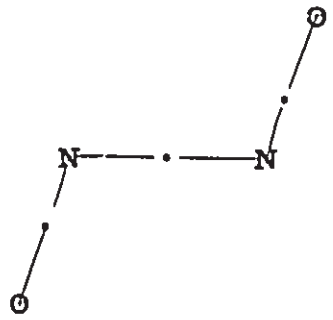

13

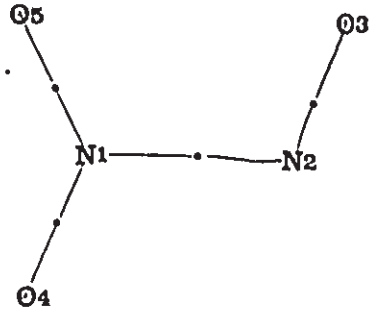

14

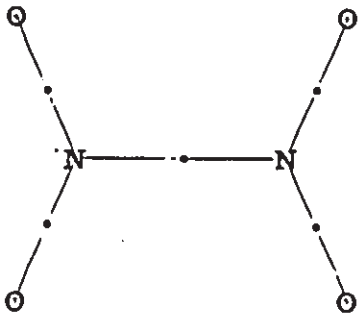

15

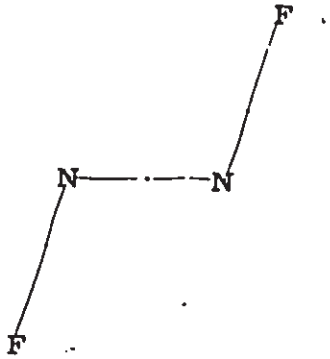

16

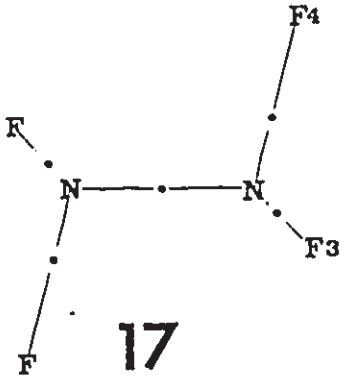

17

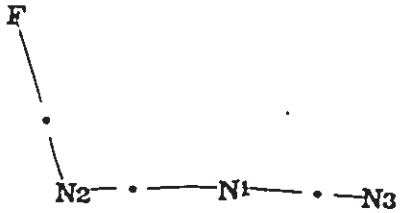

18

Figure 4.1.2

The bond order of NN bonds, n, (calculated from equation 4.1.1) versus the NN bond path length, R_b (in au). The data labels correspond to the structure labels given in Table 4.1.1 and Figure 4.1.1. If there are two nonequivalent NN bonds in a molecule, the first entry for the molecule in Table 4.1.1 is designated a in the present graph and the second entry is designated b. The correlation coefficient is -0.973.

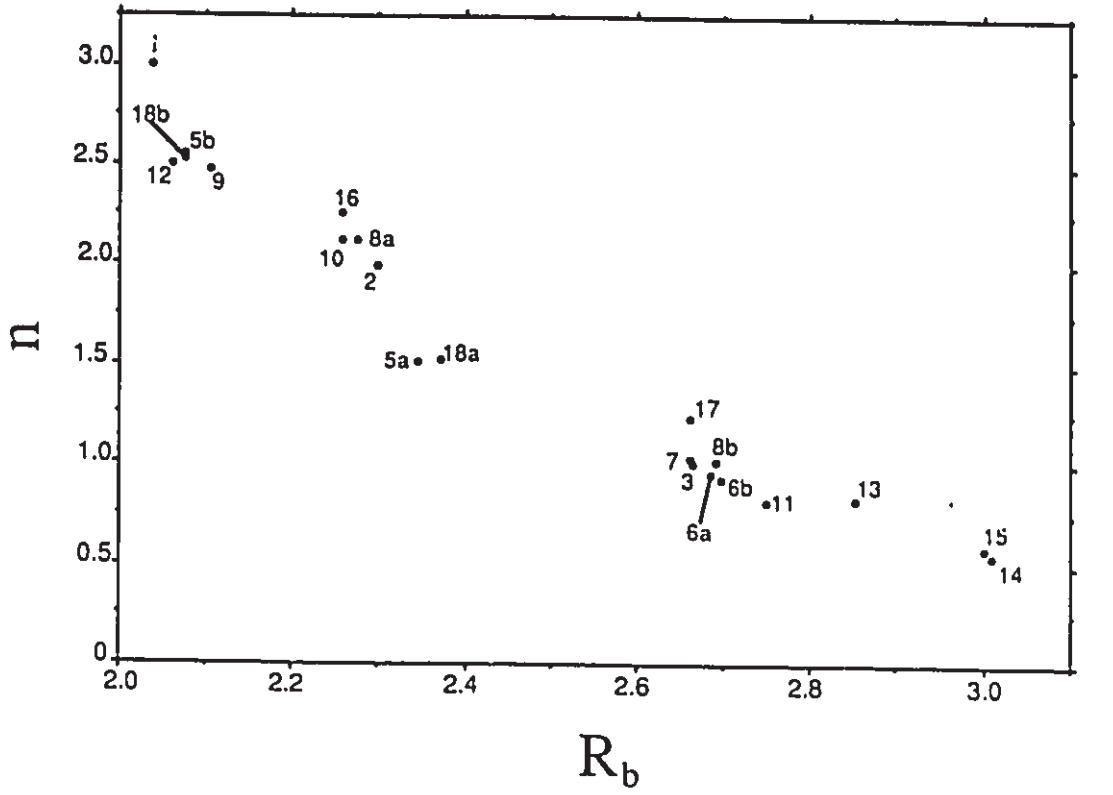
n
3.0
2.5
2.0
1.5
1.0
0.5
0
2.0
2.2
2.4
2.6
2.8
3.0
R_b
1
18b
5b
12
9
16
8a
10
2
5a
18a
17
8b
7
3
6b
11
13
6a
15
14

Table 4.1.1. Properties of Bond Critical Points of Compounds Containing NN Bonds.[a]

Species	bond	R_e	R_b	$R_{e,expt}$	ρ_b	n	$\nabla^2\rho_b$	λ_1	λ_2	λ_3	ϵ
N_2,1	NN	2.0378	2.0378	2.0680[b]	0.7102	3.00	-2.7323	-1.7013	-1.7013	0.6704	0.000
N_2H_2,2	NN	2.2952	2.2970	2.3658[c]	0.5179	1.89	-1.5308	-1.3285	-1.1110	0.9097	0.197
	NH	1.9148	1.9155	1.9426	0.3666	1.02	-2.0618	-1.4043	-1.3924	0.7151	0.009
N_2H_4,3	NN	2.6631	2.6645	2.7458[d]	0.3298	1.00	-0.7435	-0.7123	-0.7114	0.6803	0.001
	N1H3	1.8858	1.8866	1.9370	0.3677	1.03	-2.0430	-1.4366	-1.3481	0.7417	0.066
	N1H4	1.8910	1.8926	1.9370	0.3652	1.02	-2.0012	-1.3914	-1.3051	0.6953	0.066
NH_3,4	NH	1.8897	1.8899	1.9218[e]	0.3583	1.00	-1.9519	-1.3544	-1.2914	0.6953	0.049
N_3H,5	N1N2	2.3434	2.3451	2.3433[e]	0.4260	1.51	-0.8376	-0.7402	-0.4746	0.3772	0.560
	N1N3	2.0747	2.0750	2.1354	0.6203	2.53	-1.9853	-1.3153	-1.1155	0.4455	0.179
	N2H4	1.8997	1.9003		0.3522	0.98	-1.9479	-1.3716	-1.3181	0.7418	0.041
N_3H_3,6	N1N2	2.6725	2.6860		0.3192	0.85	-0.5662	-0.6794	-0.5680	0.6811	0.196
	N2N3	2.6789	2.6953		0.3149	0.83	-0.5488	-0.6740	-0.5469	0.6722	0.232
	N1H4	1.8947	1.8965		0.3736	1.04	-2.1406	-1.4799	-1.4662	0.8055	0.009
	N2H5	1.8977	1.9000		0.3719	1.04	-2.1080	-1.4336	-1.4268	0.7584	0.009
N_4,7	NN	2.6353	2.6607		0.3342	1.03	-0.5024	-0.6283	-0.5988	0.7247	0.049
N_4H_4,8	N1N2	2.2724	2.2763	2.2771[f]	0.5417	2.12	-1.6637	-1.4599	-1.1547	0.9509	0.264
	N1N3	2.6873	2.6907	2.7004	0.3312	1.01	-0.7804	-0.7771	-0.7092	0.7059	0.096
	N3H5	1.8970	1.8985	1.9086	0.3602	1.01	-1.8953	-1.3969	-1.3285	0.7301	0.051
	N3H6	1.8970	1.8989	1.9086	0.3602	1.01	-1.9957	-1.3971	-1.3288	0.7302	0.051
H_2CN_2,9	NN	2.1063	2.1063	2.1524[g]	0.6083	2.47	-2.1215	-1.3972	-1.1512	0.4269	0.214
	NC	2.4278	2.4278	2.4566	0.3029		1.1630	-0.6938	-0.3278	2.1847	1.116
	CH	2.0188	2.0188	2.0352	0.2961		-1.1551	-0.8206	-0.7413	0.4068	0.107
H_2CN_2,10	NN	2.2541	2.2574	2.3206[h]	0.5430	2.12	-1.5416	-1.3058	-1.1566	0.9209	0.129
	NC	2.7352	2.7707	2.8006	0.2614		-0.6574	-0.5244	-0.3743	0.2413	0.401
	CH	2.0295	2.0301	2.0598	0.3034		-1.2069	-0.8379	-0.7936	0.4246	0.056
H_4CN_2,11	NN	2.7448	2.7482		0.2921	0.81	-0.4050	-0.6014	-0.4316	0.6280	0.394
	NH	1.8918	1.8949		0.3692	1.03	-2.0697	-1.4237	-1.3955	0.7495	0.020
	NC	2.6882	2.7070		0.2849		-0.8582	-0.5957	-0.4434	0.1809	0.343
	CH	2.0348	2.0350		0.3029		-1.2064	-0.8254	-0.8105	0.4295	0.018
N_2O,12	NN	2.0620	2.0620	2.1278[e]	0.6153	2.50	-1.5052	-1.1339	-1.1339	0.7626	0.000
	NO	2.2310	2.2310	2.2412	0.5352		-0.9878	-1.1641	-1.1641	1.3404	0.000
N_2O_2,13	NN	2.8505	2.8511	4.1196[e]	0.2959	0.83	-0.6192	-0.7067	-0.7044	0.7919	0.003
	NO	2.1788	2.1809	2.1165	0.5934		-2.2616	-1.5990	-1.4478	0.7852	0.104
N_2O_3,14	NN	3.0072	3.0100	3.5224[i]	0.2419	0.54	-0.3519	-0.5622	-0.5388	0.7490	0.043
	N2O3	2.1326	2.1349	2.2790	0.6298		-2.6101	-1.7418	-1.5571	0.6889	0.119
	N1O5	2.2211	2.2219	2.2714	0.5665		-1.4668	-1.4427	-1.3056	1.2815	0.105
	N1O4	2.2254	2.2255	2.2998	0.5651		-1.4705	-1.4555	-1.3005	1.2854	0.119
N_2O_4,15	NN	3.0002	3.0002	3.3675[j]	0.2486	0.58	-0.4210	-0.6126	-0.5488	0.7404	0.116
	NO	2.2023	2.2032	2.2488	0.5795		-1.4627	-1.4631	-1.3194	1.3198	0.109
N_2F_2,16	NN	2.2527	2.2566	2.3244[k]	0.5681	2.26	-1.9077	-1.6857	-1.1952	0.9732	0.410
	NF	2.5306	2.5314	2.6384	0.3412		-0.5830	-0.8219	-0.7548	0.9936	0.088
N_2F_4,17	NN	2.6511	2.6615	2.[illegible]	0.3722	1.23	-1.0247	-0.9598	-0.8994	0.8345	0.067
	N1F3	2.5209	2.5230	2.6330	0.3557		-0.6773	-0.9403	-0.7762	1.0392	0.212
	N1F4	2.5289	2.5314	2.6330	0.3512		-0.6212	-0.8144	-0.7674	1.0606	0.191
N_3F,18	N1N2	2.3690	2.3711		0.4282	1.52	-1.1015	-1.0751	-0.5039	0.4776	1.134
	N1N3	2.0763	2.0764		0.6231	2.55	-2.1787	-1.4231	-1.1238	0.3672	0.266
	N2F4	2.6171	2.6184		0.2984		-0.3165	-0.6863	-0.5758	0.9456	0.192

Table 4.1.1 (con'd)
CC bonds in isoelectronic hydrocarbons:

Species	bond	R_e	R_b	R_e^{expt}	ρ_b	n	$\nabla^2\rho_b$	λ_1	λ_2	λ_3	ε
C_2H_2	C-C	2.2393	2.2393	2.2733[i]	0.4178	2.92	-1.2814	-0.5876	-0.5876	-.1062	0.000
C_2H_4	C-C	2.4888	2.4888	2.5303[i]	0.3632	2.05	-1.1917	-0.8158	-0.5643	0.1884	0.440
C_2H_6	C-C	2.8864	2.8864	2.8932[i]	0.2520	1.00	-0.6604	-0.4768	-0.4766	0.2928	0.000
C_3H_4	C-C	2.8250	2.8449	2.8629[i]	0.2436	0.85	-0.4284	-0.4379	-0.2727	0.2821	0.606
	C=C	2.4111	2.4411	2.4566[i]	0.3698	2.14	-1.0993	-0.7055	-0.5410	0.1472	0.304
C_3H_8	C-C	2.8297	2.8476	2.8535[i]	0.2490	0.98	-0.5330	-0.4892	-0.3284	0.2846	0.490
C_4H_4	C-C	2.7654	2.8047		0.2551	1.02	-0.4672	-0.3813	-0.3733	0.2874	0.021

[a] All values are in au. The bold numbers immediately to the right of each nitrogen-containing compound denote its structure (Figure 4.1.1). Only nonequivalent bonds are listed.
[b] Huber and Herzberg 1979.
[c] Carlotti et al 1974.
[d] Horino et al 1960.
[e] Greenwood and Earnshaw 1984.
[f] Veith and Schlemmer 1982.
[g] Cox et al 1958.
[h] Thomson and Glidewell 1983.
[i] Jubert et al 1984.
[j] McClelland et al 1972.
[k] Bohn and Bauer 1967.
[l] Hehre et al 1986.

Table 4.1.2. Bond Angles of Compounds Containing NN Bonds.[a]

Molecule	Parameter	Angles			
		α_c	α_b	$\Delta\alpha$	α_e[b]
N_2H_2,2	N1N2H3	108.13	99.86	-8.27	106.8
N_2H_4,3	N1N2H5	108.86	105.24	-3.62	112.0
	N1N2H6	112.97	105.72	-7.25	112.0
	H5N2H6	109.40	107.33	-2.07	108.0
NH_3,4	H2N1H3	108.80	106.31	-2.49	107.8
N_3H,5	N2N1N3	173.37	177.35	3.98	180.0
	N1N2H4	108.34	118.02	9.68	112.0
N_3H_3,6	N1N2N3	59.91	76.76	16.85	
	N2N1N3	60.18	61.40	1.22	
	N2N1H4	106.48	98.24	-8.24	
	N1N2H5	106.07	97.41	-8.66	
	N3N2H5	110.49	99.19	-11.30	
N_4,7	N3N1N4	60.00	77.83	17.83	
N_4H_4,8	N1N2N4	113.14	112.91	-0.23	109.0
	N2N4H7	107.63	99.37	-8.26	118.0
	H7N4H8	106.96	104.34	-2.62	109.8
H_2CN_2,9	N2C3H4	117.63	115.57	-2.06	116.9
	H4C3H5	124.74	128.86	4.12	126.2
H_2CN_2,10	C1N4N5	65.67	72.50	6.83	
	N4C1N5	48.67	81.18	32.51	
	H2C1N4	117.92	110.84	-7.08	118.0
	H2C1H3	118.16	124.11	5.95	117.0
H_4CN_2,11	C1N4N5	59.30	74.57	15.27	
	N4C1N5	61.40	76.40	15.00	
	H2C1N4	117.57	112.36	-5.21	
	H2C1H3	114.86	118.62	3.76	
	C1N4H6	110.64	100.20	-10.44	
	H6N4N5	106.27	98.93	-7.34	
N_2O_2,13	N1N2O3	108.58	102.30	-6.28	
N_2O_3,14	N1N2O3	109.38	105.41	-3.97	105.1
	N2N1O4	112.24	115.34	3.10	117.5
	N2N1O5	116.92	115.52	-1.40	112.7
	O4N1O5	130.84	129.15	-1.69	129.8
N_2O_4,15	N1N2O3	113.38	112.68	-0.70	112.3
	O5N1O6	133.25	134.64	1.39	135.4
N_2F_2,16	N1N2F3	106.92	100.87	-6.05	105.5
N_2F_4,17	N2N1F3	103.05	94.85	-8.20	99.0
	N2N1F4	108.33	98.06	-10.27	103.5
	F3N1F4	103.55	106.52	2.97	103.7
N_3F,18	N3N1N2	174.42	177.14	2.72	
	N1N2F4	104.07	98.47	-5.60	

[a] Angles are given in degrees. The symbols are defined in the text.
[b] References to these experimental values are given in Table 4.1.1.

Table 4.1.3. Atomic Properties of Compounds Containing NN Bonds.[a]

Molecule	Atom Ω	N(Ω)	E(Ω)	E_{rel}(Ω)	v(Ω)
N_2,1	N1(N2)	7.0000	-54.4731	0.00	129.82
-108.94702					
2.003508					
Total		14.0000	-108.9462		259.64
N_2H_2,2	N1(N2)	7.3787	-54.5200	-29.43	120.40
-110.00735	H3(H4)	0.6213	-0.4837	-11.82	30.40
2.002528					
Total		16.0000	-110.0074		301.61
N_2H_4,3	N1(N2)	7.7635	-54.6409	-105.30	114.22
-111.19124	H3(H5)	0.6034	-0.4702	-3.45	29.45
2.002389	H4(H6)	0.6332	-0.4850	-12.74	30.97
Total		18.0002	-111.1922		349.28
NH_3,4	N1	8.1663	-54.8078	-210.03	143.98
-56.20115	H2(3,4)	0.6113	-0.4647	0.00	30.40
2.002490					
Total		10.0002	-56.2019		235.19
N_3H,5	N1	7.4505	-55.0988	-392.63	83.63
-163.84839	N2	7.3850	-54.3700	64.70	128.43
2.002874	N3	6.6100	-54.9435	-295.18	122.09
	H4	0.5545	-0.4361	17.95	28.02
Total		22.0000	-164.8484		362.17
N_3H_3,6	N1	7.4249	-54.5291	-35.14	104.02
-164.95756	N2(N3)	7.3964	-54.5060	-20.64	103.36
2.001927	H4	0.5772	-0.4631	1.00	27.94
	H5(H6)	0.6025	-0.4766	-7.47	29.19
Total		23.9899	-164.9574		397.06
N_4,7	N1(2,3,4)	7.0000	-54.3846	55.53	98.11
-217.53747					
2.001514					
Total		28.0000	-217.5384		392.43
N_4H_4,8	N1(N2)	7.0714	-54.4034	43.74	97.40
-220.01144	N3(N4)	7.7521	-54.6883	-135.04	112.70
2.002222	H5(H7)	0.5882	-0.4571	4.77	29.19
	H6(H8)	0.5882	-0.4571	4.77	29.18
Total		31.9998	-220.0118		536.97
H_2CN_2,9	N1	6.7771	-54.0623	257.78	126.15
-147.85316	N2	7.8262	-55.2047	-459.09	96.98
2.002408	C3	5.4782	-37.3672	0.00	96.69
	H4(H5)	0.9592	-0.6091	-90.61	45.61
Total		21.9999	-147.8524		411.03
H_2CN_2,10	C1	5.2688	-37.3746	-4.77	66.39
-147.84298	N4(N5)	7.3543	-54.5889	-72.66	113.90
2.001792	H2(H3)	1.0112	-0.6450	-113.14	47.94
Total		21.9998	-147.8426		380.08
H_4CN_2,11	C1	5.0910	-37.3165	31.81	54.20
-149.01841	H2(H3)	1.0291	-0.6544	-119.04	49.19
2.001551	N4(N5)	7.8269	-54.7251	-158.13	112.19
	H6(H7)	0.5987	-0.4714	-4.20	28.95
Total		24.0004	-149.0183		434.86

Table 4.1.3 (con'd)

Molecule	Atom	N(Ω)	E(Ω)	E_{rel}(Ω)	V(Ω)
N_2O,12	N1	7.0711	-54.8939	-264.06	76.86
-183.68528	N2	6.5123	-53.8638	382.34	124.12
2.003040	O3	8.4166	-74.9298	0.00	117.84
Total		22.0000	-183.6875		318.82
N_2O_2,13	N1(N2)	6.4914	-54.0341	275.48	89.74
-258.42981	O3(O4)	8.5084	-75.1813	-157.82	114.64
2.002828					
Total		29.9996	-258.4308		408.77
N_2O_3,14	N1	6.2125	-53.9744	312.94	46.14
-333.24870	N2	6.3020	-53.8822	370.80	86.03
2.002852	O3	8.4865	-75.2447	-197.60	108.27
	O4	8.4967	-75.0685	-87.04	119.55
	O5	8.5024	-75.0774	-92.62	116.48
Total		38.0001	-333.2472		476.48
N_2O_4,15	N1(N2)	6.1380	-53.9027	357.93	43.66
-408.05030	O3(4,5,6)	8.4311	-75.0612	-82.45	112.81
2.002813					
Total		46.0004	-408.0502		538.95
N_2F_2,16	N1(N2)	6.6010	-54.1445	206.20	88.23
-307.59544	F3(F4)	9.3988	-99.6524	0.00	95.90
2.002729					
Total		31.9996	-307.5938		368.26
N_2F_4,17	N1(N2)	6.2389	-53.8175	411.40	60.21
-506.32590	F3(F5)	9.3801	-99.6735	-13.24	91.89
2.002616	F4(F6)	9.3812	-99.6719	-12.24	90.53
Total		50.0004	-506.3258		485.27
N_3F,18	N1	7.3749	-55.0724	-376.07	81.17
-262.61272	N2	6.6315	-53.9522	326.87	100.91
2.002864	N3	6.5743	-53.9642	319.34	117.42
	F4	9.4192	-99.6217	19.26	97.98
Total		29.9999	-262.6105		387.46

[a] All values are in au except E_{rel}(Ω) which is in kcal mol^{-1}. Immediately below each molecule are listed the values of E_{SCF} and -V/T. E_{rel}(N), E_{rel}(H), E_{rel}(C), E_{rel}(O) and E_{rel}(F) are given relative to E(N) in N_2, E(H) in NH_3, E(C) in diazomethane, E(O) in N_2O and E(F) in N_2F_2 respectively.

4.2 PROPERTIES OF COMPOUNDS CONTAINING NN BONDS: BOND ENERGIES

Electron Population in the NN Interatomic Surface

The total amount of charge density in the AB interatomic surface N(A,B) (Table 4.2.1) is given by the expression

$$N(A,B) = \oint_{AB} dS\rho(\mathbf{r}) \qquad [4.2.1]$$

For shared interactions one expects N(A,B) to parallel ρ_b in its behaviour and this is the case for NN bonds. For example, in general N(N,N) increases as ρ_b (and therefore n) increases (Figure 4.2.1a). Further, like ρ_b, N(N,N) decreases as R_b increases. Slee (1986) has shown that N(A,B) can be approximated by Nm(A,B) where

$$Nm(A,B) = 2\pi\rho_b^2/(\lambda_1\lambda_2) \qquad [4.2.2]$$

This estimate underestimates the true value (Figure 4.2.1a) for NN and other bonds (Table 4.2.1) as molecular densities fall off exponentially (slower than Gaussian functions used in deriving equation 4.2.2) at long range. Still, Nm(A,B) reproduces trends in surface populations fairly well.

Bond Energies: Theory

The bond energy E(A,B) is defined to be an energy which when summed over each bond in the molecule yields the energy of atomization ΔE_a of the molecule.

For a free, isolated atom the form of the gradient vector field reflects the existence of a single centre of force - each trajectory

lies along a radial line and terminates at the nucleus. As two atoms approach each other, their $\nabla\rho$ fields become increasingly distorted as a result of the formation of an interatomic surface (Figure 1.2.4 for example). An operator which provides a direct measure of the distortion of the $\nabla\rho$ field of an atom from its radial form is obtained from the commutator of H and r^2, r being the radial distance of the electron from the nucleus. Starting with this commutator, an expression for the bond energy between atoms A and B, E(A,B) is derived (in au) (Bader and Wiberg 1987):

$$E(A,B) = \alpha R \cdot \oint dS \nabla\rho \, n_a / R^2 \qquad [4.2.3]$$

where α is a constant of proportionality, R is the vector linking the A and B nuclei, and n_a is a unit vector directed outward from A normal to the AB interatomic surface. Equation 4.2.3 does not take into account charge transfer between A and B. In the present work, various schemes to include this are tested. With this in mind, we define the following terms: In Table 4.2.1, Eu(A,B), the uncorrected bond energy is given by

$$Eu(A,B) = R \cdot \oint dS \nabla\rho \, n_a / R^2 \qquad [4.2.4]$$

The constant of proportionality is absent in this expression as is any effects to account for charge transfer. DSGN(A,B) is given by

$$DSGN(A,B) = \oint dS \nabla \cdot \sigma \cdot n_A \qquad [4.2.5]$$

where $\sigma \cdot n_A$ is the pressure (force/area) exerted on the surface element dS of atom A. This property of the interatomic surface (absolute values given in Table 4.2.1) is noteworthy as only the surfaces with zero charge transfer across them have zero values for DSGN(A,B). The charge transfer from atom A to atom B, dq(A,B) is given by

$$dq(A,B) = |q(A) - q(B)| \qquad [4.2.6]$$

For most of the NN bonds studied here, dq(N,N) is zero or near zero. The first scheme used to calculate the bond energy is denoted E1(A,B) and

$$E1(A,B) = \alpha Eu(A,B) \qquad [4.2.7]$$

In this and the remaining two schemes, the α parameter for NN bonds is chosen such that the experimental bond energy of N_2 is reproduced. For CH bonds, the α value is taken from Bader and Wiberg (1987). For NH, NC, NO, and NF bonds it is chosen such that the experimental bond energies of NH_3, CN, N_2O_4, and N_2F_2 respectively are reproduced. In E2(A,B) charge transfer is incorporated in the following way:

$$E2(A,B) = \alpha\{Eu + R^2DSGN(A,B)\} \qquad [4.2.8]$$

where all the symbols have been previously defined. Finally, in E3(A,B) charge transfer is included in the following fashion:

$$E3(A,B) = \alpha\{Eu + q^2/(\pi R)\} \qquad [4.2.9]$$

The motive for the $q^2/(\pi R)$ term comes from diatomic studies of Bader and Wiberg (1987).

Bond Energies: Results

The results of the bond energies for the three schemes E1(A,B), E2(A,B) and E3(A,B) are given in Table 4.2.1 and the corresponding energies of atomization are given in Table 4.2.2. In general E3(A,B) performs slightly better than E1(A,B) (in terms of ΔE_a percent errors) and both these schemes perform much better than E2(A,B). Although E3(A,B) gives results closest to experiment, there are still substantial differences, the largest being for N_3H. Inclusion of

electron correlation might lower the error but it appears that a new scheme should be developed to include the effects of charge transfer.

We can still gain useful information by relating E3(A,B) to other properties of the bond. In general, E3(N,N) increases with N(N,N). Since N(N,N) increases with n and ρ_b so does E_3 and we conclude that as the value of ρ_b and n increases, so does the energy of the NN bond (Figure 4.2.1b). The equation of the line is

$$E3(N,N) = 78.246n + 11.283 \qquad [4.2.10]$$

Thus, if we know the experimental NN internuclear distance (which will be approximately equal to R_b in unstrained systems), we can calculate n from equation [4.1.2]. Then the bond energy can be calculated from equation [4.2.10]. E3(N,F) and E3(N,O) also increase as their corresponding ρ_b increase. This is not the case for NH and CH bonds but is for NO and strongly for NF.

Bond energies (E1(A,B)) for ethane and cyclopropane have been given previously (Bader and Wiberg 1987). E1(N,N) in hydrazine is 14 kcal mol^{-1} stronger than E1(C,C) in the isoelectronic ethane while E1(N,H) is 11 kcal mol^{-1} weaker than E1(C,H). E1(N,N) in N_3H_3 is 5 kcal mol^{-1} stronger than E1(C,C) in the isoelectronic cyclopropane while E1(N,H) is 15 kcal mol^{-1} weaker than E1(C,H). Thus NN bonds are stronger and NH bonds are weaker than the corresponding CC anc CH bonds respectively in the isoelectronic hydrocarbons.

Figure 4.2.1

Relationships between properties of the NN bond and the NN bond order.

a) Plot of the electron population in the NN interatomic surface, N(N,N), versus the NN bond order, n. Also included are the Nm(N,N) values calculated from equation 4.2.2. The correlation coefficient for N(N,N) vs n is 0.989 and for Nm(N,N) vs n it is 0.887.

b) Plot of the NN bond energy, E3(N,N) versus the NN bond order n. The correlation coefficient is 0.974.

a)

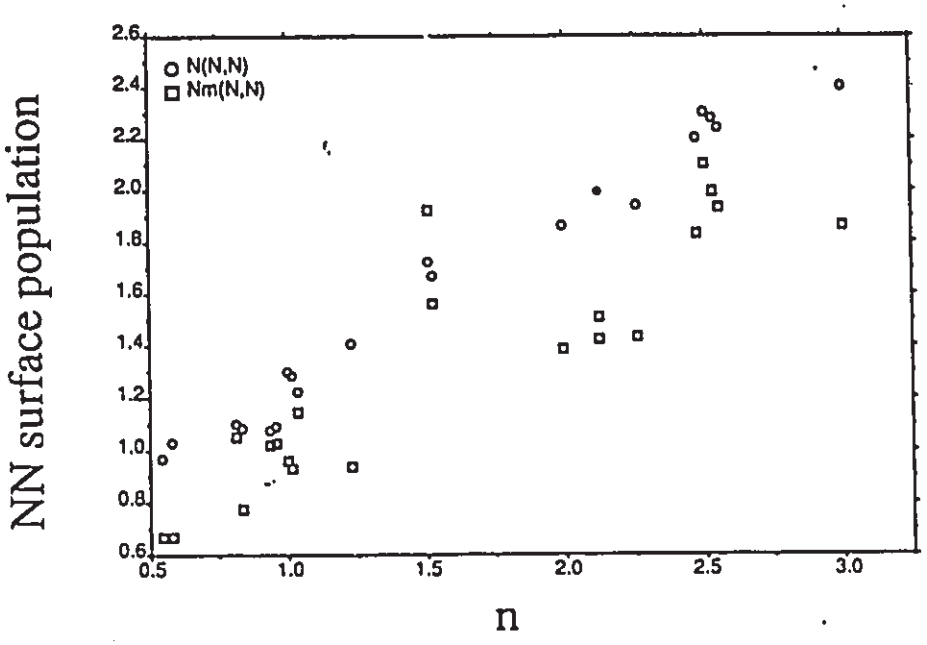
NN surface population
N(N,N)
Nm(N,N)
2.6
2.4
2.2
2.0
1.8
1.6
1.4
1.2
1.0
0.8
0.6
0.5
1.0
1.5
2.0
2.5
3.0
n

b)

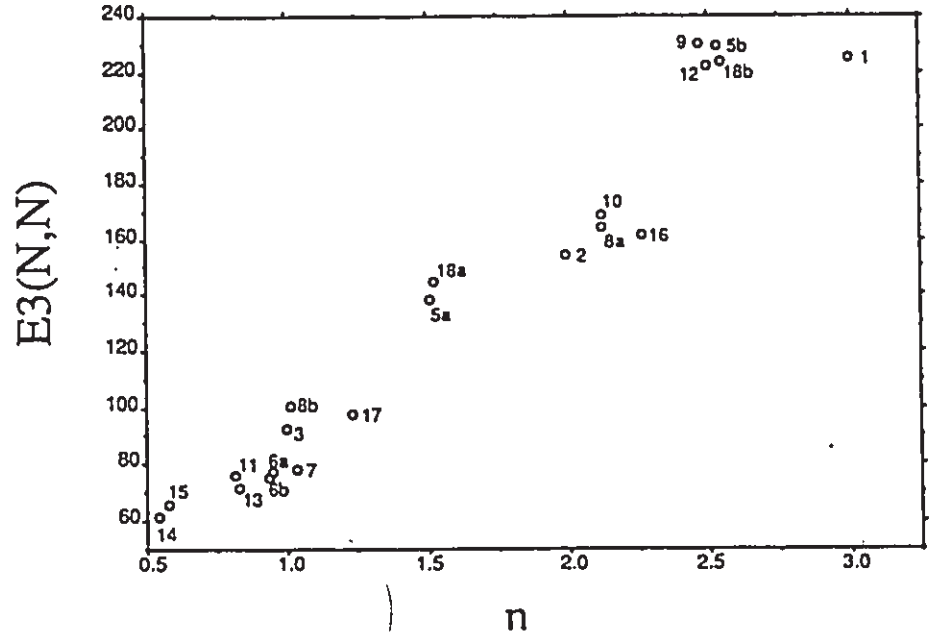
E3(N,N)
240
220
200
180
160
140
120
100
80
60
0.5
1.0
1.5
2.0
2.5
3.0
n
9
5b
12
18b
1
10
8a
16
2
18a
5a
8b
17
3
11
6a
7
15
13
6b
14

Table 4.2.1. Surface Integration Results for Compounds Containing NN Bonds.*

Species & bond	N(A,B) au	Nm(A,B) au	Eu(A,B) au	DSGN(A,B) au	dq(A,B) au	E1(A,B) kilocalories per mole	E2(A,B)	E3(A,B)
1 NN	2.4035	1.8628	1.1796	0.0000	0.0000	225.06	225.06	225.06
2 NN	1.8599	1.3867	0.8078	0.0003	0.0000	154.12	154.42	154.12
NH	0.8577	0.6039	0.4210	0.5845	0.3787	91.14	90.56	90.94
3 NN	1.2976	0.9589	0.4855	0.0000	0.0000	92.63	92.63	92.63
NH3	0.8787	0.6104	0.4312	0.6111	0.3966	93.35	91.99	93.57
NH4	0.8929	0.6219	0.4385	0.6182	0.3668	94.93	93.64	94.27
4 NH	0.8795	0.6099	0.4316	0.6203	0.3887	93.43	93.43	93.43
5 N1N2	1.7228	1.9238	0.7233	0.9263	0.0655	138.00	1109.94	138.11
N1N3	2.2743	1.9959	1.0924	2.7265	0.8405	208.42	2448.20	229.10
N2H4	0.8306	0.5796	0.4032	0.6110	0.4455	87.29	92.11	89.22
6 N1N2	1.0960	1.0305	0.4054	0.0021	0.0028	77.35	80.24	77.35
N2N3	1.0738	1.0262	0.3961	0.0000	0.0000	75.57	75.57	75.57
N1H4	0.8523	0.5954	0.4170	0.5821	0.4228	90.27	88.62	91.38
N2H5	0.8681	0.6064	0.4245	0.5946	0.3975	91.90	90.75	92.19
7 NN	1.2213	1.1441	0.4082	0.0000	0.0000	77.88	77.88	77.88
8 N1N2	1.8919	1.4200	0.8589	0.0001	0.0000	163.87	163.97	163.87
N1N3	1.2919	0.9284	0.4724	0.0270	0.6821	90.13	127.43	100.63
N3H5	0.8644	0.5984	0.4189	0.6032	0.4118	90.68	91.52	91.45
N3H6	0.8645	0.5983	0.4187	0.6031	0.4118	90.64	91.54	91.41
9 NN	2.1983	1.8332	1.0369	1.8586	1.0491	197.83	1771.06	223.57
NC	1.5432	1.2088	0.6250	1.5922	1.3480	128.06	114.60	140.94
CH	0.9945	0.7063	0.4702	0.0021	0.4810	104.94	106.85	113.08
10 NN	1.9946	1.5075	0.8823	0.0000	0.0000	168.34	168.34	168.34
NC	0.8669	0.9690	0.3040	0.6877	1.0855	62.29	63.93	71.74
CH	0.8916	0.7093	0.4709	0.0733	0.7424	105.10	172.52	124.38
11 NN	1.1008	1.0522	0.3995	0.0001	0.0000	76.22	76.37	76.22
NH	0.8718	0.6076	0.4258	0.6022	0.4013	92.18	91.35	92.58
NC	1.0606	0.9923	0.3795	0.8256	1.7359	77.76	73.62	119.81
CH	0.9925	0.7048	0.4698	0.0996	0.9381	104.85	196.90	135.57
12 NN	2.3002	2.0979	1.1144	3.1254	0.5589	212.62	2748.02	221.82
NO	1.7901	1.5460	0.7991	0.3950	1.3455	90.41	57.46	63.62
13 NN	1.0871	0.7797	0.3759	0.0000	0.0000	71.72	71.72	71.72
NO	1.9587	1.4541	0.8878	1.6326	1.0170	100.44	179.78	62.50
14 NN	0.9724	0.6680	0.3208	0.0674	0.0896	61.21	177.71	61.37
N2O3	2.0789	1.5133	0.9414	2.1089	2.1845	106.52	219.29	99.46
N1O5	1.9266	1.4692	0.8434	0.7843	2.2899	95.44	97.98	95.95
N1O4	1.8736	1.4584	0.8349	0.7587	2.2842	94.47	95.43	95.14
15 NN	1.0315	0.6697	0.3438	0.0000	0.0000	65.59	65.59	65.59
NO	1.9612	1.5187	0.8629	0.7902	2.2931	97.64	97.63	97.64
16 NN	1.9409	1.4286	0.8466	0.0001	0.0000	161.53	161.62	161.53
NF	1.2316	0.9287	0.4772	0.7455	2.7978	41.57	41.56	41.56
17 NN	1.4081	0.9368	0.5116	0.0002	0.0000	97.61	97.88	97.61
N1F3	1.3076	0.9305	0.4965	0.7422	3.1412	43.25	41.30	49.52
N1F4	1.3238	0.9251	0.4914	0.7246	3.1423	42.81	40.62	49.29
18 N1N2	1.6654	1.5652	0.6853	0.8072	0.7444	130.75	996.61	144.94
N1N3	2.2416	1.9290	1.0735	2.4455	0.8007	204.82	2216.48	223.57
N2F4	1.1577	0.8900	0.4326	0.6013	0.7877	37.68	36.02	14.45

Table 4.2.1 (con'd)

* The symbols are defined in the text. The α value in all schemes for NN and CH bonds are 0.30405 and 0.35566 respectively. The α values in E1, E2 and E3 for NH bonds are 0.34498, 0.05625 and 0.32578 respectively. For NO bonds they are 0.18030, 0.03311 and 0.09589, for NF bonds they are 0.13860, 0.01260 and 0.04532 and for NC bonds they are 0.32653, 0.01825 and 0.26019 respectively.

Table 4.2.2. Atomization Energies of Compounds Containing NN Bonds.[a]

Species	Atomization Energy (kcal mol^{-1})				percent errors		
	$\Delta E1_a$	$\Delta E2_a$	$\Delta E3_a$	ΔE_a^o	$\Delta E1_a$	$\Delta E2_a$	$\Delta E3_a$
N_2,1	225.06	225.06	225.06	225.06	0.0	0.0	0.0
N_2H_2,2	336.40	335.54	336.00	275.98	21.9	21.6	21.7
N_2H_4,3	469.18	463.89	468.31	405.45	15.7	14.4	15.5
NH_3,4	280.30	280.30	280.30	280.30	0.0	0.0	0.0
N_3H,5	433.71	3650.25	456.43	317.45	36.6	1048.9	43.8
N_3H_3,6	504.33	506.16	506.03				
N_4,7	311.53	311.53	311.53				
N_4H_4,8	706.78	784.95	730.84				
H_2CN_2,9	535.77	2099.36	596.67				
H_2CN_2,10	503.12	641.24	560.58				
H_4CN_2,11	625.80	800.11	772.14				
N_2O,12	303.04	2805.48	285.44	263.72	14.9	963.8	8.2
N_2O_2,13	272.60	431.28	196.72				
N_2O_3,14	357.63	590.41	351.92	380.21	-5.9	55.3	-7.4
N_2O_4,15	456.16	456.13	456.14	456.12	0.0	0.0	0.0
N_2F_2,16	244.66	244.75	244.65	244.65	0.0	0.0	0.0
N_2F_4,17	269.72	261.71	295.23	301.79	-10.6	-13.3	-2.2
N_3F,18	373.25	3249.11	382.96				

[a] Experimental atomization energies, ΔE_a^o are taken from Greenwood and Earnshaw 1984.

CHAPTER 5

CORRELATION ENERGIES OF ATOMS IN MOLECULES

In Chapters 2 and 3, an MP2 treatment was used to incorporate electron correlation. There are a variety of other post-SCF methods (Hehre et al 1986). In this chapter we use an alternative approach, that of density functional theory (DFT), to account for electron correlation. In Section 5.1 the reliabilities of five current local and nonlocal spin density correlation energy functionals are tested for diatomic molecules. The theory of atoms in molecules allows for an atomic correlation energy to be obtained and the resulting values are examined. In Section 5.2 we use the most reliable correlation energy functional to further explore the correlation energy and its transferability in hydrocarbons and to develop a scheme to account for the total energies of hydrocarbons.

5.1 DFT AND PERFORMANCE TESTS OF CORRELATION ENERGY FUNCTIONALS

Density functional methods have been used to calculate the total energies of atoms and molecules, as well as ionization energies, electron affinities, and molecular dissociation energies (see, for eg, the books edited by Erdahl and Smith 1986, Dreizler and da Providencia 1985, Avery and Dahl 1984). The exchange-correlation and correlation energy functionals needed for the calculation of exact ground-state energies and densities unfortunately are unknown. Local spin-density approximations (LSDA) (Kohn and Sham 1965, von Barth and Hedin 1972, Gunnarsson and Lundqvist 1976) including self-interaction corrections (Stoll et al 1978, Vosko and Wilk 1983), and gradient corrections (Langreth and Perdew 1980, Langreth and Mehl 1983) including recently developed spin-polarized versions (Hu and Langreth 1985,1986, Perdew 1986) are employed in this work in a study of the correlation part of the exchange-correlation energy functional while the exchange part is treated exactly by use of the Hartree-Fock (HF) method.

The reliability of five correlation energy functionals $E_c[\rho_\uparrow,\rho_\downarrow]$ is tested for the calculation of the correlation energy E_c for first-, second- and third-row atoms and for the calculation of E_c and the dissociation energy D_e of diatomic molecules constructed from these atoms. Energy functionals are denoted by enclosing their variables in square brackets to distinguish them from energy values. The functionals are as follows: A) The standard LSDA proposed by Kohn and Sham (1965). B) and C) LSDA with the self-interaction correction

proposed by Stoll et al (SPP) (1978) and Vosko and Wilk (VW) (1983) respectively. D) and E) Gradient corrected forms proposed by Langreth, Mehl, Perdew and Hu (1980,1983,1985) and by Perdew (1986) respectively. It is important to emphasize that both Schemes D and E accomodate spin-polarized systems. Thus, correlation and dissociation energies can now be calculated using these schemes regardless of the spin-polarizations (multiplicities) of the molecule and its separated atoms. This is an advance from what has been done in the past in which gradient corrected functionals could only give energy results for spin-compensated systems (Savin et al 1984). One can now examine a much broader cross-section of systems and discuss various trends across complete series of molecules (as is done in the present work for the second- and third-row hydrides, for example). The utility of the gradient corrected spin-polarized schemes is most evident in determining energy differences where there is potential for cancellation of errors. The tabulated results indicate that D and E are the most reliable of the five schemes (with Scheme D slightly better) for the determination of both E_e and D_e.

Molecular correlation energies have been calculated previously using both local and nonlocal correlation functionals with Hartree-Fock exchange for second-row hydrides (LiH - FH) and the corresponding homonuclear diatomics (Savin et al 1983,1984,1986, Kemister and Nordholm 1985). These workers used state functions constructed from Gaussian basis sets. In the present work results are presented for the atoms hydrogen to argon using the state functions of Clementi and Roetti (1974), and for diatomic hydrides, halides, oxides and nitrides

of both second- and third-row atoms, using near Hartree-Fock quality state functions constructed from large Slater basis sets (Cade and Huo 1973,1974,1975, McLean and Yoshimine 1968). The change in the correlation energy of an atom on forming a molecule is determined using the theory of atoms in molecules. This partitioning of the correlation energy enables one to determine how similar the correlation energy of the fluorine atom in LiF is to that in an isolated fluoride ion for example, and to determine the extent to which atomic correlation energies are transferable betweeen molecules.

The correlation energy E_c is defined (Wigner 1934, Löwdin 1959, Clementi 1963) as the difference between the exact non-relativistic ground state energy E and the corresponding Hartree-Fock energy E_{HF},

$$E_c = E - E_{HF} \qquad [5.1.1]$$

This definition fits naturally into density functional theory (DFT) as shown by the following discussion. According to the Hohenberg-Kohn theorems (1964) the ground state energy for a system of interacting electrons in the presence of a local spin-dependant potential $v^\sigma(r)$ is a functional of the spin densities $\rho_\sigma(r)$ ($\sigma=\uparrow/\downarrow$ for spin up/down densities respectively). The correct $\rho_\sigma(r)$'s minimize the functional $E_v[\rho\uparrow,\rho\downarrow]$ according to

$$\delta E_v[\rho\uparrow,\rho\downarrow]/\delta\rho_\sigma(r) - \mu_\sigma = 0 \qquad [5.1.2a]$$

where μ_σ are Lagrange multipliers arising from the constraints

$$N\sigma = \int dr\rho_\sigma(r) \qquad [5.1.2b]$$

With the correct spin densities $\rho_\sigma(r)$ as obtained from equation [5.1.2], $E = E_v[\rho\uparrow,\rho\downarrow]$. The Hohenberg-Kohn theorems are also applicable to the corresponding Hartree-Fock ground state whose energy

functional is denoted by $E_v^{HF}[\rho_\uparrow,\rho_\downarrow]$ where the correct spin densities are obtained by the analogue to equation [5.1.2] and denoted by $\rho_\sigma^{HF}(r)$. Thus, in agreement with equation [5.1.2],

$$E_c = E_v[\rho_\uparrow,\rho_\downarrow] - E_v^{HF}[\rho_\uparrow^{HF},\rho_\downarrow^{HF}] \qquad [5.1.3]$$

The above energy functionals are usually written as

$$E_v[\rho_\uparrow,\rho_\downarrow] = \Sigma_\sigma \int dr v^\sigma(r)\rho_\sigma(r) + F[\rho_\uparrow,\rho_\downarrow] \qquad [5.1.4a]$$

$$E_v^{HF}[\rho_\uparrow,\rho_\downarrow] = \Sigma_\sigma \int dr v^\sigma(r)\rho_\sigma(r) + F^{HF}[\rho_\uparrow,\rho_\downarrow] \qquad [5.1.4b]$$

where $F[\rho_\uparrow,\rho_\downarrow]$ and $F^{HF}[\rho_\uparrow,\rho_\downarrow]$ are the exact and the Hartree-Fock universal energy functionals of the sum of the kinetic and electron-electron interaction energies respectively, neither of which is known. However, $\rho_\sigma^{HF}(r)$ and E_{HF} can be obtained by a direct solution of the standard Hartree-Fock equations. Thus, if $F[\rho_\uparrow,\rho_\downarrow]$ is written as

$$F[\rho_\uparrow,\rho_\downarrow] = F^{HF}[\rho_\uparrow,\rho_\downarrow] + E_c[\rho_\uparrow,\rho_\downarrow] \qquad [5.1.5]$$

then for a given choice for $E_c[\rho_\uparrow,\rho_\downarrow]$ (i.e. its explicit $\rho_\sigma(r)$ dependence) the corresponding $\rho_\sigma(r)$ can be found. Substituting equation [5.1.5] into equation [5.1.2] and equation [5.1.4] gives

$$v^\sigma(r) + \delta F^{HF}[\rho_\uparrow,\rho_\downarrow]/\delta\rho_\sigma(r) + v_c^\sigma[\rho_\uparrow,\rho_\downarrow;r] - \mu_\sigma = 0 \qquad [5.1.6a]$$

where

$$v_c^\sigma[\rho_\uparrow,\rho_\downarrow;r] = \delta E_c[\rho_\uparrow,\rho_\downarrow]/\delta\rho_\sigma(r) \qquad [5.1.6b]$$

which is precisely the same as the Hartree-Fock problem with the "effective external potential" $v^\sigma(r) + v_c^\sigma[\rho_\uparrow,\rho_\downarrow;r]$. Thus it can be solved by standard methods to obtain the $\rho_\sigma(r)$ corresponding to a particular choice for $E_c[\rho_\uparrow,\rho_\downarrow]$ and the value of $E = E_v[\rho_\uparrow,\rho_\downarrow]$.

This work is only concerned with obtaining fairly accurate estimates of E_c corresponding to various choices for $E_c[\rho_\uparrow,\rho_\downarrow]$ (in

particular, we are not concerned with the effect of $E_c[\rho_\uparrow,\rho_\downarrow]$ on the spin densities). Because of the variational principle (equation [5.1.2]) it is sufficient to use the Hartree-Fock spin densities directly in $E_c[\rho_\uparrow,\rho_\downarrow]$ to evaluate E_c, i.e. E_c equals $E_c[\rho_\uparrow^{HF},\rho_\downarrow^{HF}]$ to within ~0.001 au which is sufficient for our purposes (Vosko and Wilk 1983, Stoll and Savin 1985, Kemister and Nordholm 1985). This difference can be seen to arise from the second and higher order spin density differences by making a functional Taylor Series expansion of $E_v[\rho_\sim^{HF},\rho_v^{HF}]$ about the correct spin densities $\rho_\sigma(r)$. Investigations of other possible uses of the Hartree-Fock density in DFT have recently been performed (Harris and Pratt 1985).

In the LSDA

$$E_c[\rho_\uparrow,\rho_\downarrow] = \int dr \rho(r)\epsilon_c(\rho_\uparrow,\rho_\downarrow) \qquad [5.1.7]$$

where $\epsilon_c(\rho_\uparrow(r),\rho_\downarrow(r))$ is the correlation energy per electron of a homogeneous electron liquid with spin densities $\rho_\sigma(r)$. In Schemes A, B, and C, $\epsilon_c(\rho_\uparrow,\rho_\downarrow)$ is calculated using the Vosko, Wilk, and Nusair (VWN) (1980) Padé interpolation of the low density ($r_s \geq 10$) Ceperley and Alder Monte Carlo data (1980) to the exact high density values (see Appendix 5.1). The LSDA (Scheme A) has been somewhat successful for the calculation of energy changes in atoms, molecules and solids in spite of the fact that the magnitude of the correlation energy itself is overestimated by a factor of two or more (see for e.g. Savin et al 1986). In any finite system, there is an unphysical self-correlation term which one would like to remove. In this work, methods to remove this are explored. SPP (1978) have proposed the following functional (Scheme B) in which the parallel-spin correlation energy is subtracted

from equation [5.1.7]:

$$E_c[\rho_\uparrow,\rho_\downarrow] = \int dr\rho(r)\epsilon_c(\rho_\uparrow,\rho_\downarrow) - \int dr\rho_\uparrow(r)\epsilon_c(\rho_\uparrow,0) - \int dr\rho_\downarrow(r)\epsilon_c(0,\rho_\downarrow) \qquad [5.1.8]$$

Scheme B gives more physically meaningful results than Scheme A. For example, the hydrogen atom (N = 1) has a correlation energy of zero in B but not in A (where it is about -0.02 au) (Savin et al 1986). Further, the energy differences, D_e, are better modelled by B in most cases. However, the complete removal of parallel-spin correlations as done in equation [5.1.8] causes E_c to be too small. A more serious drawback is that B does not collapse into A as $N \longrightarrow \infty$ for slowly varying densities.

Motivated by the inadequacy of B, Vosko and Wilk (1983) have proposed a correlation functional (Scheme C) in which $E_c = 0$ for $N = 1$ and is exact for slowly varying densities with $N \longrightarrow \infty$. They have incorporated the spin-up and spin-down electron populations, N^ and Nv, of a free atom as follows:

$$E_c[\rho_\uparrow,\rho_\downarrow] = \int dr\rho(r)\epsilon_c(\rho_\uparrow,\rho_\downarrow) - \{\int dr\rho_\uparrow(r)\epsilon_c(\rho_\uparrow(r)/N\uparrow,0) + \int dr\rho_\downarrow(r)\epsilon_c(0,\rho_\downarrow(r)/N\downarrow)\} \qquad [5.1.8]$$

where the second and third terms on the right hand side remove the self-correlation of the spin-up or spin-down electron distribution, each of density $\rho_\uparrow(r)/N\uparrow$ or $\rho_\downarrow(r)/N\downarrow$. The $N\uparrow$ (or $N\downarrow$) $\longrightarrow \infty$ limit is satisfied here as the second and third terms on the right hand side of equation [5.1.9] will then both vanish collapsing equation [5.1.9] into equation [5.1.7].

There is a question as to how to extend equation [5.1.8] to

molecules. In the present work the theory of atoms in molecules is used to allow for integrations over atoms in molecules:

$$E_c[\rho_\uparrow,\rho_\downarrow] = \int dr \rho(r)\epsilon_c(\rho_\uparrow,\rho_\downarrow) -$$

$$\Sigma_\Omega\{\int_\Omega dr \rho_\uparrow(r)\epsilon_c(\rho_\uparrow(r)/N_\uparrow(\Omega),0) + \int_\Omega dr \rho_\downarrow(r)\epsilon_c(0,\rho_\downarrow(r)/N_\downarrow(\Omega))\} \qquad [5.1.10]$$

where the spin-up electron population, spin-down electron population, and total electron population of atom Ω are

$$N_\uparrow(\Omega) = \int_\Omega dr \rho_\uparrow(r)$$

$$N_\downarrow(\Omega) = \int_\Omega dr \rho_\downarrow(r)$$

$$N(\Omega) = N_\uparrow(\Omega) + N_\downarrow(\Omega) \qquad [5.1.11]$$

Although this work demonstrates that Scheme B is more reliable than C in determining E_c and D_e, previously C has been shown to be superior in ionization energy and electron affinity calculations (Vosko and Wilk 1983).

One must remember that atoms and molecules do not have slowly varying densities nor are their electron densities uniform. To inject more realism into the LSDA, density gradient corrections to the correlation energy functional must be included. Langreth, Perdew, Mehl, and Hu, (1980,1983,1985) use a wave-vector decomposition to develop the following gradient corrected functional (Scheme D):

$$E_c[\rho_\uparrow,\rho_\downarrow] = \int dr \rho(r)\epsilon_c^{RPA}(\rho_\uparrow(r),\rho_\downarrow(r))$$

$$+ a\int dr\{|\nabla\rho|^2\rho^{-4/3}[(\rho_\uparrow/\rho)^{5/3} + (\rho_\downarrow/\rho)^{5/3}]^{-1/2}\exp(-b|\nabla\rho|\rho^{-7/8})\}$$

$$+9af^2\int dr|(|\nabla\rho_\uparrow|^2\rho_\uparrow^{-4/3} + |\nabla\rho_\downarrow|^2\rho_\downarrow^{-4/3}) \qquad [5.1.12]$$

where $a = \pi/[4(6\pi^2)^{4/3}]$, $b = (9\pi)^{1/8}f$, and the cutoff parameter $f = 0.17$. The nonlocal part of equation [5.1.12] has been calculated using the random phase approximation (Bohm and Pines 1952, von Barth and

Hedin 1972) (RPA-see Appendix 5.1) and, therefore, so must the local part of equation [5.1.12].

Recently, Perdew (1986) has developed another gradient corrected correlation functional (Scheme E):

$$E_c[\rho_\uparrow,\rho_\downarrow] = \int d\mathbf{r}\rho(\mathbf{r})\epsilon_c^{PZ}(\rho_\uparrow,\rho_\downarrow) + \int d\mathbf{r} d^{-1}e^{-\Phi}C(\rho)|\nabla\rho|^2\rho^{-4/3} \qquad [5.1.13]$$

where ϵ_c^{PZ} is the correlation energy per electron using the Perdew-Zunger parametrization (1981) of the Ceperley-Alder results (1980) (see Appendix 5.1)

$$d = 2^{1/3}[\{(1+\zeta)/2\}^{5/3} + \{(1-\zeta)/2\}^{5/3}]^{1/2} \qquad [5.1.14]$$

and the spin polarization

$$\zeta = (\rho_\uparrow-\rho_\downarrow)/\rho \qquad [5.1.15]$$

$C(\rho)$, the beyond-RPA gradient coefficient, is given by

$$C(\rho) = 0.001667 +$$

$$(0.002568+0.023266r_s+7.389\times10^{-6}r_s^2)/(1+8.723r_s+0.472r_s^2+7.389\times10^{-2}r_s^3) \qquad [5.1.16]$$

where the electron gas parameter

$$r_s = (3/(4\pi\rho))^{1/3} \qquad [5.1.17]$$

and

$$\Phi = 1.745f[C(\infty)/C(\rho)]|\nabla\rho|\rho^{-7/6} \qquad [5.1.18]$$

where the cutoff parameter $f = 0.11$ is chosen to fit the exact correlation energy of the neon atom (Veillard and Clementi 1968), and $C(\infty)=0.004235$ from equation [5.1.16]

Perdew's motivation to develop equation [5.1.13] is twofold: 1) In deriving equation [5.1.12] he claims that a somewhat artificial

separation of exchange and correlation has been performed with the $9f^2$ term arising from a piece of the gradient expansion for the exchange energy, whereas equation [5.1.13] makes the natural separation of exchange and correlation. 2) Equation [5.1.12] does not go beyond the RPA but equation [5.1.13] does.

Results for Atomic and Molecular Correlation Energies

i) Atoms

Values of E_c for the atoms H-Ar are compiled in Table 5.1.1. Two columns are included for the exact values. The first of these does not take the Lamb Shift correction into account, while the second one does. The Lamb shift corrections calculated by Veillard and Clementi (1968) while properly reported in their Table IX, were improperly combined with the values listed as EC(1) in their Table X. The "exact" E_c values reported here differ from those given by these authors by twice the value of the calculated Lamb shift. At the present time, calculated Lamb Shifts have only an indicative value and these corrections give only an order of magnitude estimate (Grant 1985, Mohr 1985, Ermolaev 1985). In view of these considerations, the remainder of this thesis deals only with exact values calculated without the Lamb Shift correction. It is seen that Scheme A overestimates the magnitude of E_c by a factor of ~3 for the lighter atoms and this factor decreases to ~2 for the heavier atoms. Scheme B gives much better agreement with the exact results but the magnitudes still are consistently too high. The values in Scheme C are sandwiched between those of A and B, being in better agreement with exact values than A

but worse than B. Scheme D provides the best agreement with exact values with a mean deviation of only 0.007 au. The magnitudes of E_c in Scheme E consistently overestimate exact values and though the agreement with experiment is better than A and C, it is worse than B and D.

The errors in E_c, defined as the exact minus the calculated values, are shown in Figure 5.1.1. So as to not obscure the details of Schemes B to E, the results of Scheme A are not plotted (the errors in E_c in Scheme A are the largest and increase fairly linearly with atomic number). The errors are greater for the third-row atoms.

ii) Molecules

Values of E_c using the five schemes for second- and third-row diatomic hydrides, second-row homonuclear diatomics and some second- and third-row diatomic fluorides, oxides, nitrides and chlorides are compiled in Table 5.1.2. In addition to the molecular correlation energy, the correlation energy of each atom in a molecule are also listed. The exact value of the correlation energy for molecule AB, $E_c(AB)$, is calculated as follows:

$$E_c(AB)=E(A)+E(B)+D_e(AB)-E_{HF}(AB)-E_{rel}(A)-E_{rel}(B) \qquad [5.1.19]$$

where E(A) and E(B) are the experimental energies of the separated atoms (Veillard and Clementi 1968), D_e is the experimental dissociation energy (Huber and Herzberg 1979), E_{HF} is the energy in the Hartree-Fock limit of AB (Cade and Huo 1973,1974,1975, Mclean and Yoshimine 1968), and $E_{rel}(A)$ and $E_{rel}(B)$ are relativistic energies of the separated atoms (Veillard and Clementi 1968). We assume that the self-consistent-field state functions generated by Cade and Huo

(1973,1974,1975) and McLean and Yoshimine (1968) yield the Hartree-Fock limit energies. This assumption is nearly correct for the second-row hydrides and homonuclear diatomics, but it is more approximate for the remainder of the molecules studied. The relativistic corrections for the atoms are assumed to be unchanged for the molecule. Figures 5.1.2a-5.1.2e display the errors in E_e. The mean deviation in E_e for all the 39 molecules studied is 0.470, 0.035, 0.075, 0.028, and 0.036 au for Schemes A to E respectively.

Just as with the atoms, the magnitudes of E_e calculated using Scheme A for the second-row hydrides consistently overestimate the exact values. An improvement occurs when B is used but C again gives worse values than B. Scheme D gives more reliable results than B, and E gives even slightly better results than D. Results of the third-row hydrides are similar to those of the second-row hydrides except that here Scheme D is much more reliable than E (the mean deviation in D is only half that of E).

As with the above two series, the magnitudes of E_e calculated using Scheme A for the second-row homonuclear diatomics consistently overestimate the exact values while an improvement is obtained using B. However, here Scheme C gives even better results than B, D, and E whereas in the above two series C ranked second worst in terms of mean deviation. Each of the five schemes gives its largest error for the molecule C_2.

The results for the diatomic fluorides are similar to the third-row hydrides but here Scheme D is only slightly more reliable than E. In these latter two schemes, OF and AlF exhibit the largest

errors.

The results for the diatomic oxides are similar to those for the fluorides but the mean deviations in D and E are about twice those of the fluorides. The molecules BeO and its third-row analogue MgO exhibit the largest errors in the latter two schemes.

The results for the diatomic nitrides and chlorides are similar to those of the oxides. The error in CN is ~3 times that of PN in the latter two schemes D and E. The error for NaCl is slightly larger than that for LiCl in the same two schemes.

Dissociation Energies (D_e)

Although E_c comparisons are informative, energy differences are chemically more interesting. It is also hoped that errors present in the DFT schemes may cancel when taking differences. The calculated dissociation energies of all of the above molecules are compiled in Table 5.1.3. They are calculated for each scheme using the following expression:

$$D_e(AB)=E_{HF}(A)+E_c(A)+E_{HF}(B)+E_c(B)-E_{HF}(AB)-E_c(AB) \quad [5.1.20]$$

where $E_{HF}(A)$, $E_{HF}(B)$, and $E_{HF}(AB)$ are the Hartree-Fock energies of the separated atoms and the molecule (Clementi and Roetti 1974, Cade and Huo 1973,1974,1975, McLean and Yoshimine 1968), and $E_c(A)$, $E_c(B)$, and $E_c(AB)$ are the corresponding correlation energies calculated using a particular scheme. Relativistic effects are assumed to cancel in taking energy differences. The errors in D_e are displayed in Figures 5.1.3a-5.1.3e. The mean deviation in D_e from experiment for all 39 molecules studied is 2.20 eV for the Hartree-Fock method and 1.22,

1.35, 1.38, 0.69, and 1.00 eV for schemes A to E respectively and hence all five schemes improve on the HF results.

Scheme D gives results about twice as good as those given by A, B, and C, and about one and one-half times as good as those given by E for the second-row hydrides. All schemes consistently overestimate D_e for BeH and underestimate it for FH. For BeH the Hartree-Fock result is correct implying that the correlation energy of the separated atoms is identical to that in the molecule. This result is accounted for in the Discussion section. The smallest spread in values of the five schemes occurs for CH. Only Scheme D reflects the experimental trend of increasing D_e from BH to CH.

For the third-row hydrides, Scheme E gives the best results and, next to Hartree-Fock, D gives the worst results in terms of mean deviation. No general trends between the five schemes are observed. The smallest spread in values of the five schemes occurs for SiH, the third-row analogue of CH. Only Schemes D and E correctly reflect the experimental trends in D_e.

Scheme A gives better results for the second-row homonuclear diatomics than B and C but it is not as good as E or D. Even though D gives the most reliable results, the mean deviation (1.37 eV) is substantial. The largest errors in all five schemes are exhibited by C_2. It should be noted that Hartree-Fock predicts the energies of the terms $^3\Sigma_g^-$, $^1\Delta_g$ and $^1\Sigma_g^+$ arising from the excited configuration $\ldots 1\pi_u^2 3\sigma_g^2$ to lie lower in energy than the experimental ground state $^1\Sigma_g^+$ arising from the configuration $\ldots 1\pi_u^4$. Clearly, the Hartree-Fock single determinant approximation to the ground state is inadequate for

C_2 and both $^1\Sigma_g^+$ states should be mixed to obtain a minimal description of the charge density for the ground state of this molecule. The smallest spread in values of the five schemes occurs for H_2. It is important to note from the tabulated values in Table 5.1.3 that the dissociation energy of F_2 is predicted to be negative by all five schemes. A simple two-state mixing ($3\sigma_g^2 \rightarrow 3\sigma_u^2$) that takes "left-right" correlation into account, increases D_e by 2 ev and gives it a positive value (Das and Wahl 1966). As for C_2, the Hartree-Fock single determinant state function for F_2 gives an inadequate description of the ground state. It is possible that a spin-unrestricted Hartree-Fock wavefunction may yield positive D_e's for the schemes studied.

The results for the diatomic fluorides, oxides and nitrides are similar to those for the second-row homonuclear diatomics in that Scheme D gives the best overall results. The mean deviations in the dissociation energy are however, considerably less for the fluorides and oxides than for the homonuclear diatomics and in Scheme D, the errors are approximately half of those in Scheme E. The open-shell systems NF and OF exhibit the largest errors of the fluorides with schemes B and C yielding negative values for the dissociation energy of OF. The smallest spread in values of D_e for the fluorides occurs for NaF and none of the schemes predict the experimental trend of decreasing D_e values from LiF to BeF. Just as with the total correlation energies, schemes D and E exhibit their largest errors among the diatomic oxides for the closed-shell systems BeO and MgO. The Hartree-Fock dissociation energy and those predicted by schemes A

to C are negative for MgO. The smallest spread in values of the five schemes occurs for LiO. Only schemes D and E correctly reflect the experimental trend in the values of D_e.

For the two diatomic chlorides, Scheme A gives better agreement with experiment than do schemes B, C, and D. Scheme E however, gives the most reliable results with a mean deviation of only 0.04 ev.

Discussion

The above results show that the gradient corrected functional, Scheme D, is the most reliable for the calculation of both the correlation and dissociation energies. Thus, the results obtained using Scheme D are used in the Discussion.

The Discussion concentrates on $E_c(\Omega)$, the contribution of atom Ω to the molecular correlation energy, to obtain an increased understanding of the variations in E_c through each series of molecules. These values, listed in Tables 5.1.2, are obtained by integrating the Scheme D functional of the charge density over the atomic basins.

In principle, one should be able to account for the variations in E_c using only the variables of DFT, ρ, $\rho_\uparrow$ and $\rho_\downarrow$ as recently exemplified in a study of atomic ionization energies and electron affinities (Vosko and Lagowski 1986). However, generalization of this technique to predict variations in E_c for molecules is yet to be investigated and may prove to be difficult. Therefore, it is useful to consider other properties of atoms in molecules in an attempt to further our understanding of the results.

An important quantity in the analysis of the atomic contributions to the total correlation energy is the atomic average of the Fermi correlation. The exchange or Fermi correlation determines the extent to which some number of electrons are localized to a given region of space (Bader and Stephens 1974,1975, Bader et al 1988), and consequently, the extent to which their motions are correlated with the motions of the remaining electrons in the system. An electron has a "shadow", its Fermi hole. The electron can travel only where its Fermi hole travels. If the Fermi hole is localized, then so is the electron.

For single-determinantal state functions (used in this chapter), the degree of localization of some number of electrons in Ω within a molecule is determined as follows: Define a correlation function $f(\mathbf{r}_1,\mathbf{r}_2)$ in an expression which determines the extent to which the pair density deviates from a simple product of number densities (McWeeny 1960)

$$D_2(\mathbf{r}_1,\mathbf{r}_2) = D_1(\mathbf{r}_1)D_1(\mathbf{r}_2)[1 + f(\mathbf{r}_1,\mathbf{r}_2)] \qquad [5.1.21]$$

where a number density $D_1(\mathbf{r})$ (which equals $\rho(\mathbf{r})$) integrates to the total number of electrons N and the pair density integrates to the number of electron pairs N(N-1). The quantity $D_1(\mathbf{r}_2)f(\mathbf{r}_1,\mathbf{r}_2)$ is called the Fermi hole and is identical to Slater's average exchange charge density (Slater 1951). Its integral over the coordinate $\mathbf{r}_2$ equals -1 for any value of $\mathbf{r}_1$. Thus it corrects equation [5.1.21] for the improper counting of pairs and as pointed out by Slater, it corrects for the self-pairing of electrons of parallel spin and hence for the self-repulsion of the electrons in the Coulomb terms in the SCF potential.

For a density arising from a single-determinantal state function

$$F(\Omega) = \int_{\Omega} dr_1 \int_{\Omega} dr_2 D_1(r_1) D_1(r_2) f(r_1, r_2) \qquad [5.1.22]$$

is a measure of the total Fermi correlation associated with the motions of the electrons in the region of real space Ω. When Ω equals all space, the value of this integral is -N, the correction for the self-pairing of N electrons. Its limiting value for an atom in a molecule is $-N(\Omega)$. This limiting value corresponds to the Fermi hole of each electron being completely confined within Ω and hence to the complete localization of the $N(\Omega)$ electrons to Ω. In this limit there is no exchange of the electrons in Ω with those in the remainder of the molecule. The ratio $F(\Omega)/N(\Omega)$ is the fraction of the total possible Fermi correlation per particle and this ratio multiplied by 100 is $L(\Omega)$, the per cent localization of the electrons in Ω. When $F(\Omega)/N(\Omega)$ attains its limiting value of minus one, the probability of finding $N(\Omega)$ electrons in Ω is unity and all other probabilities are zero - the electrons are totally localized to Ω. Such complete localization is possible only for an isolated system. What is notable however, is the extent to which the electrons of both atoms in an ionic molecule approach this limit of perfect localization, with $L(\Omega)$ values in excess of 95% not being uncommon. For example, in lithium fluoride L(Li) = 95.5% and L(F) = 99.1%. In such ionic systems the zero flux surface minimizes the fluctuation in the atomic population, and so, the magnitude of the correlation hole per particle is an extremum for such atoms. Thus the correlation of the motions of the electrons within the atom is maximized while their correlative interactions with electrons

in neighbouring atoms is minimized. The observation that the interatomic correlation decreases with increasing localization of the Fermi hole is important in understanding the variations in the total correlation energies through series of molecules.

The diatomic hydrides AH are discussed first, Table 5.1.4. The atomic contributions to E_c(AH) are shown plotted in Figure 5.1.4a. The charge distribution of LiH has the appearance of a nearly spherical closed-shell Li^+ ion adjacent to a polarized hydride ion, a picture that is consistent with the net charges of ±0.91e and the large degree of localization of the Fermi correlation in both atoms. The distribution approaches that of two separately localized pairs of electrons. The magnitudes of E_c(H) and E_c(Li) are both slightly greater than the corresponding exact values (Pedroza 1986, Vosko and Lagowski 1986) for an isolated H^- (0.040 au) and Li^+ (0.044 au) ion, due in part to the contribution from the interpair correlation between the two atoms. (The small mean error in E_c for the atoms in Scheme D justifies these comparisons with exact values of E_c). The value of E_c(H) remains almost unchanged through to BH in spite of a small decrease in N(H). There is a concomitant decrease in L(H) and consequently an increase in interatomic correlation, sufficient to counteract the decrease in N(H).

More surprising at first glance is the relatively small increase in the magnitude of E_c(Be) compared to E_c(Li). The beryllium atom in BeH approaches Be^+ and has one valence electron outside of the $1s^2$ core. From the display of the charge distribution for this molecule, Figure 1.6.1, it is clear that the remaining valence density

on Be is strongly polarized into and separately localized in the nonbonded region of the Be atom. Thus there is little correlative interaction of this extra electron with either the core of Be or with the hydrogen distribution. The same is true of an isolated Be^+ ion, for which the exact value of E_c is -0.047 au (Vosko and Lagowski 1986), differing by only 0.003 au from that for Li^+. This model of the charge density and correlation energy for BeH accounts for the observation made earlier that the Hartree-Fock value for D_e is nearly exact, because the sum of the E_c values for Be^+ and H^- is almost the same as the correlation energy for the Be atom.

Past BH, the magnitude of $E_c(H)$ undergoes a monotonic decrease, paralleling the decrease in the population of H. Figure 5.1.4b shows that the variation in the magnitude of $E_c(H)$ with N(H) from its value in FH is nearly linear up to BH. The localization of the hydridic electrons is considerably greater for BeH and LiH and consequently there is a decrease in interpair correlation. Thus the magnitude of $E_c(H)$ decreases for these two members in spite of a further increase in N(H). One can also argue that the increase in $E_c(H)$ in LiH to BH is a result of an increasing contraction of the charge density in H assuming that the local contribution to E_c in equation [5.1.12] is the dominant one. The otherwise linear behaviour and the decreasing values of L(H) from CH to FH suggests that the motions of the electrons in hydrogen in these molecules are intimately correlated with the valence electrons of A. There is a sharp increase in the magnitude of E_c for the boron atom in BH as a consequence of B^+ possessing a $2s^2$ pair of electrons in addition to the $1s^2$ core. As with the single unpaired valence electron

on Be in BeH, the valence density on boron is strongly polarized into its nonbonded region, thereby reducing its correlative interactions with the electrons on H. The value of $E_o(B)$ is also very close in value to that for an isolated B^+ ion, for which E_o equals -0.111 au (Vosko and Lagowski 1986). Past BH, there is a monotonic increase in the magnitude of $E_o(A)$ which, because of the accompanying decrease in N(H), approaches the molecular value. The value of $E_o(F)$ is only slightly greater than the value for an isolated fluoride ion for which E_o equals -0.392 au (Vosko and Lagowski 1986). The charge distribution for HF approaches that of the united F^- ion perturbed by an imbedded proton.

The corresponding data for the third-row diatomic hydrides are displayed in Figures 5.1.5a and 5.1.5b. The overall behaviour parallels that found for the second-row. As with the second-row, the magnitude of $E_o(H)$ increases with N(H) until the localization of the electrons on hydrogen exceeds 80% as found in AlH, MgH and NaH.

Figure 5.1.6 shows a plot of $E_o(F)$ versus N(F) for the diatomic fluorides listed in Table 5.1.2. The net charges and localizations for the atoms in these molecules are listed in Table 5.1.5. The form of this plot is identical to that for the hydrogen in the diatomic hydrides. The magnitude of $E_o(F)$ increases in a nearly linear manner from its value in F_2 as a consequence of an increasing degree of charge transfer from its bonded neighbour until, at BF, the charge distribution of the fluorine atom approaches the limiting localized distribution of the fluoride ion. In the fluorides of Li, Na, Be, B and Al, fluorine has a nearly closed-shell structure as reflected in

its charge and localization which approach -1 and 100% respectively. The value of $E_c(F)$ in these systems is close to -0.392 au, the exact value for an isolated fluoride ion. At this limit, the magnitude of $E_c(F)$ decreases as the electrons on F become more localized and approach the situation of zero exchange with the electrons on the neighbouring atom. The importance of the localization in determining the atomic correlation may be seen by noting that the F atoms in LiF and NaF, which are both 98% localized, have identical values $E_c(F)$ in spite of a population spread of 0.07e.

From the L(F) values in Table 5.1.5, it is clear that the charge distribution of a bound fluorine atom is always strongly localized within the basin of the atom, as well as being tightly bound. While this behaviour leads to strong bonding where there is considerable charge transfer, it is the antithesis of that required for the formation of a strong bond in the shared or covalent limit. Thus the difficulty in disrupting the very pronounced intraatomic correlation in a flourine atom limits the interatom exchange and the pairing of electrons between the atoms, and provides an explanation of the weak binding in F_2. In the more tightly bound N_2 and C_2 molecules, the extent of intraatomic exchange is much greater as reflected in lower atomic localizations of 78 and 73% respectively.

Charges and atomic localizations are given in Table 5.1.6 for some diatomic oxides. The transfer of the single valence electron of Li is nearly complete in LiO. The resulting localization of the Li $1s^2$ core results in an extreme localization for the oxygen as well and as a consequence, the magnitude of $E_c(O)$ in LiO is less than that found in

NO for which the degree of charge transfer is considerably less. The magnitude of $E_c(O)$ for the oxides of B, Mg and Si is greater than 0.328 au, the exact value for an O^- ion (Vosko and Lagowski 1986). The net charges and localization values indicate however, that the oxygen in these ionic molecules does not approach its limiting closed-shell structure of O^{2-} as closely as H and F do their limiting singly-charged structures.

Table 5.1.7 compares the atomic and total correlation energies for the N = 12 isoelectronic series of molecules. The first three members are ionic and approach, to varying degrees, two closed-shell configurations of ten and two electrons. The atomic contributions from these two configurations to the total correlation energies in these molecules are very similar. There is a general decrease in the magnitude of E_c as the difference between the nuclear charges decreases, with the lowest value occurring for BN, the only open-shell system in the series.

Tables 5.1.8 and 5.1.9 list corresponding values for the N = 13 and N = 14 isoelectronic series. As in the diatomic hydrides, the Be atom in BeF has a correlation energy characteristic of the two-electron systems. The single remaining valence electron on Be is, as in BeH, very strongly polarized into the nonbonded region and its motions are separately localized from both the core on Be and the flourine atom distribution. The values of E_c exhibit less variation for the 13- and 14-electron series than they do for the 12-electron set of molecules. The magnitude of E_c per electron, the quantity $|E_c/N|$ equals 0.034, 0.035 and 0.036 for N = 12, 13 and 14 respectively suggesting that

$|E_e/N|$ increases with increasing N. Figure 5.1.7 shows that this is true for series from N = 10 to 18.

Summary

The predicted values of E_e and D_e for the 38 diatomic molecules are not of sufficient accuracy to be generally useful. Even the most reliable scheme, D, leaves considerable room for improvement. One is now faced with several options. One may continue to treat exchange exactly and search for more reliable correlation functionals or describe both exchange and correlation by functionals as was done originally by Kohn and Sham (1965) and more recently by Kitaura et al (1979), Becke (1986), and others. One would think that any method in which exchange was approximated would be less reliable than a method (Schemes A-E) in which exchange was treated exactly. Table 5.1.10 illustrates, however, that this is not the case. Becke has examined the second-row dimers using schemes similar to A and D except he has treated exchange and correlation both as density functionals (A_{xc} and D_{xc}) where the LSDA exchange functional is given as

$$E_x^{LSDA} = -(3/2)(3/(4\pi))^{1/3}\int dr(\rho\uparrow^{4/3} + \rho\downarrow^{4/3}) \qquad [5.1.23]$$

A_{xc} has a mean deviation almost twice as small as A and D_{xc} has a mean deviation almost three times as small as D.

However, the success of A_{xc} and D_{xc} rely on a very large cancellation of errors. For example, A_{xc} gives a D_e closer to experiment for N_2 than does Scheme A but the error in the N atom exchange energy calculated by equation [5.1.23] is over nineteen eV. When exchange is treated exactly as Hartree-Fock exchange (as in A),

the error in the N atom exchange energy is zero by definition. The huge cancellation of errors in the exchange-correlation (xc) schemes fortuitously yield accurate D_e's in many cases but no physical explanation can be given as to why this is so. In fact, approximate exchange functionals model long range potentials and anionic sytems poorly. Scheme A and Scheme D have the advantage of not relying on cancellation of errors in the exchange energy. Further, when exchange is treated exactly, the correlation functional is easily implemented into an SCF calculation. Kemister and Nordholm (1985) have done this for Scheme B and have solved the now modified SCF equations iteratively to obtain bondlength and energy data.

It remains to discuss why Scheme D performs better than Scheme E. It seems that Scheme D's somewhat artificial separation of exchange and correlation is adequate compared with the greater assumptions made in deriving equation [5.1.12]. Hu and Langreth (1985) have explored local beyond-RPA terms and have concluded that these terms represent a spurious self-interaction error which is removed when the nonlocal beyond-RPA terms are included as well. Scheme E does not make use of this information but, rather, crudely attempts to build in both local and nonlocal beyond-RPA terms with less than satisfying results.

Schemes D and E are the most reliable of the five correlation functionals surveyed. Density gradient corrections play a significant role in determining both total correlation energies and energy differences. The electron density is not uniform in an atom or molecule. Spin-polarized functionals which incorporate gradient corrections, therefore, are expected to give more reliable results for

atoms and molecules than LSDA approaches alone, and we have shown this to be the case.

Figure 5.1.1

Error in the atomic correlation energy for hydrogen to argon.

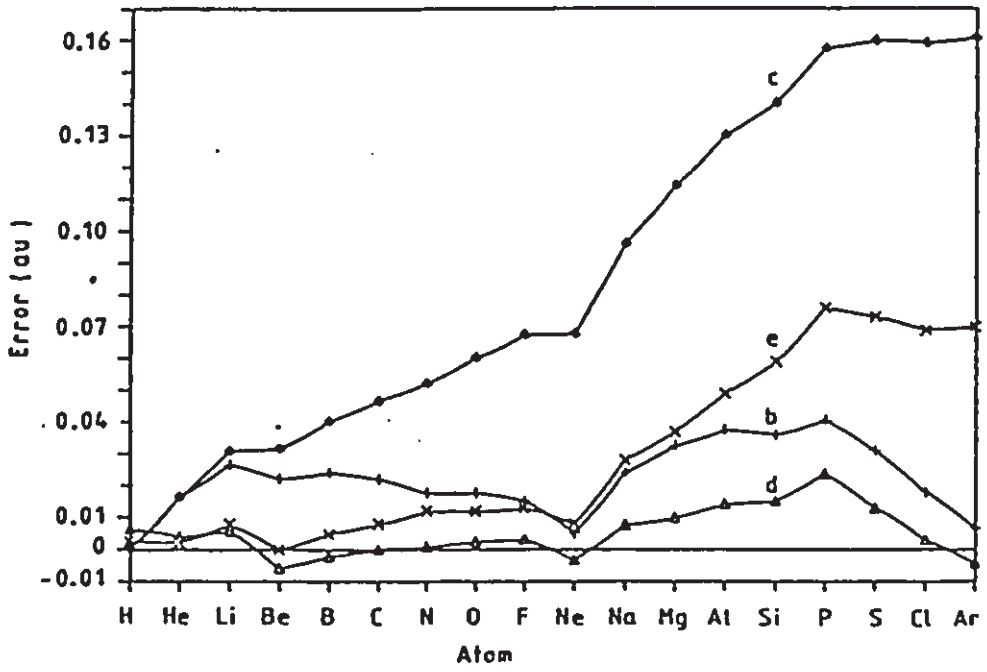
0.16
0.13
0.10
0.07
0.04
0.01
0
-0.01
Error (au)
c
e
b
d
H He Li Be B C N O F Ne Na Mg Al Si P S Cl Ar
Atom

Figure 5.1.2

Error in the molecular correlation energy for diatomic molecules.

(a) second-row hydrides

(b) third-row hydrides

(c) second-row homonuclear diatomics

(d) second- and third-row fluorides

(e) second- and third-row oxides

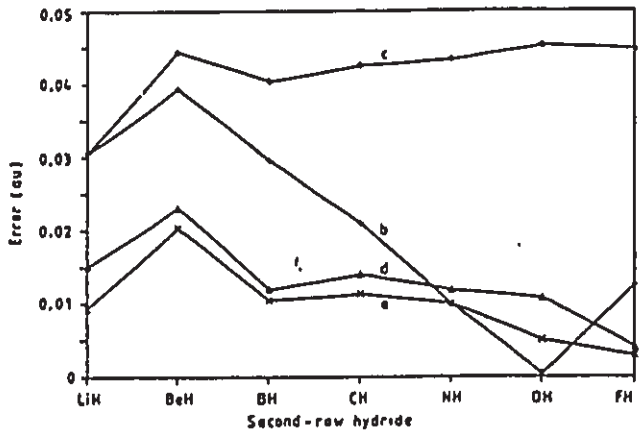
0.05
0.04
0.03
0.02
0.01
0
Error (au)
c
b
f
d
e
LiH
BeH
BH
CH
NH
OH
FH
Second-row hydride

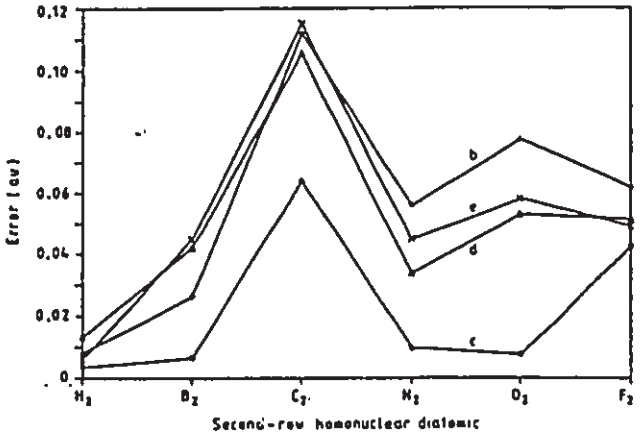
0.12
0.10
0.08
0.06
0.04
0.02
0
Error (au)
b
e
d
c
H_2
B_2
C_2
N_2
O_2
F_2
Second-row homonuclear diatomic

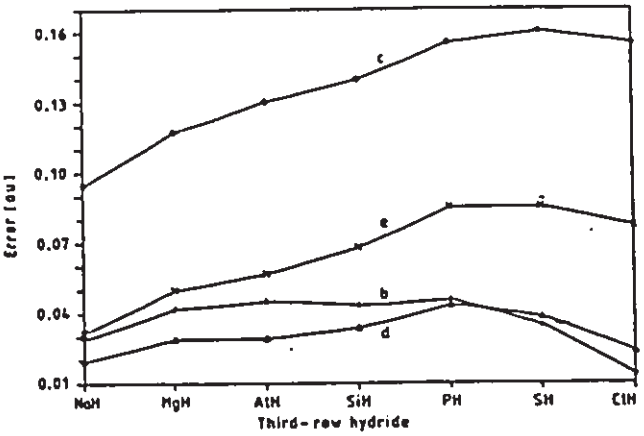
0.16
0.13
0.10
0.07
0.04
0.01
Error (au)
c
e
b
d
NaH
MgH
AlH
SiH
PH
SH
ClH
Third-row hydride

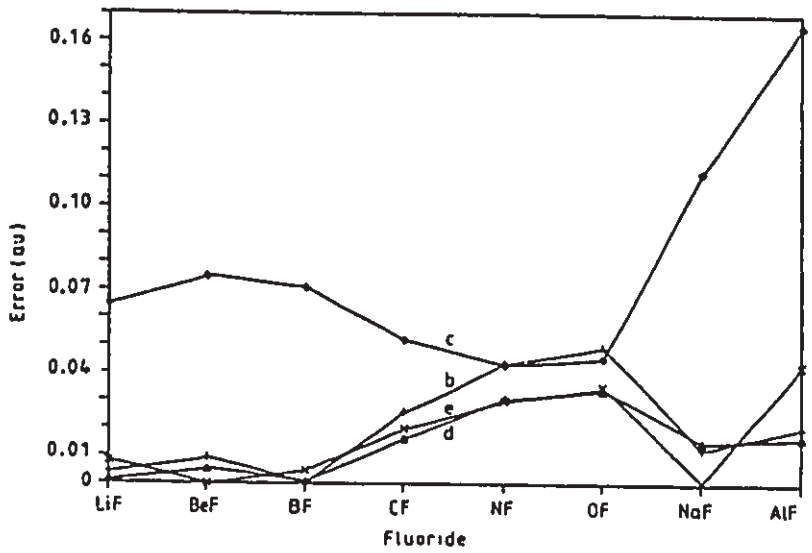
0.16
0.13
0.10
0.07
0.04
0.01
0
Error (au)
c
b
e
d
LiF
BeF
BF
CF
NF
OF
NaF
AlF
Fluoride

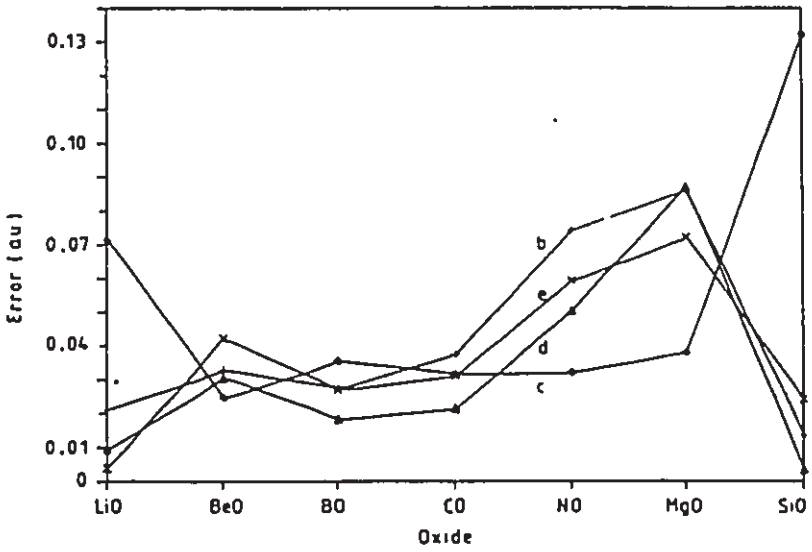
0.13
0.10
0.07
0.04
0.01
0
Error (au)
b
e
d
c
LiO
BeO
BO
CO
NO
MgO
SiO
Oxide

Figure 5.1.3

Error in the dissociation energy for diatomic molecules.

(a) second-row hydrides

(b) third-row hydrides

(c) second-row homonuclear diatomics

(d) second- and third-row fluorides

(e) second- and third-row oxides

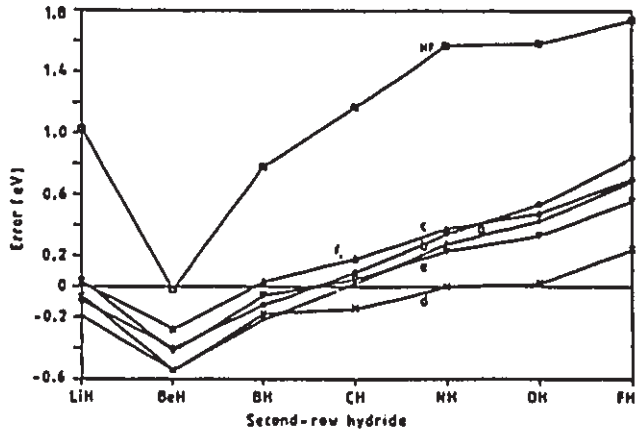
1.8
1.4
1.0
0.6
0.2
0
-0.2
-0.6
Error (eV)
HF
c
b
a
e
d
LiH
BeH
BH
CH
NH
OH
FH
Second-row hydride

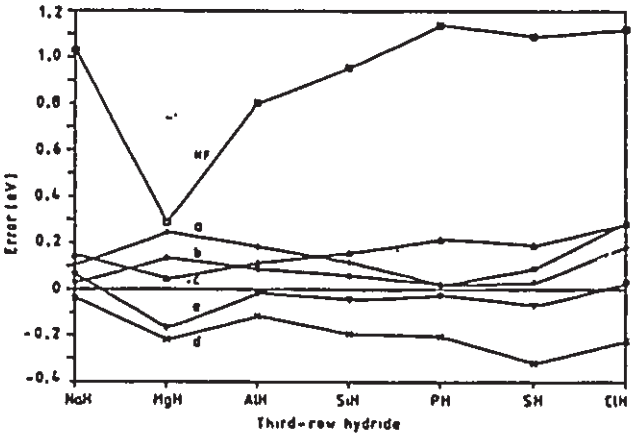
1.2
1.0
0.8
0.6
0.4
0.2
0
-0.2
-0.4
Error (eV)
HF
a
b
c
e
d
NaH
MgH
AlH
SiH
PH
SH
ClH
Third-row hydride

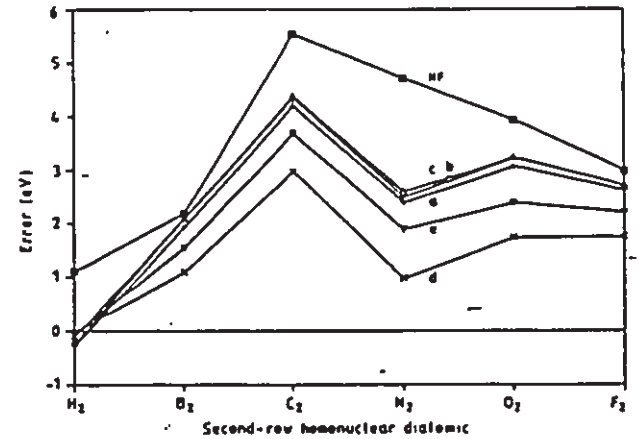
6
5
4
3
2
1
0
-1
Error (eV)
HF
c b
a
e
d
H2
B2
C2
N2
O2
F2
Second-row homonuclear diatomic

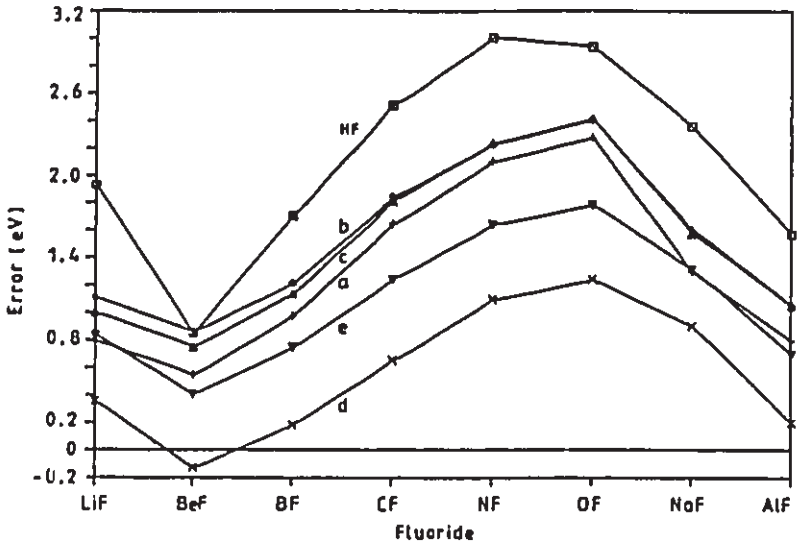
3.2
2.6
2.0
1.4
0.8
0.2
0
-0.2
Error (eV)
HF
b
c
a
e
d
LiF
BeF
BF
CF
NF
OF
NaF
AlF
Fluoride

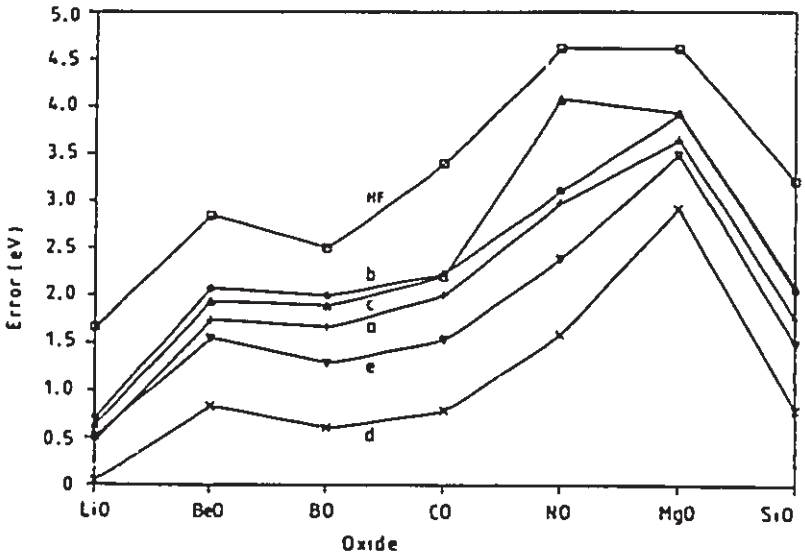
5.0
4.5
4.0
3.5
3.0
2.5
2.0
1.5
1.0
0.5
0
Error (eV)
HF
b
c
a
e
d
LiO
BeO
BO
CO
NO
MgO
SiO
Oxide

Figure 5.1.4

(a) Magnitude of the correlation energy of the atoms in the second-row hydrides. The total correlation energy is the sum of the correlation energies of the atoms in the hydrides.

(b) Magnitude of the correlation energy of hydrogen in the second-row hydrides plotted against the electron population of hydrogen in the second-row hydrides.

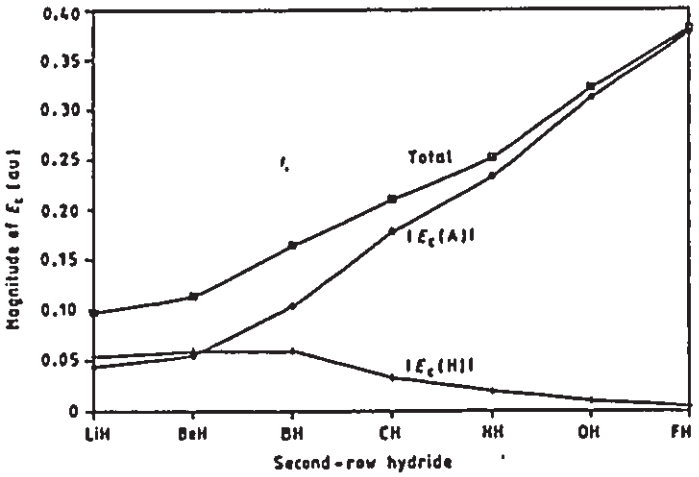
0.40
0.35
0.30
0.25
0.20
0.15
0.10
0.05
0
Magnitude of E_c (au)
Total
$|E_c(A)|$
$|E_c(H)|$
LiH
BeH
BH
CH
NH
OH
FH
Second-row hydride

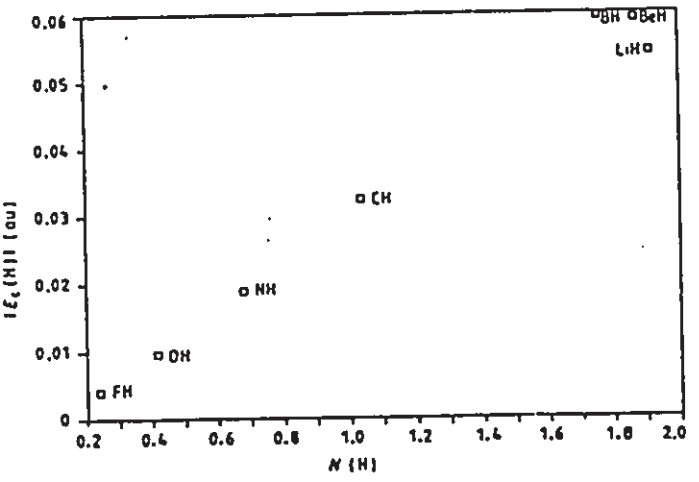
0.06
0.05
0.04
0.03
0.02
0.01
0
$|E_c(H)|$ (au)
BH
BeH
LiH
CH
NH
OH
FH
0.2
0.4
0.6
0.8
1.0
1.2
1.4
1.6
1.8
2.0
N (H)

Figure 5.1.5

(a) Magnitude of the correlation energy of the atoms in the third-row hydrides. The total correlation energy is the sum of the correlation energies of the atoms in the hydrides.

(b) Magnitude of the correlation energy of hydrogen in the third-row hydrides plotted against the electron population of hydrogen in the third-row hydrides.

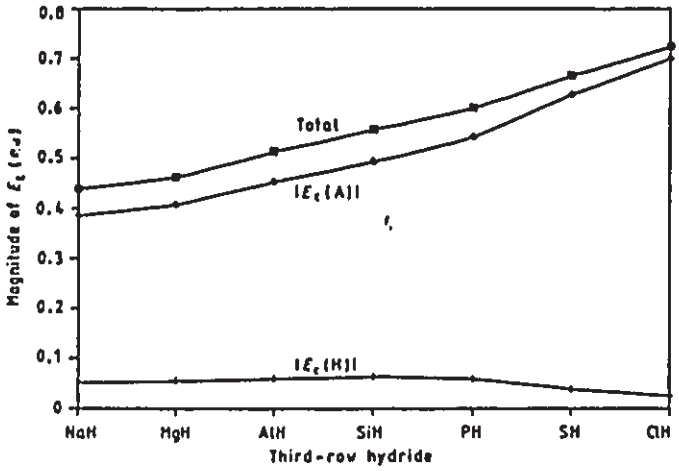
Total
$|E_c(A)|$
$|E_c(H)|$
Magnitude of E_c (a.u.)
0.8
0.7
0.6
0.5
0.4
0.3
0.2
0.1
0
NaH
MgH
AlH
SiH
PH
SH
ClH
Third-row hydride

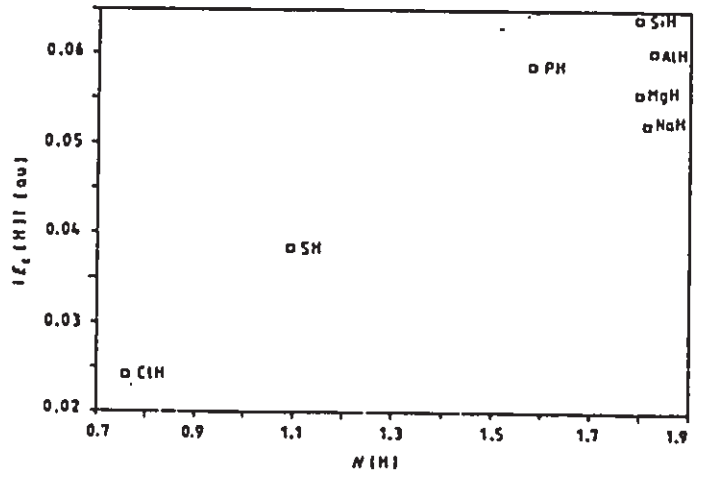
SiH
AlH
MgH
NaH
PH
SH
ClH
$|E_c(H)|$ (au)
0.06
0.05
0.04
0.03
0.02
0.7
0.9
1.1
1.3
1.5
1.7
1.9
$N(H)$

Figure 5.1.6

Magnitude of the correlation energy of fluorine in the fluorides plotted against the electron population of fluorine in the fluorides.

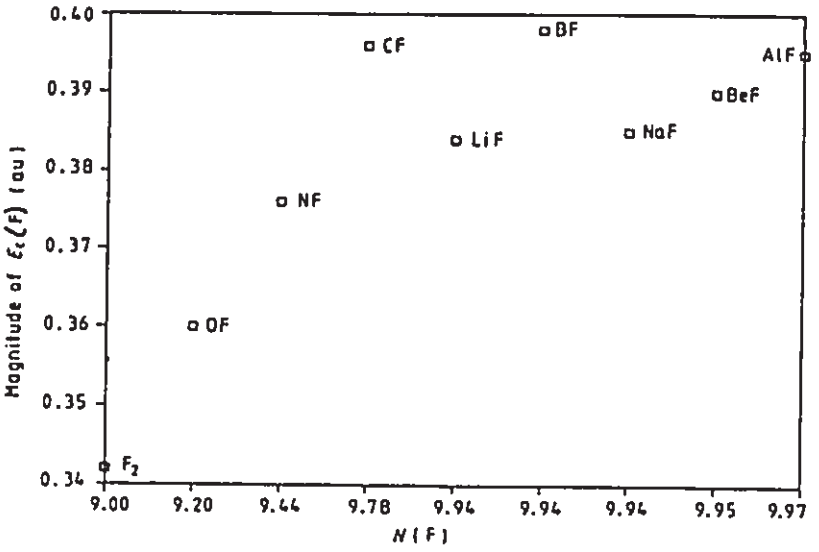
0.40
0.39
0.38
0.37
0.36
0.35
0.34
Magnitude of $\epsilon_t(F)$ (au)
CF
BF
AlF
BeF
LiF
NaF
NF
OF
F_2
9.00
9.20
9.44
9.78
9.94
9.94
9.94
9.95
9.97
$N(F)$

Figure 5.1.7

Magnitude of the average correlation energy of an N-electron system divided by N plotted against N for N = 10 to 22.

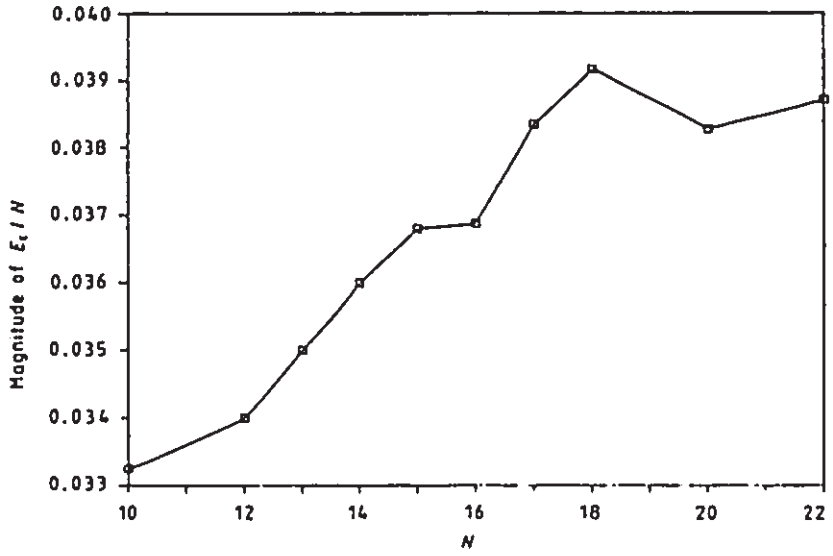
0.040
0.039
0.038
0.037
0.036
0.035
0.034
0.033
Magnitude of E_t / N
10
12
14
16
18
20
22
N

Table 5.1.1. Ground State Atomic Correlation Energies (au) Calculated Using Clementi and Roetti State Functions[a]

Atom		E_o						
		A	B	C	D	E	Exact[b]	Exact[c]
H	^2S	-0.022	0	0	-0.006	-0.003	0	0
He	^1S	-0.113	-0.059	-0.059	-0.046	-0.044	-0.042	-0.042
Li	^2S	-0.151	-0.072	-0.076	-0.051	-0.053	-0.045	-0.046
Be	^1S	-0.225	-0.116	-0.126	-0.088	-0.094	-0.094	-0.094
B	^2P	-0.291	-0.148	-0.164	-0.122	-0.129	-0.124	-0.125
C	^3P	-0.360	-0.177	-0.202	-0.155	-0.163	-0.155	-0.158
N	^4S	-0.430	-0.204	-0.239	-0.187	-0.198	-0.186	-0.189
O	^3P	-0.539	-0.272	-0.315	-0.257	-0.266	-0.254	-0.258
F	^2P	-0.644	-0.331	-0.383	-0.319	-0.329	-0.316	-0.322
Ne	^1S	-0.746	-0.386	-0.449	-0.378	-0.389	-0.381	-0.390
Na	^2S	-0.805	-0.410	-0.482	-0.394	-0.414	-0.386	-0.398
Mg	^1S	-0.892	-0.461	-0.542	-0.438	-0.465	-0.428	-0.444
Al	^2P	-0.966	-0.497	-0.589	-0.473	-0.508	-0.459	-0.479
Si	^3P	-1.042	-0.530	-0.634	-0.509	-0.553	-0.494	-0.520
P	^4S	-1.119	-0.562	-0.679	-0.545	-0.597	-0.521	-0.553
S	^3P	-1.228	-0.626	-0.755	-0.608	-0.668	-0.595	-0.634
Cl	^2P	-1.330	-0.685	-0.826	-0.670	-0.736	-0.667	-0.714
Ar	^1S	-1.431	-0.738	-0.893	-0.728	-0.802	-0.732	-0.787
Mean Dev'n	b	0.358	0.022	0.085	0.007	0.030		
	c	0.343	0.017	0.070	0.012	0.014		

[a] Clementi and Roetti (1974).
[b] Veillard and Clementi (1968) (without Lamb Shift corrections).
[c] Veillard and Clementi (1968) (with Lamb Shift corrections included, see text).

Table 5.1.2. Molecular Correlation Energies (au) of Second-Row Hydrides, Third-Row Hydrides, Second-Row Homonuclear Diatomics, Second- and Third-Row Diatomic Fluorides, Oxide, Nitrides and Chlorides Using Near-Hartree-Fock Quality State Functions[a]

System	Ω	$E_c(\Omega)$					
		A	B	C	D	E	Exact
second-row hydrides:							
LiH	Li	-0.140	-0.072	-0.073	-0.044	-0.048	
	H	-0.079	-0.041	-0.041	-0.054	-0.044	
	Total	-0.218	-0.113	-0.113	-0.098	-0.092	-0.083
BeH	Be	-0.183	-0.087	-0.092	-0.055	-0.064	
	H	-0.083	-0.043	-0.043	-0.059	-0.047	
	Total	-0.266	-0.130	-0.135	-0.114	-0.111	-0.091
BH	B	-0.266	-0.138	-0.149	-0.104	-0.114	
	H	-0.084	-0.043	-0.043	-0.059	-0.048	
	Total	-0.350	-0.181	-0.192	-0.164	-0.162	-0.152
CH	C	-0.374	-0.191	-0.215	-0.177	-0.180	
	H	-0.050	-0.026	-0.024	-0.032	-0.027	
	Total	-0.424	-0.217	-0.238	-0.210	-0.207	-0.196
NH	N	-0.466	-0.232	-0.268	-0.232	-0.233	
	H	-0.033	-0.017	-0.015	-0.019	-0.016	
	Total	-0.499	-0.249	-0.282	-0.251	-0.249	-0.239
OH	O	-0.583	-0.300	-0.347	-0.311	-0.306	
	H	-0.020	-0.011	-0.008	-0.010	-0.009	
	Total	-0.604	-0.310	-0.355	-0.321	-0.315	-0.310
FH	F	-0.693	-0.358	-0.417	-0.377	-0.370	
	H	-0.012	-0.006	-0.004	-0.004	-0.004	
	Total	-0.704	-0.364	-0.421	-0.381	-0.374	-0.377
Mean Deviation		0.231	0.020	0.042	0.013	0.010	
third-row hydrides:							
NaH	Na	-0.795	-0.411	-0.477	-0.387	-0.410	
	H	-0.074	-0.038	-0.038	-0.052	-0.042	
	Total	-0.869	-0.449	-0.515	-0.440	-0.452	-0.420
MgH	Mg	-0.856	-0.436	-0.512	-0.408	-0.440	
	H	-0.077	-0.040	-0.039	-0.056	-0.044	
	Total	-0.933	-0.476	-0.551	-0.463	-0.484	-0.434
AlH	Al	-0.943	-0.487	-0.573	-0.453	-0.493	
	H	-0.082	-0.042	-0.042	-0.060	-0.048	
	Total	-1.024	-0.529	-0.614	-0.514	-0.541	-0.484
SiH	Si	-1.021	-0.525	-0.622	-0.494	-0.542	
	H	-0.083	-0.043	-0.042	-0.064	-0.050	
	Total	-1.104	-0.567	-0.664	-0.558	-0.592	-0.524
PH	P	-1.108	-0.564	-0.675	-0.542	-0.586	
	H	-0.075	-0.039	-0.037	-0.059	-0.046	
	Total	-1.183	-0.603	-0.712	-0.600	-0.642	-0.557
SH	S	-1.234	-0.635	-0.763	-0.628	-0.682	
	H	-0.053	-0.028	-0.025	-0.038	-0.031	
	Total	-1.287	-0.663	-0.788	-0.666	-0.713	-0.628

Table 5.1.2 (con'd)

System	Ω	$E_o(\Omega)$					
		A	B	C	D	E	Exact
ClH	Cl	-1.348	-0.698	-0.841	-0.702	-0.759	
	H	-0.037	-0.019	-0.017	-0.024	-0.020	
	Total	-1.386	-0.716	-0.857	-0.726	-0.779	-0.702
Mean Deviation		0.577	0.036	0.136	0.031	0.065	
second-row homonuclear diatomics:							
H_2	Total	-0.095	-0.049	-0.044	-0.054	-0.047	-0.041
B_2	Total	-0.592	-0.300	-0.333	-0.284	-0.281	-0.326
C_2	Total	-0.769	-0.398	-0.446	-0.405	-0.395	-0.510
N_2	Total	-0.945	-0.489	-0.555	-0.511	-0.500	-0.545
O_2	Total	-1.110	-0.570	-0.655	-0.594	-0.589	-0.647
F_2	Total	-1.301	-0.673	-0.778	-0.684	-0.688	-0.735
Mean Deviation		0.335	0.057	0.022	0.050	0.053	
fluorides:							
LiF	Li	-0.139	-0.072	-0.072	-0.044	-0.048	
	F	-0.698	-0.381	-0.421	-0.384	-0.373	
	Total	-0.837	-0.433	-0.494	-0.428	-0.421	-0.428
BeF	Be	-0.179	-0.085	-0.080	-0.053	-0.061	
	F	-0.700	-0.362	-0.423	-0.390	-0.377	
	Total	-0.879	-0.447	-0.513	-0.443	-0.438	-0.438
BF	B	-0.259	-0.134	-0.144	-0.099	-0.110	
	F	-0.703	-0.364	-0.424	-0.398	-0.383	
	Total	-0.962	-0.498	-0.569	-0.497	-0.493	-0.498
CF	C	-0.338	-0.172	-0.191	-0.146	-0.157	
	F	-0.697	-0.361	-0.420	-0.396	-0.382	
	Total	-1.035	-0.533	-0.611	-0.543	-0.539	-0.559
NF	N	-0.428	-0.213	-0.243	-0.200	-0.209	
	F	-0.678	-0.351	-0.407	-0.376	-0.368	
	Total	-1.106	-0.564	-0.650	-0.576	-0.577	-0.607
OF	O	-0.543	-0.279	-0.320	-0.278	-0.281	
	F	-0.664	-0.344	-0.398	-0.360	-0.356	
	Total	-1.207	-0.623	-0.717	-0.638	-0.637	-0.672
NaF	Na	-0.791	-0.409	-0.474	-0.382	-0.409	
	F	-0.697	-0.361	-0.421	-0.385	-0.372	
	Total	-1.488	-0.769	-0.895	-0.767	-0.781	-0.782
AlF	Al	-0.937	-0.484	-0.568	-0.448	-0.490	
	F	-0.701	-0.363	-0.423	-0.395	-0.379	
	Total	-1.638	-0.847	-0.992	-0.843	-0.869	-0.828
Mean Deviation		0.543	0.021	0.079	0.015	0.018	
oxides:							
LiO	Li	-0.139	-0.072	-0.072	-0.043	-0.048	
	O	-0.595	-0.306	-0.356	-0.323	-0.313	
	Total	-0.734	-0.378	-0.428	-0.366	-0.361	-0.357

Table 5.1.2 (con'd)

System	Ω	$E_c(\Omega)$ A	B	C	D	E	Exact
BeO	Be	-0.167	-0.086	-0.088	-0.045	-0.057	
	O	-0.638	-0.330	-0.386	-0.374	-0.350	
	Total	-0.804	-0.416	-0.474	-0.418	-0.407	-0.449
BO	B	-0.221	-0.107	-0.115	-0.068	-0.083	
	O	-0.641	-0.332	-0.387	-0.380	-0.356	
	Total	-0.861	-0.439	-0.501	-0.448	-0.438	-0 466
CO	C	-0.314	-0.163	-0.178	-0.129	-0.143	
	O	-0.636	-0.329	-0.383	-0.378	-0.355	
	Total	-0.950	-0.492	-0.560	-0.508	-0.498	-0.529
NO	N	-0.440	-0.227	-0.256	-0.221	-0.224	
	O	-0.586	-0.304	-0.351	-0.334	-0.322	
	Total	-1.029	-0.531	-0.573	-0.555	-0.546	-0.605
MgO	Mg	-0.846	-0.437	-0.508	-0.398	-0.435	
	O	-0.620	-0.321	-0.374	-0.358	-0.337	
	Total	-1.466	-0.758	-0.882	-0.757	-0.772	-0.844
SiO	Si	-0.993	-0.513	-0.602	-0.469	-0.523	
	O	-0.642	-0.332	-0.388	-0.386	-0.359	
	Total	-1.634	-0.845	-0.990	-0.855	-0.882	-0.858
Mean Deviation		0.482	0.042	0.052	0.031	0.037	
nitrides:							
CN	C	-0.328	-0.170	-0.186	-0.143	-0.153	
	N	-0.528	-0.272	-0.314	-0.306	-0.288	
	Total	-0.857	-0.442	-0.500	-0.449	-0.441	-0.503
PN	P	-1.070	-0.553	-0.652	-0.511	-0.574	
	N	-0.559	-0.290	-0.336	-0.346	-0.317	
	Total	-1.630	-0.842	-0.988	-0.857	-0.891	-0.870
Mean Deviation		0.557	0.044	0.061	0.034	0.042	
chlorides:							
LiCl	Li	-0.139	-0.072	-0.072	-0.043	-0.048	
	Cl	-1.377	-0.711	-0.862	-0.730	-0.780	
	Total	-1.516	-0.783	-0.934	-0.773	-0.827	-0.744
NaCl	Na	-0.792	-0.409	-0.474	-0.384	-0.409	
	Cl	-1.377	-0.711	-0.861	-0.731	-0.779	
	Total	-2.168	-1.120	-1.336	-1.114	-1.188	-1.082
Mean Deviation		0.929	0.039	0.222	0.031	0.095	

[a] Cade and Huo 1973, 1974, 1975, McLean and Yoshimine 1968.

Table 5.1.3. Dissociation Energies (eV) of Second-Row Hydrides, Third-Row Hydrides, Second-Row Homonuclear Diatomics, Second- and Third-Row Diatomic Fluorides, Oxide, Nitrides and Chlorides Using Near-Hartree-Fock Quality State Functions[a]

System	D_e						
	HF	A	B	C	D	E	Expt[b]
second-row hydrides:							
LiH	1.49	2.71	2.61	2.50	2.58	2.48	2.52
BeH	2.18	2.70	2.56	2.44	2.70	2.58	2.16
BH	2.78	3.78	3.68	3.53	3.74	3.62	3.57
CH	2.47	3.62	3.55	3.46	3.78	3.59	3.64
NH	2.10	3.39	3.33	3.29	3.67	3.44	3.67
OH	3.03	4.19	4.09	4.14	4.60	4.29	4.62
FH	4.38	5.43	5.28	5.41	5.88	5.56	6.12
Devn[c]	1.13	0.34	0.35	0.30	0.17	0.24	
third-row hydrides:							
NaH	0.92	2.06	1.98	1.80	1.99	1.88	1.95
MgH	1.14	1.68	1.57	1.38	1.65	1.60	1.43
AlH	2.36	3.35	3.25	3.05	3.28	3.18	3.16
SiH	2.23	3.30	3.24	3.03	3.38	3.23	3.19
PH	2.03	3.19	3.14	2.95	3.37	3.19	3.17
SH	2.63	3.69	3.63	3.53	4.04	3.79	3.72
ClH	3.48	4.43	4.33	4.33	4.84	4.59	4.62
Devn	0.92	0.13	0.10	0.16	0.19	0.06	
second-row homonuclear diatomics:							
H_2	3.64	5.02	4.97	4.85	4.76	4.77	4.75
B_2	0.89	1.15	0.88	0.89	1.89	1.54	3.08
C_2	0.79	2.13	1.98	1.94	3.36	2.64	6.32
N_2	5.20	7.52	7.41	7.31	8.93	8.02	9.91
O_2	1.28	2.15	1.99	1.98	3.49	2.84	5.21
F_2	-1.32	-0.93	-1.03	-1.03	-0.09	-0.53	1.66
Devn	3.41	2.41	2.51	2.52	1.37	1.82	
fluorides:							
LiF	4.04	5.18	4.86	4.96	5.61	5.13	5.87
BeF	5.07	5.38	5.07	5.17	6.06	5.52	5.93
BF	6.19	6.92	6.68	6.76	7.72	7.15	7.80
CF	3.24	4.11	3.91	3.94	5.10	4.51	5.75
NF	0.57	1.47	1.34	1.33	2.47	1.93	3.57
OF	-0.64	0.02	-0.11	-0.12	1.06	0.51	2.29
NaF	3.00	4.07	3.76	3.78	4.47	4.05	5.36
AlF	5.37	6.14	5.88	5.89	6.74	6.24	6.94
Devn	2.11	1.30	1.54	1.50	0.59	1.08	

Table 5.1.3 (con'd)

System	D_e						
	HF	A	B	C	D	E	Expt[b]
oxides:							
LiO	1.88	3.07	2.83	2.90	3.48	3.02	3.54
BeO	1.85	2.86	2.62	2.76	3.86	3.15	4.69
BO	5.91	6.74	6.41	6.52	7.80	7.12	8.40
CO	7.84	9.23	9.00	9.03	10.45	9.70	11.23
NO	2.00	3.63	3.50	2.54	5.03	4.23	6.61
MgO	-1.03	-0.06	-0.33	-0.35	0.67	0.09	3.58
SiO	5.13	6.58	6.30	6.25	7.55	6.85	8.34
Devn	3.26	2.03	2.29	2.39	1.08	1.74	
nitrides:							
CN	3.37	5.20	5.03	5.00	6.29	5.52	7.89
PN	1.80	4.02	3.89	3.74	5.20	4.39	6.44
Devn	4.58	2.56	2.70	2.80	1.42	2.21	
chlorides:							
LiCl	3.81	4.78	4.55	4.68	5.23	4.84	4.88
NaCl	3.17	4.11	3.87	3.87	4.54	4.22	4.25
Devn	1.08	0.12	0.36	0.29	0.32	0.04	

[a] Cade and Huo (1973,1974,1975), McLean and Yoshimine (1968).
[b] Huber and Herzberg (1979).
[c] These values are the mean deviations from the experimental dissociation energies.

Table 5.1.4 Net Charges and Localizations in the Hydrides AH.

AH	q(H)[a]	L(H)	L(A)
LiH	-0.812	84.8	95.2
BeH	-0.868	88.4	92.6
BH	-0.754	80.8	92.0
CH	-0.032	46.7	90.6
NH	0.323	30.5	93.2
OH	0.585	18.5	96.0
FH	0.761	10.8	97.8
NaH	-0.812	89.4	98.1
MgH	-0.798	86.4	97.8
AlH	-0.825	84.7	97.7
SiH	-0.795	75.1	96.6
PH	-0.579	64.6	96.2
SH	-0.093	45.6	96.2
ClH	0.241	32.1	97.0

a) $q(H) = -q(A)$

Table 5.1.5. Net Charge and Localization of Fluorine in the Fluorides AF

AF	q(F)	L(F)
F_2	0.000	83.1
OF	-0.201	83.1
NF	-0.438	83.2
CF	-0.780	84.9
LiF	-0.937	88.1
BF	-0.939	86.3
NaF	-0.944	89.0
BeF	-0.945	87.8
AlF	-0.972	87.4

Table 5.1.6. Net Charge and Localization of Oxygen in the Oxides AO

AO	q(O)	L(O)
O2	0.000	85.0
NO	-0.485	87.6
LiO	-0.932	99.0
CO	-1.348	91.6
MgO	-1.412	94.7
BO	-1.553	94.2
SiO	-1.622	94.1

Table 5.1.7. Correlation Energies[a] (au) and Localization Values of the N=12 Isoelectronic Series.

System AB	ΔZ[b]	N(A)	N(B)	|Ec(A)|	|Ec(B)|	|Ec(AB)|[c]	L(A)	L(B)
NaH	10	10.189	1.812	0.387	0.052	0.438	88.1	89.4
FLi	6	9.837	2.063	0.384	0.044	0.428	99.1	95.5
OBe	4	9.693	2.307	0.374	0.045	0.419	96.8	86.4
NB	2	7.836	4.174	0.269	0.106	0.375	94.6	90.0
CC	0	0	0	0.202	0.202	0.404	73.2	73.2

$|E_c/N| = 0.034$

[a] calculated using Scheme D

[b] $\Delta Z = Z_A - Z_B$

[c] $E_c(AB) = E_c(A) + E_c(B)$

Table 5.1.8. Correlation Energies (au) and Localization Values of the N=13 Isoelectronic Series

System AB	ΔZ	N(A)	N(B)	|Ec(A)|	|Ec(B)|	|Ec(AB)|	L(A)	L(B)
MgH	11	11.206	1.798	0.408	0.056	0.464	87.8	86.4
FBe	5	9.845	3.058	0.390	0.053	0.443	87.8	92.8
OB	3	9.553	3.451	0.380	0.068	0.448	84.2	83.2
NC	1	8.083	4.917	0.306	0.143	0.449	89.4	82.4

$|Ec/N| = 0.035$

Table 5.1.8. Correlation Energies (au) and Localization Values of the N=14 Isoelectronic Series

System AB	ΔZ	N(A)	N(B)	|Ec(A)|	|Ec(B)|	|Ec(AB)|	L(A)	L(B)
AlH	12	12.175	1.825	0.453	0.060	0.513	97.7	84.7
FB	4	8.939	4.071	0.398	0.099	0.497	96.3	91.1
OC	2	8.346	4.654	0.378	0.129	0.507	91.6	83.2
NN	0	7.000	7.000	0.256	0.256	0.512	78.3	78.3

$|Ec/N| = 0.036$

Table 5.1.10. Second-Row Homonuclear Diatomic Dissociation Energy (eV) Comparison: Exact Hartree-Fock Exchange Treatment (A,D)[a] Versus Approximate Exchange Functional Treatment (Axc,Dxc)[b]

System	A	Axc	D	Dxc	Expt[c]
H_2	5.0	4.9	4.8	5.0	4.7
B_2	1.2	3.9	2.0	3.3	3.1
C_2	2.1	7.3	3.4	6.1	6.3
N_2	7.5	11.6	8.9	10.2	9.9
O_2	2.2	7.6	3.5	6.4	5.2
F_2	-0.9	3.4	-0.1	2.4	1.7
Mean Deviation	2.4	1.3	1.4	0.5	

[a] Present work.
[b] Becke (1988).
[c] Huber and Herzberg (1979).

5.2 TOTAL HYDROCARBON ENERGIES CALCULATED USING DENSITY FUNCTIONAL THEORY

Both the Hartree-Fock energy and the correlation energy calculated using Scheme D has been found to be transferable among the methyl and methylene groups in a homologous series of normal alkanes (Section 1.5). Thus in principle the theory of atoms in molecules allows for the determination of the total energies of the groups responsible for energy additivity schemes. In practice, a functional expression for the correlation energy, such as Scheme D, is not of sufficent chemical accuracy as we will see shortly. Still, it is a worthwhile endeavor to detail the methodology to determine the total energies of a series of molecules (such as the hydrocarbons) because in the future this functional may become available.

To this end, we present results for a variety of hydrocarbons. Table 5.2.1 lists the electron populations, $N(\Omega)$, of each nonequivalent atom in a given molecule, RHF/6-31G**//6-31G* energies (labelled $E(\Omega)$), Scheme D correlation energies (labelled $\epsilon(\Omega)$) determined from the charge density arising from the RHF/6-31G**//6-31G* scheme, and the calculated total energy of each atom (labelled $E_t(\Omega)$ where $E_t(\Omega) = E(\Omega) + \epsilon(\Omega)$). Table 5.2.2 lists corresponding values for the total molecule and its constituent groups. From these tables we see that the carbons of the branched alkanes increase in electron population and stability (both $E(C)$ and $\epsilon(C)$ increase in magnitude) in comparison to their straight-chain counterparts. The magnitudes of $N(C)$ and $E_t(C)$ are

greater in neopentane than isobutane, and so, it can be concluded that the stability and electron population of a carbon atom increases with the extent of methyl substitution, as methyl is less electron withdrawing than is hydrogen. This observation has been previously made only for E(C) (Bader et al 1987a) so what is encouraging in the present work is that the ϵ(C) values follow the same trends as the E(C) values.

In the series C_2H_6, C_2H_4 and C_2H_2, N(C) and |E(C)| increase as carbon changes its hybridization from sp^3 to sp^2 to sp. Orbital theories predict the electronegativity and stability of a carbon to increase relative to that of its bonded hydrogens with an increase in s electrons, as s electrons are bound more tightly than p electrons (Coulson 1961). While |E(C)| increases, $|\epsilon(C)|$ decreases, and so, as a carbon increases its s character, its correlation energy becomes less negative.

The cyclic molecules have been discussed in detail by Bader et al (1987a) and Wiberg et al (1987a,b). For the series cyclohexane, cyclobutane and cyclopropane, N(C) and |E(C)| increase with increasing geometric strain but ϵ(C) shows no pattern. The magnitude of ϵ(C) for the bridgehead carbon in [1.1.1]propellane is smaller than the corresponding value in the less geometrically strained bicyclo[1.1.0]butane molecule, and so, the bridgehead carbon in the former molecule has a greater s character than in the latter.

In general the trends in the ϵ(C) values parallel the trends in the E(C) values for the carbocations. A detailed discussion of the atomic properites of carbocations is given by Bader (1988).

Table 5.2.3 gives atomization energy values. The columns are denoted E_a, E_{at}, E_a^o, E_{ac} and E_{at}'. These terms are defined as follows: E_a is the calculated RHF/6-31G**//6-31G* atomization energy; E_{at} incorporates Scheme D correlation into the atomization energy calculation yielding a total atomization energy for the molecule; E_a^o is the experimental atomization energy extrapolated to zero Kelvin (Fliszár et al 1988). In all cases E_{at} is greater than E_a^o, and so, we wish to scale down the correlation energy contribution as follows:

$$E_{ac} = E_a^t - E_a \qquad [5.2.1]$$

and the scaled total calculated atomization energy for the molecule is

$$E_{at}' = E_a + \alpha E_{ac} \qquad [5.2.2]$$

where α is a parameter (α = 0.63065) chosen to yield E_{at}' which will minimize the range in the deviation of E_{at}' values from E_a^o values.

Inspection of Table 5.2.3 reveals that propane, cyclopropane, butane, pentane and their branched isomers deviate the least from experiment. The deviations are largest for methane, hexane and cyclohexane. Overall, the deviations are too large for an accurate energy additivity scheme to be produced.

We have used a one-parameter fit to determine E_{at}'. Of course, in addition to scaling down E_{ac}, we could scale up E_a. We could also have a separate parameter for each functional group. This task will not be undertaken here because increasing the number of fitting parameters, though perhaps improving agreement with experiment, will obscure the physics of the systems.

Table 5.2.1. Atomic Populations and Energies of Hydrocarbons[a]

Hydrocarbon	Ω	N(Ω)	-E(Ω)	-ϵ(Ω)	-E_t(Ω)
i)saturated straight-chain					
CH_4	C	5.754	37.6087	0.2276	37.8373
	H	1.062	0.6480	0.0357	0.6837
C_2H_6	C	5.762	37.6328	0.2350	37.8678
	H	1.079	0.6621	0.0368	0.6989
C_3H_8	C	5.774	37.6502	0.2366	37.8868
	H	1.079	0.6615	0.0369	0.6984
	H	1.082	0.6625	0.0375	0.7000
	C	5.778	37.6539	0.2420	37.8959
	H	1.092	0.6744	0.0380	0.7124
C_4H_{10}	C	5.773	37.6470	0.2365	37.8835
	H	1.079	0.6622	0.0369	0.6991
	H	1.082	0.6632	0.0376	0.7008
	C	5.791	37.6695	0.2434	37.9129
	H	1.095	0.6750	0.0387	0.7137
C_5H_{12}	C	5.773	37.6469	0.2365	37.8834
	H	1.079	0.6621	0.0369	0.6990
	H	1.082	0.6629	0.0376	0.7005
	C	5.791	37.6716	0.2435	37.9151
	H	1.095	0.6747	0.0387	0.7134
	C	5.803	37.6910	0.2449	37.9359
	H	1.098	0.6753	0.0394	0.7147
C_6H_{14}	C	5.775	37.6480	0.2366	37.8846
	H	1.079	0.6615	0.0369	0.6984
	H	1.082	0.6627	0.0375	0.7002
	C	5.790	37.6707	0.2434	37.9141
	H	1.095	0.6751	0.0387	0.7138
	C	5.804	37.9884	0.2448	37.9332
	H	1.098	0.6756	0.0394	0.7150
ii)saturated branched					
isobutane	C	5.781	37.6649	0.2380	37.9029
	H	1.084	0.6625	0.0381	0.7006
	H	1.082	0.6627	0.0376	0.7003
	C	5.808	37.6759	0.2489	37.9248
	H	1.102	0.6845	0.0390	0.7235
neopentane	C	5.786	37.6746	0.2391	37.9137
	H	1.084	0.6634	0.0382	0.7016
	C	5.851	37.6938	0.2559	37.9497
iii)cyclic					
cyclopropane	C	5.894	37.7115	0.2430	37.9545
	H	1.053	0.6557	0.0357	0.6914
cyclobutane	C	5.830	37.6905	0.2428	37.9333
	H	1.086	0.6683	0.0371	0.7054
	H[a]	1.084	0.6686	0.0374	0.7060
cyclohexane	C	5.809	37.6896	0.2448	37.9344
	H	1.091	0.6729	0.0379	0.7108
	H[a]	1.089	0.6754	0.0392	0.7146

Table 5.2.1 (con'd)

Hydrocarbon	Ω	N(Ω)	-E(Ω)	-ϵ(Ω)	-Et(Ω)
bicyc110butane	C	5.813	37.6702	0.2389	37.9091
	H[b]	1.062	0.6577	0.0363	0.6940
	H	1.055	0.6557	0.0356	0.6913
	C	6.081	37.8253	0.2530	38.0783
	H	1.008	0.6322	0.0335	0.6657
111propellane	C	5.864	37.7330	0.2436	37.9766
	H	1.033	0.6484	0.0353	0.6837
	C	6.102	37.8041	0.2496	38.0537
iv)unsaturated acyclic					
ETHENE	C	5.919	37.7250	0.2312	37.9562
	H	1.041	0.6473	0.0346	0.6819
ETHYNE	C	6.121	37.8418	0.2280	38.0698
	H	0.879	0.5590	0.0276	0.5866
v)cations					
CH3+	C	5.757	37.6826	0.1970	37.8796
	H	0.748	0.5179	0.0211	0.5390
C2H5+	C	5.785	37.7028	0.2323	37.9351
	H	0.871	0.5421	0.0281	0.5702
	H	0.904	0.5827	0.0290	0.6117
	C	5.910	37.8065	0.2210	38.0275
	H	0.814	0.5518	0.0241	0.5759
C3H7+	C	5.793	37.7081	0.2338	37.9419
	H	0.951	0.6082	0.0315	0.6397
	H	0.909	0.5752	0.0294	0.6046
	C	6.010	37.8794	0.2370	38.1164
	H	0.866	0.5803	0.0266	0.6069
C4H9+	C	5.796	37.7136	0.2353	37.9489
	H[d]	0.969	0.6170	0.0326	0.6496
	H	0.934	0.5897	0.0309	0.6206
	C	6.099	37.9288	0.2502	38.1790
isolated atoms					
C	C	6.000	37.6771	0.1382	37.8153
H	H	1.000	0.4982	0.0078	0.5060

[a] All results are in atomic units and are calculated from the density generated using RHF/6-31G**//6-31G*.

[b] The carbon atom of a methyl group, if present, is listed first. This is followed by the unique H of a methyl and then by one of the two equivalent hydrogens of a methyl. Given next are the carbon and hydrogen atoms of methylene. The final entries are for carbon and hydrogen of methine and finally a single carbon as in neopentane.

[c] axial

[d] in plane

Table 5.2.2. Total Energies (in au) of Hydrocarbon Molecules and Their Functional Groups

hydrocarbon and group	-E	-ϵ	-E_t
i)saturated straight-chain			
CH_4	40.2017	0.3704	40.5721
CH_3	39.5537	0.3347	39.8884
C_2H_6	79.2382	0.6908	79.9290
CH_3	39.6191	0.3454	39.9645
C_3H_8	118.2761	1.1050	119.2911
CH_3	39.6367	0.3485	39.9852
CH_2	39.0027	0.3180	39.3207
C_4H_{10}	157.3102	1.3388	158.6490
CH_3	39.6356	0.3486	39.9842
CH_2	39.0195	0.3208	39.3403
C_5H_{12}	198.3532	1.6627	198.0159
CH_3	39.6348	0.3486	39.9834
CH_2	39.0210	0.3209	39.3419
CH_2^a	39.0416	0.3237	39.3653
C_6H_{14}	235.3908	1.9858	237.3766
CH_3	39.6349	0.3485	39.9834
CH_2	39.0209	0.3208	39.3417
CH_2^a	39.0398	0.3236	39.3632
ii)saturated branched			
isobutane	157.3188	1.3418	158.6606
CH_3	39.6528	0.3513	40.0041
CH	38.3604	0.2879	38.6483
neopentane	196.3530	1.6707	198.0237
CH_3	39.6648	0.3537	40.0185
C	37.6938	0.2559	37.9497
iii)cyclic			
cyclopropane	117.0687	0.9432	118.0119
CH_2	39.0229	0.3144	39.3373
cyclobutane	156.1096	1.2692	157.3788
CH_2	39.0274	0.3173	39.3447
cyclohexane	234.2274	1.9314	236.1588
CH_2	39.0378	0.3219	39.3598
bicyc110butane	154.8822	1.1946	156.0768
CH_2	38.9836	0.3108	39.2944
CH	38.4575	0.2865	38.7440
111propellane	192.7036	1.4418	194.1454
CH_2	39.0318	0.3142	39.3460
C	37.8041	0.2496	38.0537
iv)unsaturated acyclic			
ethene	78.0382	0.6008	78.6400
CH_2	39.0196	0.3004	39.3200
ethyne	76.8216	0.5112	77.3328
CH	38.4108	0.2556	38.6664

Table 5.2.2 (con'd)

hydrocarbon and group v)cations	-E	-ϵ	-E_t
CH_3^+	39.2363	0.2603	39.4966
$C_2H_5^+$	78.3204	0.5876	78.9080
CH_3	39.4103	0.3184	39.7287
CH_2	38.9101	0.2692	39.1793
$C_3H_7^+$	117.3931	0.9118	118.3049
CH_3	39.4667	0.3241	39.7908
CH	38.4597	0.2636	38.7233
$C_4H_9^+$	156.4588	1.2393	157.6981
CH_3	39.5100	0.3297	39.8397
C	37.9288	0.2502	38.1790

[a] These methylenes are bonded only to other methylenes.

Table 5.2.3. Hydrocarbon Atomization Energies (kcal mol^{-1})

Hydrocarbon and group	E_a	E_{at}	E_a^o	E_{ae}	E_{at}'	devn[a]
i)saturated straight-chain						
CH_4	333.6	459.8	419.2	128.2	413.2	6.0
C_2H_6	561.4	792.2	710.5	230.8	707.0	3.5
C_3H_8	790.0	1127.8	1004.1	337.8	1003.0	1.1
C_4H_{10}	1018.5	1463.1	1298.2	444.6	1298.9	-0.7
C_5H_{12}	1247.0	1798.3	1592.2	551.3	1594.7	-2.5
C_6H_{14}	1475.5	2133.1	1886.0	657.6	1890.2	-4.2
ii)saturated branched						
isobutane	1018.9	1465.3	1299.7	446.4	1300.4	-0.7
neopentane	1247.5	1803.9	1595.9	556.4	1598.4	-2.5
iii)cyclic						
cyclopropane	657.8	960.3	849.9	302.5	848.6	1.3
cyclobutane	888.0	1298.6		410.6	1146.9	
cyclohexane	1370.9	2004.2	1760.8	633.3	1770.3	-9.5
bicyclobutane	743.3	1116.8	981.4	373.5	978.8	2.6
111Propellane	832.1	1274.1		442.0	1110.8	
iv)unsaturated acyclic						
ethene	434.0	618.1		184.1	550.1	
ethyne	295.6	433.2		137.6	382.4	

mean deviation= 3.1

[a] devn = $E_a^o - E_{at}'$. The symbols have been defined in the text.

5.3 CONCLUDING REMARKS

The aim of this thesis has been to apply and extend the theory of atoms in molecules to various chemical systems. The theory has been reviewed in Chapter 1. The transferabilities of atomic properties (including dipoles, volumes and correlation energies) of normal hydrocarbon groups has been discussed. A comprehensive compilation of the topological and atomic properties of second- and third-row diatomic molecules has been given in this chapter and it is hoped that the tables and diagrams will be useful both for research and pedagogical purposes.

The redistribution of charge when two reactants attach to form a hydrogen-bonded complex has been the main focus of Chapter 2. A survey of weak BASE-HF and BASE-HCl complexes have been analyzed in Section 2.1. It is hoped that this study will stimulate further research into subsets of this survey. For example, we have examined HCN-HF and HCN-HCl while Boyd and Choi (1986, 1985) have examined a range of RCN-HF systems (R = H,Li,F,Cl,HO,LiO,NC,HCC,H_3C and H_3CO) and RCN-HCl systems (R = H,Li,F,Cl,HO,NC and H_3C) to gain a greater understanding of nitrile hydrogen-bond formation.

A study of trimerization and further complexation (eg, the HF trimer and tetramer) will yield insights into the cooperative effects associated with H-bond formation. We have touched upon these effects in our water trimer study (Section 2.2).

Section 2.3 has explored a conjugated hydrogen-bonded system, the

formamide dimer, and Section 2.4 has compared various OH-O complexes of differing hydrogen-bond lengths. In Section 2.5, point charges have been used to simulate crystal fields associated with OH-O complexes and the corresponding redistribution of charge due to the crystal field effects has been detailed.

We have developed and tested a model to predict the structure and geometry of H-bonded complexes (Section 3.1) based on $\nabla^2\rho$ and have found it to work well in the vast majority of cases studied. Thus, we can predict which atoms will hydrogen-bond, what the geometry of the complex will be, and then explain the nature, energetics and mechanism of the hydrogen-bond formation.

In Section 3.2, $\nabla^2\rho$ is used to predict the reactivity of carbon ca:bon activated double bonds to nucleophilic Michael addition. We have shown that the greater toxicity of the acrylates compared to the methacrylates is predicted from the properties of $\nabla^2\rho$. It is hoped that this work will stimulate further applications of the theory of atoms in molecules to biochemistry.

Chapter 4 extends the concepts of bond order and bond energy to complexes containing nitrogen nitrogen bonds. Given the NN bond path length, we can predict its bond order and bond energy.

The theory of atoms in molecules is extended in Chapter 5 by introducing an atomic property $E_c(\Omega)$ which gives the correlation energy of an atom in a molecule. This property is derived using density functional theory. Various correlation energy density functionals have been proposed and to date a nonlocal gradient corrected expression gives the best agreement with experiment (Section 5.1). Still, these

fuctionals are not of sufficient chemical accuracy for energy additivity schemes (Section 5.2) and it is hoped that this work will stimulate further interest in the development of more accurate correlation energy density functionals.

Appendix 5.1: Parametrizations of $\epsilon_c(\rho_\uparrow,\rho_\downarrow)$

The most accurate expression to date for the correlation energy per electron of a homogeneous electron liquid is given by (VWN 1980)

$$\epsilon_c(r_s) = 0.5A\{\ln(x^2/X(x)) + (2b/Q)\tan^{-1}(Q/(2x+b)) - (bx_o/X(x_o))[\ln((x-x_o)^2/X(x)) + (2(b+2x_o)/Q)\tan^{-1}(Q/(2x+b))]\} \quad [A5.1.1]$$

where $r_s = (3/(4\pi)\rho(r))^{1/3}$, $x = r_s^{0.5}$, $X(x) = x^2+bx+c$, $Q = (4c-b^2)^{0.5}$, and the constants A, x_o, b, and c are 0.0621814, -0.10498, 3.72744, 12.9352, and 0.0310907, -0.32500, 7.06042, and 18.0578 for ϵ_c^P and ϵ_c^F respectively, where P implies a spin-compensated system (ς=0) and F implies a spin-polarized system (ς=1). To interpolate between ς=0 and ς=1, the VWN (1980) parametrization is used:

$$\epsilon_c(r_s,\varsigma)=\epsilon_c^P(r_s)+(\alpha_c(r_s)/f''(0))f(\varsigma)+[\epsilon_c^F(r_s)-\epsilon_c^P(r_s)-\alpha_c(r_s)/f''(0)]\varsigma^4 f(\varsigma) \quad [A5.1.2]$$

where $\alpha_c(r_s)$, the correlation part of the spin stiffness also is given by equation [A5.1.1] but with A = $-1/(3\pi^2)$, x_o = -0.00475840, b = 1.13107, and c = 13.0045. Further,

$$f(\varsigma) = [(1+\varsigma)^{4/3} + (1-\varsigma)^{4/3} -2]/[2(2^{1/3}-1)] \quad [A5.1.3]$$

Equations [A5.1.1] to [A5.1.3] inclusive are used in Schemes A, B, and C.

Scheme D uses the RPA of von Barth and Hedin (1972):

$$\epsilon_c^{RPA}(r_s,\varsigma) = \epsilon_P^{RPA}(r_s) + [\epsilon_F^{RPA}(r_s)-\epsilon_P^{RPA}(r_s)]f(\varsigma) \quad [A5.1.4]$$

where $\epsilon_i^{RPA}(r_s) = -c_i[(1+x_i^3)\ln(1+1/x_i) + 0.5x_i - x_i^2 - 1/3]$ (i=P,F)

[A5.1.5]

with $c_P = 0.0252$, $c_F = 0.0127$, $x_P = r_s/30.0$, and $x_F = r_s/75.0$.

Scheme E uses the Perdew-Zunger parametrization (1981):

$$\epsilon_c^i = \Phi_i/(1+\beta_1^i r_s^{0.5} + \beta_2^i r_s) \quad (r_s \geq 1)$$

$$\epsilon_c^i = A_i \ln r_s + B_i + C_i r_s \ln r_s + D_i r_s \quad (r_s < 1) \qquad (i=P,F)$$

[A5.1.6]

where $\Phi_P = -0.1423$, $\Phi_F = -0.0843$, $\beta_{1P} = 1.0529$, $\beta_{1F} = 1.3981$, $\beta_{2P} = 0.3334$, $\beta_{2F} = 0.2611$, $A_P = 0.0311$, $A_F = 0.01555$, $B_P = -0.048$, $B_F = -0.0269$, $C_P = 0.0002$, $C_F = 0.0007$, $D_P = -0.0116$, and $D_F = -0.0048$. Then, the interpolation formula is

$$\epsilon_c^{PZ}(r_s,\zeta) = \epsilon_{cP}(r_s) + [\epsilon_{cF}(r_s) - \epsilon_{cP}(r_s)]f(\zeta) \qquad [A5.1.7]$$

REFERENCES

Allen, T. L. (1959). J. Chem. Phys. 31, 1039.

Allred, A. L. (1961). J. Inorg. Nucl. Chem. 17, 215.

Bachrach, S. M. and Streitwieser, A. (1984). J. Am. Chem. Soc. 106, 2283.

Bader, R. F. W. (1989). In "Molecules in Physics, Chemistry and Biology". (ed. Maruani, J.). Vol. III, 73. Kluwer Academic Publishers.

Bader, R. F. W. and Chang, C. (1989). J. Phys. Chem. in press.

Bader, R. F. W. (1988). J. Pure Appl. Chem. 60, 145.

Bader, R. F. W., Gillespie, R. J., MacDougall, P. J. (1988). J. Am. Chem. Soc. 110, 7329.

Bader, R. F. W. and Wiberg, K. B. (1987). In "Density Matrices and Density Functionals". (eds. Erdahl, R. M. and Smith, V. H.). 677. D. Reidel Publishing Co.: Dordricht, Holland.

Bader, R. F. W., Carroll, M. T., Cheeseman, J. R., Chang, C. (1987a). J. Am. Chem. Soc. 109, 7968.

Bader, R. F. W., Larouche, A., Gatti, C., Carroll, M. T., MacDougall, P. J., Wiberg, K. B. (1987b). J. Chem. Phys. 87, 1142.

Bader, R. F. W. (1986). Can. J. Chem. 64, 1036.

Bader, R. F. W. (1985). Acc. Chem. Res. 18, 9.

Bader, R. F. W. and MacDougall, P. J. (1985). J. Am. Chem. Soc. 107, 6788.

Bader, R. F. W. and Essén, H. (1984). J. Chem. Phys. 80, 1943.

Bader, R. F. W., MacDougall, P. J., Lau, C. D. H. (1984). J. Am. Chem. Soc. 106, 1584.

Bader, R. F. W., Slee, T. S., Cremer, D., Kraka, E. (1983). J. Am. Chem. Soc. 105, 5061.

Bader, R. F. W. and Nguyen-Dang, T. T. (1981). Adv. Quant. Chem. 14, 63.

Bader, R. F. W., Nguyen-Dang, T. T., Tal, Y. (1981). Rep. Prog. Phys. 44, 893.

Bader, R. F. W. and Stephens, M. E. (1975). J. Am. Chem. Soc. 97, 7391.

Bader, R. F. W. and Stephens, M. E. (1974). Chem. Phys. Lett. 26, 445.

Bader, R. F. W. and Messer, R. R. (1974). Can. J. Chem. 52, 2268.

Bader, R. F. W. and Beddall, P. M. (1973). J. Am. Chem. Soc. 95, 305.

Bader, R. F. W. and Beddall, P. M. (1972). J. Chem. Phys. 56, 3320.

Bader, R. F. W., Beddall, P. M., Cade, P. E. (1971). J. Am. Chem. Soc. 93, 3095.

Bader, R. F. W. and Preston, H. J. T. (1970). Theor. Chim. Acta 17, 384.

Baiocchi, F. A., Reiher, W., Klemperer, W. (1983). J. Chem. Phys. 79, 6428.

Basilevsky, M. V. and Berenfeld, M. M. (1972). Intern. J. Quantum Chem. 6, 555.

Becke, A. D. (1986). J. Chem. Phys. 84, 1888.

Bell, R. P. (1973). "The Proton in Chemistry". Cornell University Press: Ithaca, N.Y.

Benzel, M. A. and Dykstra, C. E. (1983). J. Chem. Phys. 78, 4052.

Benson, S. W. (1968). "Thermochemical Kinetics". Wiley: New York.

Biegler-König, F. W., Bader, R. F. W., Tang, T.-H. (1982). J. Comp. Chem. 13, 317.

Bohm, D. and Pines, D. (1952). Phys. Rev. 85, 332.

Bohn, R. K. and Bauer, S. H. (1967). Inorg. Chem. 6, 304.

Born, M. and Oppenheimer, J. R. (1927). Ann. Phys. 84, 457.

Boyd, R. J. and Edgecombe, K. E. (1988). J. Am. Chem. Soc. 110, 4182.

Boyd, R. J. and Edgecombe, K. E. (1987). J. Comput. Chem. 8, 489.

Boyd, R. J. and Choi, S. C. (1986). Chem. Phys. Lett. 129, 62.

Boyd, R. J. and Choi, S. C. (1985). Chem. Phys. Lett. 120, 80.

Boys, S. F. and Bernardi, F. (1970). Mol. Phys. 19, 553.

Brobjer, J. T. and Murrell, J. N. (1982). J. Chem. Soc., Faraday Trans. 2 78, 1853.

Buckingham, A. D., Fowler, P. W., Hutson, J. M. (1988). Chem. Rev. 88, 963.

Buckingham, A. D. and Fowler, P. W. (1985). Can. J. Chem. 63, 2018.

Cade, P. E. and Huo, W. M. (1975). At. Data Nucl. Data Tables 15, 1.

Cade, P. E. and Huo, W. M. (1974). At. Data Nucl. Data Tables 13, 339.

Cade, P. E. and Huo, W. M. (1973). At. Data Nucl. Data Tables 12, 415.

Caldin, E. and Gold, V. (1975). (eds.) "Proton-Transfer Reactions". Chapman and Hall: London.

Cao, W. L., Gatti, C., MacDougall, P. J., Bader, R. F. W. (1987). Chem. Phys. Lett. 141, 380.

Carlon, H. R. and Harden, C. A. (1980). Appl. Optics 19, 1776.

Carlotti, M., Johns, J. W. C., Trombetti, A. (1974). Can. J. Phys. 52, 340.

Carroll, M. T. and Bader, R. F. W. (1988). Mol. Phys. 65, 695.

Carroll, M. T., Chang, C., Bader, R. F. W. (1988). Mol. Phys. 63, 387.

Carroll, M. T., Bader, R. F. W, Vosko, S. (1987). J. Phys. B 20, 3589.

Ceperley, D. M. and Alder, B. J. (1980). Phys. Rev. Lett. 45, 566.

Cheeseman, J. R., Carroll, M. T., Bader, R. F. W. (1988). Chem. Phys. Lett. 143, 450.

Clementi, E., Chin, S., Logan, D. (1986). Israel J. Chem. 27, 127.

Clementi, E. and Roetti, C. (1974). At. Data Nucl. Data Tables 14, 177.

Clementi, E. (1963). J. Chem. Phys. 38, 2248.

Collins, J. R. and Gallup, G. A. (1986). Chem. Phys. Lett. 129, 329.

Coulson, C. A. (1961). "Valence". Oxford University Press: Oxford.

Coulson, C. A. (1957). Research (London) 10, 149.

Cox, A. P., Thomas, L. F., Sheridan, J. (1958). Nature (London) 181, 1000.

Das, G. and Wahl, A. C. (1966). J. Chem. Phys. 44, 87.

Daudey, J. P. (1974). Intern. J. Quantum Chem. 8, 29.

del Bene, J. E. (1983). J. Phys. Chem. 87, 367.

Domalski, E. S. and Hearing, E. D. (1988). J. Phys. Chem. Ref. Data 17, 1637.

Dunning, T. H. (1970). J. Chem. Phys. 53, 2823.

Dyke, T. R. (1984). Top. Curr. Chem. 120, 85.

Dykstra, C. E. (1988). J. Comp. Chem. 9, 476.

Eder, E., Henschler, D., Neudecker, T. (1982). Xenobiotica 12, 831.

Ermolaev, A. M. (1985). In "Atomic Theory Workshop on Relativistic and QED Effects in Heavy Atoms". (eds. Kelly, H. P. and Kim, Y.). American

Institute of Physics: New York.

Fillery-Travis, A. J. and Legon, A. C. (1986). J. Chem. Phys. 85, 3180.

Fliszár, S., Rioux, S., Andzelm, J., Minichino, C., Vauthier, E. C. (1988). Can. J. Chem. 66, 3166.

Franklin, J. L. (1949). Ind. Eng. Chem. 41, 1070.

Frisch, M. J., Head-Gordon, M., Schlegel, H. B., Raghavachari, K., Binkley, J. S., Gonzalez, C., Defrees, D. J., Fox, D. J., Whiteside, R. A., Seeger, R., Melius, C. F., Baker, J., Martin, R. L., Kahn, L. R., Stewart, J. J. P., Fluder, E. M., Topiol, S., Pople, J. A. (1988). GAUSSIAN88. Gaussian Inc: Pittsburgh, PA.

Frisch, M. J., Del Bene, J. E., Binkley, J. S., Schaefer III, H. F. (1986). J. Chem. Phys. 84, 2279.

Fujimoto, H., Kato, S., Yamabe, S., Fukui, K. (1974). J. Chem. Phys. 60, 572.

Gatti, C., MacDougall, P. J., Bader, R. F. W. (1988). J. Chem. Phys. 88, 3792.

Gatti, C., Fantucci, P., Pacchioni, G. (1987). Theor. Chim. Acta 72, 433.

Gillespie, R. J. (1972). "Molecular Geometry". Van Nostrand-Reinhold: London

Glasstone, S. (1946). "Textbook of Physical Chemistry". Van Nostrand: New York.

Grant, I. P. (1985). In "Atomic Theory Workshop on Relativistic and QED Effects in Heavy Atoms". (eds. Kelly, H. P. and Kim, Y.). American Institute of Physics: New York.

Greenwood, N. N. and Earnshaw, A. (1984). "Chemistry of the Elements". Pergamon Press: Oxford.

Gunnarsson, O. and Lundqvist, B. I. (1976). Phys. Rev. B 13, 4274.

Gutowski, M., Van Duijneveldt, F. B., Chalasinski, G., Piela, L. (1986). Chem. Phys. Lett. 128, 325.

Harris, R. A. and Pratt, L. R. (1985). J. Chem. Phys. 83, 4024.

Hayes, I. C., Hurst, G. J. B., Stone, A. J. (1984). Mol. Phys. 53, 107.

Hehre, W. J., Radom, L., Schleyer, P. V. R., Pople, J. A. (1986). "Ab Initio Molecular Orbital Theory". Wiley: New York.

Hermansson, K., Tellgren, R., Lehmann, M. S. (1983). Act. Cryst. C. 38, 1507.

Hermansson, K. and Lunell, S. (1982). Act. Cryst. B. 38, 2563.

Hobza, P. and Zahradnik, R. (1988). Chem. Rev. 88, 871.

Hobza, P. and Sandorfy, C. (1987). J. Am. Chem. Soc. 109, 1302.

Hohenberg, P. and Kohn, W. (1964). Phys. Rev. 136, B864.

Hu, C. D. and Langreth, D. C. (1986). Phys. Rev. B 33, 943.

Hu, C. D. and Langreth, D. C. (1985). Physica Scripta 32, 391.

Huber, K. P. and Herzberg, G. (1979). "Molecular Spectra and Molecular Structure". van Nostrand: New York.

Hurst, G. J. B., Fowler, P. W., Stone, A. J , Buckingham, A. D. (1986). Int. J. Quantum Chem. 29, 1223.

Janda, K. C., Steed, J. M., Novick, S. E., Klemperer, W. (1977). J. Chem. Phys. 67, 5162.

Joesten, M. D. and Schaad, L. J. (1974). "Hydrogen Bonding". Marcel Dekker: New York.

Jones, F. M. and Arnett, E. M. (1974). In "Progress in Physical and Organic Chemistry". (eds. Streitwiesser, A. and Taft, R. W.). Wiley: New York.

Joswig, W., Fuess, H., Ferraris, G. (1982). Act. Cryst. B. 38, 2798.

Jubert, A. H., Varetti, E. L., Villar, H. O., Castro, E. A. (1984). Theoret. Chim. Acta (Berl.) 64, 313.

Jug, K. (1978). J. Am. Chem. Soc. 100, 6581.

Kemister, G. and Nordholm S. (1985). J. Chem. Phys. 83, 5163.

Kitaura, K., Satoko, C., Morokuma, K. (1979). Chem. Phys. Lett. 65, 206.

Kitaura, K., and Morokuma, K. (1976). Intern. J. Quantum Chem. 10, 325.

Kohn, W. and Sham, L. J. (1965). Phys. Rev. 140, A1133.

Kollman, P. (1977). J. Am. Chem. Soc. 99, 4875.

Kollman, P., Johansson, A., Rothenberg, S. (1974). Chem. Phys. Lett. 24, 199.

Kollman, P. and Allen, L. (1971). J. Am. Chem. Soc. 83, 4981.

Kolos, W. (1979). Theor. Chim. Acta 51, 219.

Kopp, H. (1855) as reported in: Glasstone, S. (1946). "Textbook of Physical Chemistry". Van Nostrand: New York.

Kraka, E. (1984). Ph.D. Thesis. University of Köln.

Krijn, M. P. C. M. and Feil, D. (1988). J. Chem. Phys. 88, 5787.

Langreth, D. C. and Mehl, M. J. (1983). Phys. Rev. B 28, 1809.

Langreth, D. C. and Perdew, J. P. (1980). Phys. Rev. B 21, 5469.

Lau, C. D. H., Bader, R. F. W., Hermansson, K., Berkovitch-Yellin, Z. (1986). Chem. Scripta 28, 476.

Latimer, W. M. and Rodebush, W. H. (1920). J. Am. Chem. Soc. 42, 1419.

Legon, A. C. and Millen, D. J. (1987). Acc. Chem. Res. 20, 39.

Legon, A. C. and Millen, D. J. (1986). Chem. Rev. 88, 635.

Legon, A. C., Soper, P. D., Flygare, W. H. (1981). J. Chem. Phys. 74, 4944.

Levine, I. N. (1983). "Quantum Chemistry". Third Edition. Allyn and Bacon: Boston.

Lewis, G. N. (1916). J. Am. Chem. Soc. 38, 762.

Lide, D. R. (1960). J. Chem. Phys. 33, 1514.

Lohr, L. L., Schlegel, H. B., Morokuma, K. (1984). J. Phys. Chem. 88, 1981.

Löwdin, P. O. (1959). Adv. Chem. Phys. 2, 207.

MacDougall, P. J., Schrobilgen, G. J., Bader, R. F. W. (1989). Inorg. Chem. 28, 763.

Marcus, Y. (1977). "Introduction to Liquid State Chemistry". Wiley: New York.

Mayer, I. (1987). Theor. Chim. Acta 72, 207.

McClelland, B. W., Gundersen, G., Hedberg, K. (1972). J. Chem. Phys. 56, 4541.

McLean, A. D. and Yoshimine, M. (1968). IBM Journal of Research and Development 12, 206.

McWeeny, R. (1960). Rev. Mod. Phys. 32, 335.

Mó, O., de Paz, J.L.G., Yanez, M. (1988). Theor. Chim. Acta 73, 307.

Mohr, P. J. (1985). In "Atomic Theory Workshop on Relativistic and QED Effects in Heavy Atoms" (eds. Kelly, H. P. and Kim, Y.). American Institute of Physics: New York.

Møller, C. and Plesset, M. S. (1934). Phys. Rev. 46, 618.

Moore, M. M., Amtower, A., Doerr, C., Brock, K. H., Dearfield, K. L. (1988). Environ. Mol. Mutag. 11, 49.

Morino, Y., Iijima, T., Murata, Y. (1960). Bull. Chem. Soc. Jpn. 33, 46.

Morokuma, K. (1971). J. Chem. Phys. 55, 1236.

Morton, M. and Landfield, H. (1952). J. Am. Chem. Soc. 74, 3523.

Mulliken, R. S. (1955). J. Chem. Phys. 23, 1833, 1841, 2338, 2343.

Osman, R., Namboodiri, K., Weinstein, H., Rabinowitz, J. R. (1988). J. Am. Chem. Soc. 110, 1701.

Patai, S. and Rappoport, Z. (1964). In "The Chemistry of Alkenes" (ed. Patai, S.). Wiley: New York.

Pedroza, A. C. (1986). Phys. Rev. A 33, 804.

Perdew, J. P. (1986). Phys. Rev. B 33, 8822.

Perdew, J. P. and Zunger, A. (1981). Phys. Rev. B 23, 5048.

Pauling, L. (1944). "The Nature of the Chemical Bond". Second Edition. Cornell University Press: Ithaca, N.Y.

Pauling, L. (1960). "The Nature of the Chemical Bond". Third Edition. Cornell University Press: Ithaca, N.Y.

Pimentel, G. C. and McClellan, A. D. (1960). "The Hydrogen Bond". Freeman: San Francisco.

Politzer, P. and Mulliken, R. S. (1971). J. Chem. Phys. 55, 5135.

Prosen, E. J., Johnson, W. H., Rossini, F. D. (1946). J. Res. Natl. Bur. Stand. 37, 51.

Rappoport, Z. (1981). Acc. Chem. Res. 14, 7.

Reed, A. E., Curtiss, L. A., Weinhold, F. (1988). Chem. Rev. 898.

Roothaan, C. C. J. (1951). Rev. Mod. Phys. 23, 69.

Rudenberg, K. (1975). Fortsch. Chem. Forsch. 23, 31.

Sapse, A. M. (1983). J. Chem. Phys. 78, 5733.

Savin, A., Stoll, H., Preuss, H. (1986). Theor. Chim. Acta 70, 407.

Savin, A., Wedig, U., Preuss, H., Stoll, H. (1984). Phys. Rev. Lett. 53, 2087.

Savin, A., Stoll, H., Preuss, H. (1983). In "Local Density Approximations in Quantum Chemistry and Solid State Physics" (eds. Avery, J. and Dahl, J. P.).

Plenum: New York.

Scherer, N. F., Khundkar, L. R., Bernstein, R. B., Zewail, A. H. (1987). J. Chem. Phys. 87, 1451.

Schrödinger, E. (1926). Ann. d. Phys. 79, 361.

Schulman, J. M. and Disch, R. L. (1985). Chem. Phys. Lett. 113, 291.

Schuster, P. (1976). In "The Hydrogen Bond" (eds. Schuster, P., Zundel, G., Sandorfy, C.). North-Holland Publishing Company: Amsterdam, 25.

Schwenke, D. W. and Truhlar, D. G. (1985). J. Chem. Phys. 82, 2418.

Slater, J. C. (1951). Phys. Rev. 81, 385.

Slee, T. S. (1986). Ph.D. Thesis. McMaster University.

Solomon, J. J., Fedyk, J., Mukai, F., Segal, A. (1985). Cancer Res. 45, 3465.

Solomon, J. J., Cote, I. L., Wortman, M., Decker, K., Segal, A. (1984). Chem.-Biol. Interactions 51, 167.

Stewart, R. F. (1979). Chem. Phys. Lett. 65, 335.

Stoll, H. and Savin, A. (1985). In "Density Functional Methods in

Physics" (eds. Dreizler, R. M. and da Providencia, J.). Plenum: New York.

Stoll, H., Pavlidou, C. M. E., Preuss, H. (1978). Theoret. Chim. Acta (Berl.) 49, 143.

Szczesniak, M. M. and Scheiner, S. (1986). Chem. Phys. Lett. 131, 230.

Taurian, O. E., Lunell, S., Tellgren, R. (1987). J. Chem. Phys. 86, 5053.

Thomson, C. and Glidewell, C. (1983). J. Comp. Chem. 4, 1.

Tsubomura, H. (1954). Bull. Chem. Soc. 27, 445.

Townes, C. H. and Dailey, B. P. (1949). J. Chem. Phys. 17, 782.

Veillard, A. and Clementi, E. (1968). J. Chem. Phys. 49, 2415.

Veith, V. M. and Schlemmer, G. (1982). Z. Anorg. Allg. Chem. 494, 7.

Vinogradov, S. N. and Linnell, R. H. (1971). "Hydrogen Bonding". Van Nostrand Reinhold: New York.

von Barth, U. and Hedin, L. (1972). J. Phys. C. 5, 1629.

Vosko, S. H. and Lagowski, J. B. (1986). In "Density Matrices and Density Functionals" (eds. Erdahl, R. M. and Smith Jr., V. H.). Reidel:Dordrecht.

Vosko, S. H. and Wilk, L. (1983). J. Phys. B. 16, 3687.

Vosko, S. H., Wilk, L., Nusair, M. (1980). Can. J. Phys. 58, 1200.

Wiberg, K. B., Bader, R. F. W., Lau, C. D. H. (1987a). J. Am. Chem. Soc. 109, 1001.

Wiberg, K. B., Bader, R. F. W., Lau, C. D. H. (1987b). J. Am. Chem. Soc. 109, 985.

Wiberg, K. B. (1984). J. Comput. Chem. 5, 197.

Wiberg, K. B. and Wendolowski, J. J. (1981). Proc. Nat. Acad. Sci. US

78, 6561.

Wigner, E. (1934). Phys. Rev. 48, 1002.

Wojcik, M. J., Hirakawa, A. Y., Tsuboi, M., Kato, S., Morokuma, K. (1983). Chem. Phys. Lett. 100, 523.